

Application of mechanoenergy in accessing graphene composite functional nanomaterials

by

Mohd Haniff Wahid

Dissertation Submitted to the

Faculty of Science & Engineering of Flinders University in Candidacy for the

Degree of Doctor of Philosophy in Chemistry

School of Chemical and Physical Sciences

Flinders University

August 2015



Flinders
UNIVERSITY

CONTENTS

Abstract	4
Declaration	6
Acknowledgements	7
List of Figures	8
List of Tables	16
List of Publications	17
Conference Proceedings	19
Abbreviations	21
1. Introduction	23
1.1 Thesis overview	23
1.2 General introduction	25
1.3 Graphene.....	25
1.4 Properties of Graphene	28
1.4.1 Chemical properties	28
1.4.2 Electronic properties	28
1.4.3 Mechanical properties	29
1.4.4 Optical properties	30
1.4.5 Thermal properties	31
1.5 Graphene synthesis	31
1.5.1 Micromechanical cleavage.....	32
1.5.2 Liquid phase exfoliation.....	33
1.5.3 Chemical vapour deposition.....	36
1.5.4 Epitaxial growth on silicon carbide	37
1.6 Characterization of graphene	39
1.7 Graphene oxide	43
1.8 Functionalization of graphene	43
1.9 Application of mechanoenergy in access to composite functional nanomaterials	49
1.9.1 Vortex Fluidic Device	49
1.9.2 Sonication.....	53
1.10 References.....	54
2. Preparation of functional multi-layer graphene-algae hybrid material using vortex fluidics	69
2.1 Abstract.....	70
2.2 Introduction.....	70
2.3 Experimental methods	73
2.4 Results and discussion	74
2.5 Conclusions.....	82
2.6 Acknowledgements.....	83
2.7 References.....	83
3. Entrapment of <i>Chlorella vulgaris</i> cells within graphene oxide layers	88
3.1 Abstract.....	89
3.2 Introduction.....	89

3.3 Experimental methods	90
3.4 Results and discussion	92
3.5 Conclusion	97
3.6 Acknowledgements.....	98
3.7 References.....	98
4. Microencapsulation of bacterial strains with graphene oxide nano-sheets using vortex fluidics.....	102
4.1 Abstract.....	103
4.2 Introduction.....	103
4.3 Experimental methods	105
4.4 Results and discussion	108
4.5 Conclusions.....	117
4.6 Acknowledgements.....	118
4.7 References.....	118
5. Aqueous based synthesis of antimicrobial-decorated	124
graphene	124
5.1 Abstract.....	125
5.2 Introduction.....	125
5.3 Experimental methods	128
5.4 Results and discussion	130
5.5 Conclusion	143
5.6 Acknowledgements.....	143
5.7 References.....	143
6. Amphiphilic graphene oxide stabilisation of hexagonal BN and MoS₂ sheets	148
6.1 Abstract.....	149
6.2 Introduction.....	149
6.3 Experimental methods	150
6.4 Results and discussion	153
6.5 Conclusion	158
6.6 Acknowledgements.....	159
6.7 References.....	159
Appendices	163
7. Conclusions and Future Work	174
7.1 Conclusions.....	174
7.1.1 Overall.....	177
7.2 Future work.....	178
7.3 References.....	179

ABSTRACT

Graphene, the monoatomic layer of the graphite mineral has been a subject of intense research interest among the scientific community. Given the exceptional electrical, thermal, mechanical and optical properties of graphene, it shows huge potential for wide-ranging applications and this is further extended through functionalization. In this dissertation various hybrid materials of graphene have been synthesised, characterized in detail, and some of their potential applications explored. Multi-layers of graphene have been synthesised using a vortex fluidic device (VFD) in water and subsequently they were interfaced with the surface of microalgal cells, *Chlorella vulgaris*. This functionalization of microalgae with multi-layer graphene has resulted in enhanced nitrate-removal activity compared to pristine microalgal cells. Viability tests show that the graphene is non-toxic towards the cells. This work demonstrates the advantage of hybridization of microalgae with graphene.

Secondly, taking advantage of the bio-interfacing of graphene towards cells, encapsulation of microalgae, *Chlorella vulgaris*, with ultra-thin layers of graphene oxide (GO) using the VFD has been established. The entrapment of algal cells within GO layers enabled the temporal confinement of the growth of microalgae which is promising as an immobilization technique for the microalgal cells. Furthermore, using the VFD, improved wrapping efficiency is obtained which is evidenced by the morphology of the samples and the growth curve of the cells post wrapping. This work demonstrates for the first time the wrapping of single cell algae with graphene oxide.

GO encapsulation of two types of bacteria has been established using the VFD, for spherical shaped *Staphylococcus aureus*, and rod shaped *Rhodococcus opacus*. Similar to the previous study with microalgae, GO wrapping of the bacteria resulted in a temporal confinement of the bacterial growth and AFM, TEM and SEM microscopy images of the samples demonstrate the wrapping of bacterial cells within GO layers. This work demonstrates the effectiveness of the VFD processing on wrapping different shapes of bacteria with the scope of extending functionality of the bacterial cells.

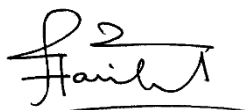
Functionalization of graphene was also carried out using an antimicrobial agent, 1,3,5-tris[(1E)-2'-(4'-benzoic acid) vinyl]benzene, namely Ramizol[®]. Ramizol[®] is essentially a planar molecule and can interact with the surface of graphene *via* extended π - π interactions thus potentially stabilising the graphene in water. Moreover, the shape of Ramizol[®] lends itself to facilitate the exfoliation of graphene from graphite by acting as a molecular 'wedge' during sonication where the graphene sheets are prized apart. The ensuing stabilized composite material demonstrates antibacterial activity against *Staphylococcus aureus* bacteria and it has potential in biomedical applications such as wound dressing materials with the graphene acting as a drug carrier as well as enhancing the structural strength of the composite material.

The amphiphilic property of graphene oxide has been utilised as a surfactant for the stabilization of 2D monoatomic crystals, namely boron nitride and molybdenum disulphide, in water. One of the intricacies of processing 2D atomic crystals is due to their insolubility in water and common organic solvents. If they can be made soluble, this can significantly facilitate their processing. An alternative route to overcome this problem has been established, involving the use of graphene oxide. This work demonstrates a facile approach of preparing 2D atomic crystals in aqueous solution, which can be further developed for the large scale synthesis of 2D layered materials and hetero-laminar material in general.

Overall, the synthesis of novel functional materials through hybridization with graphene derivatives has been established, with the ability to gain access to various products with novel properties. The unique properties of graphene and other materials are combined to generate potentially useful materials such as water treatment agents, surface functionalized biological cells, antibacterial materials and 2D hetero-atomic materials. Moreover, samples were prepared using facile preparation methods which are scalable, and therefore have potential for industrial applications.

DECLARATION

I certify that this thesis does not incorporate without acknowledgement any material previously submitted for a degree or diploma in any university; and that to the best of my knowledge and belief it does not contain any material previously published or written by another person except where due reference is made in the text.

A handwritten signature in black ink, appearing to read 'Hailu', written over a horizontal line.

Signed.....

08 August 2015

Date.....

ACKNOWLEDGEMENTS

Herein I would like to express my sincere appreciation to my supervisors, friends, colleagues and family. Indeed, I could not have completed my PhD project without their invaluable advice, support, and love.

I would like to thank my excellent supervisors Professor Colin L. Raston and Dr. Ela Eroglu for their generous guidance and help. Professor Raston's passion for research, positive attitude, encouragement, and ideas always motivated me in my PhD journey. Dr. Ela Eroglu was always there to provide invaluable advice, and encouraged me to get involved in collaborations with colleagues.

I would like to take this opportunity to thank Dr Xianjue Chen (Sam) who provided great support in TEM characterizations, and Dr Christopher Gibson who provided the AFM and Raman training. I would also like to express my gratitude to our collaborators, especially Dr. Sarah Harmer who provided great support in the bacteria work.

I would like to sincerely thank Universiti Putra Malaysia and Ministry of Education, Malaysia for their financial support for my PhD. I would like to thank the staff from the School of Chemical and Physical Sciences, School of Biology, and Centre for Microscopy, Characterisation and Analysis at the University of Adelaide for their kind help.

I would like to say thank you to all the members of the Raston group, for creating an upward and harmonious environment in which I have been enjoying every day. All the members have been very friendly and supportive throughout the PhD.

Finally I must thank my family for their love, support and understanding during my candidature. My parents in Malaysia who barely saw their son in the last three years and I owe them many big warm hugs. But I bet they will be proud when I eventually complete my PhD. My wife and kids who accompanied me from throughout my PhD study until the finishing. Her lasting love and patience have encouraged me to get over every barrier in the process of my PhD.

LIST OF FIGURES

- Figure 1.1.** (a) General classification of nanomaterials. (A) 0D clusters and particles. (B) 1D nanotubes and nanowires. (C) 2D nanoplates and layers. (D) 3D nanostructure. In the case of isotropic or 0D particles (e.g. sphere), due to the confinement of electrons to the same extent in all the three dimensions, properties will be more or less the same regardless of directions. Anisotropic materials show direction and dimension dependent physical and chemical properties. They come under the category of 1, 2, and 3D nanostructures, and electron motions are possible in the different dimensions. Taken from Sajanlal et al. [5]. (b) The ‘Mother’ of all graphitic forms. Graphene (on top), can be wrapped up to form 0D Buckminster fullerene (left), rolled into 1D nanotubes (centre) or stacked into 3D graphite(right). Taken from Geim and Novoselov [8].....27
- Figure 1.2.** (a) Scanning electron micrograph image of a large graphene flake spanning an array of circular holes (1 μm and 1.5 μm in diameter). Area I shows a hole partially covered by graphene, area II is fully covered, and area III is fractured from indentation (Scale bar, 3 μm) and (b) Schematic illustration of AFM nanoindentation on a suspended graphene membrane. Taken from Lee et al. [14] ...29
- Figure 1.3.** The molecular structure with rough electronic density distribution. Geometric gap calculated from van der Waals (vdw) radius of carbon is smaller than the size of helium. The C–C bond length of 0.142 nm in graphene implies that considering the nuclei alone, the pore size would be 0.246 nm. If we add the vdw radius of carbon as 0.11 nm, this geometric pore size would decrease to 0.064 nm which is is small enough not to allow molecules to pass through. Illustration taken from Berry [26].30
- Figure 1.4.** Photograph of a 50- μm aperture partially covered by graphene and its bilayer. The line scan profile shows the intensity of transmitted white light along the wide line. Inset image shows the sample design: A 20- μm thick metal support structure having several apertures of 20, 30 and 50 μm in diameter with graphene crystallites placed over them. Taken from Nair et al. [16].....31
- Figure 1.5.** Micromechanically exfoliated graphene sheets (a) Optical micrograph image (in normal white light) of a relatively large multilayer graphene with ~ 3 nm thickness and (b) Atomic force microscope (AFM) image of single-layer graphene. Taken from Novoselov et al. [7].....32

Figure 1.6. (a) Schematic illustration of graphite exfoliation in aqueous solution in the presence of sodium cholate as a surfactant, and (b) Photograph of a $90 \mu\text{g mL}^{-1}$ graphene dispersion by six weeks after its preparation. Image taken from Green et al. [40].33

Figure 1.7. (a) Chemical structure of graphite oxide. Image taken from He et al. [42] and (b) scheme showing the chemical route to the synthesis of aqueous graphene dispersions. (1) Oxidation of graphite-to-graphite oxide with greater interlayer distance. (2) Exfoliation of graphite oxide in water by sonication to obtain GO colloids that are stabilized by electrostatic repulsion. (3) Controlled conversion of GO colloids to conducting graphene colloids through deoxygenation by hydrazine reduction. Taken from Li et al. [44] 34

Figure 1.8. Schematic illustration of aqueous graphene dispersions stabilized with TCNQ anion. (a) pristine expanded graphite; (b) TCNQ intercalation within graphite layers (c) after sonication, TCNQ-anion-stabilized graphene in water; (d) photograph of TCNQ anion adsorbed graphene suspension in different solvents: water, ethanol, DMF and DMSO. Images taken from Hao et al. [48]. 35

Figure 1.9. (a) Cartoon illustrating shear exfoliation of graphene in the VFD, (b) TEM image of exfoliated few layer graphene sheets with the selected area electron diffraction pattern in the inset. Images taken from Chen et al. [51], (c) High-shear mixer with mixing head in a 5 litre beaker of graphene dispersion, (d,e) Close-up view of a D=32mm mixing head (d) and a D=16mm mixing head with rotor (left) separated from stator (e). (f) Graphene–NMP dispersions produced by shear exfoliation. Photos taken from Paton et al. [52]..... 36

Figure 1.10. (a) SEM image of graphene grown on copper foil via chemical vapour deposition method, (b) graphene films transferred onto SiO_2/Si substrate. Images taken from Li et al. [54], (c) schematic illustration of roll-to-roll production of graphene films grown on copper foil, (d) a transparent ultralarge-area graphene film transferred on a 35-inch polyethylene terephthalate (PET) sheet and (e) an assembled graphene/PET touch panel showing outstanding flexibility. Images taken from Bae et al. [55]..... 37

Figure 1.11. Graphene growth by the confinement controlled sublimation (CCS) method. (a) An SiC chip is placed in a graphite enclosure that is provided with a small leak, and inductively heated. The growth rate is controlled by the enclosure aperture (leak), and the background gas pressure. (b) Photograph of the furnace and

(c) Schematic of graphene on SiC (silicon, yellow; carbon, black). The bottom face (C face) is covered with two graphene layers, whereas the top face (Si face) schematically terminates in a covalently bonded buffer layer. In subsequent growth on this face, the buffer layer is converted into a graphene layer by the new buffer layer that grows under it. Images taken from De Heer et al. [60,61]...... 38

Figure 1.12. (a) Direct image of a single-layer graphene membrane (atoms appear white) using aberration corrected HRTEM. Image taken from Meyer et al. [65]. Evidence of monolayer graphene from TEM. (b) HRTEM image of solution-cast monolayer graphene (scale bar: 500 nm) and (c) the SAED pattern of the graphene sheet in (b) with the peaks labelled by Miller-Bravais indices. Images taken from Hernandez et al. [30]. 40

Figure 1.13. (a) Raman spectra at 514 nm for graphite and monolayer graphene. (b,c) Evolution in 2D band as a function of layers at 514 nm and 633 nm excitations respectively. (d) Comparison of the D band at 514 nm at the edge of bulk graphite and monolayer graphene. The fit of the D1 and D2 components of the D band of bulk graphite is shown. (e) The four components of the 2D band in bilayer graphene at 514 and 633 nm. Images taken from Ferrari et al. [71]..... 42

Figure 1.14. Energy band gap in graphene induced by covalent chemical functionalization. (a) Schematic illustration of nitro phenyl functionalized epitaxial graphene, (b) angle resolved photoemission spectroscopy (ARPES) measured band structure of nitrophenyl-functionalized graphene and (c) constant energy cuts clearly shows that a band gap of 0.36 eV has been created. Images taken from Niyogi et al. [78]. 44

Figure 1.15. Photographic images of reduced graphite oxide (left) and 1-pyrenebutyrate functionalized graphene (right) dispersions in water. Image taken from Xu et al. [92]. 45

Figure 1.16. Various graphene based functional hybrid bionanomaterials. (a) DNA coating of graphene oxide (GO) and reduced graphene oxide (RGO), which were then used as interfaces for a homogeneous assembly of metal-carbon hetero-nanostructure. Images taken from Liu et al. [116], (b) TEM image of bacteria, *Escherichia coli* encapsulated in graphene layers and cross section image of a wrapped bacterium in the inset. Wet-phase imaging was possible after graphene encapsulation. Images taken from Mohanty et al. [117], (c) Yeast cells interfaced with chemically reduced graphene (CRG) sheets resulting in electrically conductive

and higher resistance towards osmotic pressure. Inset image shows the presence of the Au particles on the cell–CRG sheets. Taken from Kempaiah et al. [118] and (d) schematic illustration of various curcumin-graphene composites; double oxidized graphene oxide (DGO), graphene oxide (GO) and graphene quantum dot (GQD) and their anti-cancer effects. Taken from Some et al. [119]......47

Figure 1.17. Schematic view of an SDP and a photograph of a 20 cm diameter spinning disc housed in such a unit. (b) Schematic view of an RTP showing high mass and heat transfer and a photograph of an RTP, which has a rotating tube of 30 cm in length and 6 cm in diameter. Images taken from Chen et al. [134]. 50

Figure 1.18. Vortex fluidic device (VFD). (a) Cross section showing components of the device. (b) Average film thickness (mm) versus tilt angle θ , (c) Photographs showing the film of liquid developed for different speeds, for 3 mL of an aqueous solution, for $\theta = 45^\circ$ and (d) Photograph of a VFD housing a 10 mm diameter borosilicate NMR tube inclined at 45 degrees. Images (a-c) taken from Yasmin et al. [139].52

Figure 2.1. Cartoon showing the formation of a thin fluid film in the rapidly rotating tube of the VFD which has shearing force associated with the Stewartson-Ekman layers [31]. For continuous flow processing the liquid is directed to the bottom of the tube, through the central pipe.72

Figure 2.2. Schematic illustration of the overall hybridization process, involving the exfoliation of graphite flakes into multi-layer graphene sheets followed by the hybridization of these sheets with algal cells using a VFD; each sheet represents ≥ 5 layers of graphene.73

Figure 2.3. SEM and (b) TEM images of exfoliated MLG sheets obtained in water using the VFD..... 75

Figure 2.4. (a) AFM image of exfoliated MLG sheets obtained in water using VFD and (b) height profiles of the selected area in (a) 76

Figure 2.5. Raman spectroscopy of graphite flakes (a) before, and (b) after VFD processing.77

Figure 2.6. Bright field and fluorescence microscopy images using Texas-Red filters for microalgae cells processed under various VFD speeds, (a) 2000 rpm, (b) 4000 rpm, (c) 6000 rpm, (d) 8000 rpm, and (e) 9000 rpm. Note the autofluorescence of “chlorophyll b” in microalgae cells. Scale bars: 20 μm 78

Figure 2.7.	SEM images of pristine microalgae after processing in the VFD at (a) 5000 rpm, and (b) 7000 rpm min; (c) algae-graphene hybrid samples processed at 5000 rpm, and (d) 7000 rpm; (e-f) algae and MLG mixed without VFD process. Scale bars: 1 μ m.	79
Figure 2.8.	Total chlorophyll (Chl a + Chl b) content measured as a function of growth time MLG coated (red rectangles for 5000 rpm and purple spheres for 7000 rpm); uncoated free <i>C. vulgaris</i> cells (blue diamonds for 5000 rpm and green triangles for 7000 rpm); and MLG-algae mixture without VFD processing (grey spheres).	80
Figure 2.9.	Nitrate-nitrogen (NO_3^- -N) concentration (mg/L) of liquid medium versus time. Free algal cells after VFD processing at 5000 rpm and 7000 rpm are represented with blue and green columns, respectively. MLG-hybrid algal cells after VFD processing at 5000 rpm and 7000 rpm are given as red and purple columns, respectively. MLG and algae without VFD processing is shown in grey.	82
Figure 3.1.	Schematic illustration of the algae wrapping using VFD.	91
Figure 3.2.	(a, b) TEM images of graphene oxide (GO) sheets with the inset in (b) showing the SAED pattern and (c) an AFM image of a selected graphene oxide (GO) sheet, with the height profile in (d).	92
Figure 3.3.	SEM images of (a, b) pure algae cells and (c, d) GO wrapped algal cells using mild sonication, and (e, f) GO wrapped algal cells using VFD.	93
Figure 3.4.	Bright field and fluorescence microscopy images of (a, b) GO wrapped algal cells using mild sonication, and (c, d) GO wrapped algal cells using VFD. Texas-Red filters were used for monitoring the autofluorescence of “chlorophyll B” pigment in microalgal cells. Scale bars: 20 μ m.	94
Figure 3.5.	Total chlorophyll (Chl a and b) content as a function of time. Pure algae cells (green column), GO wrapped algal cells formed using mild sonication (blue column), and GO wrapped algal cells formed using VFD (red column).	96
Figure 3.6.	Nitrate-nitrogen (NO_3^- -N) concentration (mg/L) of liquid effluent versus time. Pure algae cells (green column), GO wrapped algal cells by mild sonication (blue column), and GO wrapped algal cells using VFD (red column).	97
Figure 4.1.	Schematic illustration of the preparation of GO wrapped bacteria using VFD	108
Figure 4.2.	Flow cytometry analysis of <i>S. aureus</i> (top row) and <i>R. opacus</i> (bottom row). Sa and Ro-untreated and heat ‘killed’ represents control samples and	

Sa and Ro-5000 & 8000 rpm / 1 min shows cytogram of bacteria after processing in the VFD at 5000 and 8000 rpm for 1 minute respectively 109

Figure 4.3. SEM images of bacteria (a) *S. aureus* interfaced with GO sheets, and (b) *S. aureus* only. Both (a) and (b) were imaged without pre-coating with a platinum metal film. (c) *S. aureus* only (d) GO wrapped *S. aureus* (e) *R. opacus* only, and (f) GO wrapped *R. opacus*. (c-f) samples were pre-coated with platinum prior to SEM imaging. (Scale bars: 5 μm). 110

Figure 4.4. TEM images of (a) *S. aureus* only, (b) *S. aureus* wrapped with GO, (c) *R. opacus* only, and (d) *R. opacus* wrapped with GO and the selected area electron diffraction pattern in the inset. (Scale bars: 500 nm) 111

Figure 4.5. AFM images of bacteria (a) *S. aureus* only, (b) GO wrapped *S. aureus*, (c) *R. opacus* only, and (d) GO wrapped *R. opacus*. Inset images display phase images of the same samples. 112

Figure 4.6. (a) AFM image acquired in approximately the same region as the optical micrographs of the *S. aureus* bacteria. (b) Optical microscope image (x100) of GO wrapped *S. aureus* deposited on a cleaned silicon surface and (c) Zoomed in image of (b). (d) Raman image, plotting the intensity of the 1600 cm^{-1} peak typical for the graphitic band of GO. (e) Optical microscope image of GO wrapped *R. opacus*, (f) Raman image of (e), (g,h) Zoomed in image of (e,f) respectively. (i,j) Raman single spectra acquired on samples d and h respectively. 113

Figure 4.7. Bacterial growth curves for *S. aureus* cells regrown in nutrient media after wrapping with GO. Inset information of each figure shows the logistic model constants of equation-1 (a, b, and c), and the coefficient of determination (R^2). 115

Figure 4.8. Bacterial growth curves for *R. opacus* cells regrown in nutrient media after wrapping with GO. Inset information of each figure shows the logistic model constants of equation-1 (a, b, and c), and the coefficient of determination (R^2). 116

Figure 5.1. (a) Structure of Ramizol[®] (1,3,5-tris[(1E)-2'-(4'-benzoic acid vinyl)]benzene and a molecular dynamic simulation of it on the surface of graphene (Appendix A8). (b) Photograph of solutions derived from sonication of mixtures of different ratios of graphite and Ramizol[®] in water (G:R). 127

Figure 5.2. (a) Graphene/Ramizol[®] sample at the initial graphite to Ramizol[®] ratio, G:R (1:0.1) produced after sonication (image on the left) and a control sample prepared with the same starting material without sonication (image on the right). Sonication was carried out following the reported procedure, and the sample

prepared without sonication involved manual shaking and left overnight) and (b) Photograph image of graphite in water, in the presence and absence of Ramizol[®]. Samples were sonicated following the described procedure and left overnight. In the case where no Ramizol[®] is present, any exfoliation is followed by rapid restacking. ...

..... 131

Figure 5.3. Photograph images of stabilised graphene/Ramizol[®] solutions, (a) before addition of aqueous NaOH (1 M), and (b) after the addition followed by mild sonication and centrifugation. AFM (c1-3) and SEM (d1-3) images at different regions of graphene/Ramizol[®] sample (initial graphite to Ramizol[®] ratio, G:R (1:0.1)) upon addition of NaOH followed by mild sonication and centrifugation. Rectangular dotted loops show formation of aggregates of restacked graphene sheets.

..... 133

Figure 5.4. (a) UV-visible spectra of Ramizol[®] and graphene/Ramizol[®] composites at different ratios of graphite to Ramizol[®] (G:R) after centrifugal washing and redispersing in milli-Q water. (b) Bright field image (top row) of Ramizol[®] functionalised graphene and the corresponding fluorescence microscopy images (bottom row) at different w/w ratios of G:R (1:1), (1:0.1) and (1:0.01), respectively. (Scale bar: 100 μm).

134

Figure 5.5. (a) Raman spectra at 532 nm of graphite flakes and graphene/Ramizol[®] composites at different ratios of graphite to Ramizol[®] (G:R). Dotted loops indicate a shoulder at 1900 cm⁻¹, and (b) comparison of scaled 2D band of the samples.

136

Figure 5.6. TEM images of graphene sheets prepared at different w/w ratios of graphite to Ramizol[®] (G:R). (a) 1:1. The inset TEM image shows significant traces of Ramizol[®] observed on graphene sheets from different area of the sample (b) 1:0.1 and (c) 1:0.01, and (d) electron diffraction pattern of a selected area in sample (c) (Scale bar: 100 nm).

137

Figure 5.7. AFM height images of graphene/Ramizol[®] G:R (1:1) (a) with phase image in the inset, (1:0.1) (b), and (1:0.01) (c), respectively.

139

Figure 5.8. SEM images of (a) pristine graphite and graphene/Ramizol[®] samples; (b) G:R (1:1), (c) G:R (1:0.1) and (d) G:R (1:0.01) respectively. (Scale bar: 5μm)

140

Figure 5.9. SEM images of graphene/Ramizol[®], G:R (a) 1:1 , (b) 1:0.1 and (c) 1:0.01, and (d) EDS analysis of lumpy sites in (a) and inset image showing EDS

analysis on a clear surface for comparison. Red arrows indicating lumpy features on graphene sheets (Scale bar: 1 μ m)..... 141

Figure 5.10. Bacterial growth monitoring by optical density measurements at 600 nm for pure Ramizol[®], pure graphite sonicated in water and graphene/Ramizol[®] composites of *S. aureus* in Mueller-Hinton media over a period of 20 hours. Inset photograph shows image of samples after incubation for 20 hours. First image on the left is bacteria only in media followed by pure Ramizol[®], G:R 1:1, G:R 1:0.1, G:R 1:0.01 and ultrasonicated graphite in water with bacteria in media, respectively.... 142

Figure 6.1. Schematic illustration of the sample preparation and corresponding photographs of the dispersions. 153

Figure 6.2. TEM images of (a,b) GO, (c) exfoliated BN and (d) MoS₂ sheets, (e,f) GO/BN and (g,h) GO/MoS₂. Electron diffraction patterns for all samples are as shown in the inset. 155

Figure 6.3. AFM images and height profiles of the indicated area in (a,b) GO, (c,d) GO/BN, and (e,f,g) MoS₂ samples..... 157

Figure 6.4. Raman spectra of pristine (a) GO, (b) BN, (c) MoS₂ and composite material of (d) GO/BN and (e) GO/MoS₂, respectively. Zoomed-in images of the peaks labelled as (i), (ii) and (iii) are shown on the right..... 158

LIST OF TABLES

<i>Table 1.1</i> Properties of graphene synthesized through different methods.....	39
<i>Table 4.1</i> Kinetic model parameters for <i>S. aureus</i> and <i>R. opacus</i> bacteria; k_c is the apparent growth rate in h^{-1} , and μ_{exp} is the specific growth rate of the exponential phase in h^{-1}	117
<i>Table 5.1</i> Composition of graphite and Ramizol [®] starting material	129
<i>Table 5.2</i> Composition of graphene and Ramizol [®] in graphene/Ramizol [®] composites used for antibacterial test against <i>S. aureus</i>	130

LIST OF PUBLICATIONS

1. **Wahid, M. H.**, Eroglu, E., Chen, X., Smith, S. M. and Raston, C. L. (2013). Functional multi-layer graphene–algae hybrid material formed using vortex fluidics. *Green Chemistry*, 15(3), 650-655.

Authors Contributions: Raston and Eroglu designed the research; Wahid carried out the primary experiments, Eroglu assisted with the algal cell cultivation and investigation of nitrate removal and viability of the cells; Chen assisted with the transmission electron microscopy (TEM) analyses; Wahid, Eroglu, Chen, Smith, and Raston finalized the manuscript. (Overall contribution by Wahid: 70%)

2. **Wahid, M. H.**, Eroglu, E., Chen, X., Smith, S. M. and Raston, C. L. (2013). Entrapment of *Chlorella vulgaris* cells within graphene oxide layers. *RSC Advances*, 3(22), 8180-8183.

Authors Contributions: Wahid designed the research and carried out the primary experiments and scanning electron microscopy (SEM) analysis, Eroglu assisted with the algal cell cultivation and investigation of nitrate removal and viability of the cells; Chen synthesized graphene oxide and assisted with the TEM analyses; Wahid, Eroglu, Chen, Smith, and Raston finalized the manuscript. (Overall contribution by Wahid: 70%)

3. **Wahid, M. H.**, Stroehler, U. H., Eroglu, E., Chen, X., Vimalanathan, K., Raston, C. L. and Boulos, R. A. (2015). Aqueous based synthesis of antimicrobial-decorated graphene. *Journal of Colloid and Interface Science*, 443, 88-96.

Authors Contributions: Ramiz and Eroglu designed the research; Wahid carried out the primary experiments, atomic force microscope (AFM) and SEM analyses; Stroehler conducted the antibacterial test; Chen assisted with the TEM analyses; Vimalanathan carried out the Raman spectroscopy; Wahid, Stroehler, Eroglu, Chen, Vimalanathan, and Raston finalized the manuscript. (Overall contribution by Wahid: 70%)

4. **Wahid, M. H.**, Eroglu, E., LaVars, S. M., Newton, K., Gibson, C. T., Stroehler, U. H., Chen, X., Boulos, R. A., Raston, C. L. and Harmer, S-L. (2015).

Microencapsulation of bacterial strains with graphene oxide nano sheets using vortex fluidics. *RSC Advances*, 5, 37424-37430

Authors Contributions: Raston and Harmer designed the research; Wahid carried out the primary experiments, AFM, TEM and SEM analyses; Eroglu assisted with the modelling of the bacterial growth; LaVars and Newton assisted with the bacterial cell cultivation; Gibson performed Raman spectroscopy; Stroehler assisted with the bacterial cell counting; Chen assisted with TEM analysis; Wahid, Eroglu, Chen, Smith, and Raston finalized the manuscript. (Overall contribution by Wahid: 80%)

5. **Wahid, M. H.**, Chen, X., Gibson, C. T., Boulos, R. A. and Colin L. Raston. (2015). Amphiphilic graphene oxide stabilisation of hexagonal BN and MoS₂ sheets. *Chemical Communications*, 51, 11709-11712

Authors Contributions: Chen designed the research; Wahid carried out the sample preparation, Chen assisted with AFM and TEM analyses, Gibson assisted with the Raman analysis; Wahid, Chen, Gibson, Boulos, and Raston finalized the manuscript. (Overall contribution by Wahid: 60%)

6. Eroglu, E., Zang, W., Eggers, P. K., Chen, X., Boulos, R. A., **Wahid, M. H.**, Smith, S. M. and Raston, C. L. (2013). Nitrate uptake by p-phosphonic acid calix [8] arene stabilized graphene. *Chemical Communications*, 49(74), 8172-8174.

Authors Contributions: Eroglu designed the research and carried out the primary experiments; Zang provided the graphene samples; Chen assisted with TEM analysis; Boulos assisted with the computer modelling; Wahid assisted with the Zeta potential analysis; Eroglu, Zang, Eggers, Chen, Boulos, Wahid, Smith, and Raston finalized the manuscript. (Overall contribution by Wahid: 20%)

7. Chen, X., Gibson, C. T., Britton, J., Eggers, P. K., **Wahid, M. H.** and Raston, C. L. (2015). p-Phosphonic acid calix [8] arene assisted dispersion and stabilisation of pea-pod C₆₀ @ multi-walled carbon nanotubes in water. *Chemical Communications*, 51, 2399-2402.

Authors Contributions: Chen designed the research and carried out the primary experiments; Gibson performed Raman analysis; Britton assisted with the nuclear magnetic resonance (NMR) analysis; Haniff assisted with the sample preparation;

Chen, Gibson, Britton, Eggers, Wahid, and Raston finalized the manuscript. (Overall contribution by Wahid: 20%)

CONFERENCE PROCEEDINGS

1. **M. Haniff Wahid**, Kelly Newton, Sian M. La Vars, Ramiz A. Boulos, Sarah L. Harmer and Colin L. Raston. Graphene oxide encapsulation of bacteria using vortex fluids. *RACI National Congress*, December 7-12, 2014, Adelaide, Australia.
2. **M. Haniff Wahid**, Kelly Newton, Sian M. La Vars, Ramiz A. Boulos, Sarah L. Harmer and Colin L. Raston. Graphene oxide encapsulation of bacteria using vortex fluids. *Flinders Centre for Nanoscale Science and Technology (CNST) Annual Conference*, June 18, 2014, Adelaide, Australia.
3. Ela Eroglu, **M. Haniff Wahid**, Ramiz A. Boulos, , Xianjue Chen, Paul K. Eggers, Jeremiah Toster, Nicholas J. D'Alonzo, Steven M. Smith, & Colin L. Raston. Novel nanohybrid materials for the effective removal of phosphates and nitrates from liquid effluents. *European Geosciences Union (EGU) General Assembly Conference 2014*, April 27 – May 2, 2014, Vienna, Austria.
4. **M. Haniff Wahid**, Ela Eroglu, Xianjue Chen, Colin L. Raston and Ramiz A. Boulos. In situ exfoliation and functionalization of graphene with an anti-microbial agent (Ramizol[®]). *International Conference on Nanoscience and Nanotechnology (ICONN 2014)*, February 2- 6, 2014, Adelaide, Australia.
5. **M. Haniff Wahid**, Ela Eroglu, Xianjue Chen, Steven M. Smith and Colin L. Raston. Graphene oxide encapsulation of microalgae via vortex fluidics. *Flinders Centre for Nanoscale Science and Technology (CNST) Annual Conference*, June 19, 2013, Adelaide, Australia.
6. **M. Haniff Wahid**, Ela Eroglu, Xianjue Chen, Steven M. Smith and Colin L. Raston. Functional multi-layer graphene-algae hybrid material formed using vortex fluidics. *2013 RACI SA Student Polymer & Bionanotechnology Symposium (SASPBS'13)*, October 4, 2013, Adelaide, Australia.

7. Ela Eroglu, **M. Haniff Wahid**, Xianjue Chen, Steven M. Smith, & Colin L. Raston. Removal of nitrate from liquid effluents with bio-nano hybrid materials. *European Geosciences Union (EGU) General Assembly Conference 2013*, April 7-12, 2013, Vienna, Austria.
8. **M. Haniff Wahid**, Ela Eroglu, Xianjue Chen and Colin L. Raston. Preparation of Graphene-algae hybrid material using vortex fluidics. *The 5th International Symposium on Functional Materials (ISFM)*, December 17-20, 2012, Perth, Western Australia.
9. **M. Haniff Wahid**, Ela Eroglu, Xianjue Chen and Colin L. Raston. Graphene-wrapped Algae using Vortex Fluids. *International Conference on Nanoscience and Nanotechnology (ICONN 2012)*, February 5-9, 2012, Perth, Western Australia.

ABBREVIATIONS

0D: Zero-dimensional

1D: One-dimensional

2D: Two-dimensional

3D: Three-dimensional

AFM: Atomic force microscope

CCS: Confinement controlled sublimation

Chl: Chlorophyll

CMG: Chemically modified graphene

CNTs: Carbon nanotubes

CVD: Chemical vapour deposition

DMF: Dimethyl formamide

DMSO: Dimethyl sulfoxide

FWHM: Full width at half maximum

GO: Graphene oxide

GIC: Graphite intercalated compound

HAADF: High angular annular dark-field

h-BN / BN: Hexagonal boron nitride

HRTEM: High resolution transmission electron microscopy

ITO: Indium tin oxide

MLG: Multi-layer Graphene

MoS₂: Molybdenum disulphide

NMP: *N*-methyl-pyrrolidone

NMR: Nuclear magnetic resonance

PmPV: Poly(m-phenylenevinylene-co-2,5-dioctoxy-p-phenylenevinylene)

PET: Polyethylene terephthalate

RTP: Rotating tube processor

SAED: Selected area electron diffraction

SDP: Spinning disc processor

SEM: Scanning electron microscope

SiC: Silicon carbide

STEM: Scanning transmission electron microscopy

TCD: Total colour difference

TEM: Transmission electron microscope/microscopy

VFD: Vortex fluidic device

1. INTRODUCTION

1.1 Thesis overview

The aim of this research was to explore a feasible method to functionalize graphene and graphene oxide through hybridization, using process intensification technologies, namely the vortex fluidic device and ultrasonic mechanoenergy. Graphene hybridization was carried out with various biological entities including microalgae, bacteria, or inorganic laminar material such as antimicrobial drug (Ramizol[®]) and 2D layered materials namely; molybdenum disulphide (MoS₂) and hexagonal boron nitride.

Accordingly, the first chapter reviews the literature to date relating to graphene and its derivatives, functionalization of graphene, which includes the synthesis of hybrid materials with graphene and the application of mechanoenergy to access composite functional nanomaterials. Given the large amount of existing graphene-related publications, only the most relevant literature was selected to represent the work, and they are presented in a systematic way as an outline of the pathway to the following sections. The introduction begins with the general introduction on nanomaterials. This is followed by the introduction of graphene and its properties. Various graphene synthesis routes are also covered. Next there is a focus on the synthesis of hybrid bionanomaterials, with more emphasis on graphene, discussing the potential of hybrid materials of graphene oxide with other 2D inorganic layered materials.

Chapter 2 reports the preparation of graphene-algae hybrid material using a vortex fluidic device (VFD). This study features an enhanced nitrate removal activity of the hybrid material compared to pristine algal cells or multi-layer graphene alone. Furthermore, the samples which are prepared using the vortex fluidic device were found to possess higher nitrate removal activity. The chapter includes the method of synthesis, characterization data, results and discussion.

Chapter 3 presents the encapsulation of microalgae *Chlorella vulgaris* within graphene oxide layers using the VFD. Confinement of microalgal cells in graphene oxide layers successfully limits the rapid growth of the cells while maintaining their

biological activity. The study also shows that wrapping of algal cells using the VFD are more effective in delaying the growth of the cells.

Chapter 4 presents the encapsulation of two different strains of bacterial cells, *Staphylococcus aureus* and *Rhodococcus opacus*, within graphene oxide layers using the VFD. Wrapping different shapes of bacteria with ultrathin layers of graphene oxide is demonstrated in this study. Graphene oxide wrapped bacterial cells were found to be still biologically active, and that the graphene oxide imparts electrical conducting properties to the surface of the cells, allowing SEM imaging without the need for prior coating with metal substrates.

Chapter 5 reports a successful synthesis of antimicrobial decorated graphene in aqueous suspensions using an ultrasonication technique and (1,3,5-tris[(1E)-2'-(4'-benzoic acid)vinyl]benzene), Ramizol[®] as a surfactant. Ramizol[®] acts as a molecular wedge in facilitating the exfoliation of graphene and subsequently stabilizing the sheets in water. Graphene / Ramizol[®] composite material shows antibacterial activity towards gram positive bacteria *Staphylococcus aureus*.

Chapter 6 presents a benign aqueous synthesis of hetero-laminar structures consisting of graphene oxide, hexagonal boron nitride and molybdenum disulphide (MoS₂). This study proposes an alternative route of building hetero atomic 2D layers which could lead to materials with unique properties. The method is scalable and thus it is potentially attractive for large scale production of hetero-laminar structures.

Chapter 7 provides a conclusion of the results and highlights the significance of the research. Future directions are also discussed, along with potential applications of the materials.

1.2 General introduction

There is a growing global drive to discover and develop renewable energy resources for sustainable technologies for the future. To date remarkable developments are being implemented such as the use of solar cells to generate electricity and hydrogen fuel cells to power cars. However, the application of these emerging technologies are still limited mainly due to the high cost of raw materials and processes compared to the use of conventional fossil fuel based energy systems [1]. While extensive efforts are being made to overcome the limitations, nanomaterials are gaining considerable interest due to their intriguing properties and potentials to overcome the challenges in the widespread use of renewable energy resources and this includes the use of graphene and its related materials.

Nanomaterials such as graphene refer to materials that have at least one dimension in the 1 – 100 nm range [1]. In general, as the size approaches the nanometer scale, the material's property changes due to the higher percentage of atoms at the surface of the material compared to its bulk form. In this state, the material tends to behave more like molecules than as bulk material [1,2]. Several advantages arise from this including enhanced optical, mechanical, electrical, structural, magnetic and chemical properties [3]. Hence, by taking advantage of the size/shape dependant properties of nanomaterials, the synthesis of materials with desirable properties is possible through controlling the size and shape of the nanomaterials. This has led to the use of nanomaterials in various applications such as catalysts, functional polymer fillers, nanowires and nanotube arrays for electromagnetic interference shielding, chemical gas sensing, electronics, energy conversion, textile fibres, permanent coatings, catalysts, fuel cell and many others [3].

1.3 Graphene

Nanomaterials can be classified into four main categories based on the dimensionality: (a) 0D clusters and particles, (b) 1D nanotubes and nanowires, (c) 2D nanoplates and layers, and (d) 3D nanostructure (Fig.1 a) [4-6]. One of the most prominent nanomaterials in this era is the 2D layered material, graphene which is the monoatomic layer of graphite (Fig. 1). Historically, free-standing 2D atomic crystals such as graphene were not expected to exist due to its thermodynamic instability at ambient conditions [7,8]. It was merely conceived that they only exist as a part of

larger 3D structures and are usually grown epitaxially on top of monocrystals with matching crystal lattices [9,10]. This concept was dispelled following the successful isolation and characterization of monoatomic-layer graphene by A. K. Geim and K. S. Novoselov in 2004 [7,8]. Starting from a rather simplistic micro-mechanical exfoliation step by simply using an adhesive tape, this unexpected discovery has triggered enormous interest among the scientific communities to embark on graphene research and inevitably paved the way for the exploration of other 2D atomic crystals in search of new phenomena and potential applications [8].

Graphene is a flat mono-layer of carbon atoms tightly arranged in a honeycomb lattice structure and possesses outstanding properties such as large theoretical surface area ($2630 \text{ m}^2 \text{ g}^{-1}$) [11], high intrinsic mobility ($200\,000 \text{ cm}^2 \text{ V}^{-1} \text{ s}^{-1}$) [12,13], high Young's modulus ($\sim 1.0 \text{ TPa}$) [14] and thermal conductivity ($\sim 5000 \text{ W m}^{-1} \text{ K}^{-1}$) [15] and good optical transmittance ($\sim 97.7 \%$) [16]. Furthermore, graphene is the building block for other allotropes of carbon, namely fullerene and carbon nanotubes (Fig.1) [8]. The remarkable properties of graphene stems from its structure where the hybridization of s , p_x and p_y atomic orbitals leads to a trigonal planar hexagonal arrangement of sp^2 carbons with a formation of a σ bond between carbon atoms with a bond length of $\sim 0.142 \text{ nm}$ [17]. This provides the exceptional chemical and mechanical stability of graphene. Meanwhile, the unaffected p_z orbital which is perpendicular to the planar surface covalently binds to the neighbouring carbon atoms forming the π -electron band (half-filled π -band), which is responsible for the excellent electrical, optical and thermal properties [17].

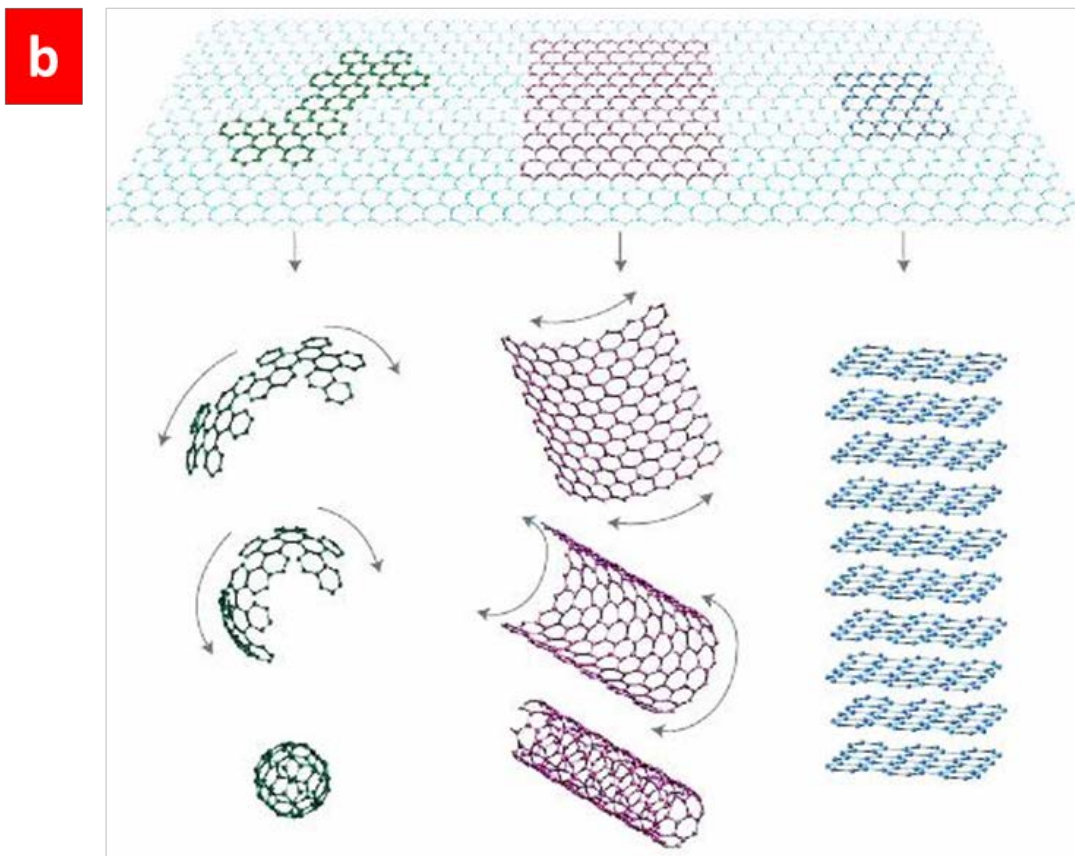
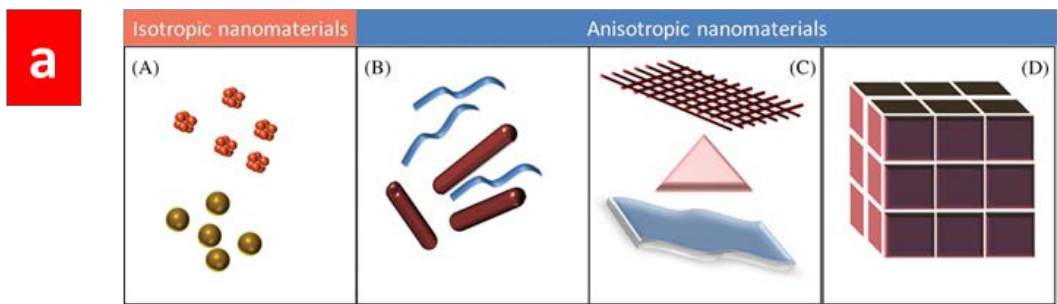


Figure 1.1. (a) General classification of nanomaterials. (A) 0D clusters and particles. (B) 1D nanotubes and nanowires. (C) 2D nanoplates and layers. (D) 3D nanostructure. In the case of isotropic or 0D particles (e.g. sphere), due to the confinement of electrons to the same extent in all the three dimensions, properties will be more or less the same regardless of directions. Anisotropic materials show direction and dimension dependent physical and chemical properties. They come under the category of 1, 2, and 3D nanostructures, and electron motions are possible in the different dimensions. Taken from Sajanlal et al. [5]. (b) The ‘Mother’ of all graphitic forms. Graphene (on top), can be wrapped up to form 0D Buckminster fullerene (left), rolled into 1D nanotubes (centre) or stacked into 3D graphite(right). Taken from Geim and Novoselov [8].

1.4 Properties of Graphene

1.4.1 Chemical properties

Graphene possesses similar surface chemistry as graphite, such as the ability to adsorb and desorb various atoms and molecules [18]. However, compared to graphite, chemically induced changes for graphene are more pronounced due to the absence of influence from the bulk [18]. In principle, weakly attached adsorbates often act as donors or acceptors thus leading to changes in the carrier concentration [18]. This mechanism has been utilized to develop solid-state gas sensors and interestingly compared to other solid-state gas sensors, graphene is capable of detecting individual gas molecules as a 'low-noise material' [19]. There are several contributing factors rendering graphene as a low-noise material such as it has its whole volume exposed to surface adsorbates, high conductivity, and few crystal defects which minimizes the noise caused by thermal switching [19]. In addition, graphene allows electrical measurements using the four point probe on a single crystal device with electrical contacts that have low resistance [19]. All these factors help to maximize the signal-to-noise ratio thus enables detection of changes in a local concentration by less than one electron charge at room temperature. Furthermore the corrugated surface of graphene can enhance the reactivity, where reagents can possibly attach on both sides of its surface to which alters the energetics, thus allowing formation of chemical bonds that would be unstable if only one surface was exposed [18]. Also noteworthy is that the graphene tends to form irreversible agglomerates or even restacks into graphite through van der Waals interactions, unless graphene layers are well separated from each other.

1.4.2 Electronic properties

Long before the successful isolation of atomic layers of graphene, its structure was already used in theoretical models to predict the electronic properties of graphite. The first theoretical reference for this system was reported in 1947 by P.R. Wallace [20]. He demonstrated the use of a nearest neighbour, tight-binding model for determining the electronic band structure pertaining to the π -bonds of a monolayer of graphite which now is known as graphene [20]. Following to the successful exfoliation of graphene by Novoselov *et al.* in 2004, the first exceptional property unveiled was a strong ambipolar electric field effect with a carrier concentration of

10^{13} cm^{-2} and a room temperature mobility of $10,000 \text{ cm}^2 \text{ V}^{-1} \text{ s}^{-1}$ [7]. Follow-up experiments led to the confirmation that its charge carriers are massless Dirac fermions [21,22]. A few years later, mobility values of up to $250,000 \text{ cm}^2 \text{ V}^{-1} \text{ s}^{-1}$ was reported for suspended sheets after minimizing carrier scattering [12,13]. This value is exceptionally high which could not be attained in semiconductors or non-suspended graphene. Moreover, since graphene itself is atomically thin, it favours the ballistic electronic transport at submicrometer distances [23].

1.4.3 Mechanical properties

Another outstanding property of graphene is its mechanical strength. The mechanical properties of monolayer graphene have been experimentally investigated using atomic force microscope (AFM) nanoindentation on a strip of graphene suspended over open holes (Fig. 1.2) [14]. It was reported that defect-free graphene has a Young's modulus of 1.0 TPa and a breaking strength of 42 N m^{-1} which leads to the announcement of graphene as the strongest and stiffest material ever measured. This remarkable property facilitates the micropatterning of graphene using lithography technique which is ideal for fabrication of ultra-small devices such as supercapacitors, field effect transistors and more [24].

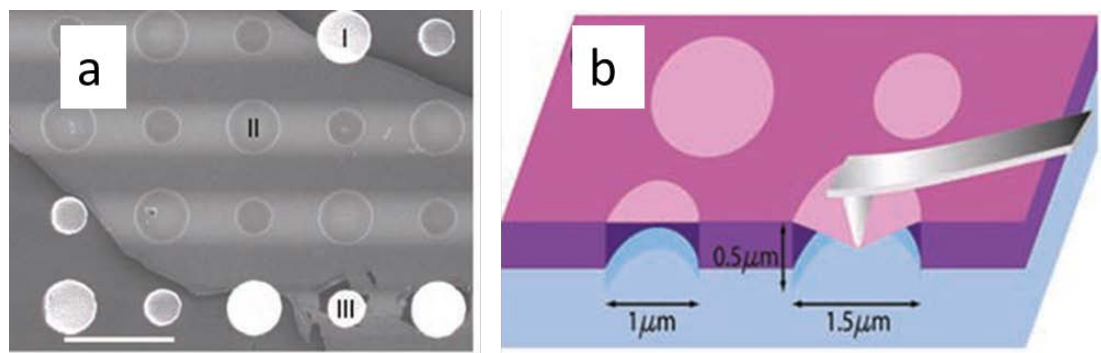


Figure 1.2. (a) Scanning electron micrograph image of a large graphene flake spanning an array of circular holes ($1 \mu\text{m}$ and $1.5 \mu\text{m}$ in diameter). Area I shows a hole partially covered by graphene, area II is fully covered, and area III is fractured from indentation (Scale bar, $3 \mu\text{m}$) and (b) Schematic illustration of AFM nanoindentation on a suspended graphene membrane. Taken from Lee *et al.* [14]

Another interesting mechanical property of graphene is its impermeability to standard gases including helium [25]. Bunch *et al.* (2008) demonstrated that graphene membranes, despite being one atomic thick, are impermeable and can

support pressure differences larger than one atmosphere. The impermeability of graphene is due to its π -orbitals which form a dense delocalized cloud that blocks the gap within its atomic rings (Fig. 1.3) [26]. Thus, the use of graphene as a membrane can provide a unique atomic layer thick separation barrier between two distinct regions.

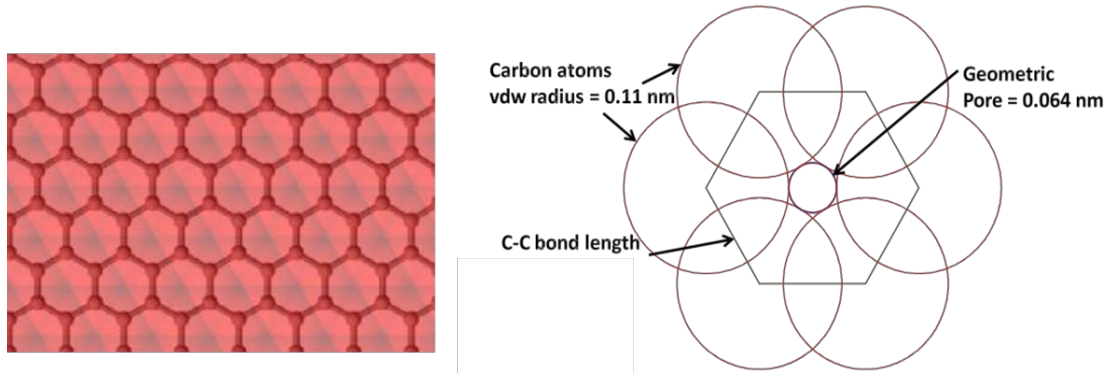


Figure 1.3. The molecular structure with rough electronic density distribution. Geometric gap calculated from van der Waals (vdw) radius of carbon is smaller than the size of helium. The C–C bond length of 0.142 nm in graphene implies that considering the nuclei alone, the pore size would be 0.246 nm. If we add the vdw radius of carbon as 0.11 nm, this geometric pore size would decrease to 0.064 nm which is small enough not to allow molecules to pass through. Illustration taken from Berry [26].

1.4.4 Optical properties

Few phenomena in condensed matter physics can be defined by the fundamental constants without depending on the material parameters, and graphene is one of them. Nair *et al.* (2008) demonstrated that the opacity of graphene is defined uniquely by the fine structure constant, $\alpha = e^2/\hbar c \approx 1/137$ (where e is the electron charge, \hbar is the Planck's constant and c is the speed of light) [16]. Furthermore, monoatomic layer of graphene absorbs 2.3% of incident white light due to its unique electronic structure [16]. As shown in Figure 1.4, the opacity of graphene increases directly with membrane's thickness with each graphene layer adding another 2.3%.

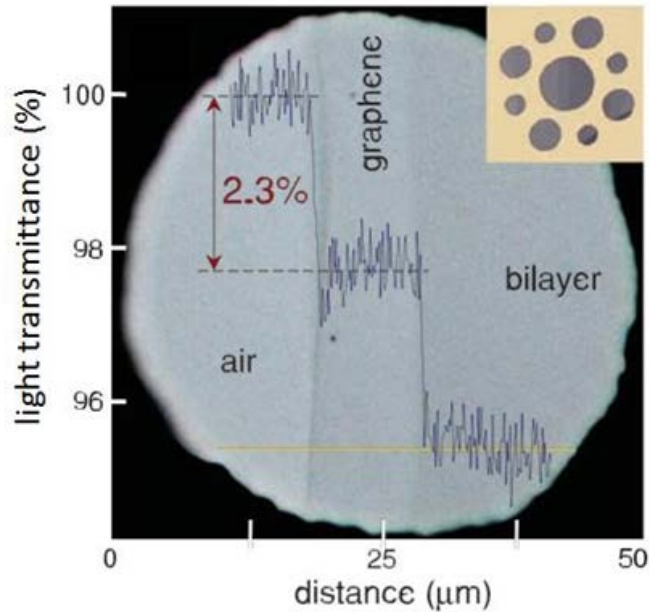


Figure 1.4. Photograph of a 50- μm aperture partially covered by graphene and its bilayer. The line scan profile shows the intensity of transmitted white light along the wide line. Inset image shows the sample design: A 20- μm thick metal support structure having several apertures of 20, 30 and 50 μm in diameter with graphene crystallites placed over them. Taken from Nair *et al.* [16].

1.4.5 Thermal properties

Graphene also possess remarkable thermal properties. Balandin *et al.* (2008) reported that single layer graphene has thermal conductivity of up to 5300 W/mK at room temperature [27]. This value supersedes the values obtained for suspended carbon nanotubes (CNTs) which is approximately 3500 W/mK and matches the highest values reported for single-wall CNT bundles, which has values as high as 5800 W/mK [28]. The remarkable thermal conductivity and other characteristics of graphene render it as an excellent material for electronic applications.

1.5 Graphene synthesis

Graphene and other two dimensional layered analogues such as boron nitride, tungsten disulphide, molybdenum disulphide and many others display strong chemical bonding in-plane but a relatively weak out-plane bonding which renders the material possible for exfoliation [29]. Exfoliation of these 2D layered materials is interesting given that they possess unusual electronic properties and large specific surface areas [29]. Monoatomic layer, graphene, can be exfoliated directly from

graphite mineral as a relatively cheap and abundant material. However, it requires overcoming the van der Waals interactions between the adjacent graphitic layers and also stabilizing the sheets after exfoliation, which is important for further processing of graphene [30]. To date, various methods have been reported for the production of graphene, using either the bottom-up approach or the top-down approach starting with graphite. Nevertheless, there are still on-going efforts aiming towards development of synthesis methods which can produce high quality, scalable, low-cost, and environmentally friendly graphene. Some of the major methods are as follows:

1.5.1 Micromechanical cleavage

Mechanically ‘peeling off’ the thin layers of graphite using adhesive tape is the method used by Geim and co-workers to isolate graphite sheets, which led to the first successful isolation of monoatomic layer graphene (Fig. 1.5) [7,31]. Through this rather simplistic approach high quality graphene sheets were obtained and their characterization has led to the discovery of remarkable properties of this material [7,8,11-16]. Nevertheless, even though high quality sheets are accessible, the yields are low, and also the sheets obtained are typically small with lateral dimensions on the order of tens to hundreds of micrometers [29,32]. Thus, it is unlikely that this method will be suitable for industrial scale production [29].

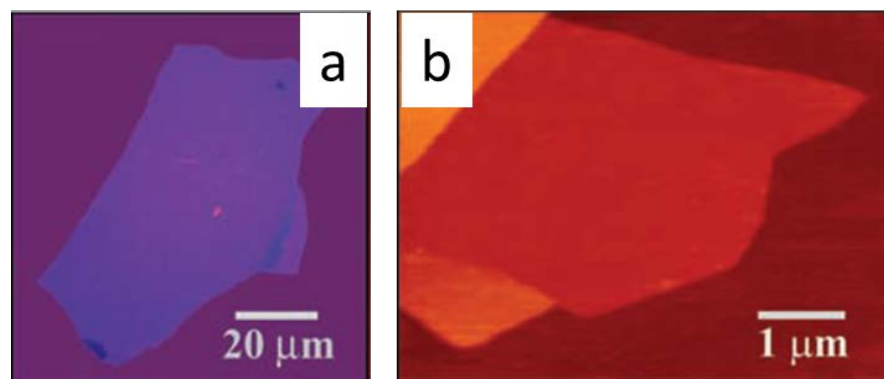


Figure 1.5. Micromechanically exfoliated graphene sheets (a) Optical micrograph image (in normal white light) of a relatively large multilayer graphene with ~ 3 nm thickness and (b) Atomic force microscope (AFM) image of single-layer graphene. Taken from Novoselov et al. [7].

1.5.2 Liquid phase exfoliation

Liquid phase exfoliation of graphite is one of the promising routes for scaling up the production of graphene [29]. The principle behind this method is the selection of solvents with surface energies matching to those of graphite which facilitates the interlayer separation of graphitic layers [30,33-35]. Solvents typically used are non-aqueous; however aqueous solutions with the presence of surfactants are also possible routes for graphene exfoliation (Fig. 1.6) [36-40]. By applying an external force such as sonication, exfoliation of graphene sheets takes place and prolonged treatment leads to the isolation of individual or few layer sheets.

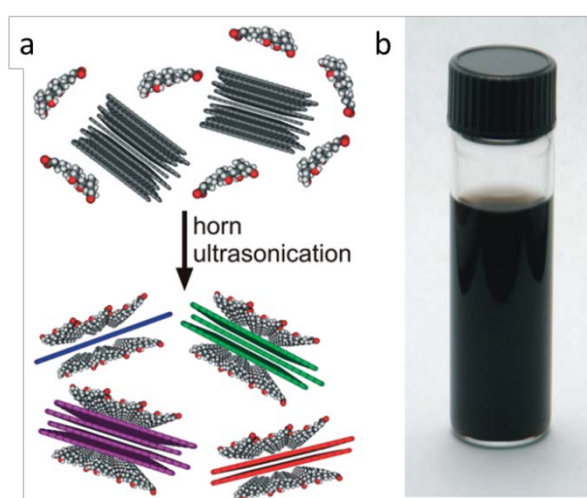


Figure 1.6. (a) Schematic illustration of graphite exfoliation in aqueous solution in the presence of sodium cholate as a surfactant, and (b) Photograph of a $90 \mu\text{g mL}^{-1}$ graphene dispersion by six weeks after its preparation. Image taken from Green et al. [40].

Another common route is the graphene oxide (GO) route. This method involves the oxidation of bulk graphite using strong oxidizers such as sulphuric acid and potassium permanganate resulting in the introduction of hydroxyl and epoxide groups to the basal plane (Fig. 1.6a) [41,42]. Upon introduction of oxygen rich functional groups onto graphene's surface, it becomes hydrophilic and thus it can be easily dispersed in water.

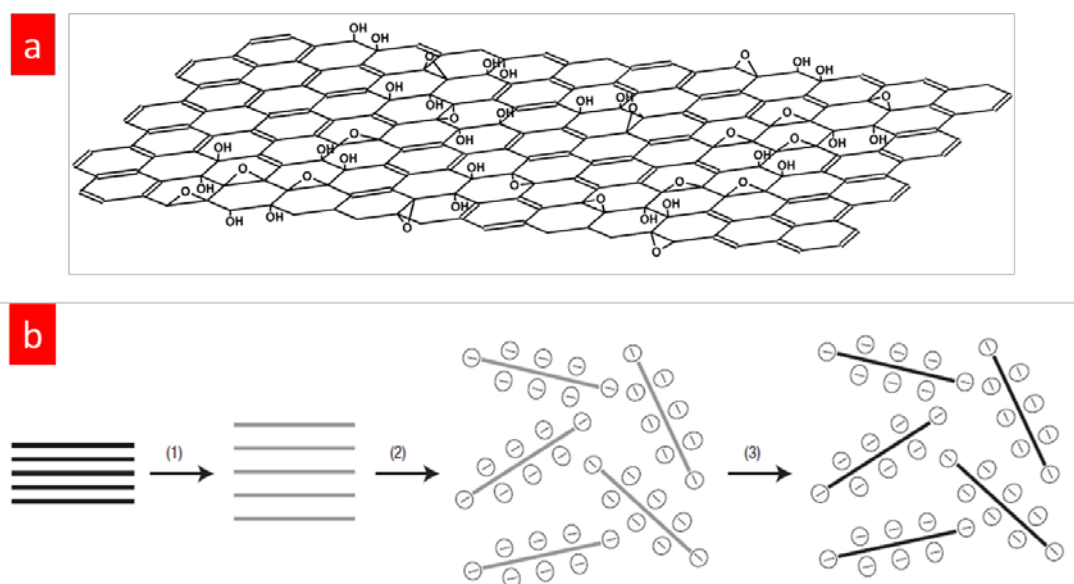


Figure 1.7. (a) Chemical structure of graphite oxide. Image taken from He et al. [42] and (b) scheme showing the chemical route to the synthesis of aqueous graphene dispersions. (1) Oxidation of graphite-to-graphite oxide with greater interlayer distance. (2) Exfoliation of graphite oxide in water by sonication to obtain GO colloids that are stabilized by electrostatic repulsion. (3) Controlled conversion of GO colloids to conducting graphene colloids through deoxygenation by hydrazine reduction. Taken from Li et al. [44]

The interlayer spacing of graphitic layers also increases relative to the unoxidized graphite, which facilitates the exfoliation process with the negative surface charge acquired, preventing the sheets from restacking (Fig. 1.6b) [43-45]. Dispersed graphene oxide can be reduced back to graphene, though graphene obtained through this method possess structural defects which lead to the degradations in its electrical, thermal and mechanical properties [45].

The formation of graphite intercalation compounds (GICs), or expanded graphite are the other possible routes for obtaining graphene [46]. Through intercalation of small molecules, the interlayer spacing of graphite layers are increased thus reducing the van der Waals forces between the layers and can lead to the exfoliation of graphene layers (Fig. 1.8) [46,48]. However, despite the use of several GICs such as $K(THF)_x C_{24}$, poly(*m*-phenylenevinylene-co-2,5-dioctoxy-*p*-phenylenevinylene) (PmPV) and 7,7,8,8-Tetracyanoquinodimethane (TCNQ) [47-49], the efficiencies of graphene production have been extremely low (1 – 12 wt %), thus raising the cost of the synthesis and limiting the wide-spread implementation.

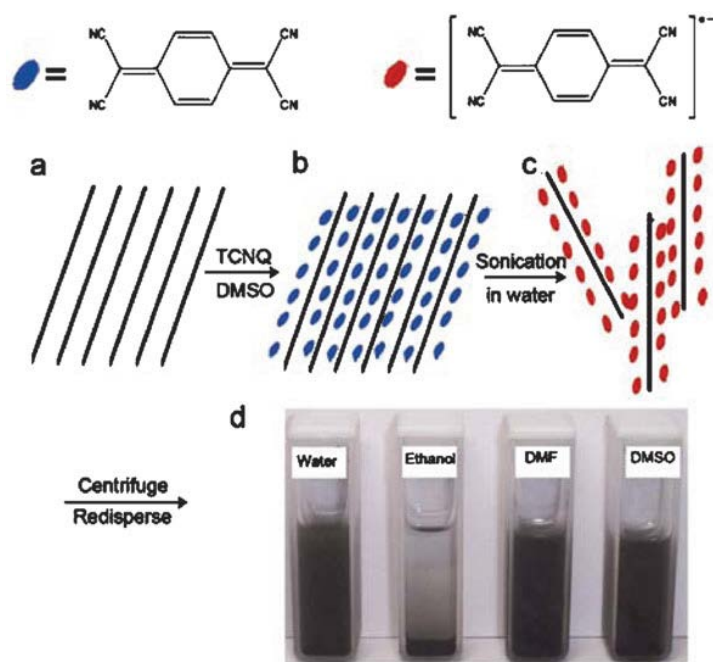


Figure 1.8. Schematic illustration of aqueous graphene dispersions stabilized with TCNQ anion. (a) pristine expanded graphite; (b) TCNQ intercalation within graphite layers (c) after sonication, TCNQ-anion-stabilized graphene in water; (d) photograph of TCNQ anion adsorbed graphene suspension in different solvents: water, ethanol, DMF and DMSO. Images taken from Hao et al. [48].

Graphene exfoliation using intense shear forces has also been demonstrated with initial efforts carried out by Raston and co-workers in 2012 [50]. By mixing graphite in N-methyl pyrrolidone (NMP) followed by shear processing in a rapidly rotating tube, called the vortex fluidic device (VFD), they managed to obtain monolayers and few-layers of graphene (Fig. 1.9a,b). Similar results were also obtained for other 2D layered materials namely; boron nitride and molybdenum disulphide. However, this method produces small quantities of graphene and requires further efforts for a scale up. Enhancement in the production rates and yields of graphene has been demonstrated by Paton and co-workers, using a high-shear mixer with potential for large scale production (Fig. 1.9c-f) [51]. The advantage of shear exfoliation is production of defect-free and unoxidized graphene sheets [50,51]. This rather simplistic approach is of particular interest and a recent study demonstrated that graphene can be produced through a similar approach using a household kitchen blender [52].

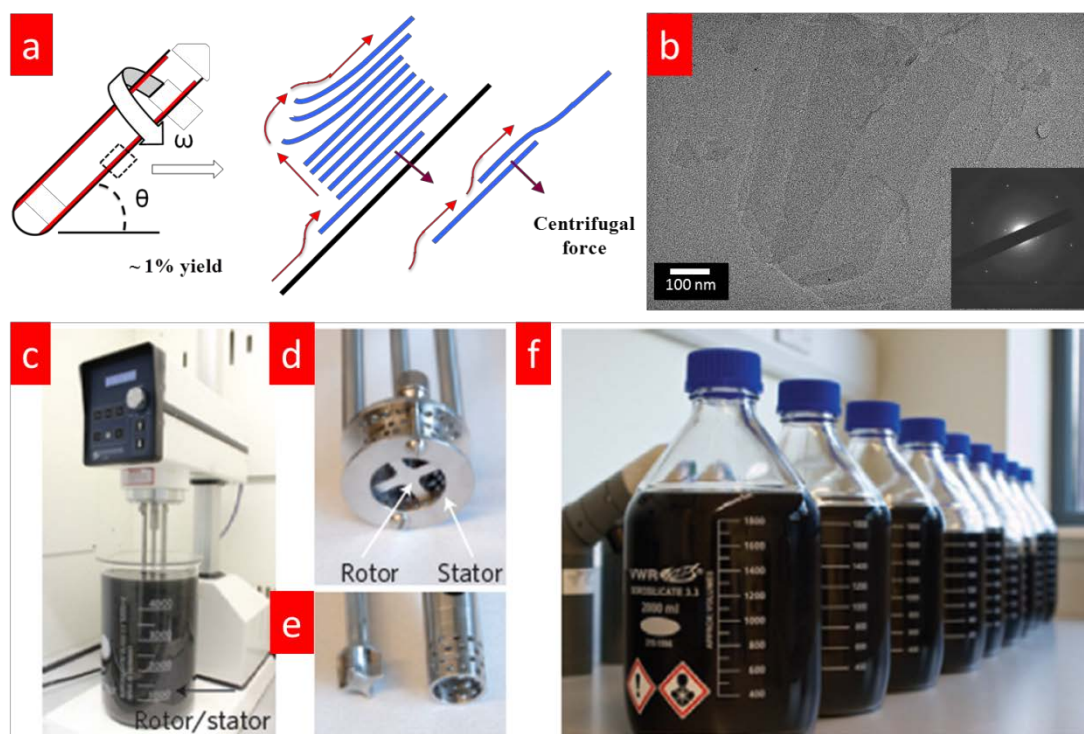


Figure 1.9. (a) Cartoon illustrating shear exfoliation of graphene in the VFD, (b) TEM image of exfoliated few layer graphene sheets with the selected area electron diffraction pattern in the inset. Images taken from Chen *et al.* [51], (c) High-shear mixer with mixing head in a 5 litre beaker of graphene dispersion, (d,e) Close-up view of a $D=32\text{mm}$ mixing head (d) and a $D=16\text{mm}$ mixing head with rotor (left) separated from stator (e). (f) Graphene–NMP dispersions produced by shear exfoliation. Photos taken from Paton *et al.* [52]

1.5.3 Chemical vapour deposition

Besides mechanical and liquid phase exfoliation, chemical vapour deposition (CVD) on metal surfaces is also promising for graphene synthesis especially for large-scale production of mono- or few-layer graphene films. In the CVD method, the nucleation and growth of graphene occurs by the exposure of the transition metal surface to a hydrocarbon gas under low pressure or ultra-high vacuum conditions [53]. Recently, large-area uniform polycrystalline graphene films had successfully been grown on copper foils and films, and showed good potential for many applications (Fig. 1.10) [54,55]. Li *et al.* (2009) demonstrated that graphene films grow directly on the surface of copper by a surface catalysed process and in contrast to nickel, due to the low solubility of carbon in copper, a time-independent nucleation based growth of graphene (as large as 30 inch sheets) was observed which was self-limiting (> 95 % of area were mono-layered) [54,55]. However, at present, there are several

challenges that need to be addressed such as its high cost due to large energy consumption and removal of the underlying metal layer for the film transfer process [56].

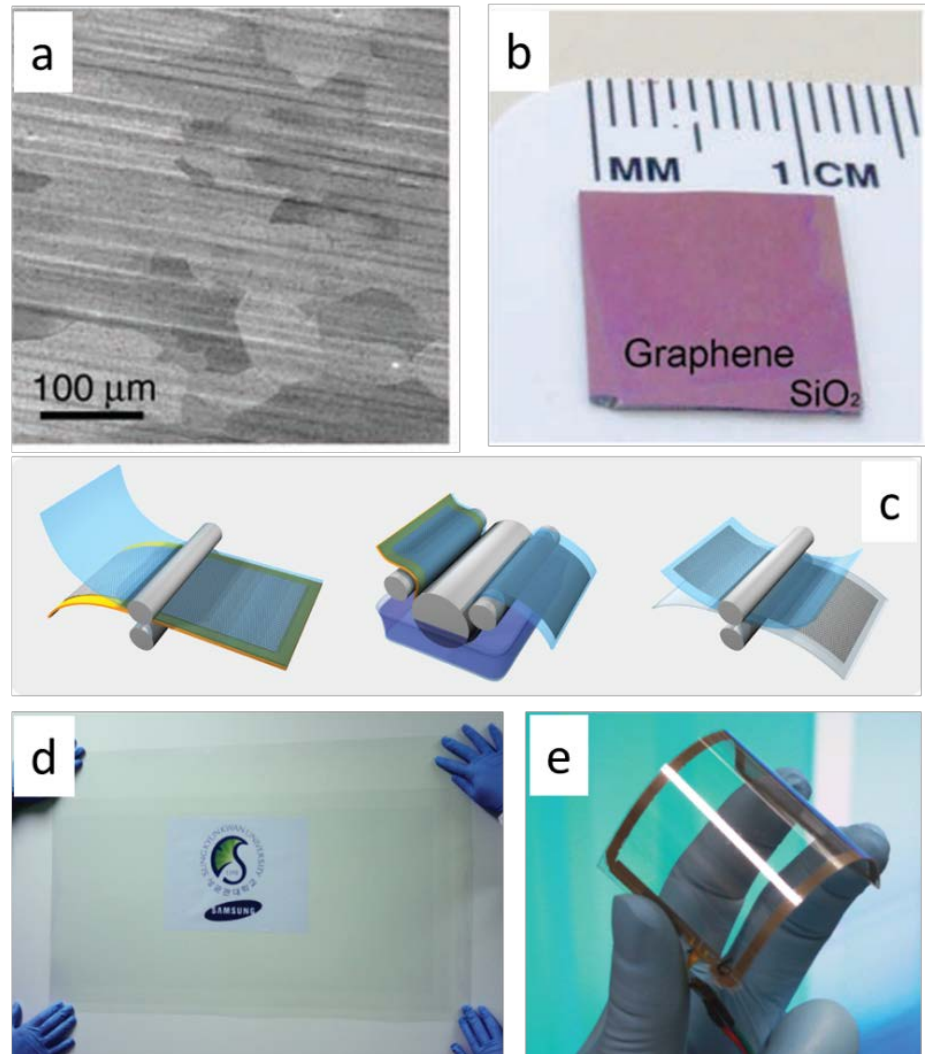


Figure 1.10. (a) SEM image of graphene grown on copper foil via chemical vapour deposition method, (b) graphene films transferred onto SiO₂/Si substrate. Images taken from Li *et al.* [54], (c) schematic illustration of roll-to-roll production of graphene films grown on copper foil, (d) a transparent ultralarge-area graphene film transferred on a 35-inch polyethylene terephthalate (PET) sheet and (e) an assembled graphene/PET touch panel showing outstanding flexibility. Images taken from Bae *et al.* [55].

1.5.4 Epitaxial growth on silicon carbide

It has been demonstrated that graphitic layers can be grown on silicon or carbon faces of a silicon carbide (SiC) wafer through sublimation of Si atoms [57]. Further studies conducted by Charrier *et al.* (2002) leads to the formation of few layers of

graphene that had a lattice parameter comparable to graphite [58]. In 2004, Berger *et al.*, were the first to demonstrate that graphene holds good potential for large-scale electronics [59]. Epitaxially grown graphene on SiC possess several advantages over graphene deposited on substrates such as avoiding the need for transferring graphene on other substrates. This simplifies the patterning process and the interface of graphene and SiC substrate is formed at temperatures in excess of 1500 °C, thus avoiding water or impurities trapped under graphene (Fig. 1.11) [60]. However, the high cost of the SiC wafers and the high temperatures required are not compatible with the silicon electronics technology, and this is likely to limit the use of SiC-grown graphene to a small number of applications.

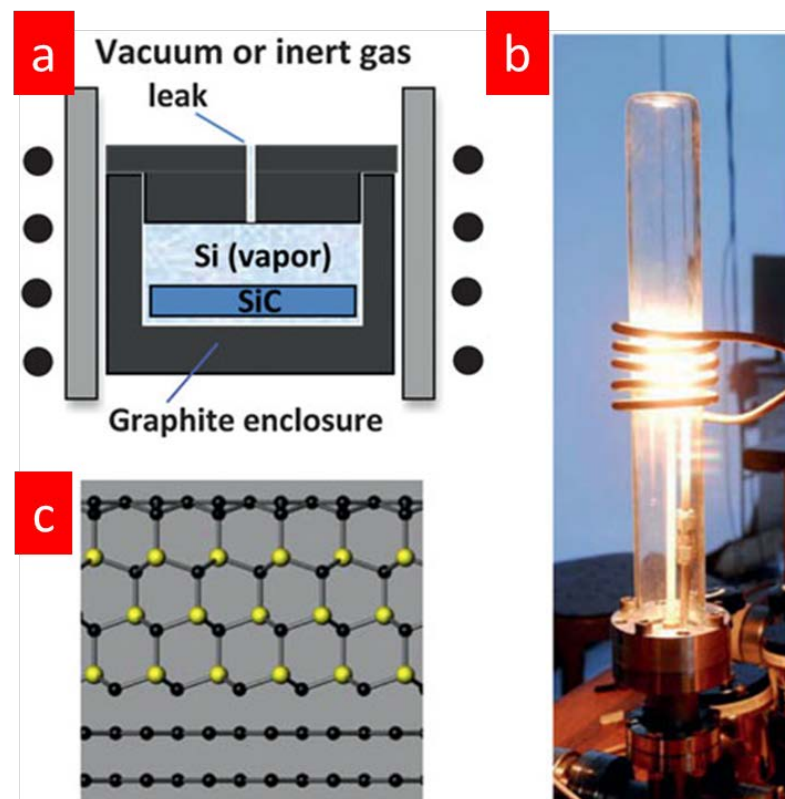


Figure 1.11. Graphene growth by the confinement controlled sublimation (CCS) method. (a) An SiC chip is placed in a graphite enclosure that is provided with a small leak, and inductively heated. The growth rate is controlled by the enclosure aperture (leak), and the background gas pressure. (b) Photograph of the furnace and (c) Schematic of graphene on SiC (silicon, yellow; carbon, black). The bottom face (C face) is covered with two graphene layers, whereas the top face (Si face) schematically terminates in a covalently bonded buffer layer. In subsequent growth on this face, the buffer layer is converted into a graphene layer by the new buffer layer that grows under it. Images taken from De Heer *et al.* [60,61].

It is noteworthy that different preparation methods of graphene results in different dimensions, shapes and quality of graphene produced. A summary of different properties of graphene produced using the most common techniques are as shown in Table 1.1.

Table 1.1 Properties of graphene synthesized through different methods

Preparation methods	Cost	Electronic quality	Size	Quantity	Reference
Mechanical exfoliation	Low	High	< 10 μm	Low	7
Liquid phase exfoliation from graphite	Low	High	Smaller fragments to tens of μm	High	35-37
Chemical exfoliation via graphene oxide	Low	Low	Tens of nanometres to 100 μm	High	43-45
Chemical vapour deposition	High	High	> 100 μm	Low	53,54
Epitaxial growth on SiC	High	High	> 50 μm	Low	61,62

1.6 Characterization of graphene

Due to graphene being atomically thin, its characterization is challenging. Nevertheless, graphene identification is crucial for studying its structure and properties which is important in developing its applications. To date, a range of reliable techniques are available, including atomic force microscopy (AFM), transmission electron microscopy (TEM), optical microscopy, and Raman spectroscopy.

AFM analysis can effectively determine the layer thickness of graphene in nanometre scale. However, due to its low throughput, imaging a large-area graphene is cumbersome. AFM analysis provides topographic contrast, which cannot distinguish between graphene oxide and pristine graphene under normal operation. Nevertheless, phase imaging is one of the attractive features of tapping-mode AFM which is able to distinguish between a defect free pristine graphene and its functionalized version

[63]. Apart from imaging and analysing the thickness of graphene, AFM have also been used to investigate mechanical properties of graphene as it can resolve small forces involved in the deformation process [14]. The study of frictional, electrical and magnetic properties of graphene is also possible using different modes of AFM [64].

TEM is widely used for imaging nano sized materials up to the atomic scale resolution, where a transmitted electron beam passes through the ultra-thin sample and reaches the imaging lenses and detector. As compared to AFM, TEM analysis is more useful in preliminary identification of graphene. Furthermore, as graphene is atomic layer thick, TEM is an ideal tool which can resolve atomic features of the graphene. Recently, Meyer and co-workers have demonstrated that high resolution images of the graphene lattice can be obtained using an aberration corrected TEM in combination with a monochromator, providing 1 Å resolution at an acceleration voltage of only 80 kV (Figure 1.12) [65]. Meanwhile, using another imaging technique, Gass *et al.* (2008) have shown atomic lattice, defects and surface contamination in high angle annular dark-field (HAADF) images using scanning transmission electron microscopy (STEM) [66]. The selected area electron diffraction (SAED) technique offers insights for distinguishing monolayer graphene as shown in Figure 1.12b,c [30].

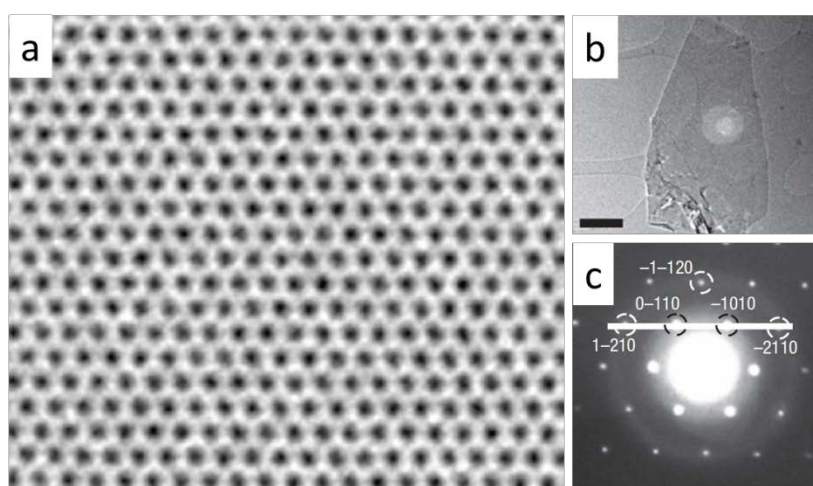


Figure 1.12. (a) Direct image of a single-layer graphene membrane (atoms appear white) using aberration corrected HRTEM. Image taken from Meyer *et al.* [65]. Evidence of monolayer graphene from TEM. (b) HRTEM image of solution-cast monolayer graphene

(scale bar: 500 nm) and (c) the SAED pattern of the graphene sheet in (b) with the peaks labelled by Miller-Bravais indices. Images taken from Hernandez *et al.* [30].

Optical microscopy was primarily used after the first discovery of graphene, mainly because it is the cheapest among other techniques, non-destructive and can be easily found in laboratories. Prior to optical imaging, graphene samples must be placed on silicon dioxide substrate to obtain good contrast imaging [7]. Over the past few years, several routes have been proposed to enhance the visibility of thin sheets such as narrow band illumination [67], selection of appropriate substrate [68], the use of reflection and contrast spectroscopy [69] and the use of total colour difference (TCD) method [70]. At present SiO_2 and Si_3N_4 are the most commonly used overlay materials on silicon for enhancing the contrast of graphene samples [67]. Thus far, the detection of graphene using optical microscope is dependent on the thickness of the substrate and wavelength of the incident light. In order to facilitate the visualization of graphene by this technique, more work is needed to develop methods that can enable the visualization of graphene sheets independent from the support material.

Raman spectroscopy is another useful tool for graphene characterization. It offers fast, non-destructive, high resolution analysis and also access to structural and electronic information. Furthermore it is applicable in both laboratory and mass production scales [71]. Graphene and other carbon allotropes show their fingerprints under Raman spectroscopy mainly by D, G, and 2D peaks around 1350 cm^{-1} , 1580 cm^{-1} and 2700 cm^{-1} respectively, due to the change in electron bands [72]. Analysis of these features provides insights into characterization of graphene layers in terms of number of layers [71] and their effect of strain [73], doping concentration [74], effect of temperature [75] and the presence of any defects [76]. The two most prominent peaks for graphene are the G and the 2D peaks. The G peak is associated to the doubly degenerate zone center E_{2g} phonon mode. This band arises due to the in-plane vibration of the sp^2 carbon atoms, whereas the 2D band is at almost double the frequency of the D band. The 2D band originates from second order Raman scattering process which is due to the presence of atomic disorders or edge effects of the graphene sheet, ripples and charge puddles [71,72]. Ferrari *et al.* (2006) have compared the Raman spectra of graphite, single and few layer graphene as shown in Figure 1.13 [72]. D peak was not observed at the centre of the graphene layers which

confirms the absence of defects. In addition, a significant change in shape and intensity was observed for 2D band of graphene and graphite (Figure 1.13b,c). Ferrari *et al.* (2006) have also demonstrated that the 2D band splits into two components for bulk graphite and into four components for bi-layer graphene [72]. As the number of layer increases, the relative intensity of 2D peak decreases and its FWHM shift to higher wavenumber. The single sharp 2D peak was reported for monolayer that is four times more intense than the G peak [72]. Nonetheless, for more than 5 layers the Raman spectrum becomes hardly distinguishable from bulk graphite. As the properties of graphene crucially depend on the number of layers and purity, Raman spectra has been widely used as a tool to characterize and also for the quality control of mono and few layers of graphene.

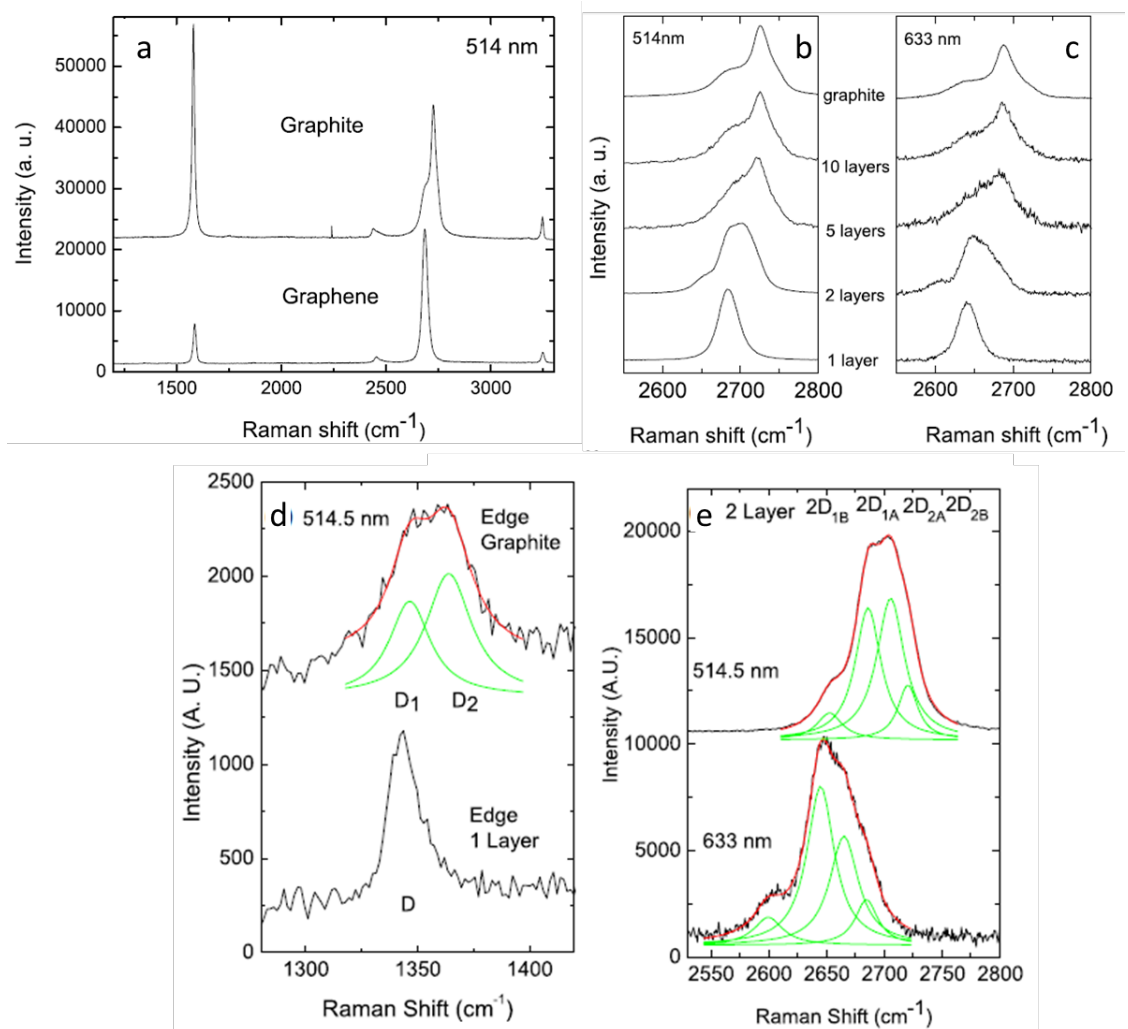


Figure 1.13. (a) Raman spectra at 514 nm for graphite and monolayer graphene. (b,c) Evolution in 2D band as a function of layers at 514 nm and 633 nm excitations respectively.

(d) Comparison of the D band at 514 nm at the edge of bulk graphite and monolayer graphene. The fit of the D1 and D2 components of the D band of bulk graphite is shown. (e) The four components of the 2D band in bilayer graphene at 514 and 633 nm. Images taken from Ferrari et al. [71]

1.7 Graphene oxide

Apart from pristine graphene, the derivatives of graphene such as graphene oxide (GO), and reduced graphene oxide (rGO) are also attracting significant interest due to the feasibility for large scale production [43-45]. Despite the fact that pristine graphene possess superior properties, it is insoluble in water and therefore its synthesis and processing requires the use of organic solvents which are generally more expensive, toxic and difficult to handle. On the other hand, GO is hydrophilic due to the high affinity of oxygen containing groups on the surface of GO towards water molecules, and thus can be dissolved in water. GO can be prepared by oxidizing bulk graphite, which leads to the increase of the basal spacing between graphitic planes consequently facilitating its exfoliation [43-45]. Furthermore, the hydroxyl and carboxyl groups on its surface allow GO to be efficiently modified by reaction with a wide range of chemicals, using standard procedures of organic chemistry [45]. Recent studies have revealed that GO is amphiphilic with an edge-to-center distribution of hydrophilic and hydrophobic sites which enables them to adhere to interfaces and lower the interfacial energy, potentially acting as a surfactant [76]. GO is electrically insulating but can be reduced to which partly restores the structure and properties of graphene [43-45].

1.8 Functionalization of graphene

Due to the remarkable properties of graphene and its derivatives, they show a great number of potential applications in a wide-ranging area; from electronics [7,8,11-13,78], energy storage [79-81], sensors [81,82], optical [16,83], to bioremediation [84,85] and biomedical applications [86,87]. At the same time, significant efforts are being made to further extend the functionality of graphene either through modification of the graphene structure itself or through the synthesis of hybrid or composite materials with graphene [88,89].

Several studies have reported successful modification of graphene structure via covalent and non-covalent functionalization of graphene with different functional moieties [88,89]. For example, the modification of pristine graphene through covalent functionalization with several organic functional groups has been carried out to enhance dispersibility of graphene in organic solvents which facilitates the formation of nanocomposite materials with graphene [88]. It is also important to note that covalent attachment of organic molecules to graphene results in perturbation of its sp^2 conjugation. Due to the zero band gap property of graphene, there is a limitation in developing devices with on/off functions [90]. To overcome this limitation, there have been a number of efforts in band gap engineering, including through covalent attachment of organic molecules. Niyogi *et al.* (2011) demonstrated that the band structure of graphene can be modified through covalent attachment of graphene which enables the control of its electronic properties, and through precise functionalization it can further extend the application of graphene application in electronic devices (Fig. 1.14) [78].

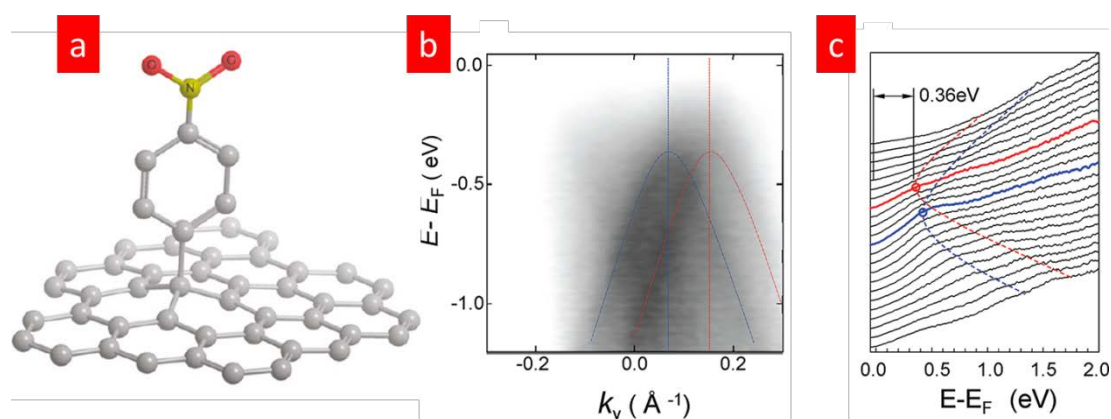


Figure 1.14. Energy band gap in graphene induced by covalent chemical functionalization. (a) Schematic illustration of nitro phenyl functionalized epitaxial graphene, (b) angle resolved photoemission spectroscopy (ARPES) measured band structure of nitrophenyl-functionalized graphene and (c) constant energy cuts clearly shows that a band gap of 0.36 eV has been created. Images taken from Niyogi *et al.* [78].

Graphene can also be functionalized non-covalently which involves hydrophobic, van der Waals, electrostatic interactions and also physical adsorption of suitable molecules on the graphene surface [88,91]. Such an example is the attachment of pyrene moieties and other organic molecules on their surfaces [88]. Unlike covalent functionalization, non-covalent functionalization by π -interactions offers possibility

of attaching functional groups to graphene without disturbing the electronic network [88,91]. Xu *et al.* (2008) demonstrated that functionalizing reduced graphene oxide with water soluble pyrene-derivative leads to the formation of stable aqueous dispersion of graphene sheets (Fig. 1.15) [92]. They also demonstrated that conductivity of the functionalized graphene film was about 2×10^2 S/m, almost 7 orders of magnitude larger than that of GO film prepared by the same method.

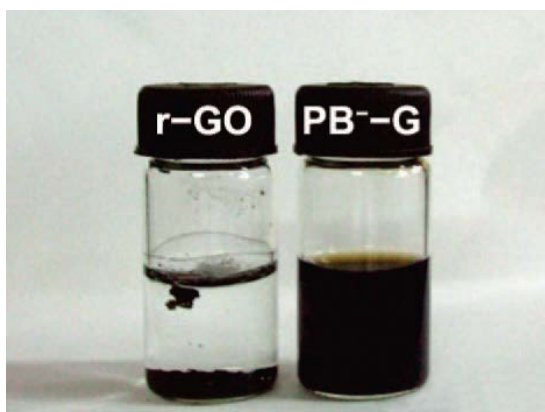


Figure 1.15. Photographic images of reduced graphite oxide (left) and 1-pyrenebutyrate functionalized graphene (right) dispersions in water. Image taken from Xu *et al.* [92].

In another study, Wang *et al.* (2009) demonstrated that non-covalent attachment of thermally reduced graphene with pyrene butanoic acid succidymidyl ester (PBSA) improved the power conversion efficiency of photovoltaic devices to 1.71% compared to non-functionalized thermally reduced graphene, which had 0.26% power conversion efficiency. This establishes the possibility for replacement of the expensive indium tin oxide (ITO) material with low-cost graphene in photovoltaic devices [93]. Nonetheless several other advantages of non-covalent functionalization of graphene with pyrene moieties has been revealed which is promising for the development of portable electronic and optoelectronic devices, solar cells and many others [94,95].

Another emerging interest is to build heterolayers of graphene and other 2D layered materials which are non-covalently bounded. These materials are identified as van der Waals solids due to the interaction between the layers [96,97]. As opposed to covalent bonding, the relatively weak van der Waals interaction barely affects the electronic properties of each layer material and stacking different layers can result in tunable properties of the heterostructures [98]. Gao *et al.* (2012) demonstrated that

hybrid film of h-BN (hexagonal boron nitride) and graphene nanosheets can be prepared by mixing the exfoliated h-BN dispersion with that of graphene. Furthermore, by varying the volume ratio of h-BN and graphene different compositions of h-BN/G can be obtained thus paving the way for generating material a tunable band gap [99]. In comparison to pristine graphene, the van der Waals solids are more promising to perform as electronic switches and optoelectronic devices which remain challenging for pristine graphene due to the absence of a band gap [99]. Thus far, significant efforts have been made towards preparation of these materials such as using the scotch-tape approach similar to the method used by Geim and Novoselov in their discovery of graphene [100]. Even though high quality material can be obtained through this method, the process is not suitable for large scale production. Other techniques such as chemical vapour deposition [101], and solution phase methods [99] are gaining interest for building heterostructures in large scale. The solution phase method is particularly interesting given that it is cheaper and feasible [29,30]. It would be more desirable to render the material soluble in water or common low-boiling point organic solvents. In the case of graphene, it can be chemically modified to render it hydrophilic thus facilitating the processing. However for other 2D layered materials such as h-BN and molybdenum disulphide (MoS_2), their chemical modification is restricted and due to their hydrophobic nature, processing in aqueous solutions without surfactant is inherently difficult. Therefore, it is important to develop methods to produce aqueous based dispersion of van der Waals solids. Given the amphiphilic properties of graphene oxide, they have been used as surfactants for carbon nanotubes [102] with amphiphilic properties fine tuned by adjusting the pH of the system [103]. Herein we utilized the amphiphilic property of graphene oxide to build van der Waals solids consisting of graphene oxide and other 2D layered materials namely h-BN and MoS_2 .

Synthesis of graphene hybrid materials has also shown intriguing results leading to the generation of novel functional materials. Given the large specific surface area of graphene, it can act as an ideal substrate for deposition of functional materials or nanoparticles which already have established applications such as for noble metals [104-106], metal oxides [107-109] and quantum dots [110]. Graphene has also been incorporated into polymers as graphene/polymer nanocomposites, which exhibit enhanced electrical and thermal conductivity, tensile strength, and flame retardancy

compared to polymers without graphene [111-114]. Furthermore, graphene contributes to the formation of strong yet lightweight composite materials [112,114]. The unique chemical and physical properties of graphene and its derivatives have also attracted strong interest for its hybridization with biological entities [115]. Thus far graphene has been hybridized with various biomolecules such as proteins, nucleic acids, peptides, drugs and also with biological cells such as bacteria and yeast (Fig. 1.16) [115]. It has been reported that biofunctionalization of graphene with biomolecules, the biocompatibility, solubility and selectivity of graphene can be enhanced [115].

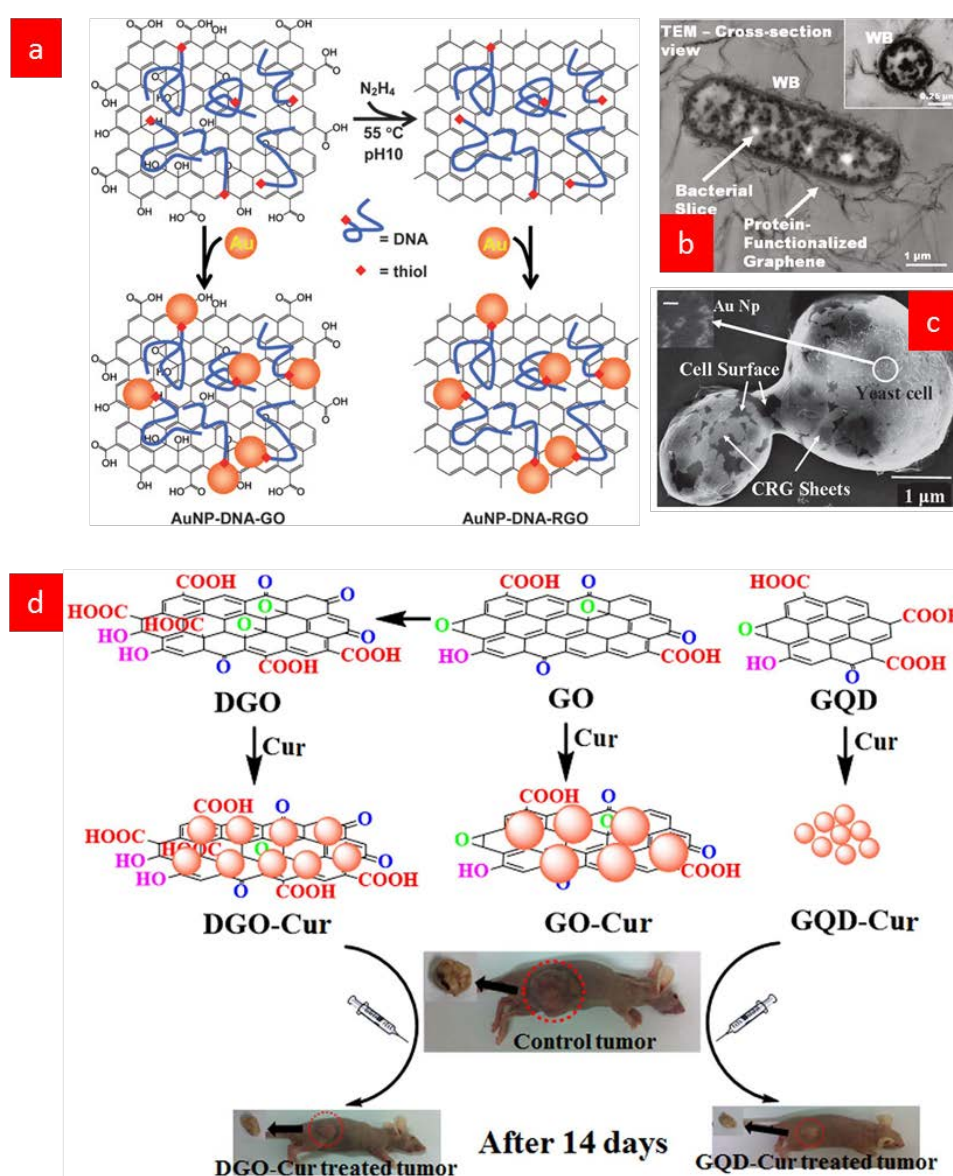


Figure 1.16. Various graphene based functional hybrid bionanomaterials. (a) DNA coating of graphene oxide (GO) and reduced graphene oxide (RGO), which were then used

as interfaces for a homogeneous assembly of metal–carbon hetero-nanostructure. Images taken from Liu *et al.* [116], (b) TEM image of bacteria, *Eschericia coli* encapsulated in graphene layers and cross section image of a wrapped bacterium in the inset. Wet-phase imaging was possible after graphene encapsulation. Images taken from Mohanty *et al.* [117], (c) Yeast cells interfaced with chemically reduced graphene (CRG) sheets resulting in electrically conductive and higher resistance towards osmotic pressure. Inset image shows the presence of the Au particles on the cell–CRG sheets. Taken from Kempaiah *et al.* [118] and (d) schematic illustration of various curcumin-graphene composites; double oxidized graphene oxide (DGO), graphene oxide (GO) and graphene quantum dot (GQD) and their anti-cancer effects. Taken from Some *et al.* [119].

Graphene has also been proven to be an effective drug carrier for drug delivery applications [86,119,120]. Sun *et al.* (2008) demonstrated the use of nano-graphene oxide sheets covalently attached to polyethylene glycol (PEG) star-polymers as carriers for anti-cancer drug, doxorubicin [86]. The simple physisorption via π -stacking enables the loading of drug molecules on graphene surface, and the nano-graphene oxide sheets have been shown to possess photoluminescence properties which is useful for cellular imaging [86]. For more control over targeting sites and controlled drug release, various strategies have been developed such as introducing superparamagnetic nanoparticles and pH-dependent release mechanism, as reported by Yang *et al.* (2009 & 2011) [121,122]. Several other studies have reported an increase in the biocompatibility of graphene based drug carriers via functionalization with chitosan [123] or gelatin [124].

Another interesting work related to graphene functionalization is the interfacing of graphene sheets on the surface of microorganisms. Hybridization of graphene with microorganisms has led to the development of novel functional material. Several studies have been carried out on interfacing graphene with bacteria and yeast cells with aims of imparting electrically conductive [117,118], highly sensitive [118,124] and impermeable protective layer [117,118] to the cells. Mohanty *et al.* (2011) demonstrated that protein functionalized graphene (PFG) can specifically wrap around bacteria, and given the impermeability and high electron transparency of graphene this enables the wet-phase imaging of bacterial cells [117]. Similarly, Kempaiah *et al.* (2011) have reported that by interfacing graphene on the surface of yeast cells, their stability towards osmotic stresses increases, and also direct visualization of the cells under electron microscope became possible [118]. Mohanty

and Berry (2005) have described that interfacing chemically modified graphene (CMG) with microorganisms can result in a single bacterium resolution interfacial device [125]. This is mainly attributed to the CMGs' p-type characteristic and its sub-nanoscale thickness which results in extraordinary response from external interactions [125]. They also developed a label-free, reversible DNA detector and a polarity-specific molecular transistor for protein/DNA adsorption [125]. The new properties of the composite material involving micro-organisms are useful for developing biodevices such as bio-batteries, bioprocess analysis tools, pathogen identification devices and many others [125].

1.9 Application of mechanoenergy in access to composite functional nanomaterials

Various preparation techniques are available for the preparation of composite functional materials. A facile, efficient and environmental friendly technique is a prerequisite to develop applications with prospect of being taken up by industry. In this dissertation, samples were prepared using process intensification technology, in the form of (i) the vortex fluidic device, and (ii) ultrasonic irradiation technique. Process intensification technology is defined as a strategy for making significant increase in the production rate within a given equipment volume, decrease in energy consumption and also obvious cut in wastes or by-product formation [126].

1.9.1 Vortex Fluidic Device

The limitations of traditional batch processing method in synthesizing materials have initiated the development of novel processing technologies. This limitation often arises prior to the scaling up of the production which is due to the uneven heat transfer and uneven mixing that results in poor production in traditional batch processing [127]. This can result in batch-to-batch variations leading to reproducibility issues [128]. In lieu of this, alternative processing routes have been identified for process intensification and among these are the dynamic thin film processing methods [129,130]. As opposed to batch processing, where reactions are carried out in a pool of mixture of reactants, dynamic thin films enables intense micromixing of the reactants given the high shear rates and intense surface ripples within the thin film resulting in efficient heat and mass transfer [130]. Furthermore, the high surface area to volume ratio characteristics of thin film also promotes

interactions between the film and its surroundings [130,131]. Dynamic thin films can be generated on rapidly rotating surfaces as a result of high centrifugal accelerating force [130,131]. Such devices which implements this concepts comes in the form of a spinning disc processor (SDP) (Fig. 1.17a) [130,131], and rotating tube processor (RTP) (Fig. 1.17b) [132,133].

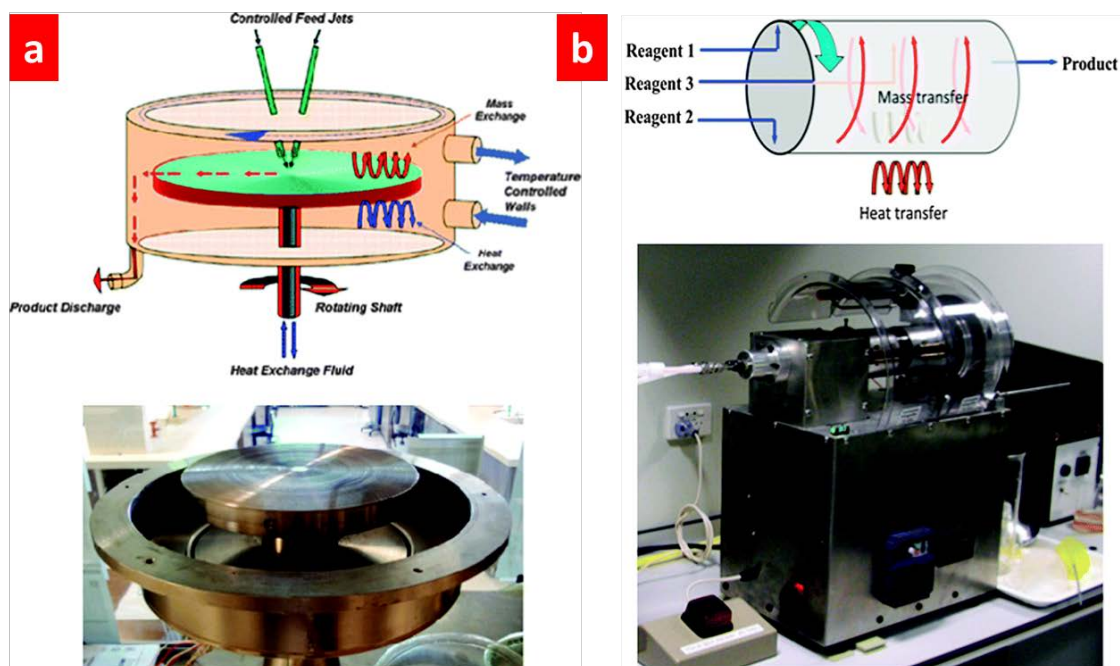


Figure 1.17. Schematic view of an SDP and a photograph of a 20 cm diameter spinning disc housed in such a unit. (b) Schematic view of an RTP showing high mass and heat transfer and a photograph of an RTP, which has a rotating tube of 30 cm in length and 6 cm in diameter. Images taken from Chen et al. [134].

Both SDP and RTP enables continuous flow production, and therefore they are useful processing routes for scaling up from the laboratory to the requirements of industry. The SDP typically functions as a horizontal rotating disc with controllable speed and temperature. Jet feeds are used to direct reagents onto the disc. Thin fluid films are generated as the disc rotates rapidly and as mentioned earlier, the thin film properties creates a favourable environment for the reactions to occur. The rapid rotation of the disc also results in short residence time for the liquid film on the surface which is desirable for processing heat sensitive liquids [129]. The RTP, on the other hand is a variant of the SDP with the ability to control the residence time. This is achieved by controlling the rate of addition and tube length [134].

The vortex fluidic device (VFD) technology used herein is closely related to the technology of RTP (Fig. 1.18). VFD is a novel microfluidic processing platform developed by Colin L. Raston [134]. The VFD essentially consists of a glass tube open at one end which can be rapidly rotated at a controllable speed along its longitudinal axis and with adjustable inclination angle ranging from 0 to 90° [134]. In the VFD, as the tube rapidly rotates, a dynamic thin film is formed along the wall of the tube. Intense shearing forces are generated within the thin fluid film as a result of the interplay between centrifugal and gravitational forces which is associated with the Stewartson-Ekman layers [135-137]. Unlike the spinning disc and rotating tube processors, VFD can operate at different tilting angles and this affects the thickness of the fluid film in the tube and the nature of the fluid flow. Reactions in the VFD are typically performed in tubes made of borosilicate glass and at present, processing is available in two different tube sizes which are the 10 mm and 20 mm outer diameter (8.45 and 18 mm inner diameter) glass tubes. Moreover, VFD can operate in either continuous flow or confined mode for a finite sub millilitre volume of liquid, which is advantageous to control the residence time. In continuous flow mode of operation, products can be collected at the open end of the tube and feed jets can be used to deliver reagents into the tube. Nonetheless, a variety of field effects such as magnetic, thermal, lasers, plasma and acoustic energy can be applied thus enriching the processing conditions of the VFD. The VFD can also be equipped with UV-Vis and also fluorescence detectors to enable real-time monitoring of the reactions.

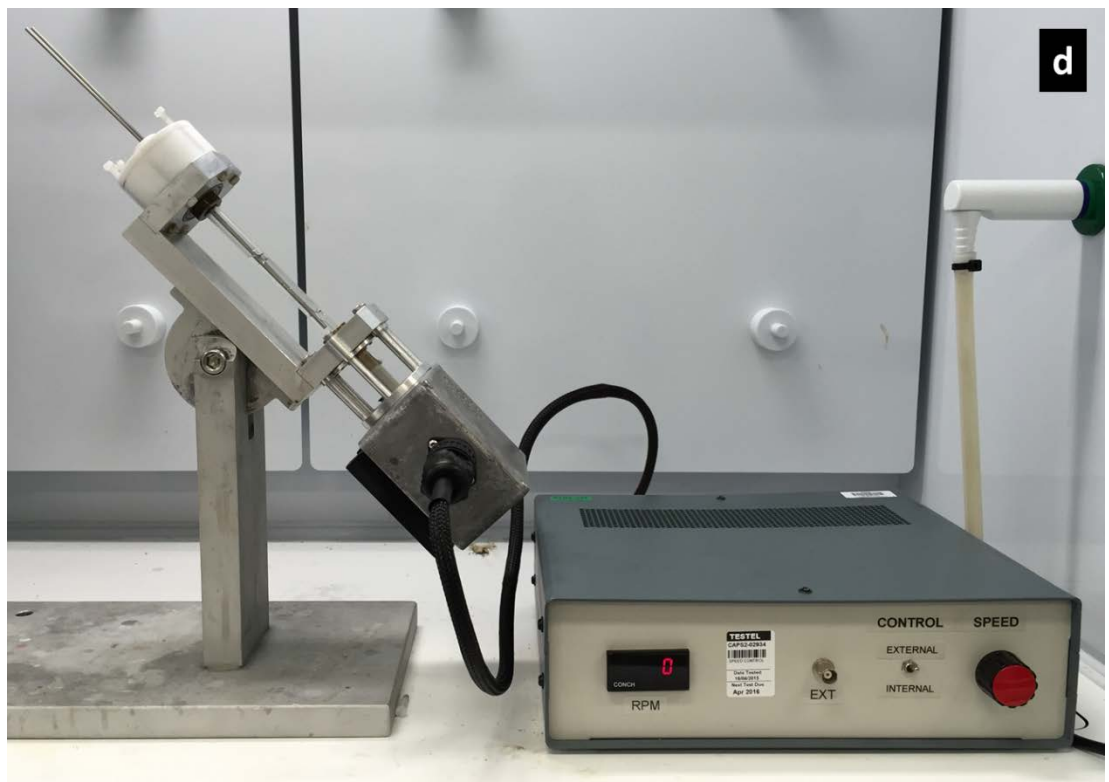
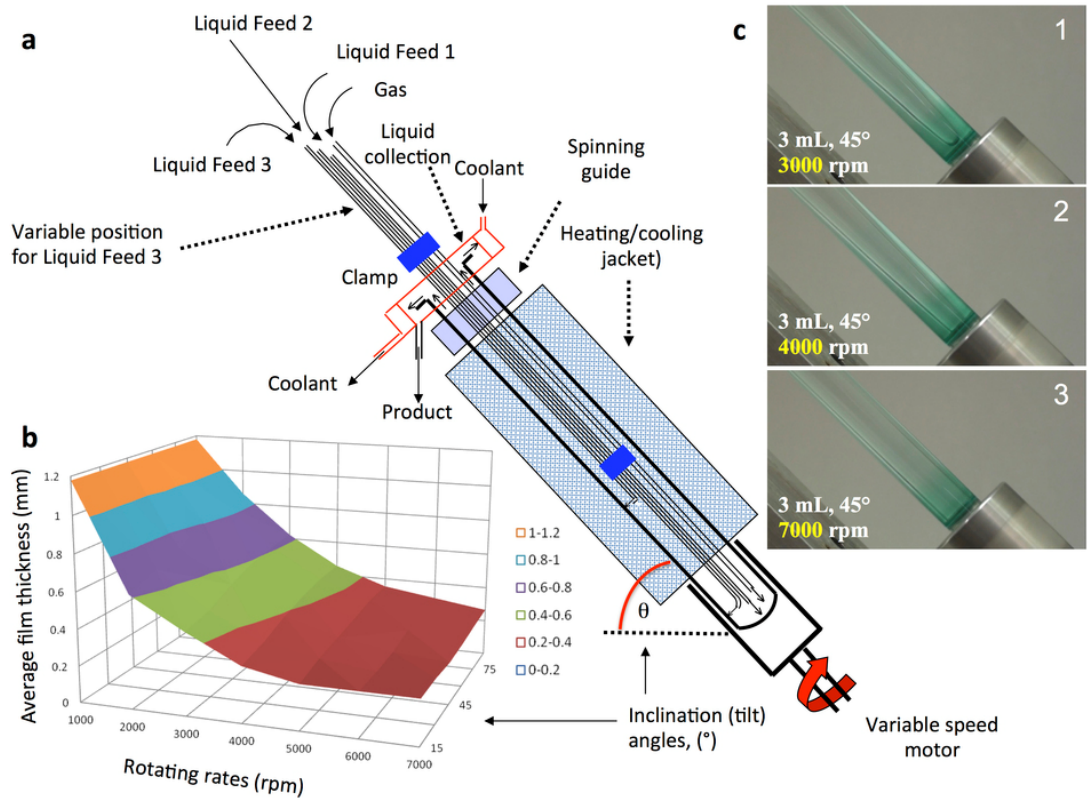


Figure 1.18. Vortex fluidic device (VFD). (a) Cross section showing components of the device. (b) Average film thickness (mm) versus tilt angle θ , (c) Photographs showing the film of liquid developed for different speeds, for 3 mL of an aqueous solution, for $\theta = 45^{\circ}$ and (d)

Photograph of a VFD housing a 10 mm diameter borosilicate NMR tube inclined at 45 degrees. Images (a-c) taken from Yasmin et al. [139].

The use of VFD in processing materials is promising, which has been demonstrated in the preparation of various types of material such as inorganic and organic syntheses including synthesis of biodiesel [139-146], exfoliation of 2D layered materials [136,137], decoration of noble metal nanoparticles on different nanostructures [146-149], controlling growth of calcium carbonate polymorphs [138], synthesis of mesoporous silica at room temperature with control over the pore size [151], compacting single walled carbon nanotube into toroidal structures [152], preparation of functional hybrid bio-nano materials [137,153-155] and the refolding of proteins [156].

1.9.2 Sonication

Another form of process intensification technology is the ultrasound irradiation or sonication [157]. The ultrasound technology is well established and is widely used in research and industry. The term ultrasound refers to the sound frequencies greater than 20 kHz [158]. The underlying mechanism behind ultrasound irradiation is the acoustic cavitation process which is the formation, growth and implosive collapse of microbubbles within an aqueous solution as a result of pressure fluctuations that occur in the applied sound field [158-160]. This implosion of microbubbles generates high local turbulence and releases heat energy which causes significant increase in temperature and pressure [158-160]. In the vicinity of the collapsed bubbles intense localized heating occurs which acts as “hot spots” having temperatures of ~5000 °C, pressures of about 2000 atm, and heating and cooling rates above 10^{10} K/s that is ideal for driving chemical reactions under extreme conditions [161]. Furthermore, liquid motion in the vicinity of the collapsed bubbles creates very large shear and strain gradients which is caused by the rapid streaming of solvent molecules around the cavitation bubble and also upon the collapse of microbubbles strong shockwaves are emanated [160]. These physical effects are primarily responsible for enhanced mass transfer within the system, emulsification, bulk thermal heating, and a variety of effects on solids. Ultrasound irradiation can be generated through the conversion of an electrical signal into a physical vibration, with certain frequencies and amplitudes that can be directed toward a substance [158].

Thus far, sonication has been widely used for different applications for instance in the case of polymers, for dispersal of fillers and other components into base polymers, encapsulation of inorganic particles with polymers, modification of particle size in polymer powders and the welding and cutting of thermoplastics. Furthermore, sonication has also been used to accelerate chemical reactions in liquid-solid heterogeneous systems and significant achievements have been made such as enhancement of reaction rates, improvement in yields and circumvention of by-products. Sonication also features in synthesis of nanostructured materials. Using the extreme conditions inside a cavitating bubble, Suslick and co-workers have produced different nanostructured materials such as amorphous metals, alloys, and carbides and examined their catalytic activity [161].

Sonication induced cavitation energy has also been used for liquid-phase exfoliation of 2D layered materials. Following to the successful isolation of graphene for the first time, tremendous amount of research have been concentrating on exfoliation of 2D layered materials using various approaches including through sonication in organic solvents or in aqueous solutions under the presence of surfactants [30,35-37]. Graphene exfoliation through this method is ideal for large scale production and not only that, graphene is produced without oxidation or defect formation which would possibly degrade its unique electrical property [35]. One of the early attempts to exfoliate graphene using ultrasonication technique was demonstrated by Coleman and co-workers (2008) by sonicating bulk graphite in organic solvents possessing similar surface energies with graphene [30]. This is followed by a detailed experiment carried out by the same group to investigate graphene concentration as a function of sonication time and optimization of other processing parameters to achieve higher yield of graphene [35,37,162].

1.10 References

- 1 Chen, X., Li, C., Gratzel, M., Kosteki, R. and Mao, S. S. (2012). Nanomaterials for renewable energy production and storage. *Chemical Society Reviews*, 41, 7909-7937.
- 2 Roduner, E. (2006). Size matters: why nanomaterials are different. *Chemical Society reviews*, 35, 583-592.
- 3 Lines, M. G. (2008). Nanomaterials for practical functional uses. *Journal of*

Alloys and Compounds, 449, 242-245.

- 4 Tiwari, J. N., Tiwari, R. N., and Kim, K. S. (2012). Zero-dimensional, one-dimensional, two-dimensional and three-dimensional nanostructured materials for advanced electrochemical energy devices. *Progress in Materials Science*, 57(4), 724-803.
- 5 Sajanalal, P. R., Sreeprasad, T. S., Samal, A. K. and Pradeep, T. (2011). Anisotropic nanomaterials: structure, growth, assembly, and functions. *Nano Reviews*, 2, 5883_1-5883_62.
- 6 Pokropivny, V. V., and Skorokhod, V. V. (2007). Classification of nanostructures by dimensionality and concept of surface forms engineering in nanomaterial science. *Materials Science and Engineering: C*, 27(5), 990-993.
- 7 Novoselov, K. S., Geim, A. K., Morozov, S. V., Jiang, D., Zhang, Y., Dubonos, S. V., Grigorieva, I. V. and Firsov, A. A. (2004). Electric field effect in atomically thin carbon films. *Science*, 306(5696), 666-669.
- 8 Geim, A. K. and Novoselov, K. S., (2007). The rise of graphene. *Nature Materials*, 6, 183-191.
- 9 Venables, J. A., Spiller, G. D. T. and Hanbucken, M. (1984). Nucleation and growth of thin films. *Reports on Progress in Physics*, 47(4), 399.
- 10 Evans, J. W., Thiel, P. A. and Bartelt, M. C. (2006). Morphological evolution during epitaxial thin film growth: Formation of 2D islands and 3D mounds. *Surface Science Reports*, 61(1), 1-128.
- 11 Stoller, M. D., Park, S., Zhu, Y., An, J. and Ruoff, R. S. (2008). Graphene-based ultracapacitors. *Nano Letters*, 8(10), 3498-3502.
- 12 Bolotin, K. I., Sikes, K. J., Jiang, Z., Klima, M., Fudenberg, G., Hone, J., Kim, P. and Stormer, H. L. (2008). Ultrahigh electron mobility in suspended graphene. *Solid State Communications*, 146(9), 351-355.
- 13 Morozov, S. V., Novoselov, K. S., Katsnelson, M. I., Schedin, F., Elias, D. C., Jaszczak, J. A. and Geim, A. K. (2008). Giant intrinsic carrier mobilities in graphene and its bilayer. *Physical Review Letters*, 100(1), 016602.
- 14 Lee, C., Wei, X., Kysar, J. W. and Hone, J. (2008). Measurement of the elastic properties and intrinsic strength of monolayer graphene. *Science*, 321(5887), 385-388.
- 15 Balandin, A. A., Ghosh, S., Bao, W., Calizo, I., Teweldebrhan, D., Miao, F. and Lau, C. N. (2008). Superior thermal conductivity of single-layer graphene. *Nano*

letters, 8(3), 902-907.

- 16 Nair, R. R., Blake, P., Grigorenko, A. N., Novoselov, K. S., Booth, T. J., Stauber, T., Peres, N. M. R. and Geim, A. K. (2008). Fine structure constant defines visual transparency of graphene. *Science*, 320(5881), 1308-1308.
- 17 Neto, A. C., Guinea, F., Peres, N. M. R., Novoselov, K. S. and Geim, A. K. (2009). The electronic properties of graphene. *Reviews of Modern Physics*, 81(1), 109.
- 18 Geim, A. K. (2009). Graphene: status and prospects. *Science*, 324(5934), 1530-1534.
- 19 Schedin, F., Geim, A. K., Morozov, S. V., Hill, E. W., Blake, P., Katsnelson, M. I. and Novoselov, K. S. (2007). Detection of individual gas molecules adsorbed on graphene. *Nature Materials*, 6(9), 652-655.
- 20 Wallace, P. R. (1947). The band theory of graphite. *Physical Review*, 71(9), 622.
- 21 Novoselov, K. S. A., Geim, A. K., Morozov, S., Jiang, D., Grigorieva, M. K. I., Dubonos, S. V. and Firsov, A. A. (2005). Two-dimensional gas of massless Dirac fermions in graphene. *Nature*, 438(7065), 197-200.
- 22 Zhang, Y., Tan, Y. W., Stormer, H. L. and Kim, P. (2005). Experimental observation of the quantum Hall effect and Berry's phase in graphene. *Nature*, 438(7065), 201-204.
- 23 Du, X., Skachko, I., Barker, A. and Andrei, E. Y. (2008). Approaching ballistic transport in suspended graphene. *Nature Nanotechnology*, 3(8), 491-495.
- 24 Hancock, Y. (2011). The 2010 Nobel Prize in physics— ground-breaking experiments on graphene. *Journal of Physics D: Applied Physics*, 44(2011), 473001.
- 25 Bunch, J. S., Verbridge, S. S., Alden, J. S., van der Zande, A. M., Parpia, J. M., Craighead, H. G. and McEuen, P. L. (2008). Impermeable atomic membranes from graphene sheets. *Nano Letters*, 8(8), 2458-2462.
- 26 Berry, V. (2013). Impermeability of graphene and its applications. *Carbon*, 62, 1-10.
- 27 Balandin, A. A., Ghosh, S., Bao, W., Calizo, I., Teweldebrhan, D., Miao, F. and Lau, C. N. (2008). Superior thermal conductivity of single-layer graphene. *Nano Letters*, 8(3), 902-907.
- 28 Hone, J., Whitney, M., Piskoti, C. and Zettl, A. (1999). Thermal conductivity of

single-walled carbon nanotubes. *Physical Review B*, 59(4), R2514.

- 29 Nicolosi, V., Chhowalla, M., Kanatzidis, M. G., Strano, M. S. and Coleman, J. N. (2013). Liquid exfoliation of layered materials. *Science*, 340(6139), 1226419.
- 30 Hernandez, Y., Nicolosi, V., Lotya, M., Blighe, F. M., Sun, Z., De, S., McGovern, I. T., Holland, B., Byrne, M., Gun'ko, Y. K., Boland, J. J., Niraj, P., Duesberg G., Krishnamurthy, S., Goodhue, R., Hutchison, J., Scardaci, V., Ferrari, A. C. and Coleman, J. N. (2008). High-yield production of graphene by liquid-phase exfoliation of graphite. *Nature Nanotechnology*, 3(9), 563-568.
- 31 Novoselov, K. S., Jiang, D., Schedin, F., Booth, T. J., Khotkevich, V. V., Morozov, S. V. and Geim, A. K. (2005). Two-dimensional atomic crystals. *Proceedings of the National Academy of Sciences of the United States of America*, 102(30), 10451-10453.
- 32 Zhu, Y., Murali, S., Cai, W., Li, X., Suk, J. W., Potts, J. R. and Ruoff, R. S. (2010). Graphene and graphene oxide: synthesis, properties, and applications. *Advanced Materials*, 22(35), 3906-3924.
- 33 Hernandez, Y., Lotya, M., Rickard, D., Bergin, S. D. and Coleman, J. N. (2009). Measurement of multicomponent solubility parameters for graphene facilitates solvent discovery. *Langmuir*, 26(5), 3208-3213.
- 34 Bourlinos, A. B., Georgakilas, V., Zboril, R., Steriotis, T. A. and Stubos, A. K. (2009). Liquid-Phase Exfoliation of Graphite Towards Solubilized Graphenes. *Small*, 5(16), 1841-1845.
- 35 Khan, U., O'Neill, A., Lotya, M., De, S. and Coleman, J. N. (2010). High-Concentration Solvent Exfoliation of Graphene. *Small*, 6(7), 864-871.
- 36 Lotya, M., Hernandez, Y., King, P. J., Smith, R. J., Nicolosi, V., Karlsson, L. S., Blighe, F. M., De, S., Wang, Z., McGovern, I. T., Dueberg, G. S. and Coleman, J. N. (2009). Liquid phase production of graphene by exfoliation of graphite in surfactant/water solutions. *Journal of the American Chemical Society*, 131(10), 3611-3620.
- 37 Lotya, M., King, P. J., Khan, U., De, S. and Coleman, J. N. (2010). High-concentration, surfactant-stabilized graphene dispersions. *ACS Nano*, 4(6), 3155-3162.
- 38 Smith, R. J., Lotya, M. and Coleman, J. N. (2010). The importance of repulsive potential barriers for the dispersion of graphene using surfactants. *New Journal of Physics*, 12(12), 125008.
- 39 Vadukumpully, S., Paul, J. and Valiyaveetil, S. (2009). Cationic surfactant mediated exfoliation of graphite into graphene flakes. *Carbon*, 47(14), 3288-

3294.

- 40 Green, A. A. and Hersam, M. C. (2009). Solution phase production of graphene with controlled thickness via density differentiation. *Nano Letters*, 9(12), 4031-4036.
- 41 Hummers Jr, W. S. and Offeman, R. E. (1958). Preparation of graphitic oxide. *Journal of the American Chemical Society*, 80(6), 1339-1339.
- 42 He, H., Klinowski, J., Forster, M. and Lerf, A. (1998). A new structural model for graphite oxide. *Chemical Physics Letters*, 287(1), 53-56.
- 43 Stankovich, S., Dikin, D. A., Piner, R. D., Kohlhaas, K. A., Kleinhammes, A., Jia, Y., Wu, Y., Nguyen, S. T. and Ruoff, R. S. (2007). Synthesis of graphene-based nanosheets via chemical reduction of exfoliated graphite oxide. *Carbon*, 45(7), 1558-1565.
- 44 Li, D., Müller, M. B., Gilje, S., Kaner, R. B. and Wallace, G. G. (2008). Processable aqueous dispersions of graphene nanosheets. *Nature Nanotechnology*, 3(2), 101-105.
- 45 Park, S. and Ruoff, R. S. (2009). Chemical methods for the production of graphenes. *Nature Nanotechnology*, 4(4), 217-224.
- 46 Allen, M. J., Tung, V. C. and Kaner, R. B. (2009). Honeycomb carbon: a review of graphene. *Chemical reviews*, 110(1), 132-145.
- 47 Vallés, C., Drummond, C., Saadaoui, H., Furtado, C. A., He, M., Roubeau, O., Ortolani, L., Monthieux, M. and Pénicaud, A. (2008). Solutions of negatively charged graphene sheets and ribbons. *Journal of the American Chemical Society*, 130(47), 15802-15804.
- 48 Hao, R., Qian, W., Zhang, L. and Hou, Y. (2008). Aqueous dispersions of TCNQ-anion-stabilized graphene sheets. *Chemical Communications*, (48), 6576-6578.
- 49 Liu, N., Luo, F., Wu, H., Liu, Y., Zhang, C. and Chen, J. (2008). One-Step Ionic-Liquid-Assisted Electrochemical Synthesis of Ionic-Liquid-Functionalized Graphene Sheets Directly from Graphite. *Advanced Functional Materials*, 18(10), 1518-1525.
- 50 Chen, X., Dobson, J. F. and Raston, C. L. (2012). Vortex fluidic exfoliation of graphite and boron nitride. *Chemical Communications*, 48(31), 3703-3705.
- 51 Paton, K. R., Varrla, E., Backes, C., Smith, R. J., Khan, U., O'Neill, A., Boland, C., Lotya, M., Istrate, O. M., King, P., Higgins, T., Barwich, S., May, P.,

- Puczkarski, P., Ahmed, I., Moebius, M., Petterson, H., Long, E., Coelho, J., O'Brien, S. E., McGuire, E. K., Sanchez, B. M., Duesberg, G. S., McEvoy, N., Pennycook, J., Downing, C., Crossley, A., Nicolosi, V. and Coleman, J. N. (2014). Scalable production of large quantities of defect-free few-layer graphene by shear exfoliation in liquids. *Nature Materials*, 13(6), 624-630.
- 52 Varrla, E., Paton, K. R., Backes, C., Harvey, A., Smith, R. J., McCauley, J. and Coleman, J. N. (2014). Turbulence-assisted shear exfoliation of graphene using household detergent and a kitchen blender. *Nanoscale*, 6(20), 11810-11819.
- 53 Reina, A., Jia, X., Ho, J., Nezich, D., Son, H., Bulovic, V., Dresselhaus, M. S. and Kong, J. (2008). Large area, few-layer graphene films on arbitrary substrates by chemical vapor deposition. *Nano Letters*, 9(1), 30-35.
- 54 Li, X., Cai, W., An, J., Kim, S., Nah, J., Yang, D., Piner, R., Velamakanni, A., Jung, I., Tutuc, E., Banerjee, K. S., Colombo, L. and Ruoff, R. S. (2009). Large-area synthesis of high-quality and uniform graphene films on copper foils. *Science*, 324(5932), 1312-1314.
- 55 Bae, S., Kim, H., Lee, Y., Xu, X., Park, J. S., Zheng, Y., Balakrishnan, J., Lei, T., Kim, H. R., Song, Y. I., Kim, Y.-J., Kim, K. S., Ozyilmaz, B., Ahn, J.-H., Hong, B. H. and Iijima, S. (2010). Roll-to-roll production of 30-inch graphene films for transparent electrodes. *Nature Nanotechnology*, 5(8), 574-578.
- 56 Novoselov, K. S., Fal, V. I., Colombo, L., Gellert, P. R., Schwab, M. G. and Kim, K. (2012). A roadmap for graphene. *Nature*, 490(7419), 192-200.
- 57 Forbeaux, I., Themlin, J. M. and Debever, J. M. (1998). Heteroepitaxial graphite on 6 H-SiC (0001): Interface formation through conduction-band electronic structure. *Physical Review B*, 58(24), 16396.
- 58 Charrier, A., Coati, A., Argunova, T., Thibaudau, F., Garreau, Y., Pinchaux, R., Forbeaux, I., Debever, J. -M., Sauvage-Simkin, M., and Themlin, J. M. (2002). Solid-state decomposition of silicon carbide for growing ultra-thin heteroepitaxial graphite films. *Journal of Applied Physics*, 92(5), 2479-2484.
- 59 Berger, C., Song, Z., Li, T., Li, X., Ogbazghi, A. Y., Feng, R., Dai, Z., Marchenkov, A. N., Conrad, E. H., First, P. N. and De Heer, W. A. (2004). Ultrathin epitaxial graphite: 2D electron gas properties and a route toward graphene-based nanoelectronics. *The Journal of Physical Chemistry B*, 108(52), 19912-19916.
- 60 Ruan, M., Hu, Y., Guo, Z., Dong, R., Palmer, J., Hankinson, J., Berger, C. and De Heer, W. A. (2012). Epitaxial graphene on silicon carbide: Introduction to structured graphene. *MRS bulletin*, 37(12), 1138-1147.
- 61 De Heer, W. A., Berger, C., Ruan, M., Sprinkle, M., Li, X., Hu, Y., Zhang, B.,

- Hankinson, J. and Conrad, E. (2011). Large area and structured epitaxial graphene produced by confinement controlled sublimation of silicon carbide. *Proceedings of the National Academy of Sciences*, 108(41), 16900-16905.
- 62 Emtsev, K. V., Bostwick, A., Horn, K., Jobst, J., Kellogg, G. L., Ley, L., McChesney, J. L., Ohta, T., Reshanov, S. A., Rohrl, J., Rotenberg, E., Schmid, A. K., Waldmann, D., Webber, H. B. and Seyller, T. (2009). Towards wafer-size graphene layers by atmospheric pressure graphitization of silicon carbide. *Nature Materials*, 8(3), 203-207.
- 63 Paredes, J. I., Villar-Rodil, S., Solis-Fernandez, P., Martinez-Alonso, A. and Tascon, J. M. D. (2009). Atomic force and scanning tunneling microscopy imaging of graphene nanosheets derived from graphite oxide. *Langmuir*, 25(10), 5957-5968.
- 64 Bertolazzi, S., Brivio, J., Radenovic, A., Kis, A., Wilson, H., Prisbrey, L., Minot, E., Tselev, A., Philips, M., Viani, M., Walters, D. and Proksch, R. (2013). Exploring flatland: AFM of mechanical and electrical properties of graphene, MoS₂ and other low-dimensional materials. *Microsc. Anal*, 27, 21-24.
- 65 Meyer, J. C., Kisielowski, C., Erni, R., Rossell, M. D., Crommie, M. F. and Zettl, A. (2008). Direct imaging of lattice atoms and topological defects in graphene membranes. *Nano Letters*, 8(11), 3582-3586.
- 66 Gass, M. H., Bangert, U., Bleloch, A. L., Wang, P., Nair, R. R. and Geim, A. K. (2008). Free-standing graphene at atomic resolution. *Nature Nanotechnology*, 3(11), 676-681.
- 67 Blake, P., Hill, E. W., Neto, A. C., Novoselov, K. S., Jiang, D., Yang, R., Booth, T. J. and Geim, A. K. (2007). Making graphene visible. *Applied Physics Letters*, 91(6), 063124.
- 68 Jung, I., Pelton, M., Piner, R., Dikin, D. A., Stankovich, S., Watcharotone, S., Hausner, M. and Ruoff, R. S. (2007). Simple approach for high-contrast optical imaging and characterization of graphene-based sheets. *Nano Letters*, 7(12), 3569-3575.
- 69 Ni, Z. H., Wang, H. M., Kasim, J., Fan, H. M., Yu, T., Wu, Y. H., Feng, Y. P. and Shen, Z. X. (2007). Graphene thickness determination using reflection and contrast spectroscopy. *Nano Letters*, 7(9), 2758-2763.
- 70 Gao, L., Ren, W., Li, F. and Cheng, H. M. (2008). Total color difference for rapid and accurate identification of graphene. *ACS Nano*, 2(8), 1625-1633.
- 71 Ferrari, A. C. and Basko, D. M. (2013). Raman spectroscopy as a versatile tool for studying the properties of graphene. *Nature Nanotechnology*, 8(4), 235-246.

- 72 Ferrari, A. C., Meyer, J. C., Scardaci, V., Casiraghi, C., Lazzeri, M., Mauri, F., Piscanec, S., Jiang, D., Novoselov, K. S., Roth, S. and Geim, A. K. (2006). Raman spectrum of graphene and graphene layers. *Physical Review Letters*, 97(18), 187401.
- 73 Mohiuddin, T. M. G., Lombardo, A., Nair, R. R., Bonetti, A., Savini, G., Jalil, R., Bonini, N., Basko, D. M., Galiotis, C., Marzari, N., Novoselov, K. S., Geim, A. K. and Ferrari, A. C. (2009). Uniaxial strain in graphene by Raman spectroscopy: G peak splitting, Grüneisen parameters, and sample orientation. *Physical Review B*, 79(20), 205433.
- 74 Ferrari, A. C. (2007). Raman spectroscopy of graphene and graphite: disorder, electron–phonon coupling, doping and nonadiabatic effects. *Solid State Communications*, 143(1), 47-57.
- 75 Calizo, I., Balandin, A. A., Bao, W., Miao, F. and Lau, C. N. (2007). Temperature dependence of the Raman spectra of graphene and graphene multilayers. *Nano Letters*, 7(9), 2645-2649.
- 76 Cançado, L. G., Jorio, A., Ferreira, E. M., Stavale, F., Achete, C. A., Capaz, R. B., Moutinho, M. V. O., Lombardo, A., Kulmala, T. S. and Ferrari, A. C. (2011). Quantifying defects in graphene via Raman spectroscopy at different excitation energies. *Nano Letters*, 11(8), 3190-3196.
- 77 Kim, J., Cote, L. J., Kim, F., Yuan, W., Shull, K. R. and Huang, J. (2010). Graphene oxide sheets at interfaces. *Journal of the American Chemical Society*, 132(23), 8180-8186.
- 78 Niyogi, S., Bekyarova, E., Hong, J., Khizroev, S., Berger, C., de Heer, W. and Haddon, R. C. (2011). Covalent chemistry for graphene electronics. *The Journal of Physical Chemistry Letters*, 2(19), 2487-2498.
- 79 Brownson, D. A., Kampouris, D. K. and Banks, C. E. (2011). An overview of graphene in energy production and storage applications. *Journal of Power Sources*, 196(11), 4873-4885.
- 80 Pumera, M. (2011). Graphene-based nanomaterials for energy storage. *Energy & Environmental Science*, 4(3), 668-674.
- 81 Pumera, M. (2009). Electrochemistry of graphene: new horizons for sensing and energy storage. *The Chemical Record*, 9(4), 211-223.
- 82 Shao, Y., Wang, J., Wu, H., Liu, J., Aksay, I. A. and Lin, Y. (2010). Graphene based electrochemical sensors and biosensors: a review. *Electroanalysis*, 22(10), 1027-1036.
- 83 Bonaccorso, F., Sun, Z., Hasan, T. and Ferrari, A. C. (2010). Graphene

photonics and optoelectronics. *Nature Photonics*, 4(9), 611-622.

- 84 Zhang, K., Kemp, K. C. and Chandra, V. (2012). Homogeneous anchoring of TiO₂ nanoparticles on graphene sheets for waste water treatment. *Materials Letters*, 81, 127-130.
- 85 Zhao, G., Li, J., Ren, X., Chen, C. and Wang, X. (2011). Few-layered graphene oxide nanosheets as superior sorbents for heavy metal ion pollution management. *Environmental Science & Technology*, 45(24), 10454-10462.
- 86 Sun, X., Liu, Z., Welsher, K., Robinson, J. T., Goodwin, A., Zaric, S. and Dai, H. (2008). Nano-graphene oxide for cellular imaging and drug delivery. *Nano Research*, 1(3), 203-212.
- 87 Park, S., Mohanty, N., Suk, J. W., Nagaraja, A., An, J., Piner, R. D., Cai, W., Dreyer, D. R., Berry, V. and Ruoff, R. S. (2010). Biocompatible, Robust Free-Standing Paper Composed of a TWEEN/Graphene Composite. *Advanced Materials*, 22(15), 1736-1740.
- 88 Georgakilas, V., Otyepka, M., Bourlinos, A. B., Chandra, V., Kim, N., Kemp, K. C., Hobza, P., Zboril, R. and Kim, K. S. (2012). Functionalization of graphene: covalent and non-covalent approaches, derivatives and applications. *Chemical Reviews*, 112(11), 6156-6214.
- 89 Guo, S. and Dong, S. (2011). Graphene nanosheet: synthesis, molecular engineering, thin film, hybrids, and energy and analytical applications. *Chemical Society Reviews*, 40(5), 2644-2672.
- 90 Schwierz, F. (2010). Graphene transistors. *Nature Nanotechnology*, 5(7), 487-496.
- 91 Kuila, T., Bose, S., Mishra, A. K., Khanra, P., Kim, N. H. and Lee, J. H. (2012). Chemical functionalization of graphene and its applications. *Progress in Materials Science*, 57(7), 1061-1105.
- 92 Xu, Y., Bai, H., Lu, G., Li, C. and Shi, G. (2008). Flexible graphene films via the filtration of water-soluble noncovalent functionalized graphene sheets. *Journal of the American Chemical Society*, 130(18), 5856-5857.
- 93 Wang, Y., Chen, X., Zhong, Y., Zhu, F. and Loh, K. P. (2009). Large area, continuous, few-layered graphene as anodes in organic photovoltaic devices. *Applied Physics Letters*, 95(6), 063302.
- 94 An, X., Butler, T. W., Washington, M., Nayak, S. K. and Kar, S. (2011). Optical and sensing properties of 1-pyrenecarboxylic acid-functionalized graphene films laminated on polydimethylsiloxane membranes. *ACS Nano*, 5(2), 1003-1011.

- 95 Su, Q., Pang, S., Alijani, V., Li, C., Feng, X. and Müllen, K. (2009). Composites of graphene with large aromatic molecules. *Advanced Materials*, 21(31), 3191-3195.
- 96 Geim, A. K. and Grigorieva, I. V. (2013). Van der Waals heterostructures. *Nature*, 499(7459), 419-425.
- 97 Duesberg, G. S. (2014). Heterojunctions in 2D semiconductors: A perfect match. *Nature Materials*, 13(12), 1075-1076.
- 98 Furchi, M. M., Pospischil, A., Libisch, F., Burgdörfer, J. and Mueller, T. (2014). Photovoltaic effect in an electrically tunable van der Waals heterojunction. *Nano Letters*, 14(8), 4785-4791.
- 99 Gao, G., Gao, W., Cannuccia, E., Taha-Tijerina, J., Balicas, L., Mathkar, A., Narayanan, T. N., Liu, Z., Gupta, B. K., Peng, J., Yin, Y., Rubio, A. and Ajayan, P. M. (2012). Artificially stacked atomic layers: toward new van der Waals solids. *Nano Letters*, 12(7), 3518-3525.
- 100 Fang, H., Battaglia, C., Carraro, C., Nemsak, S., Ozdol, B., Kang, J. S., ... and Javey, A. (2014). Strong interlayer coupling in van der Waals heterostructures built from single-layer chalcogenides. *Proceedings of the National Academy of Sciences*, 111(17), 6198-6202.
- 101 Liu, Z., Song, L., Zhao, S., Huang, J., Ma, L., Zhang, J., Lou, J. and Ajayan, P. M. (2011). Direct growth of graphene/hexagonal boron nitride stacked layers. *Nano Letters*, 11(5), 2032-2037.
- 102 Zhang, C., Ren, L., Wang, X. and Liu, T. (2010). Graphene oxide-assisted dispersion of pristine multiwalled carbon nanotubes in aqueous media. *The Journal of Physical Chemistry C*, 114(26), 11435-11440.
- 103 Cote, L. J., Kim, J., Zhang, Z., Sun, C. and Huang, J. (2010). Tunable assembly of graphene oxide surfactant sheets: wrinkles, overlaps and impacts on thin film properties. *Soft Matter*, 6(24), 6096-6101.
- 104 Luo, Z., Somers, L. A., Dan, Y., Ly, T., Kybert, N. J., Mele, E. J. and Johnson, A. C. (2010). Size-selective nanoparticle growth on few-layer graphene films. *Nano Letters*, 10(3), 777-781.
- 105 Liu, J., Takeshi, D., Sasaki, K. and Lyth, S. M. (2014). Defective Graphene Foam: A Platinum Catalyst Support for PEMFCs. *Journal of The Electrochemical Society*, 161(9), 838-844.
- 106 Granatier, J., Lazar, P., Pucek, R., Šafařová, K., Zbořil, R., Otyepka, M. and Hobza, P. (2012). Interaction of Graphene and Arenes with Noble Metals. *The Journal of Physical Chemistry C*, 116(26), 14151-14162.

- 107 Wang, D., Choi, D., Li, J., Yang, Z., Nie, Z., Kou, R., Hu, D., Wang, C., Saraf, L. V., Zhang, J., Aksay, I. A. and Liu, J. (2009). Self-assembled TiO₂-graphene hybrid nanostructures for enhanced Li-ion insertion. *ACS Nano*, 3(4), 907-914.
- 108 Wang, H., Cui, L. F., Yang, Y., Sanchez Casalongue, H., Robinson, J. T., Liang, Y., Cui, Y. and Dai, H. (2010). Mn₃O₄-graphene hybrid as a high-capacity anode material for lithium ion batteries. *Journal of the American Chemical Society*, 132(40), 13978-13980.
- 109 Jiang, J., Li, Y., Liu, J., Huang, X., Yuan, C. and Lou, X. W. D. (2012). Recent Advances in Metal Oxide-based Electrode Architecture Design for Electrochemical Energy Storage. *Advanced Materials*, 24(38), 5166-5180.
- 110 Konstantatos, G., Badioli, M., Gaudreau, L., Osmond, J., Bernechea, M., de Arquer, F. P. G., Gatti, F. and Koppens, F. H. (2012). Hybrid graphene-quantum dot phototransistors with ultrahigh gain. *Nature Nanotechnology*, 7(6), 363-368.
- 111 Stankovich, S., Dikin, D. A., Dommett, G. H., Kohlhaas, K. M., Zimney, E. J., Stach, E. A., Piner, R. D., Nguyen, S. T. and Ruoff, R. S. (2006). Graphene-based composite materials. *Nature*, 442(7100), 282-286.
- 112 Ramanathan, T., Abdala, A. A., Stankovich, S., Dikin, D. A., Herrera-Alonso, M., Piner, R. D., Adamson, D. H., Schniepp, H. C., Chen, X., Ruoff, R. S., Nguyen, S. T., Aksay, I. A., Prud'homme, R. K. and Brinson, L. C. (2008). Functionalized graphene sheets for polymer nanocomposites. *Nature Nanotechnology*, 3(6), 327-331.
- 113 Kim, H., Abdala, A. A. and Macosko, C. W. (2010). Graphene/polymer nanocomposites. *Macromolecules*, 43(16), 6515-6530.
- 114 Potts, J. R., Dreyer, D. R., Bielawski, C. W. and Ruoff, R. S. (2011). Graphene-based polymer nanocomposites. *Polymer*, 52(1), 5-25.
- 115 Wang, Y., Li, Z., Wang, J., Li, J. and Lin, Y. (2011). Graphene and graphene oxide: biofunctionalization and applications in biotechnology. *Trends in Biotechnology*, 29(5), 205-212.
- 116 Liu, J., Li, Y., Li, Y., Li, J. and Deng, Z. (2010). Noncovalent DNA decorations of graphene oxide and reduced graphene oxide toward water-soluble metal-carbon hybrid nanostructures via self-assembly. *Journal of Materials Chemistry*, 20(5), 900-906.
- 117 Mohanty, N., Fahrenholtz, M., Nagaraja, A., Boyle, D. and Berry, V. (2011). Impermeable graphenic encasement of bacteria. *Nano Letters*, 11(3), 1270-1275.
- 118 Kempaiah, R., Salgado, S., Chung, W. L. and Maheshwari, V. (2011). Graphene as membrane for encapsulation of yeast cells: protective and electrically

conducting. *Chemical Communications*, 47(41), 11480-11482.

- 119 Some, S., Gwon, A-R., Hwang, E., Bahn, G-H., Yoon, Y., Kim, Y., Kim, S-H., Bak, S., Yang, J., Jo, D-G. and Lee, H. (2014). Cancer Therapy Using Ultrahigh Hydrophobic Drug-Loaded Graphene Derivatives. *Scientific Reports*, 4.
- 120 Zhang, L., Xia, J., Zhao, Q., Liu, L. and Zhang, Z. (2010). Functional graphene oxide as a nanocarrier for controlled loading and targeted delivery of mixed anticancer drugs. *Small*, 6(4), 537-544.
- 121 Yang, X., Zhang, X., Ma, Y., Huang, Y., Wang, Y. and Chen, Y. (2009). Superparamagnetic graphene oxide-Fe₃O₄ nanoparticles hybrid for controlled targeted drug carriers. *Journal of Materials Chemistry*, 19(18), 2710-2714.
- 122 Yang, X., Wang, Y., Huang, X., Ma, Y., Huang, Y., Yang, R., Duan, H. and Chen, Y. (2011). Multi-functionalized graphene oxide based anticancer drug-carrier with dual-targeting function and pH-sensitivity. *Journal of Materials Chemistry*, 21(10), 3448-3454.
- 123 Bao, H., Pan, Y., Ping, Y., Sahoo, N. G., Wu, T., Li, L., Li, J. and Gan, L. H. (2011). Chitosan-Functionalized Graphene Oxide as a Nanocarrier for Drug and Gene Delivery. *Small*, 7(11), 1569-1578.
- 124 Liu, K., Zhang, J. J., Cheng, F. F., Zheng, T. T., Wang, C. and Zhu, J. J. (2011). Green and facile synthesis of highly biocompatible graphene nanosheets and its application for cellular imaging and drug delivery. *Journal of Materials Chemistry*, 21(32), 12034-12040.
- 125 Mohanty, N. and Berry, V. (2008). Graphene-based single-bacterium resolution biodevice and DNA transistor: interfacing graphene derivatives with nanoscale and microscale biocomponents. *Nano Letters*, 8(12), 4469-4476.
- 126 Stankiewicz, A.I. and Mouljijn, J. A. (2000). Process intensification: transforming chemical engineering. *Chemical Engineering Progress*, 96(1), 22-34.
- 127 Glasnov, T. N. and Kappe, C. O. (2011). The Microwave-to-Flow Paradigm: Translating High-Temperature Batch Microwave Chemistry to Scalable Continuous-Flow Processes. *Chemistry-A European Journal*, 17(43), 11956-11968.
- 128 Marjanovic, O., Lennox, B., Sandoz, D., Smith, K. and Crofts, M. (2006). Real-time monitoring of an industrial batch process. *Computers & Chemical Engineering*, 30(10), 1476-1481.
- 129 Jachuck, R. J. J. and Ramshaw, C. (1994). Process intensification: heat transfer characteristics of tailored rotating surfaces. *Heat Recovery Systems and CHP*,

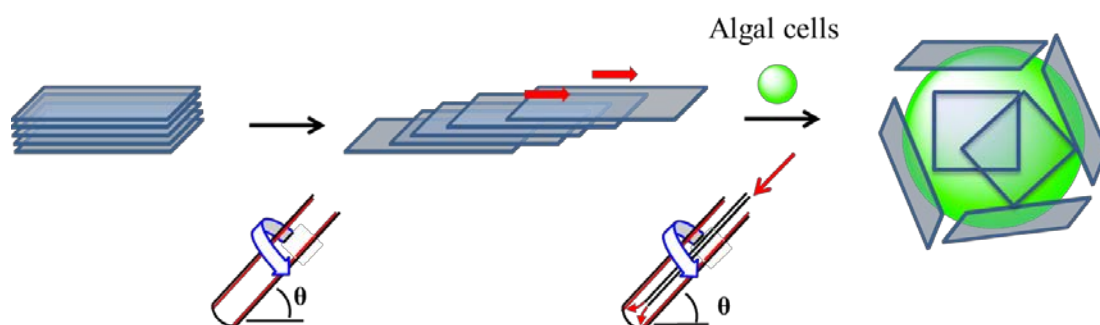
14(5), 475-491.

- 130 Aoune, A. and Ramshaw, C. (1999). Process intensification: heat and mass transfer characteristics of liquid films on rotating discs. *International Journal of Heat and Mass Transfer*, 42(14), 2543-2556.
- 131 Boodhoo, K. V. and Al-Hengari, S. R. (2012). Micromixing Characteristics in a Small-Scale Spinning Disk Reactor. *Chemical Engineering & Technology*, 35(7), 1229-1237.
- 132 Lodhar, H. and Jachuck, R. J. J. (2007, November). Intensified biodiesel reaction using continuous rotating tube reactor technology. In Proceedings of the AIChE Annual Meeting, Salt Lake City, USA.
- 133 Lodha, H., Jachuck, R. and Suppiah Singaram, S. (2012). Intensified biodiesel production using a rotating tube reactor. *Energy & Fuels*, 26(11), 7037-7040.
- 134 Chen, X., Smith, N. M., Iyer, K. S. and Raston, C. L. (2014). Controlling nanomaterial synthesis, chemical reactions and self-assembly in dynamic thin films. *Chemical Society Reviews*, 43(5), 1387-1399.
- 135 Raston, C. L. (2011). U.S. Patent Application 13/823,531.
- 136 Chen, X., Dobson, J. F. and Raston, C. L. (2012). Vortex fluidic exfoliation of graphite and boron nitride. *Chemical Communications*, 48(31), 3703-3705.
- 137 Wahid, M. H., Eroglu, E., Chen, X., Smith, S. M. and Raston, C. L. (2013). Functional multi-layer graphene–algae hybrid material formed using vortex fluidics. *Green Chemistry*, 15(3), 650-655.
- 138 Bennetts, D. A. and Hocking, L. M. (1973). On nonlinear Ekman and Stewartson layers in a rotating fluid. Proceedings of the Royal Society of London. A. *Mathematical and Physical Sciences*, 333(1595), 469-489.
- 139 Yasmin, L., Chen, X., Stubbs, K. A. and Raston, C. L. (2013). Optimising a vortex fluidic device for controlling chemical reactivity and selectivity. *Scientific reports*, 3.
- 140 Yasmin, L., Coyle, T., Stubbs, K. A. and Raston, C. L. (2013). Stereospecific synthesis of resorcin [4] arenes and pyrogallol [4] arenes in dynamic thin films. *Chemical Communications*, 49(93), 10932-10934.
- 141 Yasmin, L., Stubbs, K. A. and Raston, C. L. (2014). Vortex fluidic promoted Diels–Alder reactions in an aqueous medium. *Tetrahedron Letters*, 55(14), 2246-2248.

- 142 Yasmin, L., Eggers, P. K., Skelton, B. W., Stubbs, K. A. and Raston, C. L. (2014). Thin film microfluidic synthesis of fluorescent highly substituted pyridines. *Green Chemistry*, 16(7), 3450-3453.
- 143 Gandy, M. N., Raston, C. L. and Stubbs, K. A. (2014). Towards aryl C–N bond formation in dynamic thin films. *Organic & Biomolecular Chemistry*.
- 144 Britton, J. and Raston, C. L. (2014). Continuous flow vortex fluidic production of biodiesel. *RSC Advances*, 4(91), 49850-49854.
- 145 Britton, J. and Raston, C. L. (2015). Rapid high conversion of high free fatty acid feedstock into biodiesel using continuous flow vortex fluidics. *RSC Advances*, 5(3), 2276-2280.
- 146 Yasin, F. M., Boulos, R. A., Hong, B. Y., Cornejo, A., Iyer, K. S., Gao, L., Chua, H. T. and Raston, C. L. (2012). Microfluidic size selective growth of palladium nano-particles on carbon nano-onions. *Chemical Communications*, 48(81), 10102-10104.
- 147 Yasin, F. M., Iyer, K. S. and Raston, C. L. (2013). Palladium nano-carbon-calixarene based devices for hydrogen sensing. *New Journal of Chemistry*, 37(10), 3289-3293.
- 148 Chen, X., Yasin, F. M., Eggers, P. K., Boulos, R. A., Duan, X., Lamb, R. N., Iyer, K. S. and Raston, C. L. (2013). Non-covalently modified graphene supported ultrafine nanoparticles of palladium for hydrogen gas sensing. *RSC Advances*, 3(10), 3213-3217.
- 149 Goh, Y. A., Chen, X., Yasin, F. M., Eggers, P. K., Boulos, R. A., Wang, X., Chua, H. T. and Raston, C. L. (2013). Shear flow assisted decoration of carbon nano-onions with platinum nanoparticles. *Chemical Communications*, 49(45), 5171-5173.
- 150 Boulos, R. A., Zhang, F., Tjandra, E. S., Martin, A. D., Spagnoli, D. and Raston, C. L. (2014). Spinning up the polymorphs of calcium carbonate. *Scientific reports*, 4.
- 151 Tong, C. L., Boulos, R. A., Yu, C., Iyer, K. S. and Raston, C. L. (2013). Continuous flow tuning of ordered mesoporous silica under ambient conditions. *RSC Advances*, 3(41), 18767-18770.
- 152 Vimalanathan, K., Chen, X. and Raston, C. L. (2014). Shear induced fabrication of intertwined single walled carbon nanotube ring. *Chemical Communications*.
- 153 Eroglu, E., D'Alonzo, N. J., Smith, S. M. and Raston, C. L. (2013). Vortex fluidic entrapment of functional microalgal cells in a magnetic polymer matrix. *Nanoscale*, 5(7), 2627-2631.

- 154 Wahid, M. H., Eroglu, E., Chen, X., Smith, S. M. and Raston, C. L. (2013). Entrapment of *Chlorella vulgaris* cells within graphene oxide layers. *RSC Advances*, 3(22), 8180-8183.
- 155 Wahid, M. H., Eroglu, E., LaVars, S. M., Newton, K., Gibson, C. T., Stroehrer, U. H., Chen, X., Boulos, R. A., Raston, C. L. and Harmer, S. -L. (2015). Microencapsulation of bacterial strains in graphene oxide nano-sheets using vortex fluidics. *RSC Advances*, 5, 37424-37430.
- 156 Yuan, T. Z., Ormonde, C. F. G., Kudlacek, S. T., Kunche, Sameeran, Smith, J. N., Brown, W. A., Pugliese, K. M., Olsen, T. J., Iftikhar, M., Raston, C. L., and Weiss, G. A. (2015). Shear-Stress-Mediated Refolding of Proteins from Aggregates and Inclusion Bodies. *ChemBioChem*, 16(3), 393-396.
- 157 Stankiewicz, A. I. and Moulijn, J. A. (2000). Process intensification: transforming chemical engineering. *Chemical Engineering Progress*, 96(1), 22-34.
- 158 Leighton, T. (1994). The acoustic bubble. Academic press.
- 159 Young, F. R. Cavitation. McGraw-Hill, London (1989) pp. 1-418.
- 160 Leong, T., Ashokkumar, M. and Kentish, S. (2011). The fundamentals of power ultrasound—a review. *Acoustics Australia*, 39(2), 54-63.
- 161 Suslick, K. S. and Price, G. J. (1999). Applications of ultrasound to materials chemistry. *Annual Review of Materials Science*, 29(1), 295-326.
- 162 Khan, U., Porwal, H., O'Neill, A., Nawaz, K., May, P. and Coleman, J. N. (2011). Solvent-exfoliated graphene at extremely high concentration. *Langmuir*, 27(15), 9077-9082.

2. PREPARATION OF FUNCTIONAL MULTI-LAYER GRAPHENE-ALGAE HYBRID MATERIAL USING VORTEX FLUIDICS



This chapter is a reformatted version of the paper published in *Green Chemistry*, Year 2013, Vol. 15, Pages 650-655.

2.1 Abstract

Dynamic thin films confined in a microfluidic platform are effective in exfoliating graphite in water and then decorating the multi-layer 2D sheets on the surface of microalgal cells. The overall process incorporates green chemistry principles in using naturally available resources, namely algae and graphite, and using water as a benign reaction medium. Furthermore, the nanobio hybrid material is active for wastewater treatment, in removing all traces of nitrate from liquid effluents, more efficiently than the pristine microalgal cells, with the multi-layer graphene itself not showing any significant nitrate removal.

2.2 Introduction

There is a growing global concern for the need to develop low cost processing techniques with small footprints for facile and precise fabrication of end products which are more environmentally friendly. Also of equal importance is the use of renewable and benign materials and reaction media. In this study we report on the use of vortex fluidics for the exfoliation of multi-layered graphene sheets from graphite in water and their hybridization with algae using the same platform, the overall process incorporating sustainability/green chemistry principles at the inception of the research.

Biological systems display complex and intelligent mechanisms necessary for sustaining the organisms, and mimicking such systems or direct usage of the organisms feature in various applications. Algae are abundant in Nature and are attracting much interest in a variety of applications, as renewables for developing sustainable green technologies for the future. Depending on the species, algae have several uses as nutrient supplements [1], and in bioenergy production [2,3], biosensor applications [4], wastewater treatment [5], and CO₂ mitigation [6].

A number of research studies have reported on the intriguing properties acquired as a result of hybridization of materials with biological microorganisms. For instance, deposition of gold nanorods on bacteria forms highly conducting hybrid systems [7], and hybridization of algae with silica features in electrochemical sensors [8]. Graphene has remarkable properties, including high electrical conductivity,

transparency, high thermal stability and high strength [9], and these are being exploited in various application, as are the properties of hybrid materials, as mixtures of materials with graphene, and this includes organisms [10,11]. Graphene has been interfaced with bacteria [10] and yeast cells [11], with the hybrid materials effective in sensor technology. For instance, hybrid graphene-yeast cells are capable of distinguishing different types of alcohol based on the change of cell volume due to physiologically stressing with their exposure to these alcohols. This volume change response has been monitored as the electrical signal through graphene [11]. In addition, protein functionalized graphene has been used to encapsulate bacteria, which show high cell retention towards vacuum and enables wet-phase TEM imaging by protecting the intracellular volatile material and decreasing electrostatic charging [12]. Other types of hybrid material containing graphene include (i) coated particles of sulfur which have enhanced capacity and cycling stability of the cathode material for lithium-sulfur batteries [13], and (ii) coated nanoparticles of copper which protects the metal from oxidation [14]. Graphene has ultra-strong adhesion properties, which is attributed to its extreme flexibility allowing strong adhesion to the surface of the smoothest substrates with adhesion energies similar to solid-liquid adhesion energies [15]. Thus graphene has potential for adhesion to the surface of microalgal cells, possibly by the hydrophobic-hydrophobic surface interactions, and gaining access to a functional hybrid material is the focus of the present study. Microalgal cell walls contain polysaccharides, and the cell surface of *Chlorella* species is hydrophobic with negative surface charges [16-18].

Various methods to produce graphene sheets have been developed using either the top-down approach starting with graphite, as in micromechanical cleavage using the scotch tape method [19], ball milling [20], and sonication [21-22], or the bottom-up approach as in chemical vapor deposition [23,24], and solvothermal synthesis [25]. Recently we established the utility of a microfluidic platform vortex fluidic device (VFD) in exfoliating graphene sheets, and similarly hexagonal boron nitride in N-methyl pyrrolidone (NMP) [26]. The underlying feature of the VFD is its novel dynamic thin film regime which provides the intense shear for the exfoliation (Fig. 2.1) [26]. The graphene sheets produced by this method have minimal potential damage compared to graphene produced by sonication [26]. Several other nanomaterials and nanohybrid materials have also been prepared using similar

microfluidic devices, albeit for bottom up processing [27-30]. The present method is scalable, simple and environmentally friendly which is desirable for large scale production.

In the vortex fluidic device (VFD), as the tube rotates, a thin fluid film is formed on the wall of the tube. The average thickness of the film varies depending on the tilting angle (θ) and rotation speed. By increasing the rotation speed, intense shear occurs within the thin fluid film which arises from the interplay of gravitational and centrifugal forces, which has previously been successful in exfoliating graphene and boron nitride in N-methylpyrrolidone [26]. In this study, sample preparation involves a two-step processing: (i) exfoliation of graphite into multi-layer graphene (MLG) sheets in water, followed by (ii) hybridization with microalgal cells, using the same VFD, also in water.

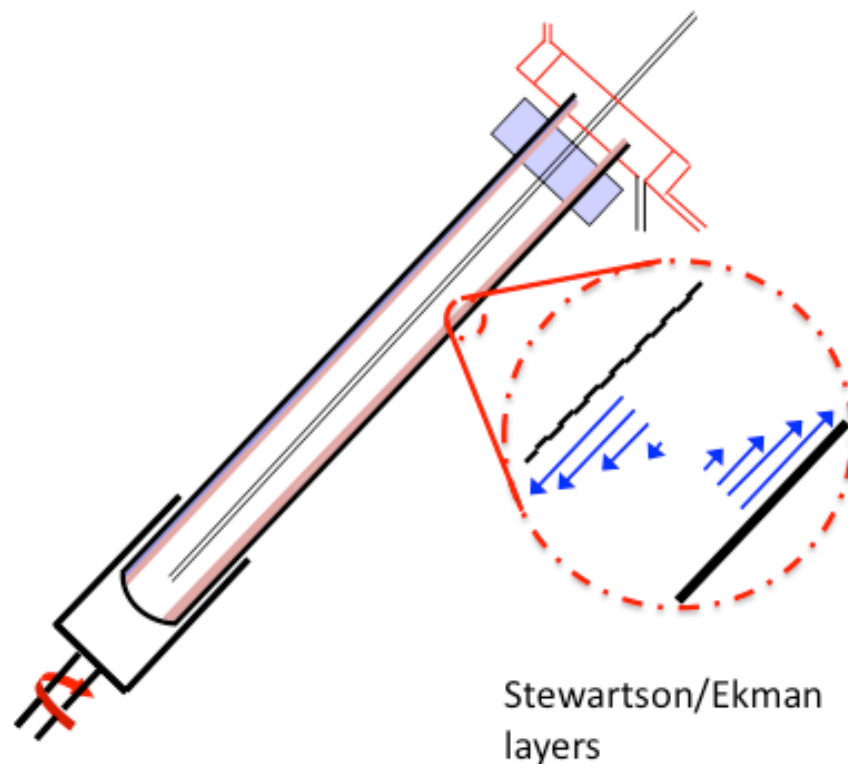


Figure 2.1. Cartoon showing the formation of a thin fluid film in the rapidly rotating tube of the VFD which has shearing force associated with the Stewartson-Ekman layers [31]. For continuous flow processing the liquid is directed to the bottom of the tube, through the central pipe.

2.3 Experimental methods

The overall process for the preparation of the material is given in Figure 2.2. Graphite flakes (7-10 μm in diameter) with a thickness in the range of a few hundred nanometers to 1 μm , were used as received from Alfa Aesar. The graphite was suspended in distilled water at a 1 mg/mL concentration. The 10 mm glass tubes used for the VFD process were sterilized with ethanol followed by drying prior to each experiment.

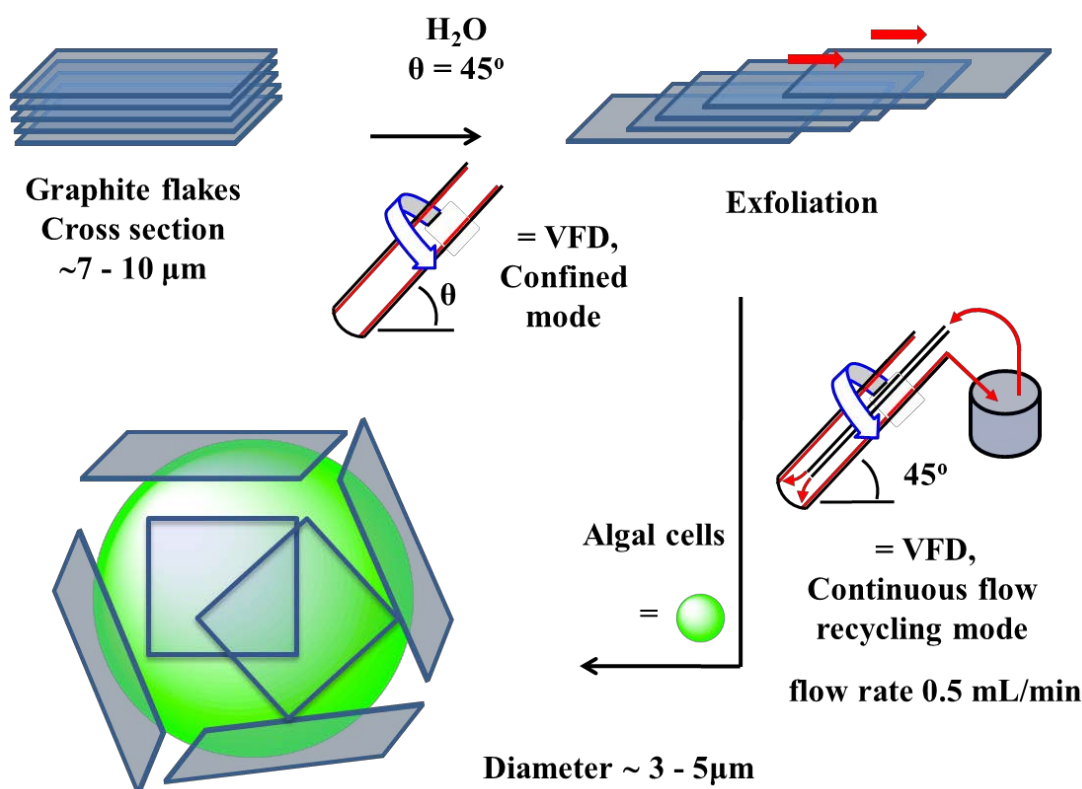


Figure 2.2. Schematic illustration of the overall hybridization process, involving the exfoliation of graphite flakes into multi-layer graphene sheets followed by the hybridization of these sheets with algal cells using a VFD; each sheet represents ≥ 5 layers of graphene.

For the exfoliation of MLG, the rotating speed was set at 7000 rpm with an inclination angle at 45° under confined mode. 1 mL of this MLG solution was then mixed with 1 mL of microalgal solution, followed by addition of 5 mL of sterilized algal growth media [32] during continuous VFD processing. For the SEM imaging, algal growth media was replaced with sterilized water ($d\text{H}_2\text{O}$) in order to avoid the presence of salts that can interfere with the imaging. While maintaining the continuous VFD processing for 30 minutes, the rotation speed for algal wrapping

was carried out at 5000 rpm and 7000 rpm respectively. Mixture was recirculated and delivered through feed jets with a flow rate of 1 mL / min. Inoculated algae cultures had an initial cell culture with a total chlorophyll content of around 4 mg/L. Wild type *Chlorella vulgaris* (Australian National Algae Culture Collection, CSIRO) was used as the microalgae source. Algal growth was carried out under the artificial illumination (16 h light/ 8 h dark cycle) at 25 °C, inside glass flasks upon orbital shaking (Thermoline Scientific) at 120 rpm. Viability test were done by using fluorescence microscopy and also by conducting spectrophotometric analysis of the chlorophyll content. The cell imaging were carried out under bright field and under fluorescence by using an upright fluorescence microscope (Olympus BX61) with Texas-Red filters having laser excitation wavelengths at 545-580 nm and emission wavelengths of 610 nm. Both bright field and fluorescence images were captured using Cell^R imaging software. Total chlorophyll content (Chl a + Chl b) was investigated by the spectrophotometric measurements of the methanol extracts obtained from the known amount of algal culture pellets [38]. SEM studies were carried out using Zeiss 1555 VP-FESEM with an accelerating voltage differing between 3-5 kV. SEM samples were coated with 3 nm Pt films. TEM studies were performed using JEOL 2100 operating at 120 keV. AFM images were recorded on Digital Instruments Dimension 3000 with a Nanoscope IIIa controller under tapping mode, using silicon cantilevers. Samples were drop cast onto freshly cleaved mica and left for drying. Raman spectra were collected with a Dilor Labram 1B dispersive Raman spectrometer using an excitation wavelength of 633 nm and laser power of 2 mW. The “cadmium reduction method” was used for the nitrate analysis, using chemical-kits in the form of powder pillows (HACH[®], NitraVer Nitrate Reagent) and a colorimeter (HACH[®] DR/870) [42]. The nitrate analysis was performed for three independent experiments and error bars were calculated based on the deviation from the mean value.

2.4 Results and discussion

Scanning electron microscopy (SEM) and transmission electron microscopy (TEM) images of exfoliated MLG sheets produced using VFD are shown in Figure 2.3. While exfoliation of graphene in NMP is favored by the surface tension of the solvent [26], exfoliation in water is also effective, although the material is mainly in

the form of multiple layers of graphene.

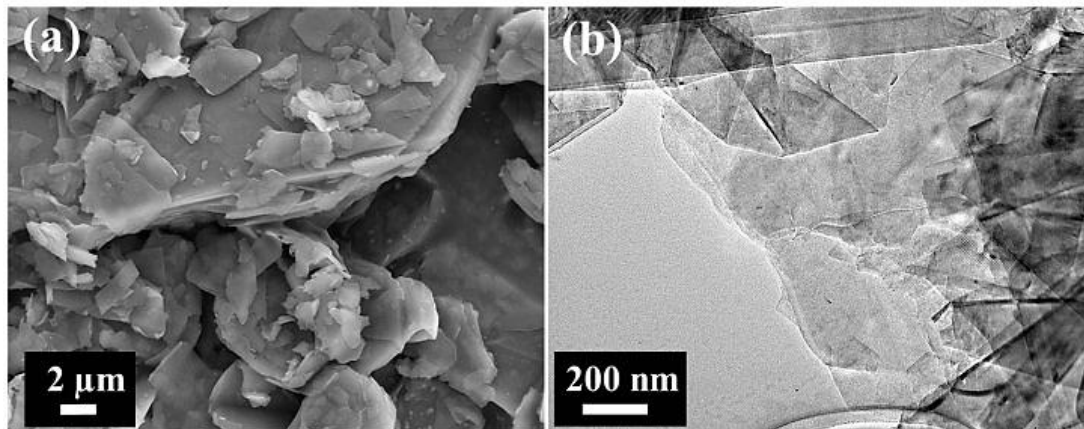
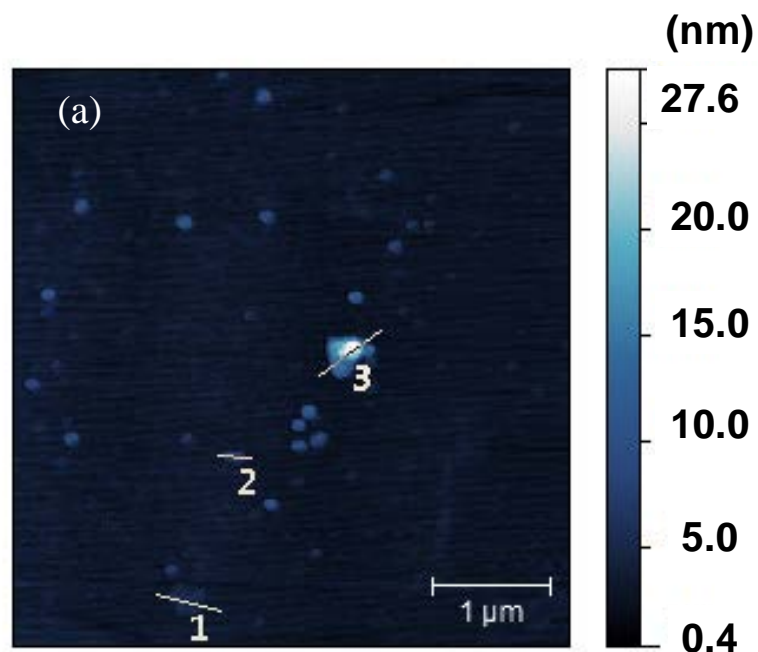


Figure 2.3. SEM and (b) TEM images of exfoliated MLG sheets obtained in water using the VFD.

Atomic force microscopy (AFM) analysis in tapping mode was carried out to investigate the thickness of the exfoliated sheets. AFM results revealed the existence of sheets as thin as ~1 nm albeit with majority existence of thicker sheets (> 20 nm) (Fig. 2.4). Herein, the use of NMP during the exfoliation process was avoided to reduce any negative effect of residual NMP on the viability of the cells. The MLG sheets obtained in water formed a hybrid material with algal cells, which enhanced the removal of nitrate from liquid effluents (Fig. 2.7).



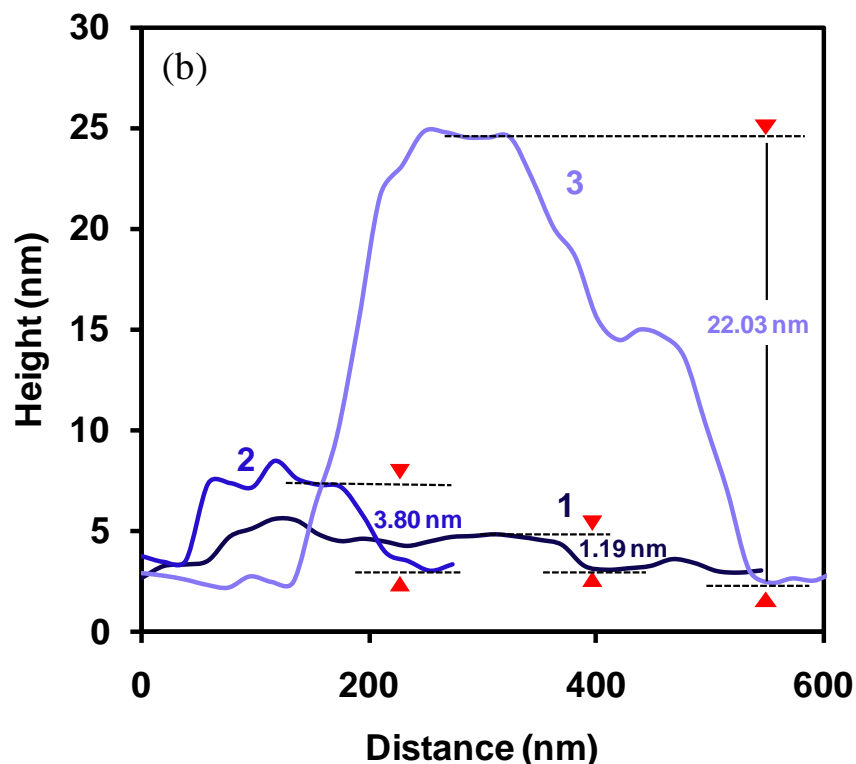


Figure 2.4. (a) AFM image of exfoliated MLG sheets obtained in water using VFD and (b) height profiles of the selected area in (a)

Raman spectroscopy was carried out to investigate the surface properties (i.e. defects and oxidation) of graphene sheets [33]. The characteristic peaks of graphite are present (Fig. 2.5) with the peak associated with the defects, the D band, is similar to unprocessed graphite, and thus the VFD processing results in minimum defects in exfoliating the material. For oxidized graphite, a broader G and D bands with higher relative intensity appears [34]. In addition Raman spectroscopy can also distinguish a monolayer graphene from bilayer and few layers (less than 5) by observing the G' band (also termed as the 2D band) [35]. For a monolayer, the 2D band profile appears as a single sharp peak about 4 times more intense than the G peak and this peak becomes broader as the number of layers, being hardly distinguishable from bulk graphite for 5 layers [35]. Thus, it can be concluded that the exfoliated sheets obtained using the VFD, for which the Raman has the same 2D peak as bulk graphite, are ≥ 5 layers thick (Fig. 2.5). This is also in accordance with results from SEM, TEM and AFM studies.

Autofluorescence of microalgae cells was used for evaluating the viability of cultures

after the VFD processing. Fluorescence microscopy employed an excitation filter around 540 nm which is near the Soret band maximum absorption of algal chlorophyll b [36,37]. Figure 2.6 shows the bright field and fluorescence microscopy images of microalgae cells processed at different VFD speeds. The red fluorescence of algal cultures (Fig. 2.6, right hand side of each pair) indicates that the cultures are mostly alive, and majority of them kept their integrity even at high VFD speeds. The functionalities of these VFD processed cells are also demonstrated with their cellular growth data (see below). After confirming the viability of the cells, two speeds were used for the VFD processing for hybridization of microalgae cells, 5000 and 7000 rpm.

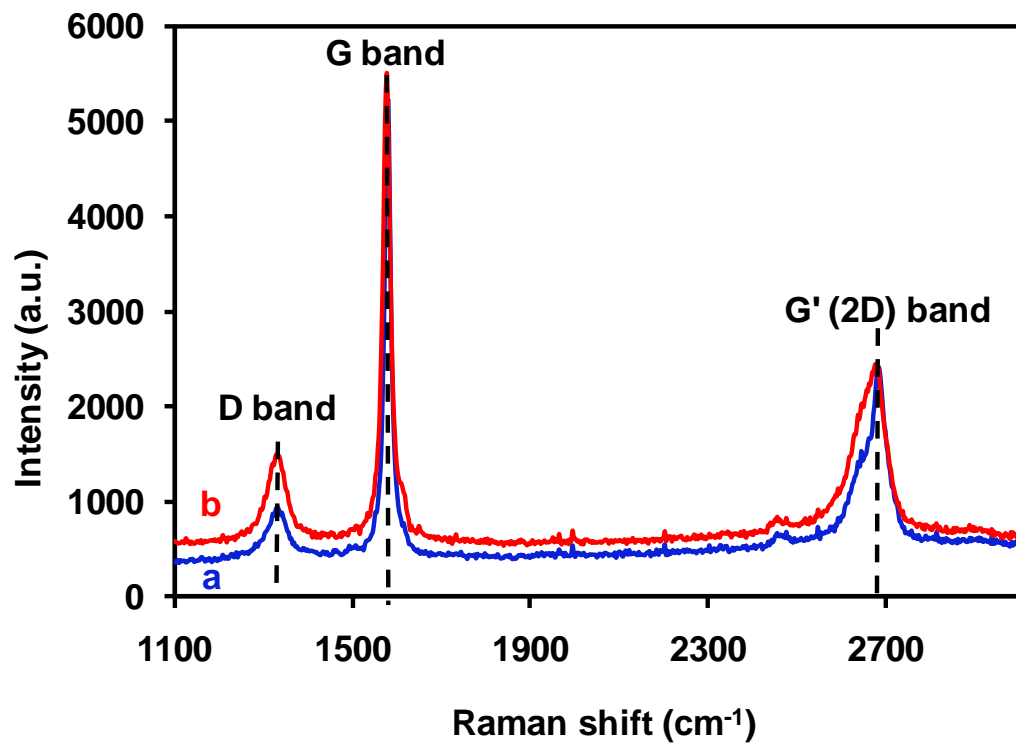


Figure 2.5. Raman spectroscopy of graphite flakes (a) before, and (b) after VFD processing.

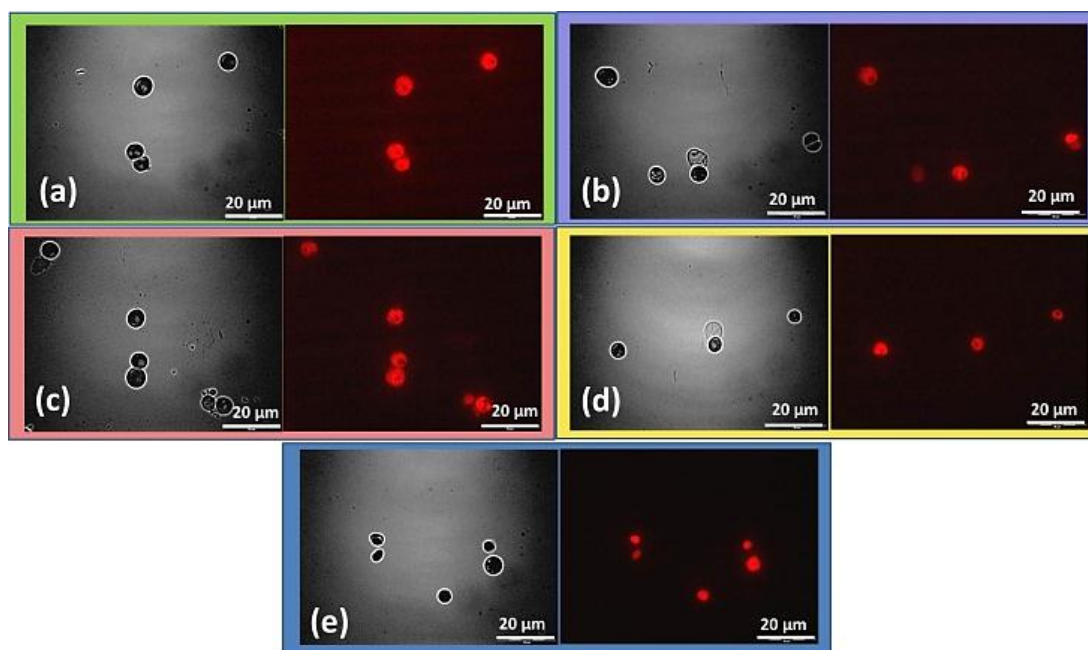


Figure 2.6. Bright field and fluorescence microscopy images using Texas-Red filters for microalgae cells processed under various VFD speeds, (a) 2000 rpm, (b) 4000 rpm, (c) 6000 rpm, (d) 8000 rpm, and (e) 9000 rpm. Note the autofluorescence of “chlorophyll b” in microalgae cells. Scale bars: 20 μm .

SEM images of free algae and algae-MLG hybrid samples were recorded and compared below. As observed in Figure 2.7 (a and b), the expected smooth surface images of free algae samples are evident. Images of hybridized samples (Fig. 2.7c and d) display the attachment of sheet-like materials on the surface of the cells thus suggesting that the algae are successfully decorated with a layered arrangement of graphene and MLG previously exfoliated from the graphite. Algae mixed with graphene without using VFD (Fig. 2.7e and f) establish that the graphene sheets are not well adhered to the algal cell wall compared to the samples prepared using VFD.

Accumulation of the total chlorophyll pigment (Chl a and b) as a function of growth time was monitored to determine the viability of the free and hybrid cells after VFD processing (Fig. 2.8). Both free and algae-MLG hybrid samples were grown in the algal growth media. Chlorophyll content was investigated using spectrophotometric measurements for methanol extracts obtained from the culture pellets [38]. As given in Fig. 2.8, hybrid cells show relatively similar growth patterns with their free counterparts. Slightly higher growth was observed for the free cells, which is consistent with their cellular surfaces being devoid of any boundary material, *i.e.*

allowing unrestricted cellular division relative to the hybrid cells. Nevertheless, even with MLG on the algae cell wall, the cells were still functional for their replication, and the MLG sheets had nonlethal effects on microalgal cell cultures at $\sim 0.14 \text{ mg L}^{-1}$ in the final mixture of MLG and algae and culture solution. The ease of replication of the cells in the hybrid material also shows that microalgal cell surfaces are decorated with MLG sheets rather than being completely immobilized within them. The graphene-algae mixture prepared without using VFD (Fig. 2.8, grey spheres) has a similar growth curve relative to the algae-only samples, indicating minimal adhesion of the MLG to the surface of the cells.

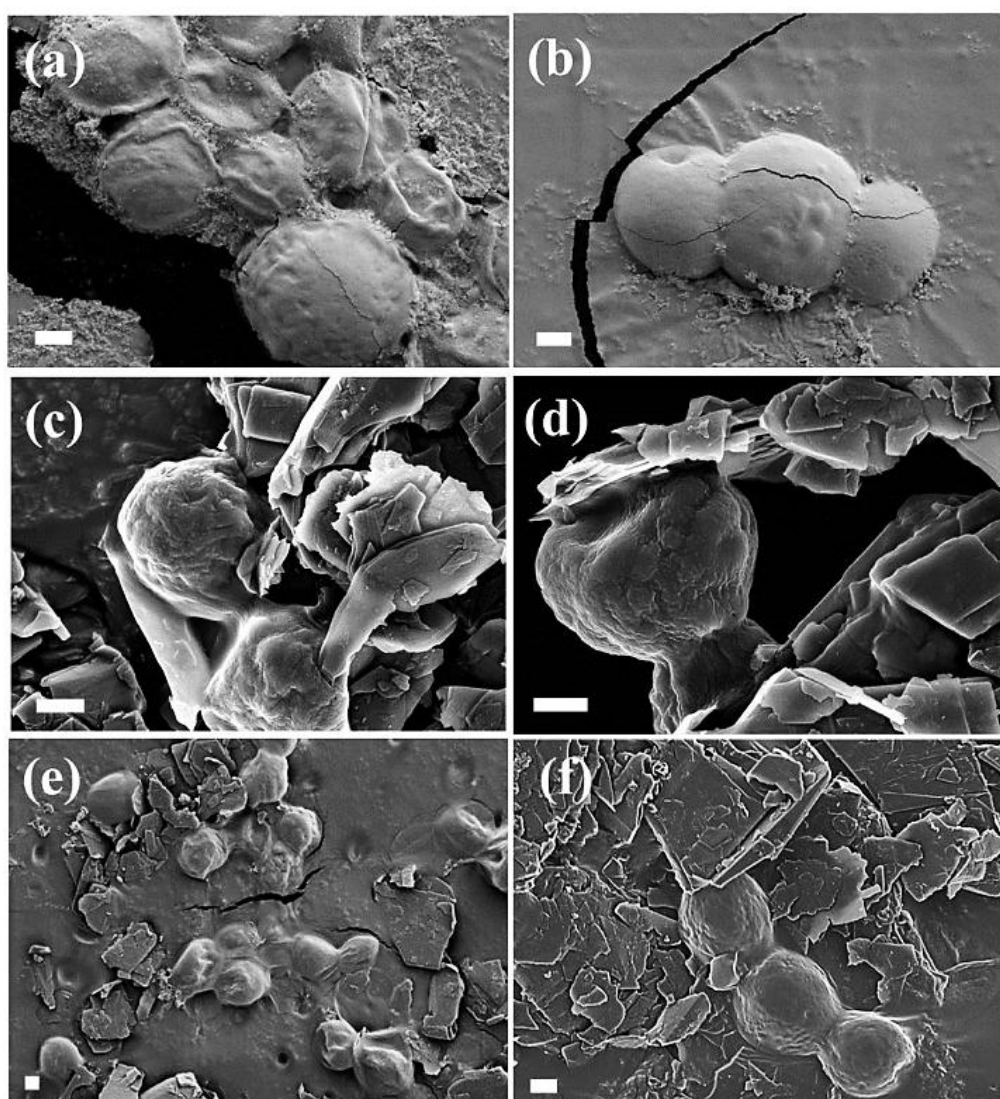


Figure 2.7. SEM images of pristine microalgae after processing in the VFD at (a) 5000 rpm, and (b) 7000 rpm; (c) algae-graphene hybrid samples processed at 5000 rpm, and (d) 7000 rpm; (e-f) algae and MLG mixed without VFD process. Scale bars: 1 μm .

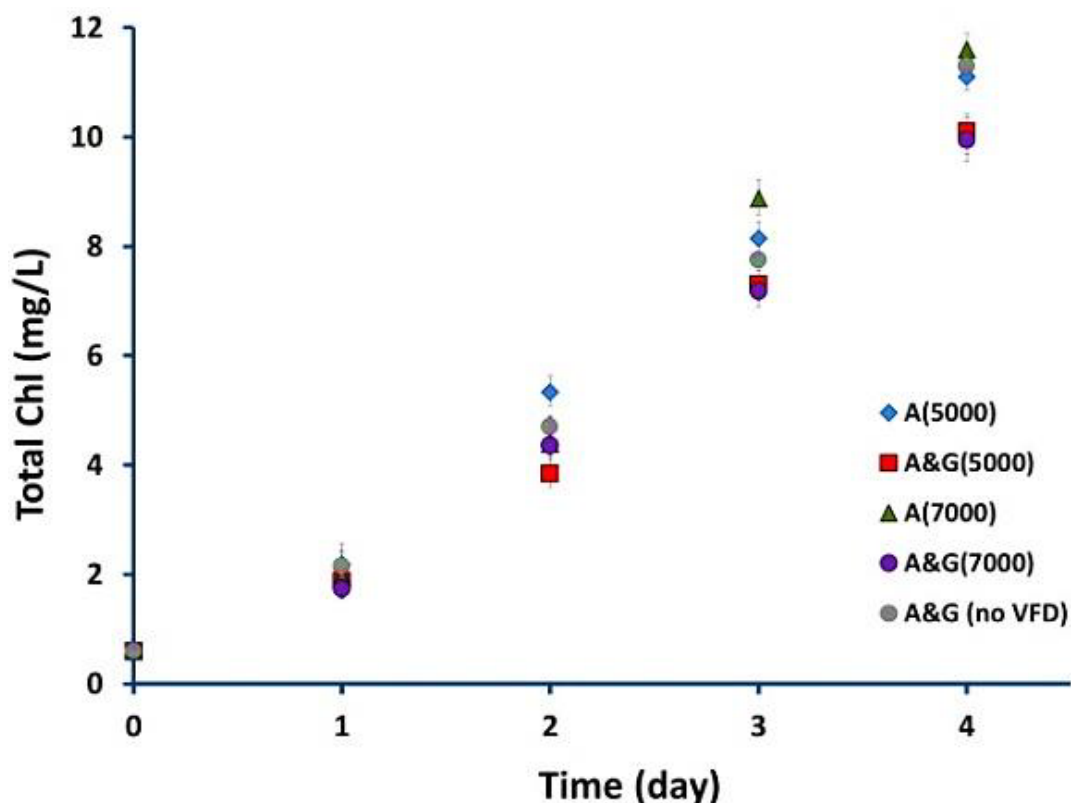


Figure 2.8. Total chlorophyll (Chl *a* + Chl *b*) content measured as a function of growth time MLG coated (red rectangles for 5000 rpm and purple spheres for 7000 rpm); uncoated free *C. vulgaris* cells (blue diamonds for 5000 rpm and green triangles for 7000 rpm); and MLG-algae mixture without VFD processing (grey spheres).

Graphene has a high sorption capacity being effective in the removal of organic or inorganic compounds, and heavy metals [39-41]. The hybrid materials composed of microalgae and MLG sheets synthesized directly from graphite flakes were used as adsorbents for the removal of nitrate ions from aqueous solutions. Figure 2.9 shows the nitrate-nitrogen (NO_3^- -N) concentration *versus* time for the free algae cells, MLG-algae hybrid material after VFD processing, and MLG-algae mixture without VFD. NO_3^- -N is an important environmental parameter showing the amount of nitrogen in liquid solutions resulting from the nitrate ions (NO_3^-) [17]. Algal cells naturally uptake nitrates for use in their cellular metabolism [17]. After the hybridization of MLG sheets with *C. vulgaris* cells, nitrate removal of the hybrid cells was enhanced relative to their free counterparts. The nitrate content of the initial liquid mixture ($[\text{NO}_3^-\text{-N}]_{\text{initial}} \sim 26 \text{ mg L}^{-1}$) was consumed completely within four days by the MLG-algae hybrids whereas this was longer for the free cultures and MLG-algae mixture without using the VFD. While MLG sheets themselves did

not result in a significant amount of nitrate reduction (~14%), the hybrid with microalgal cells after VFD processing was effective in removing nitrate, while being nontoxic to the cultures.

For free algal cells, the rate of nitrate removal was nearly linear throughout the entire process at $\sim 5.5 \text{ mg L}^{-1} \text{ d}^{-1}$. In contrast, the rate of removal of nitrate by the algae-MLG biohybrid after VFD processing was significantly higher at $\sim 9 \text{ mg L}^{-1} \text{ d}^{-1}$ within the first two days, reducing to $\sim 5 \text{ mg L}^{-1} \text{ d}^{-1}$ thereafter. A similar pattern was also observed for the MLG and algae mixture without VFD processing, where the overall nitrate removal rate was $\sim 7 \text{ mg L}^{-1} \text{ d}^{-1}$ within the first two days followed by $4.5 \text{ mg L}^{-1} \text{ d}^{-1}$. The enhancement of nitrate removal phenomenon at the initial stages mostly relates to the physicochemical adsorption of the MLG sheets, for then acting as a conduit to the attached algal cell. The adsorption of nitrate ions is likely to occur at the defect sites of the graphene sheets as reported by Eroglu *et al.* [43]. Further interactions between graphene and algae which leads to the enhancement of nitrate removal is extremely interesting and requires more investigation. Interestingly there was no significant difference in the growth of algal (Fig. 2.8) or nitrate removal (Fig. 2.9) by varying the speeds of the VFD in processing either the free or forming the biohybrid.

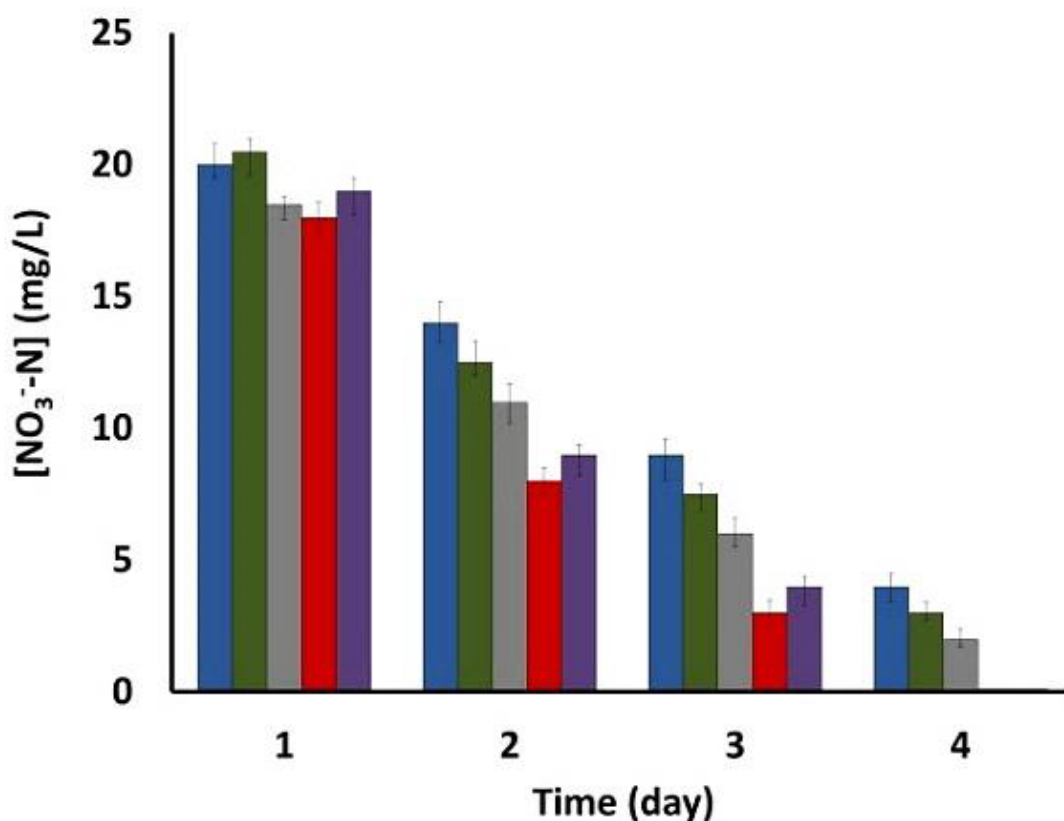


Figure 2.9. Nitrate-nitrogen (NO_3^- -N) concentration (mg/L) of liquid medium versus time. Free algal cells after VFD processing at 5000 rpm and 7000 rpm are represented with blue and green columns, respectively. MLG-hybrid algal cells after VFD processing at 5000 rpm and 7000 rpm are given as red and purple columns, respectively. MLG and algae without VFD processing is shown in grey.

2.5 Conclusions

In summary we have established a simple process for fabricating a hybrid material composed of MLG and microalgae cells by using a vortex fluidic device. The applicability of this hybrid material for the nitrate removal has been demonstrated with complete removal of initial nitrate content within four days, with an improved removal rate compared to their free cell counterparts, MLG-algae mixture without VFD, and MLG alone. The nontoxic nature of MLG for microalgae cells was also established. Even though various biohybrid materials have been previously reported, hybridization of algae cells with graphene in general is without precedent. Dynamic thin film processing where intense shearing forces facilitates the exfoliation of graphite into MLG in water, is also without precedent, and the high surface energy of the hydrophobic material in water readily attaches to the hydrophobic surface of the

cells using the VFD. In addition, this simple processing technique provides a simple control on processing parameters such as temperature, rotation speed, flow rate and others which can be attractive for larger scale productions. This technique can also find further applications for the exfoliation of several laminar materials and their subsequent hybridization with various microorganisms.

2.6 Acknowledgements

We would like to acknowledge the support of the Australian Research Council for this research. SEM analyses were carried out using the facilities in the Centre for Microscopy, Characterization and Analysis (CMCA), The University of Western Australia. Raman analyses were performed at Curtin University. M.H. Wahid and X. Chen would like to thank the Malaysian Government and China Scholarship Council for their PhD research scholarships, respectively.

2.7 References

- 1 Spolaore, P., Joannis-Cassan, C., Duran, E. and Isambert, A. (2006). Commercial applications of microalgae. *Journal of bioscience and bioengineering*, 101(2), 87-96.
- 2 Beer, L. L., Boyd, E. S., Peters, J. W. and Posewitz, M. C. (2009). Engineering algae for biohydrogen and biofuel production. *Current opinion in biotechnology*, 20(3), 264-271.
- 3 Eroglu, E. and Melis, A. (2009). "Density equilibrium" method for the quantitative and rapid in situ determination of lipid, hydrocarbon, or biopolymer content in microorganisms. *Biotechnology and bioengineering*, 102(5), 1406-1415.
- 4 Nguyen-Ngoc, H. and Tran-Minh, C. (2007). Fluorescent biosensor using whole cells in an inorganic translucent matrix. *Analytica chimica acta*, 583(1), 161-165.
- 5 Hammouda, O., Gaber, A. and Abdelraouf, N. (1995). Microalgae and wastewater treatment. *Ecotoxicology and Environmental safety*, 31(3), 205-210.
- 6 Rooke, J. C., Léonard, A., Sarmiento, H., Meunier, C. F., Descy, J. P. and Su, B. L. (2011). Novel photosynthetic CO₂ bioconverter based on green algae entrapped in low-sodium silica gels. *Journal of Materials Chemistry*, 21(4), 951-959.

- 7 Berry, V., Gole, A., Kundu, S., Murphy, C. J. and Saraf, R. F. (2005). Deposition of CTAB-terminated nanorods on bacteria to form highly conducting hybrid systems. *Journal of the American Chemical Society*, 127(50), 17600-17601.
- 8 Darder, M., Aranda, P., Burgos-Asperilla, L., Llobera, A., Cadarso, V. J., Fernández-Sánchez, C. and Ruiz-Hitzky, E. (2010). Algae–silica systems as functional hybrid materials. *Journal of Materials Chemistry*, 20(42), 9362-9369.
- 9 Chen, H., Müller, M. B., Gilmore, K. J., Wallace, G. G. and Li, D. (2008). Mechanically strong, electrically conductive, and biocompatible graphene paper. *Advanced Materials*, 20(18), 3557-3561.
- 10 Mohanty, N. and Berry, V. (2008). Graphene-based single-bacterium resolution biodevice and DNA transistor: interfacing graphene derivatives with nanoscale and microscale biocomponents. *Nano Letters*, 8(12), 4469-4476.
- 11 Kempaiah, R., Chung, A. and Maheshwari, V. (2011). Graphene as cellular interface: Electromechanical coupling with cells. *ACS nano*, 5(7), 6025-6031.
- 12 Mohanty, N., Fahrenholtz, M., Nagaraja, A., Boyle, D. and Berry, V. (2011). Impermeable graphenic encasement of bacteria. *Nano letters*, 11(3), 1270-1275.
- 13 Wang, H., Yang, Y., Liang, Y., Robinson, J. T., Li, Y., Jackson, A., ... & Dai, H. (2011). Graphene-wrapped sulfur particles as a rechargeable lithium–sulfur battery cathode material with high capacity and cycling stability. *Nano letters*, 11(7), 2644-2647.
- 14 Luechinger, N. A., Athanassiou, E. K. and Stark, W. J. (2008). Graphene-stabilized copper nanoparticles as an air-stable substitute for silver and gold in low-cost ink-jet printable electronics. *Nanotechnology*, 19(44), 445201.
- 15 Koenig, S. P., Boddeti, N. G., Dunn, M. L. and Bunch, J. S. (2011). Ultrastrong adhesion of graphene membranes. *Nature nanotechnology*, 6(9), 543-546.
- 16 Kaplan, D., Christiaen, D. and Arad, S. M. (1987). Chelating properties of extracellular polysaccharides from *Chlorella* spp. *Applied and Environmental Microbiology*, 53(12), 2953-2956.
- 17 Eroglu, E., Agarwal, V., Bradshaw, M., Chen, X., Smith, S. M., Raston, C. L. and Iyer, K. S. (2012). Nitrate removal from liquid effluents using microalgae immobilized on chitosan nanofiber mats. *Green Chemistry*, 14(10), 2682-2685.
- 18 Hadjoudja, S., Deluchat, V. and Baudu, M. (2010). Cell surface characterisation of *Microcystis aeruginosa* and *Chlorella vulgaris*. *Journal of Colloid and Interface science*, 342(2), 293-299.

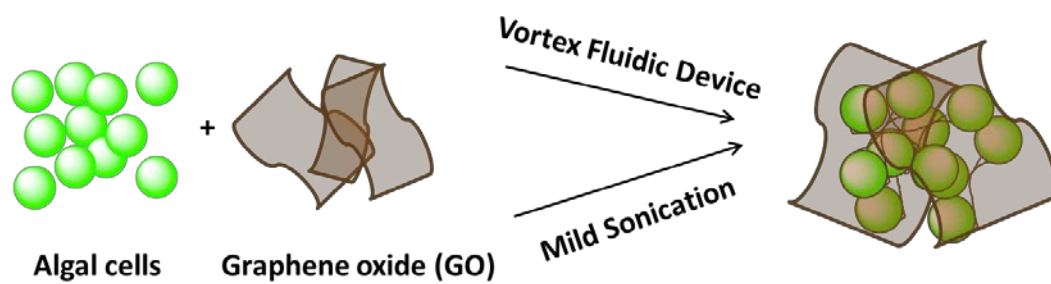
- 19 Novoselov, K. S., Geim, A. K., Morozov, S. V., Jiang, D., Zhang, Y., Dubonos, S. V., Grigorieva, I. V. and Firsov, A. A. (2004). Electric field effect in atomically thin carbon films. *Science*, 306(5696), 666-669.
- 20 Zhao, W., Fang, M., Wu, F., Wu, H., Wang, L. and Chen, G. (2010). Preparation of graphene by exfoliation of graphite using wet ball milling. *J. Mater. Chem.*, 20(28), 5817-5819.
- 21 Hernandez, Y., Nicolosi, V., Lotya, M., Blighe, F. M., Sun, Z., De, S., McGovern, I. T., Holland, B., Byrne, M., Gun'ko, Y. K., Boland, J. J., Niraj, P., Duesberg G., Krishnamurthy, S., Goodhue, R., Hutchison, J., Scardaci, V., Ferrari, A. C. and Coleman, J. N. (2008). High-yield production of graphene by liquid-phase exfoliation of graphite. *Nature Nanotechnology*, 3(9), 563-568.
- 22 Lotya, M., Hernandez, Y., King, P. J., Smith, R. J., Nicolosi, V., Karlsson, L. S., F. M. Blighe, S. De, Z. Wang, I. T. McGovern, G. S. Duesberg and Coleman, J. N. (2009). Liquid phase production of graphene by exfoliation of graphite in surfactant/water solutions. *Journal of the American Chemical Society*, 131(10), 3611-3620.
- 23 Reina, A., Jia, X., Ho, J., Nezich, D., Son, H., Bulovic, V., Dresselhaus, M. S. and Kong, J. (2008). Large area, few-layer graphene films on arbitrary substrates by chemical vapor deposition. *Nano Letters*, 9(1), 30-35.
- 24 Chae, S. J., Güneş, F., Kim, K. K., Kim, E. S., Han, G. H., Kim, S. M., Shin, H. J., Yoon, S. M., Choi, J. Y., Park, M. H., Yang, C. W., Pribat, D. and Lee, Y. H. (2009). Synthesis of Large-Area Graphene Layers on Poly-Nickel Substrate by Chemical Vapor Deposition: Wrinkle Formation. *Advanced Materials*, 21(22), 2328-2333. *Adv. Mater.*, 2009, **21**, 2328-2333.
- 25 Choucair, M., Thordarson, P. and Stride, J. A. (2008). Gram-scale production of graphene based on solvothermal synthesis and sonication. *Nature Nanotechnology*, 4(1), 30-33.
- 26 Chen, X., Dobson, J. F. and Raston, C. L. (2012). Vortex fluidic exfoliation of graphite and boron nitride. *Chemical Communications*, 48(31), 3703-3705.
- 27 Zou, J. L., Iyer, K. S. and Raston, C. L. (2012). Pd-sodium carboxymethyl cellulose nanocomposites display a morphology dependent response to hydrogen gas. *Green Chemistry*, 14(4), 906-908.
- 28 Fang, J., Guo, Y., Lu, G., Raston, C. L. and Iyer, K. S. (2011). Enhancement of quantum yield of LaPO₄: Ce³⁺: Tb³⁺ nanocrystals by carbon nanotube induced suppression of the 1-dimensional growth. *Dalton Transactions*, 40(13), 3122-3124.
- 29 Hartlieb, K. J., Raston, C. L. and Saunders, M. (2007). Controlled scalable

- synthesis of ZnO nanoparticles. *Chemistry of Materials*, 19(23), 5453-5459.
- 30 Dev, S., Iyer, K. S. and Raston, C. L. (2011). Nanosized drug formulations under microfluidic continuous flow. *Lab on a Chip*, 11(19), 3214-3217.
 - 31 Bennetts, D. A. and Hocking, L. M. (1973). On nonlinear Ekman and Stewartson layers in a rotating fluid. *Proceedings of the Royal Society of London. A. Mathematical and Physical Sciences*, 333(1595), 469-489.
 - 32 Bolch, C. J. and Blackburn, S. I. (1996). Isolation and purification of Australian isolates of the toxic cyanobacterium *Microcystis aeruginosa* Kütz. *Journal of Applied Phycology*, 8(1), 5-13.
 - 33 Ferrari, A. C. and Robertson, J. (2000). Interpretation of Raman spectra of disordered and amorphous carbon. *Physical review B*, 61(20), 14095.
 - 34 Kudin, K. N., Ozbas, B., Schniepp, H. C., Prud'Homme, R. K., Aksay, I. A. and Car, R. (2008). Raman spectra of graphite oxide and functionalized graphene sheets. *Nano Letters*, 8(1), 36-41.
 - 35 Ferrari, A. C., Meyer, J. C., Scardaci, V., Casiraghi, C., Lazzeri, M., Mauri, F., Piscanec, S., Jiang, D., Novoselov, K. S., Roth, S. and Geim, A. K. (2006). Raman spectrum of graphene and graphene layers. *Physical Review Letters*, 97(18), 187401.
 - 36 Fakhruddin, R. F., Shlykova, L. V., Zamaleeva, A. I., Nurgaliev, D. K., Osin, Y. N., García-Alonso, J. and Paunov, V. N. (2010). Interfacing Living Unicellular Algae Cells with Biocompatible Polyelectrolyte-Stabilised Magnetic Nanoparticles. *Macromolecular Bioscience*, 10(10), 1257-1264.
 - 37 Hipkins, M. F. and Baker, N. R. (1986). *Photosynthesis: energy transduction: a practical approach*. IRL Press Limited.
 - 38 Lichtenthaler, H. K. and Buschmann, C. (2001). Chlorophylls and Carotenoids: Measurement and Characterization by UV-VIS Spectroscopy. *Current Protocols in Food Analytical Chemistry*.
 - 39 Chandra, V., Park, J., Chun, Y., Lee, J. W., Hwang, I. C. and Kim, K. S. (2010). Water-dispersible magnetite-reduced graphene oxide composites for arsenic removal. *ACS Nano*, 4(7), 3979-3986.
 - 40 Zhao, G., Jiang, L., He, Y., Li, J., Dong, H., Wang, X. and Hu, W. (2011). Sulfonated graphene for persistent aromatic pollutant management. *Advanced Materials*, 23(34), 3959-3963.
 - 41 Zhao, G., Li, J., Ren, X., Chen, C. and Wang, X. (2011). Few-layered graphene

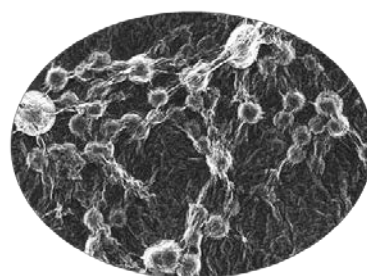
oxide nanosheets as superior sorbents for heavy metal ion pollution management. *Environmental Science & Technology*, 45(24), 10454-10462.

- 42 American Public Health Association. APHA (1992): Standard methods for the examination of water and wastewater, 18th edition. *APHA, Washington, DC*.
- 43 Eroglu, E., Zang, W., Eggers, P. K., Chen, X., Boulos, R. A., Wahid, M. H., Smith, S. M. and Raston, C. L. (2013). Nitrate uptake by p-phosphonic acid calix[8]arene stabilized graphene. *Chemical Communication*, 49, 8172-8174.

3. ENTRAPMENT OF *Chlorella vulgaris* CELLS WITHIN GRAPHENE OXIDE LAYERS



Pure algal cells



GO wrapped algal cells

This chapter is a reformatted version of the paper published in *RSC Advances*, Year 2013, Vol. 3, Pages 8180-8183.

3.1 Abstract

Confinement of microalgae cells within layers of graphene oxide (GO) effectively reduces the rate of cell division, with the microalgal wrapping being more efficient in a vortex fluidic device than using mild sonication, as determined by the cell growth and the level of nitrate removal from the liquid effluent.

3.2 Introduction

Algae have several commercial applications in nutraceuticals and cosmetics [1], with emerging potential applications in bioenergy production [2,3], wastewater treatment [4], biosensor applications [5], and CO₂ sequestration [6]. The potential utilization of algae in various areas is being realized with research focusing on the optimization of cultivation and harvesting methods. They can be economically cultivated in open ponds, although this has several drawbacks such as significant evaporative water loss, diffusion of CO₂ into the atmosphere, and the likelihood of contamination [7]. Algae can also be cultivated in photobioreactors where high quality products are produced, albeit with high inherent costs [6]. For both methods of cultivation, a common problem is the rapid replication of algal cells which leads to clogging resulting in difficulties in cellular cultivation and harvesting, especially in the photobioreactors with bio-fouling attenuating the penetration of light passing through [8,9]. This can be overcome by immobilizing the cells such that their cellular replication and movements are restricted. The benefits of this approach include better operational stability where the cell density can be controlled, ease of cell harvesting, and circumventing biofouling [10-12]. In addition, it also reduces the potential toxicity of reactants towards microalgae especially for cultivation in open ponds. Several algal cell immobilization techniques have been reported with gel entrapment using alginate or carrageenan beads as the most common methods [10]. In addition, several studies have been reported on the greater efficiency of immobilized cells relative to their free counterparts for the removal of metal ions and uptake of nutrients [12-15].

Prerequisites of coating photosynthetic microalgae include non-toxicity, photo-transparency, stability in growth medium, and robustness against cell growth [10]. In this study we have developed the use of graphene oxide (GO) as such a coating

material for microalgae, taking into account its unique properties such as flexibility, high mechanical stability and transparency to visible light. Graphene and GO have featured as a coating layer for a number of materials [16-19], and unlike pristine graphene, GO is more hydrophilic due to the high level of oxygen containing functional groups on the basal plane. Indeed, these hydroxyl and carboxyl groups allow GO to be designed for specific applications [19]. Kim *et al.* reported that GO has pH tunable amphiphilic properties and can be adsorbed onto surfaces to lower the surface and interfacial tension, and acts as a dispersing agent for graphite and carbon nanotubes in water [19]. Such combination of different materials is a route to novel materials. Recently we established that nitrate removal efficiency by algae cells from water can be enhanced as a hybrid material with multilayered graphene, generated using a vortex fluidics device (VFD) [20]. Overall the unique properties of GO renders it a promising coating material for algal immobilization, and this is developed herein.

3.3 Experimental methods

Graphene oxide used in this study was synthesized from natural graphite powder (99.9%, SP-1, Bay Carbon) using the modified Hummers method [21,22]. A colloidal solution of graphene oxide (0.5 mL of 0.4 mg/mL) was added to a microalgae suspension (0.5 mL) with an initial total Chl concentration of around 3 mg/L (wild type *Chlorella vulgaris*) grown in an MLA fresh water media [29]. Two different immobilization processes were used: (i) mild sonication in a bath sonicator for 30 seconds, or (ii) using a vortex fluidic device (VFD) which is inclined at 45° at a rotation speed of 1200 rpm for 30 minutes under the so called confined mode (Fig. 3.1). 10 mm glass tubes were used during the VFD process. The tilt angle was selected on the basis that it is the optimized angle for exfoliating graphene and also hexagonal boron nitride in N-methyl pyrrolidone [23], and the controlled growth of palladium nano-particles on carbon nano-onions [24].

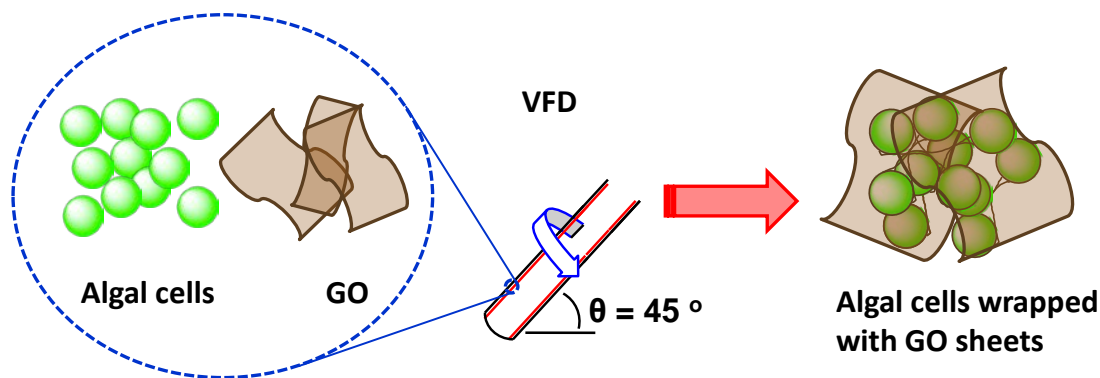


Figure 3.1. Schematic illustration of the algae wrapping using VFD

The algal cultures were diluted so that each starting solution has a total Chl concentration of around 0.25 mg/L (Fig. 3.6). Wild type *Chlorella vulgaris* was originally obtained from the CSIRO, Australian National Algae Culture Collection. Algal growth was carried out under the artificial illumination (16 h light/ 8 h dark cycle) at 25 °C, inside glass flasks upon orbital shaking (Thermoline Scientific) at 80 rpm. The as-treated suspensions were dropped onto 200 mesh holey carbon Cu grids for TEM characterization, and micrographs recorded using JEOL 2100 instruments operating at 120 keV. SEM studies were carried out using Zeiss 1555 VP-FESEM with samples coated with approximately 3 nm Pt films. AFM images were recorded on a Digital Instruments Dimension 3000 with a Nanoscope IIIa controller under tapping mode, using silicon cantilevers. Samples were drop cast onto freshly cleaved mica and left for drying. The Zeta potential measurements were carried out with a Zetasizer Nano S (ZEN1600, Malvern Instruments). Viability test were carried out by using fluorescence microscopy and also by conducting spectrophotometric analysis of the chlorophyll content. The uncoated and coated cells were examined under bright field and under fluorescence by using an upright fluorescence microscope (Olympus BX61) with Texas-Red filters having laser excitation wavelengths at 545-580 nm and emission wavelengths of 610 nm [20,27,28]. Both bright field and fluorescence images were captured using Cell^R imaging software. Total chlorophyll content (Chl a + Chl b) was investigated by the spectrophotometric measurements of the methanol extracts obtained from the known amount of algal culture pellets [30]. Nitrate concentration was analyzed by following the “cadmium reduction method” via powder pillows (HACH[®], NitraVer Nitrate Reagent) and a colorimeter (HACH[®], DR-870) [31].

3.4 Results and discussion

Transmission electron microscopy (TEM) and atomic force microscopy (AFM) of the as synthesized GO are given in Figure 3.2. TEM analyses of GO revealed monolayers of GO sheets. The electron diffraction pattern obtained by SAED was identical with the sixfold symmetry expected for graphite/graphene and the intensity of the inner spots being brighter than the outer spots establishes that the sheets observed are monolayer (inset of Figure 3.2b) [24,25]. Meanwhile, thickness measurement of GO sheets from a selected area was established using AFM as ~5 nm which is consistent with GO being comprised of a few layers of the material. Scanning electron microscopy (SEM) images of coated and uncoated algae were recorded and compared. Images of uncoated cells, Figure 3.3 (a, b), appears to be more spherical and smooth, which is typical of algal cells, whereas images of samples containing GO, Figure 3.3 c – f, have wrinkles of sheet-like material, which is consistent with the algal cells being wrapped by a few layers of GO.

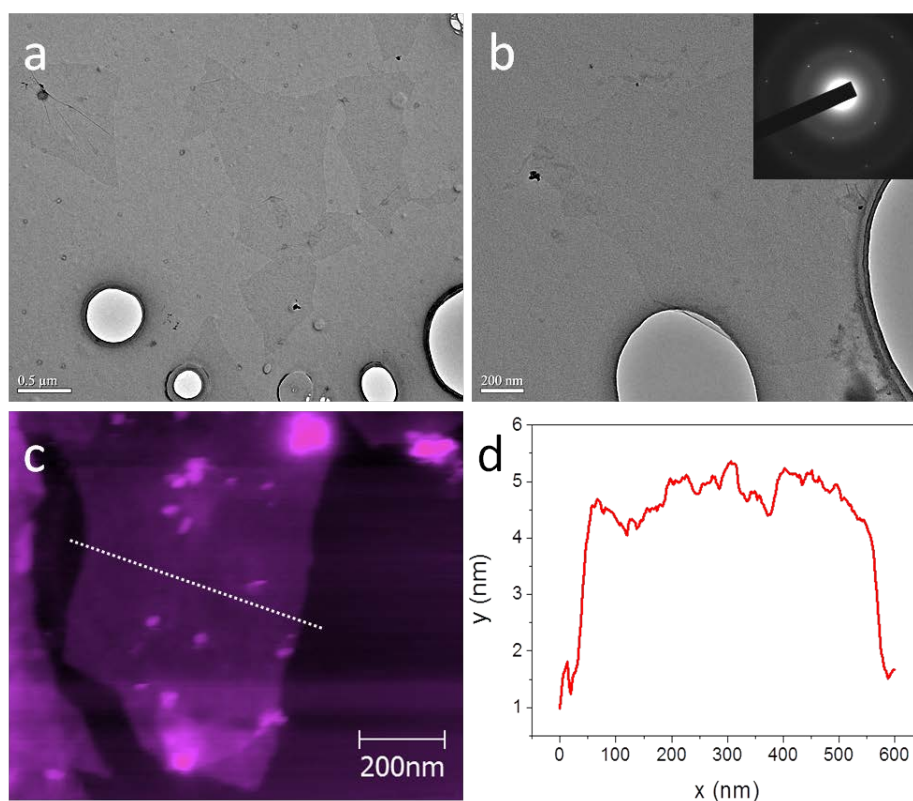


Figure 3.2. (a, b) TEM images of graphene oxide (GO) sheets with the inset in (b) showing the SAED pattern and (c) an AFM image of a selected graphene oxide (GO) sheet, with the height profile in (d).

Autofluorescence of microalgae cells was used for studying the viability of cultures after the wrapping processes. Fluorescence microscopy used an excitation filter around 540 nm which is near the Soret band maximum absorption of algal chlorophyll b [20,27,28]. Results given in Figure 3.4 show the bright field and fluorescence microscopy images of coated microalgae cells using mild sonication (a, b) and using the VFD (c, d). The red fluorescence of algal cultures, Figures 3.4b and d, indicates that the cultures are alive for both methods of wrapping the algal cells, which establishes the nonlethal effect of GO towards them. Dark layers around the cells, observed in the bright field images, arise from the GO layers.

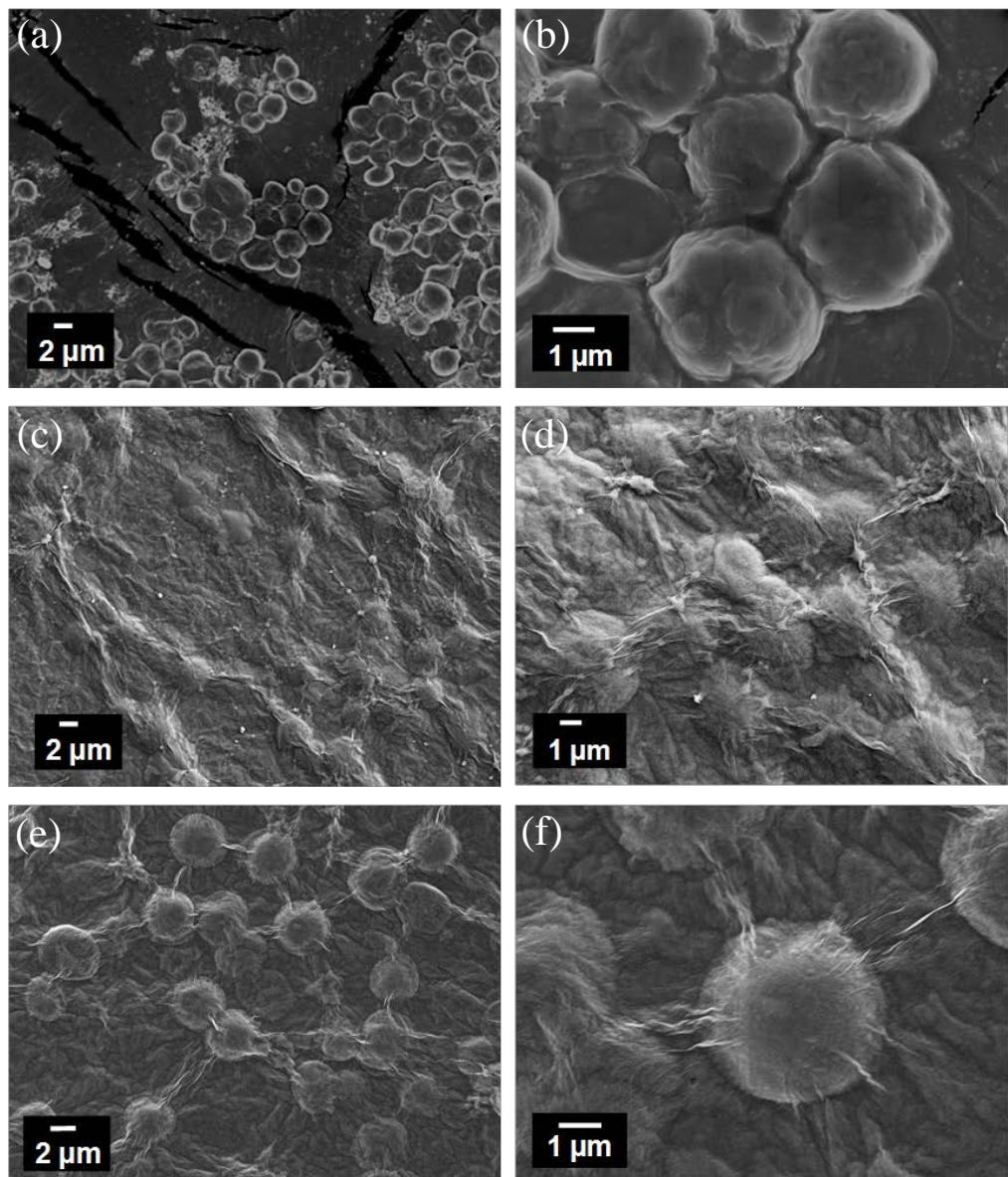


Figure 3.3. SEM images of (a, b) pure algae cells and (c, d) GO wrapped algal cells using mild sonication, and (e, f) GO wrapped algal cells using VFD.

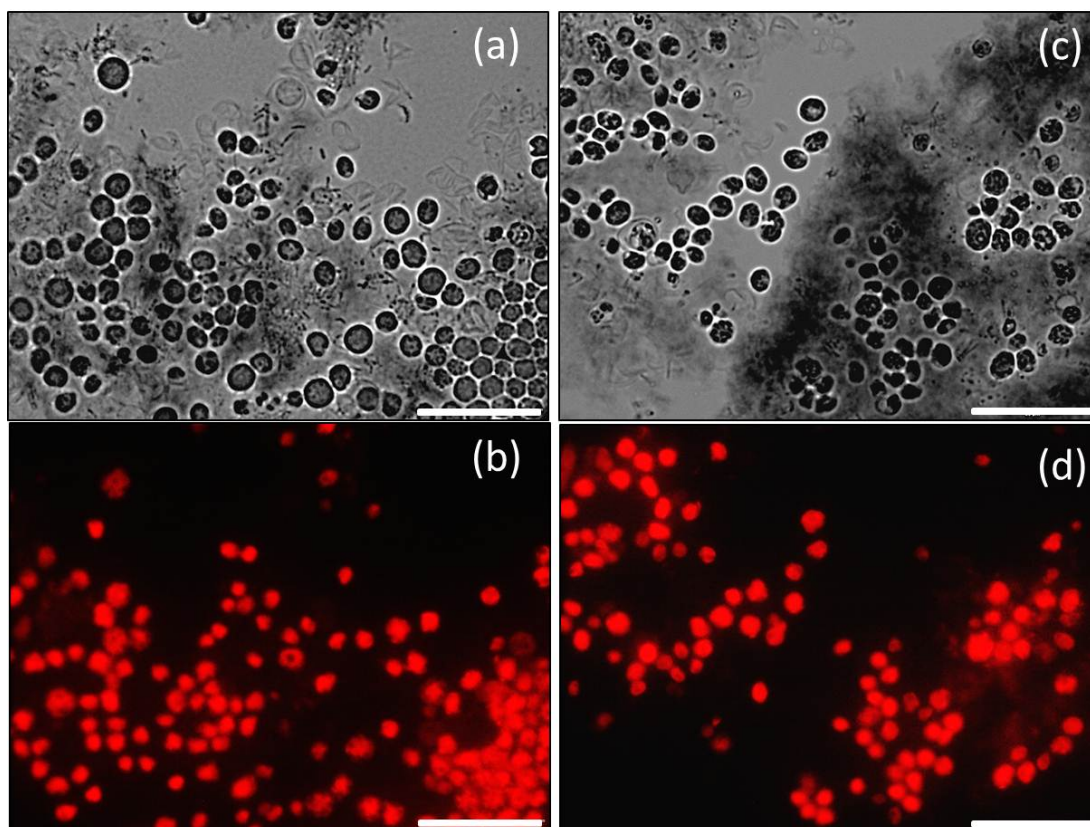


Figure 3.4. Bright field and fluorescence microscopy images of (a, b) GO wrapped algal cells using mild sonication, and (c, d) GO wrapped algal cells using VFD. Texas-Red filters were used for monitoring the autofluorescence of “chlorophyll B” pigment in microalgal cells. Scale bars: 20 μm .

Colloidal stability of the wrapped cells was studied by conducting the Zeta potential analysis. GO wrapped cells prepared by sonication and VFD resulted in having average zeta potential values of -42.0 mV and -39.9 mV respectively, meanwhile the zeta potential for free cells being less negative at -25.3 mV. This reflects an increase in colloidal stability of the cells following their wrapping with GO sheets (Appendix A1).

Growth of the cell cultures was also investigated by the periodical examination of their chlorophyll content, Figure 3.5. GO coated algae were immediately placed into the algal growth media (MLA fresh water media) [29], with a dilution rate to obtain an initial microalgal concentration of 0.25 mg/L total Chl. The chlorophyll content was analyzed by spectrophotometric measurements of the methanol extracts obtained from the algal culture pellets [30]. In addition to the fluorescence microscopic images of the cells, Figure 3.4, the ability of the cell cultures to replicate after

escaping the graphene further highlights the nontoxic effect of GO on the microalgal cells. Significantly higher growth was observed for free algal cells relative to the immobilized cells, where there is a lack of external boundaries that could attenuate cellular division. GO wrapped cells, formed using either sonication or a VFD, significantly diminished their growth until after the first three days, whereupon the cells escape the confines of the GO and then freely replicate within the external media. However, it is noteworthy mentioning that processing *via* a VFD can also be done under continuous flow mode and thus it has the potential for large scale processing. The immobilization process was not very efficient when algae and GO were simply mixed on the bench without using VFD or sonication processing, with cells yielding a similar replication pattern relative to free cells (Fig. 3.5). This shows the significance of an external force on the immobilization process, such as a VFD. In our previous study, multi-layer graphene sheets were not effective in wrapping the microalgae cells even after using a VFD, as the hybrid cells yielded a similar growth curve to their free counterparts [20]. This relates to the essentially non-oxidized graphene > 5 layers thick being less flexible when generated in water using a VFD [20].

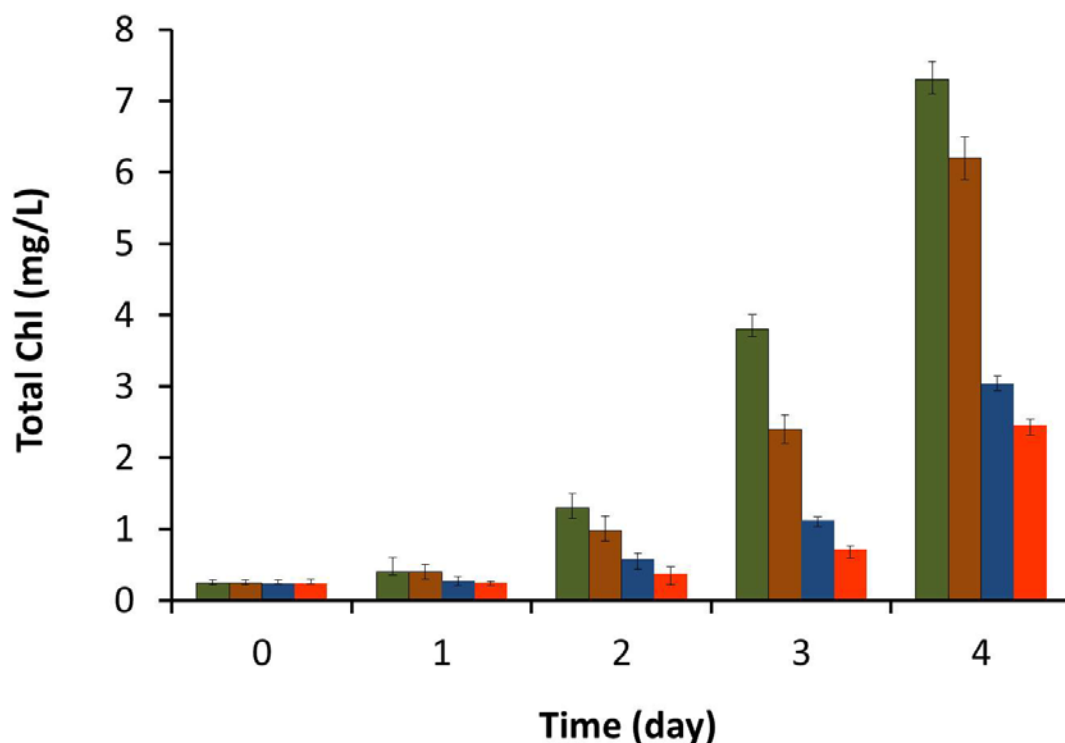


Figure 3.5. Total chlorophyll (Chl a and b) content as a function of time. Pure algae cells (green column), GO wrapped algal cells formed using mild sonication (blue column), and GO wrapped algal cells formed using VFD (red column).

Environmental remediation of the different wrapped cells has been investigated by monitoring the concentration of $[\text{NO}_3^-\text{-N}]$, which analyzes the amount of nitrogen present in the liquid solutions only due to nitrate ions (NO_3^-) (Fig. 3.6) [15,20]. The nitrate content of the initial effluent ($[\text{NO}_3^-\text{-N}]_{\text{initial}} \sim 26 \text{ mg/L}$) was significantly reduced (76.9% within 4 days) by the free *C. vulgaris* cells, in parallel with its uptake for the cellular replication and metabolism [15,20]. During the first three days, at which immobilization of the cells was significantly achieved, nitrate removal of the immobilized cells was lower, and can be mainly associated with the adsorption of nitrate on the layers of GO surrounding the cells. Dispersed GO layers in the absence of algal cells did not show significant nitrate removal with a maximum uptake of 12% by the 4th day. For the algae-GO mixture without using VFD or sonication processing, where immobilization was not very effective, the nitrate removal efficiency was always higher than its immobilized counterparts as a result of free and faster replication of the cells. In our previous study, hybrid cells with multi-layer graphene were also very effective for the removal of nitrate (complete removal

by the fourth day) [20] as a result of the unrestricted cell division of the non-immobilized cells compared to their herein GO-immobilized counterparts.

After the third day (Fig. 3.6), the wrapped cells freed themselves from the GO immobilization matrix and started replication, and this was also reflected by the enhanced nitrate removal rates. GO wrapped cells using the VFD had slightly higher nitrate removal efficiency relative to the wrapped cells formed using mild sonication (49.0% versus 40.4% after the 4th day, and this is despite the use of the VFD resulting in a slightly lower cell growth, Fig. 3.5. The dynamic thin film in the VFD, in providing a form of ‘soft energy’ [20], is likely to form a more uniform layer of GO relative to using high energy localized cavitation using sonication. More uniform layers of GO would potentially have greater nitrate removal efficiencies while also successfully attenuating the cell replication.

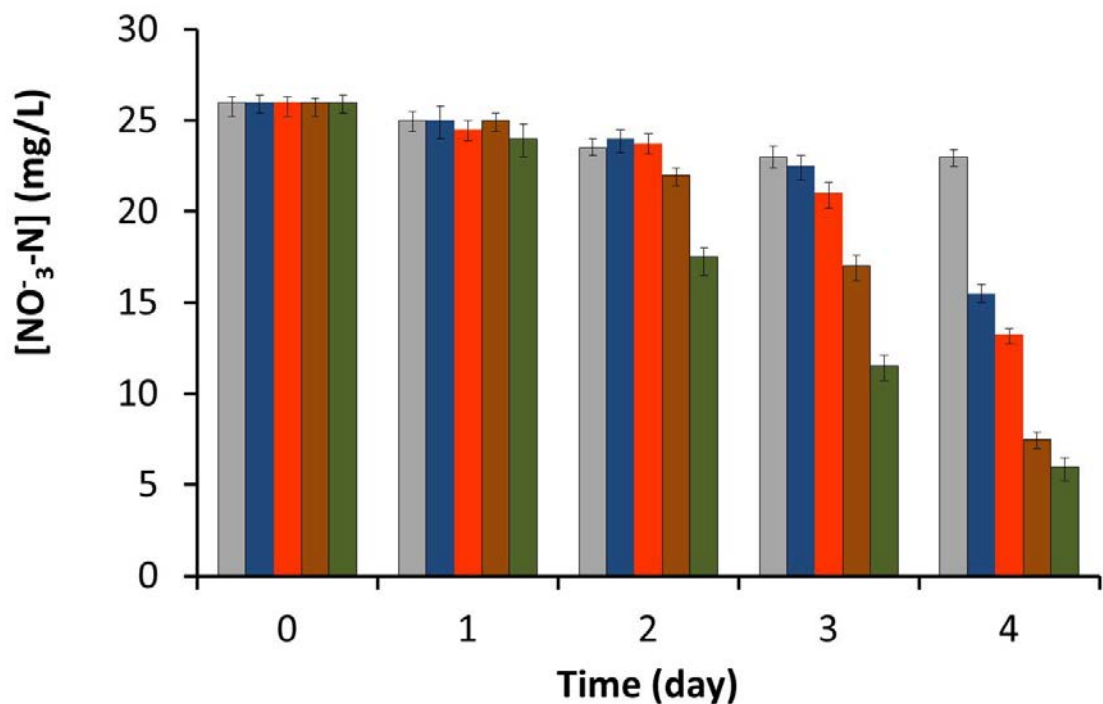


Figure 3.6. Nitrate-nitrogen (NO_3^- -N) concentration (mg/L) of liquid effluent versus time. Pure algae cells (green column), GO wrapped algal cells by mild sonication (blue column), and GO wrapped algal cells using VFD (red column).

3.5 Conclusion

In summary we have achieved a simple process for the immobilization of the

microalgal cells with graphene oxide layers. Even though various immobilization techniques have already been introduced in the literature, wrapping algae cells with GO is without precedent. The nonlethal nature of graphene oxide for microalgal cell cultures was also proven with various viability tests. Both sonication and vortex fluidics were efficient for wrapping the cells with the material of interest, while VFD processing is slightly more efficient for the immobilization and overall nitrate removal.

3.6 Acknowledgements

We gratefully acknowledge support of this work by the Australian Research Council for this research. TEM and SEM studies were carried out using facilities in the Centre for Microscopy, Characterization and Analysis, The University of Western Australia. AFM studies were carried out at Curtin University. M.H. Wahid and X. Chen would like to thank the Malaysian Government and China Scholarship Council for their PhD research scholarships, respectively.

3.7 References

- 1 Spolaore, P., Joannis-Cassan, C., Duran, E. and Isambert, A. (2006). Commercial applications of microalgae. *Journal of Bioscience and Bioengineering*, 101(2), 87-96.
- 2 Beer, L. L., Boyd, E. S., Peters, J. W. and Posewitz, M. C. (2009). Engineering algae for biohydrogen and biofuel production. *Current Opinion in Biotechnology*, 20(3), 264-271.
- 3 Eroglu, E. and Melis, A. (2009). "Density equilibrium" method for the quantitative and rapid in situ determination of lipid, hydrocarbon, or biopolymer content in microorganisms. *Biotechnology and Bioengineering*, 102(5), 1406-1415.
- 4 Hammouda, O., Gaber, A. and Abdelraouf, N. (1995). Microalgae and wastewater treatment. *Ecotoxicology and Environmental Safety*, 31(3), 205-210.
- 5 Nguyen-Ngoc, H. and Tran-Minh, C. (2007). Fluorescent biosensor using whole cells in an inorganic translucent matrix. *Analytica Chimica Acta*, 583(1), 161-165.
- 6 Rooke, J. C., Léonard, A., Sarmiento, H., Meunier, C. F., Descy, J. P. and Su, B. L. (2011). Novel photosynthetic CO₂ bioconvertor based on green algae

entrapped in low-sodium silica gels. *Journal of Materials Chemistry*, 21(4), 951-959.

- 7 Pulz, O. (2001). Photobioreactors: production systems for phototrophic microorganisms. *Applied Microbiology and Biotechnology*, 57(3), 287-293.
- 8 Ugwu, C. U., Aoyagi, H. and Uchiyama, H. (2008). Photobioreactors for mass cultivation of algae. *Bioresource Technology*, 99(10), 4021-4028.
- 9 Tredici, M. R. (2002). Bioreactors, photo. *Encyclopedia of Bioprocess Technology*.
- 10 Mallick, N. (2002). Biotechnological potential of immobilized algae for wastewater N, P and metal removal: a review. *BioMetals*, 15(4), 377-390.
- 11 Mallick, N. and Rai, L. C. (1993). Influence of culture density, pH, organic acids and divalent cations on the removal of nutrients and metals by immobilized *Anabaena doliolum* and *Chlorella vulgaris*. *World Journal of Microbiology and Biotechnology*, 9(2), 196-201.
- 12 Rai, L. C. and Mallick, N. (1992). Removal and assessment of toxicity of Cu and Fe to *Anabaena doliolum* and *Chlorella vulgaris* using free and immobilized cells. *World Journal of Microbiology and Biotechnology*, 8(2), 110-114.
- 13 Wilkinson, S. C., Goulding, K. H. and Robinson, P. K. (1990). Mercury removal by immobilized algae in batch culture systems. *Journal of Applied Phycology*, 2(3), 223-230.
- 14 Travieso, L., Canizares, R. O., Borja, R., Benitez, F., Dominguez, A. R., Dupeyrón y, R. and Valiente, V. (1999). Heavy metal removal by microalgae. *Bulletin of environmental contamination and toxicology*, 62(2), 144-151.
- 15 Eroglu, E., Agarwal, V., Bradshaw, M., Chen, X., Smith, S. M., Raston, C. L. and Iyer, K. S. (2012). Nitrate removal from liquid effluents using microalgae immobilized on chitosan nanofiber mats. *Green Chemistry*, 14(10), 2682-2685.
- 16 Mohanty, N., Fahrenholtz, M., Nagaraja, A., Boyle, D. and Berry, V. (2011). Impermeable graphenic encasement of bacteria. *Nano Letters*, 11(3), 1270-1275.
- 17 Wang, H., Yang, Y., Liang, Y., Robinson, J. T., Li, Y., Jackson, A., Cui, Y. and Dai, H. (2011). Graphene-wrapped sulfur particles as a rechargeable lithium-sulfur battery cathode material with high capacity and cycling stability. *Nano letters*, 11(7), 2644-2647.
- 18 Luechinger, N. A., Athanassiou, E. K. and Stark, W. J. (2008). Graphene-stabilized copper nanoparticles as an air-stable substitute for silver and gold in

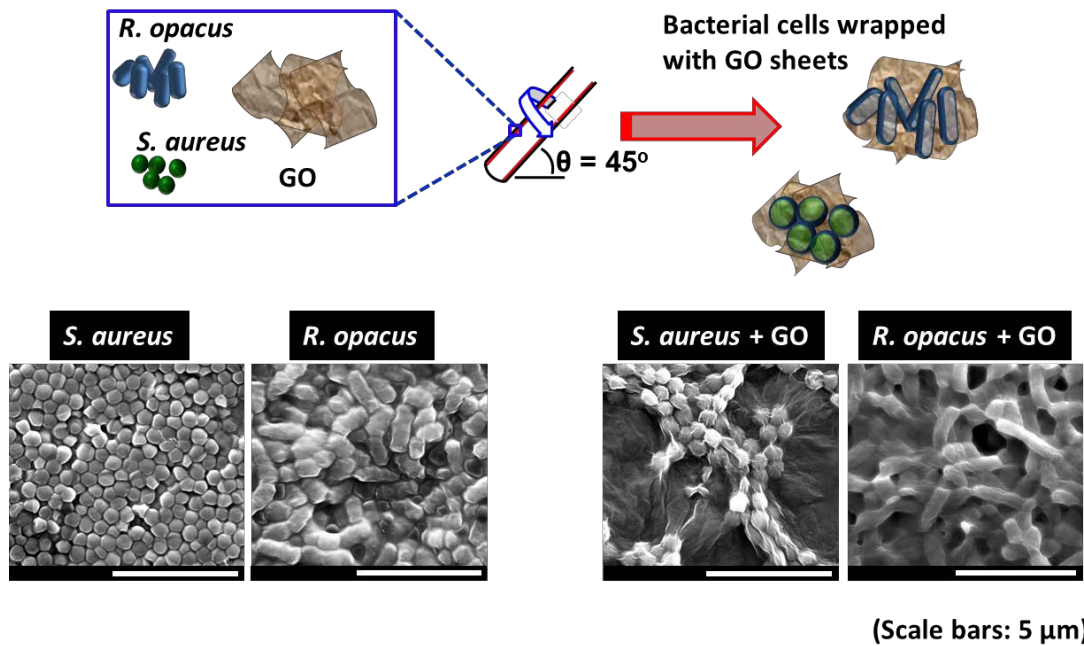
low-cost ink-jet printable electronics. *Nanotechnology*, 19(44), 445201.

- 19 Kim, J., Cote, L. J., Kim, F., Yuan, W., Shull, K. R. and Huang, J. (2010). Graphene oxide sheets at interfaces. *Journal of the American Chemical Society*, 132(23), 8180-8186.
- 20 Wahid, M. H., Eroglu, E., Chen, X., Smith, S. M. and Raston, C. L. (2013). Functional multi-layer graphene–algae hybrid material formed using vortex fluidics. *Green Chemistry*, 15(3), 650-655.
- 21 Kovtyukhova, N. I., Ollivier, P. J., Martin, B. R., Mallouk, T. E., Chizhik, S. A., Buzaneva, E. V. and Gorchinskiy, A. D. (1999). Layer-by-layer assembly of ultrathin composite films from micron-sized graphite oxide sheets and polycations. *Chemistry of Materials*, 11(3), 771-778.
- 22 Hummers Jr, W. S. and Offeman, R. E. (1958). Preparation of graphitic oxide. *Journal of the American Chemical Society*, 80(6), 1339-1339.
- 23 Chen, X., Dobson, J. F. and Raston, C. L. (2012). Vortex fluidic exfoliation of graphite and boron nitride. *Chemical Communications*, 48(31), 3703-3705.
- 24 Yasin, F. M., Boulos, R. A., Hong, B. Y., Cornejo, A., Iyer, K. S., Gao, L., Chua, H. T. and Raston, C. L. (2012). Microfluidic size selective growth of palladium nano-particles on carbon nano-onions. *Chemical Communications*, 48(81), 10102-10104.
- 25 Hernandez, Y., Nicolosi, V., Lotya, M., Blighe, F. M., Sun, Z., De, S., McGovern, I. T., Holland, B., Byrne, M., Gun'Ko, Y. K., Boland, J. J., Niraj, P., Duesberg, G., Krishnamurthy, S., Goodhue, R., Hutchison, J., Scardaci, V., Ferrari, A. C. and Coleman, J. N. (2008). High-yield production of graphene by liquid-phase exfoliation of graphite. *Nature Nanotechnology*, 3(9), 563-568.
- 26 Wilson, N. R., Pandey, P. A., Beanland, R., Young, R. J., Kinloch, I. A., Gong, L., Liu, Z., Suenaga, K., Rourke, J. P., York, S. J. and Sloan, J. (2009). Graphene oxide: structural analysis and application as a highly transparent support for electron microscopy. *ACS Nano*, 3(9), 2547-2556.
- 27 Fakhrullin, R. F., Shlykova, L. V., Zamaleeva, A. I., Nurgaliev, D. K., Osin, Y. N., García-Alonso, J. and Paunov, V. N. (2010). Interfacing Living Unicellular Algae Cells with Biocompatible Polyelectrolyte-Stabilised Magnetic Nanoparticles. *Macromolecular Bioscience*, 10(10), 1257-1264.
- 28 Hipkins, M. F. and Baker, N. R. (1986). *Photosynthesis: energy transduction: a practical approach*. IRL Press Limited.
- 29 Bolch, C. J. S. and Blackburn, S. I. (1996). Isolation and purification of Australian isolates of the toxic cyanobacterium *Microcystis aeruginosa*

Kütz. *Journal of Applied Phycology*, 8(1), 5-13.

- 30 Lichtenthaler, H. K. and Buschmann, C. (2001). Chlorophylls and Carotenoids: Measurement and Characterization by UV-VIS Spectroscopy. *Current Protocols in Food Analytical Chemistry*.
- 31 American Public Health Association. APHA (1992): Standard methods for the examination of water and wastewater, 18th edition. *APHA, Washington, DC*.

4. MICROENCAPSULATION OF BACTERIAL STRAINS WITH GRAPHENE OXIDE NANO-SHEETS USING VORTEX FLUIDICS



This chapter is a reformatted version of the paper published in *RSC Advances*, Year 2015, Vol. 5, Pages 37424–37430. Additional information in the Experimental methods has been added from the supplementary information of the published paper.

4.1 Abstract

Wrapping bacterial cells with graphene oxide sheets using a vortex fluidic device (VFD) effectively limits cellular growth for a certain time period whilst sustaining biological activity. This simple and benign method in preparing such composite material relies on the shear within the film in the device without compromising on cellular viability. In principle, the process is scalable for large volumes, for operating the VFD(s) under continuous flow mode. Moreover, acquiring SEM images were possible without pre-coating the composite material with a metallic film, with limited charging effects. This establishes the potential for interfacing material with graphene oxide, which could be extended to more conductive graphene layers, as an effective approach for simplifying characterization using SEM.

4.2 Introduction

Microorganisms such as bacteria have attracted considerable interest for their use in commercial applications. Being abundant in nature, they also exhibit many different morphologies and metabolic pathways, some of which are unique to bacteria [1]. Accordingly microorganisms have potential in prospective sustainable technologies for the future. Thus far bacteria have been used in a wide range of sustainable applications, ranging from food manufacturing, the production of antibiotics, drugs, enzymes, biofuels and solvents [1,2] to biomining [3,4] and bioremediation [5,6]. Additionally, with the emerging advances in nanotechnology, innovative approaches such as the integration of nanomaterials and microorganisms provide access to novel functional materials. Some of these studies focus on interfacing nanomaterials with biological cells to detect biocomponents or to investigate biological phenomena [7], in particular bioremediation [8-10], the synthesis of bio-templated materials for various novel applications such as supercapacitors [11], surface enhanced Raman scattering (SERS) substrates [12], and lithium storage [13], or for immobilization purposes [14-16].

Despite the number of promising applications of bacteria, their direct usage is challenging because bacterial activity depends critically on several environmental factors. For instance, the delivery of probiotics bacteria to the gastrointestinal tract is usually hindered due to the adverse pH conditions of the tract [17]. Various

techniques have been implemented in order to increase the applicability of bacteria through cellular protection. This includes microencapsulation [17-22] which is effective in providing cells with a protective layer, which can enhance their viability during processing and facilitate their delivery to targeted sites such as in the case of probiotics bacteria [17-19]. In addition, such encapsulated cells have featured in bioremediation [20,21] and targeted agricultural deliveries where extended shelf-life and controlled microbial release were achieved [22]. Given that the majority of encapsulated bacteria are used in the food industry, common materials used for the encapsulation are food grade polymers such as calcium-alginate gel, kappa-carrageenan, gellan gum, gelatin and starch [17,23]. Nevertheless, due to the growing potential applications of bacteria in diverse fields, there is a need to seek alternative coating materials with the scope of protecting the cells as well as imparting additional functionality to them. Several examples have recently been reported, including introducing superparamagnetic nanoparticles for magnetic field responses [24,25], silica to enhance thermal durability [26], and graphene to impart electrical conductivity [27,28]. Another potential encapsulating material for microorganisms is graphene oxide (GO) which has a number of advantageous properties such as biodegradability [29], flexibility [30], robustness [30], transparency [30] and amphiphilicity [31]. We recently reported on the encapsulation of microalgae, *Chlorella vulgaris* with GO layers while maintaining biological activity of the cells [16]. The encapsulation was proven to reduce the rate of cell division for a certain time interval and thus established the potential of the approach for immobilization purposes in general. Furthermore, a recent study showed that GO can act as a scaffold for bacterial attachment, proliferation and biofilm formation for *Escherichia coli* [29].

Although substantial efforts have been made to interface biological cells with various functional nanomaterials, the preparation techniques are limited and require further development [23]. A facile, efficient and environmentally friendly technique is a prerequisite in developing industrial applications [23]. Herein we develop the use of a vortex fluidic device (VFD) to effectively interface graphene oxide (GO) sheets to the surface of two different strains of bacterial cells, *Staphylococcus aureus* and *Rhodococcus opacus*, in order to impart novel function to the cells in the hybrid materials. Related to this work is the use of the VFD to prepare functional multi-

layer graphene-algae and graphene oxide (GO)-algae hybrid materials [10,16]. In the VFD, a rapidly rotating tube generates a thin microfluidic film with rapid micro-mixing of reagents therein, and the mechanoenergy in the film is effective in increasing reaction rates, and therefore reducing the processing times [33]. Importantly, the VFD can be operated in the confined mode and also continuous flow mode, and it has a diversity of processing capabilities, including in organic synthesis [33-37], controlled growth of the polymorphs of calcium carbonate [38], formation of mesoporous silica at room temperature with control over the pore size [39], compacting single walled carbon nanotube into toroidal structures [40], exfoliation of graphene and boron nitride [41], controlled decoration of nanoparticles on 2D nanomaterials [42-44], preparation of functional hybrid bio-nanomaterials [10,16,45], and the refolding of proteins [46].

Selection of the bacterial strains for this study was based on the disparate physical structures of spherical *S. aureus* and rod shaped *R. opacus* cells. Exploring different cellular morphologies can be useful to understand the effects of shearing forces generated within the microfluidic film in the VFD, towards the bacteria, and subsequently towards the GO in inducing the wrapping process. While *S. aureus* are easy to grow and could represent a model to study the VFD wrapping efficiency and the effects of shear on bacteria, *R. opacus* has the advantage of being able to degrade pollutants [47]. Since wrapping with GO also has the advantage of water treatment [48], its hybrid with bacterial cells like *R. opacus* is attractive in developing more efficient waste treatment systems.

4.3 Experimental methods

In a typical experiment, bacterial cultures were first prepared in a nutrient media solution [1] until the cells reached their stationary phase prior to use in these experiments (Fig. 4.1). *Staphylococcus aureus* (ATCC 6538) and *Rhodococcus opacus* (DSN 43205) were maintained on nutrient agar and were grown to stationary phase in Luria-Bertani and GYM *Streptomyces* medium respectively. Before being used for VFD experiments, both strains were grown in broth culture until stationary phase, as determined by spectroscopic optical density measurements at 600 nm (Varian Cary 50 Bio UV/Visible spectrophotometer). Graphene oxide used in this study was synthesized from natural graphite powder (99.9%, SP-1, Bay Carbon)

using the modified Hummers method [49,50]. For the cell viability assay of the bacteria (without GO addition) processed in the VFD, bacteria were initially processed at different rotational speeds ranging from 2000 to 8000 rpm for one minute per sample, using a VFD housing a 10 mm OD diameter borosilicate NMR tube, inclined at 45 degrees. Processed cells were then stained with the fluorescent dyes, SYBR Green I, for live cells staining, and propidium iodide (PI) for dead cells staining. Accordingly, untreated and heat 'killed' bacteria were prepared as controls for VFD processed bacteria. Viability of all samples was analysed using flow cytometry. For flow cytometric analysis, a tube of each of the bacterial species without VFD processing was prepared as a positive control. For VFD processed bacteria, samples were prepared in triplicates. In order to establish the regions in the flow cytometric analysis that corresponded to live and dead cells, cells were heat injured at 60 °C for 1 h and used as a dead control, whereas untreated cells were used as a live control. Cells were stained (15 min at room temperature, in the dark) with the cell-permeant double-stranded DNA fluorochrome, SYBR green I (Sigma-Aldrich) at a final concentration of the commercial stock solution of 1:10,000 (v/v) in Tris-Acetate EDTA buffer and with propidium iodide (PI) (Sigma-Aldrich) at a final concentration of 10 $\mu\text{g}\cdot\text{mL}^{-1}$ in water. SYBR stains the nucleic acids in all cells, while PI stains the nucleic acids in cells with damaged membranes. Sample analysis was performed using a LSR Fortessa flow cytometer (Becton Dickinson Biosciences, San Diego, CA, USA) equipped with an air-cooled 488-nm argon ion laser. Each cell was characterized by four optical parameters: side-angle scatter (SSC), forward-angle scatter (FSC), green fluorescence for SYBR (525 nm) and red fluorescence for PI (675 nm). Data were collected using FACS Diva Software version 8.0 supplied by BD Biosciences. Following to the selection of the optimal VFD processing speeds; GO wrapping of the bacteria was carried out in the VFD tube at 5000 and 8000 rpm for 1 minute after mixing 0.5 mL of GO solution (0.1 mg mL^{-1}) with 0.5 mL of bacterial solution at the stationary phase of their growth. The mixture was then transferred into nutrient media solution and their growth was monitored using the standard optical density method. Samples of *S. aureus* and *R. opacus* were diluted at a ratio of 1:2 (v/v) with graphene oxide suspension (0.1 mg $\cdot\text{mL}^{-1}$ prepared in sterile MilliQ™ water), and vortexed using the VFD under aseptic conditions for one minute in triplicate. The 10 mm OD diameter NMR tube in the VFD was cleaned with 70 % ethanol and rinsed with sterile MilliQ™ water between samples. Vortexed

samples were then aseptically placed in fresh media (10 % initial concentration) and incubated at 37 °C and 28 °C with a shaking speed at 155 rpm using CERTOMAT®R and Ratek shakers respectively. To determine the growth curves, optical density measurements of the aliquots were immediately taken after VFD treatment in parallel with the control at proper dilutions at every 4 hours for *S. aureus* and every 8 hours for *R. opacus* until they reach their stationary phase. Sterile media with graphene oxide particles (5 % final concentration) was used to blank the spectrophotometer.

As a control, samples of *S. aureus* and *R. opacus* (5 % of initial concentration) were cultured without graphene oxide particles and without vortexing, then incubated alongside the treated samples. Sterile media was used as a blank for the optical density measurements of the bacteria-only samples.

As a further control to determine the effect of graphene oxide without VFD processing, samples of *S. aureus* and *R. opacus* were diluted at a ratio of 1:2 (v/v) with graphene oxide (10 % of final concentration), placed in fresh media and incubated alongside the treated samples. Sterile media with graphene oxide particles (5 % of final concentration) was used as a blank for the optical density measurements of the GO treated samples.

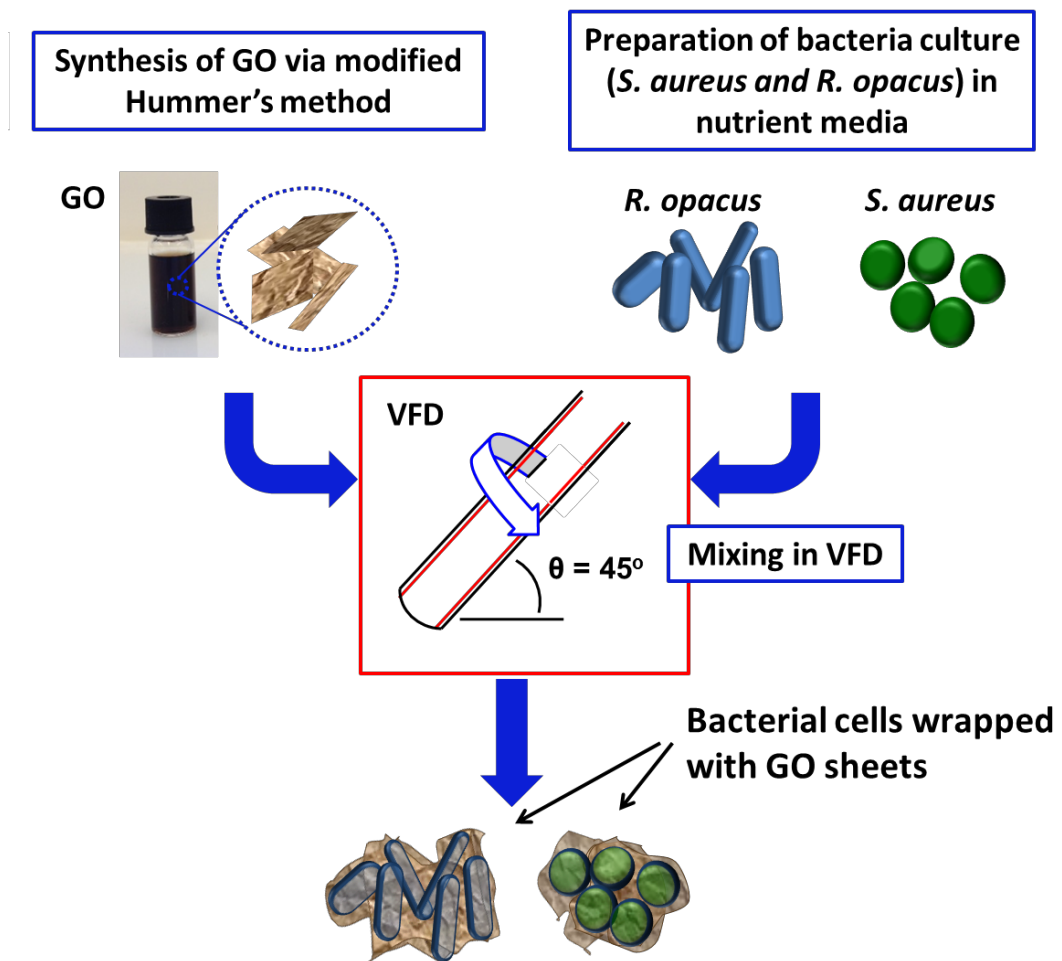


Figure 4.1. Schematic illustration of the preparation of GO wrapped bacteria using VFD

4.4 Results and discussion

Flow cytometry analysis data in Figure 4.2 shows that *S. aureus* and *R. opacus* exhibit slightly different cytometric characteristics, potentially due to the different cell morphologies and surface structures present on the bacteria [51]. Initial experiments demonstrate the efficacy of SYBR and PI for distinguishing between live and dead bacterial cells which was useful for understanding the effect of VFD processing towards the viability of the bacteria (Fig. 4.2). Regardless of the different processing speeds, flow cytometric analysis of the VFD processed samples showed similar cytometric characteristics for all speeds, ranging from 2000 rpm to 8000 rpm, which was also similar to those exhibited by untreated cells, where a high density of live cells was observed (Appendix A2). This suggests that there was only a minimal effect on the cells from their processing in the VFD. Figure 4.2 shows the results for

S. aureus and *R. opacus* processed at two different speeds (5000 and 8000 rpm) as a representation of the VFD processed samples. After confirming the viability of the cells, these two speeds, i.e. 5000 and 8000 rpm, were selected for wrapping the bacteria with GO sheets using the VFD. Of note is that the same speeds were also used in our previous study for the preparation of multi-layer graphene/algae hybrid material [10].

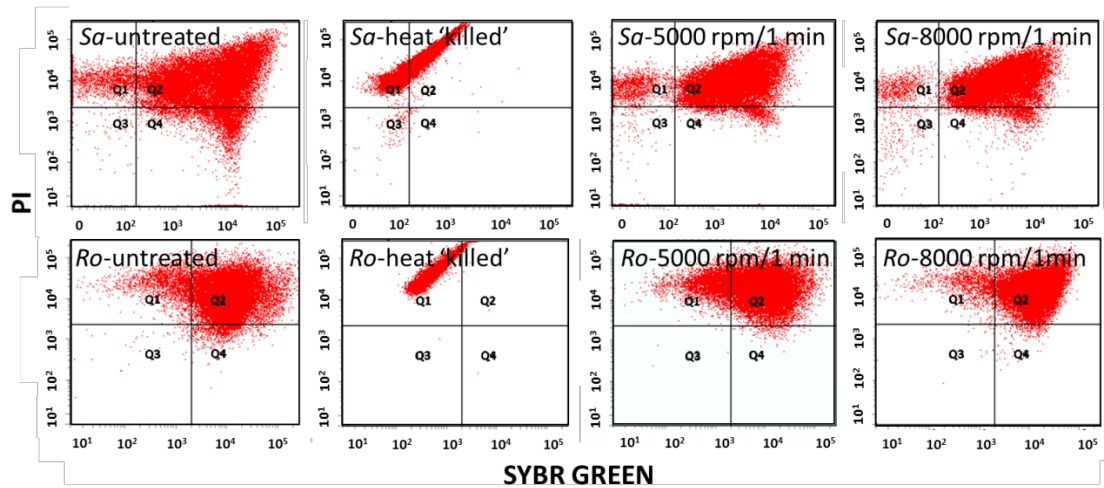


Figure 4.2. Flow cytometry analysis of *S. aureus* (top row) and *R. opacus* (bottom row). *Sa* and *Ro*-untreated and heat 'killed' represents control samples and *Sa* and *Ro*-5000 & 8000 rpm / 1 min shows cytogram of bacteria after processing in the VFD at 5000 and 8000 rpm for 1 minute respectively

Scanning electron microscopy (SEM) images of only bacterial cells, and GO wrapped bacterial cells were recorded and are compared in Figure 4.3. Preliminary results showed that bacteria interfaced with GO can be imaged under SEM without pre-coating with a metallic film, although there is small charging effects (Fig. 4.3a). However for untreated bacterial cells not coated with either a metallic film or GO, charging effects were prevalent, distorting the images (Fig. 4.3b). Hence, it can be anticipated that by interfacing the cells with more conductive graphene sheets such as reduced graphene oxide or pure graphene, clear SEM images can be acquired. Nevertheless, in order to minimize the charging effects due to the less electron conductive property of GO, all samples were pre-coated with 5 nm platinum prior to SEM imaging. As shown in Figure 4.3c-d, untreated bacteria samples have smooth surfaces and there were pronounced charging effects. In contrast, the bacteria interfaced with GO clearly have the bacteria wrapped with GO sheets.

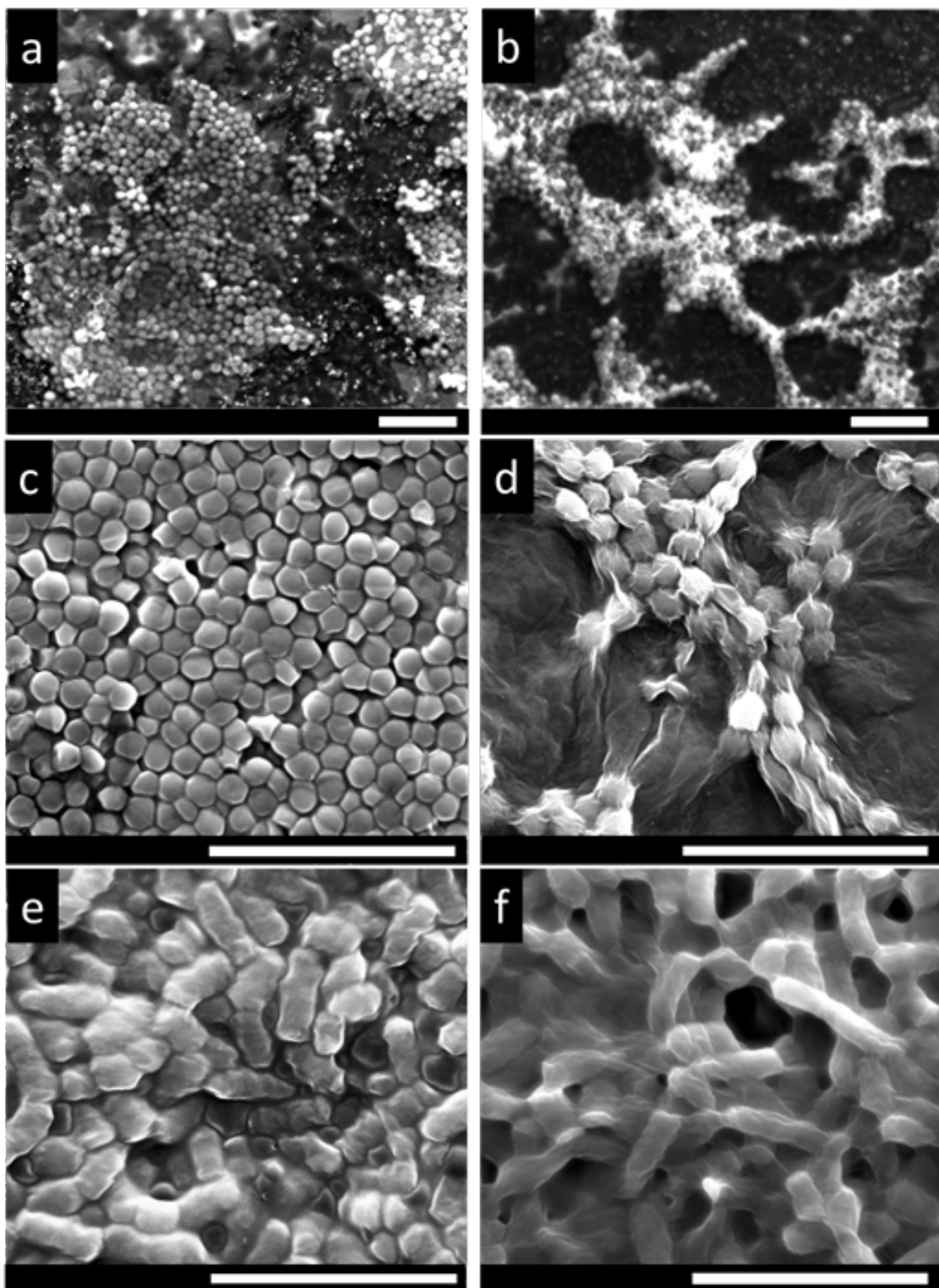


Figure 4.3. SEM images of bacteria (a) *S. aureus* interfaced with GO sheets, and (b) *S. aureus* only. Both (a) and (b) were imaged without pre-coating with a platinum metal film. (c) *S. aureus* only (d) GO wrapped *S. aureus* (e) *R. opacus* only, and (f) GO wrapped *R. opacus*. (c-f) samples were pre-coated with platinum prior to SEM imaging. (Scale bars: 5 μm).

The SEM results are supported by transmission electron microscopy (TEM), atomic force microscopy (AFM) and Raman spectroscopy. TEM images of the GO wrapped bacteria exhibit wrinkles at the interface of the bacteria, revealing wrapping features of the GO on the surface of the bacteria, which was not observed in untreated bacteria samples (Fig. 4.4). Furthermore, selected area electron diffraction pattern of the graphene wrapped bacteria shows typical electron diffraction for GO layers, as shown in the inset of Figure 4.4(d). AFM analysis under tapping mode revealed different surface topography for bacterial cells with and without GO (Fig. 4.5) (For details of AFM analysis see appendix A3). For bacterial cells without GO, smooth surfaces were observed whereas features of wrinkles are demonstrated for GO encapsulated cells, which is characteristic of GO sheets. The difference in surface properties can also be seen in the phase images of AFM shown in the inset images in Figure 4.5.

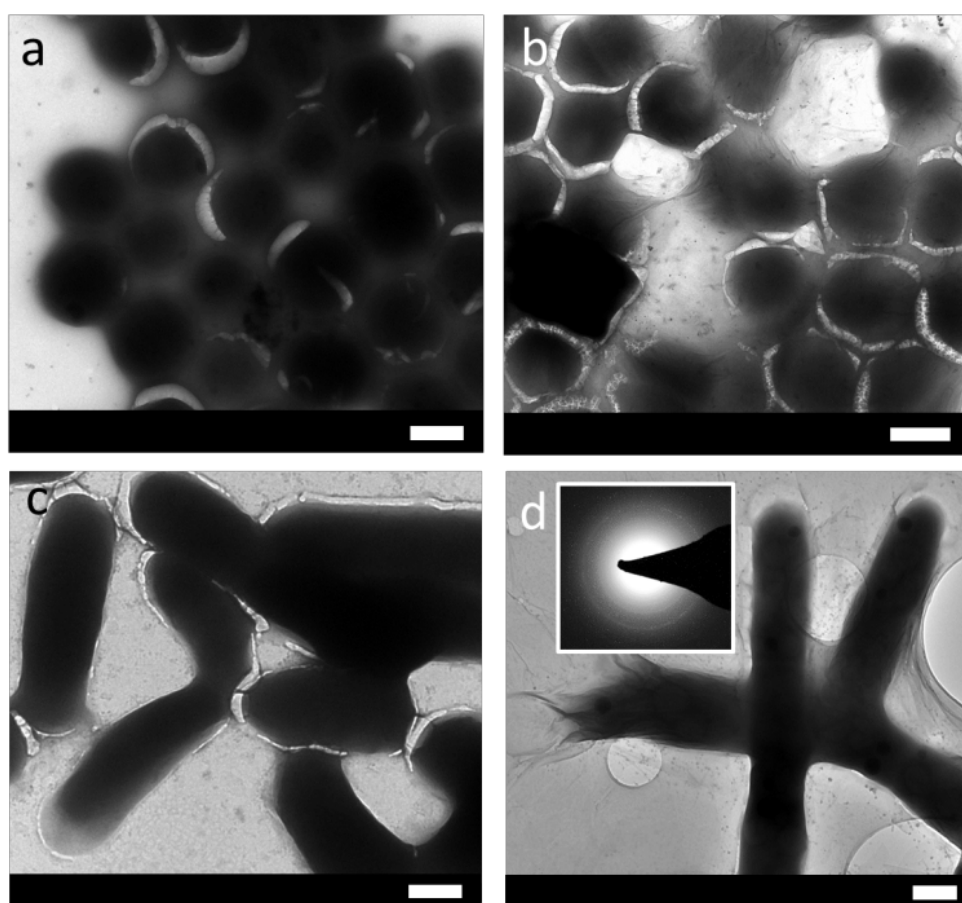


Figure 4.4. TEM images of (a) *S. aureus* only, (b) *S. aureus* wrapped with GO, (c) *R. opacus* only, and (d) *R. opacus* wrapped with GO and the selected area electron diffraction pattern in the inset. (Scale bars: 500 nm)

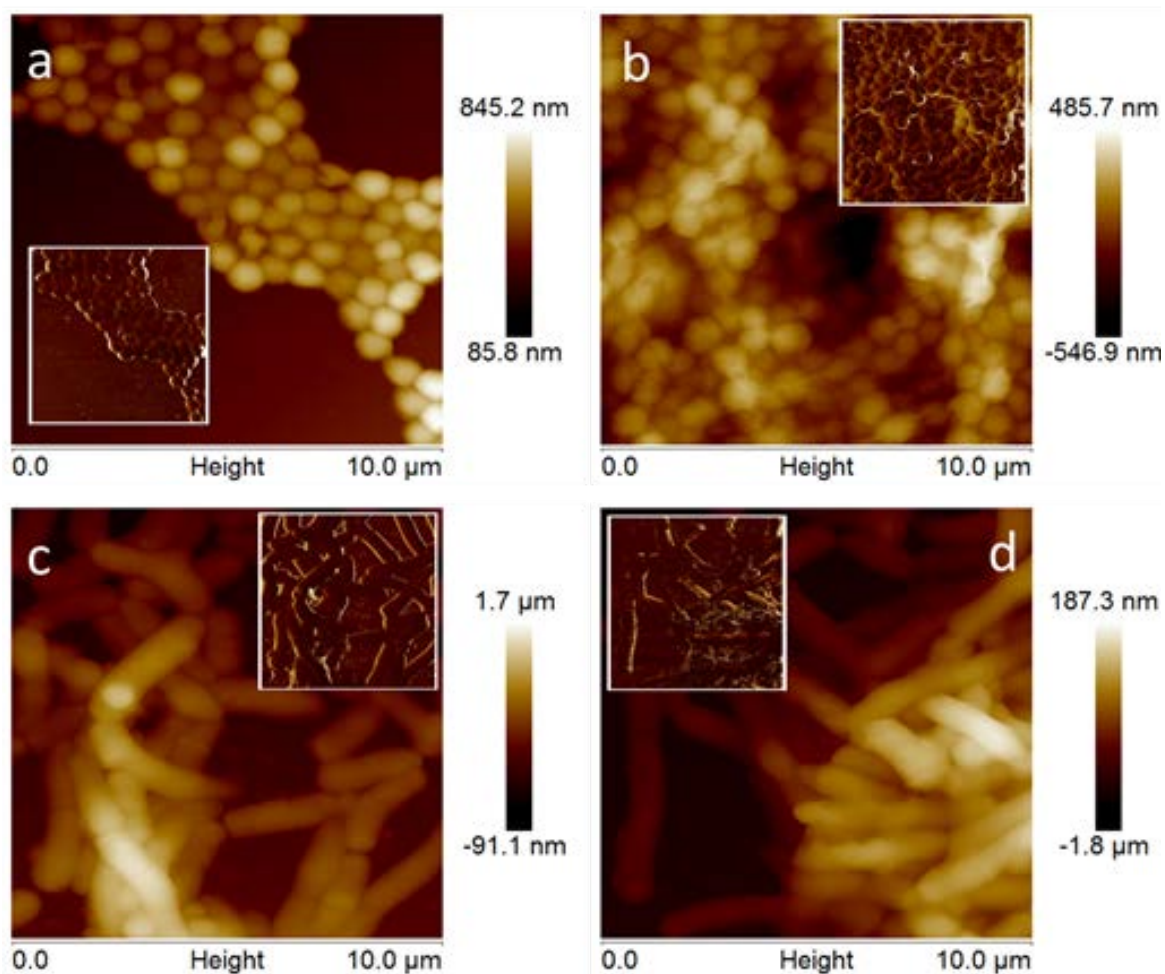


Figure 4.5. AFM images of bacteria (a) *S. aureus* only, (b) GO wrapped *S. aureus*, (c) *R. opacus* only, and (d) GO wrapped *R. opacus*. Inset images display phase images of the same samples.

Raman spectra and images of GO wrapped bacteria are shown in Figure 4.6, with Figure 4.6(b) and (c) showing x100 optical microscope images of GO wrapped *S. aureus* deposited on a cleaned silicon surface (For details of Raman analysis see Appendix A4). The surface coverage of the *S. aureus* is quite high and given their small size (approximately 1 μm or less) it is difficult to discern individual bacteria. AFM images were acquired in approximately the same region as these optical micrographs and show the typical shape and structure of the *S. aureus* bacteria (Fig. 4.6(a)). Figure 4.6(d) is a Raman image plotting the intensity of the 1600 cm^{-1} peak typical for the graphitic band of GO. Clearly from the bright regions on Figure 4.6(c), the GO is covering the *S. aureus* bacterial surface. Figure 4.6(i) is a Raman single spectra acquired on the image and shows the distinctive peaks of the D and G bands, at 1350 and 1600 cm^{-1} respectively, for GO, being consistent with previously

reported values [50]. The peaks at 520 and 965 cm^{-1} are also shown, which are from the underlying silicon substrate. Figure 4.6(e-h) and (j) show optical images, Raman images and a Raman spectrum for the *R. opacus* bacteria covered in GO. Figure 4.6e is an optical image and due to the much larger size of the rod-shaped *R. opacus* (1 μm wide and \sim 4-5 μm long) they are easily discernible using the x100 objective on the Raman microscope. Figure 4.6(f) shows the same region as the image in 4.6(e) as a Raman image generated from the GO graphitic band at 1600 cm^{-1} . The bright regions again indicate the presence of GO on the bacteria, which coincide with the position of the bacteria. Figure 4.6(g and h) are zoomed in optical and Raman images of a particular bacterium, highlighted in Figure 4.6(e and f). The data in Figure 4.6(g) and (h) further demonstrate the covering of the bacteria with GO. The Raman image in Figure 4.6(h) is, once again, corresponds to the GO graphitic band at 1600 cm^{-1} . Figure 4.6(j) shows a typical spectrum from the image and shows the distinctive peaks D and G bands at 1350 and 1600 cm^{-1} respectively for GO [52].

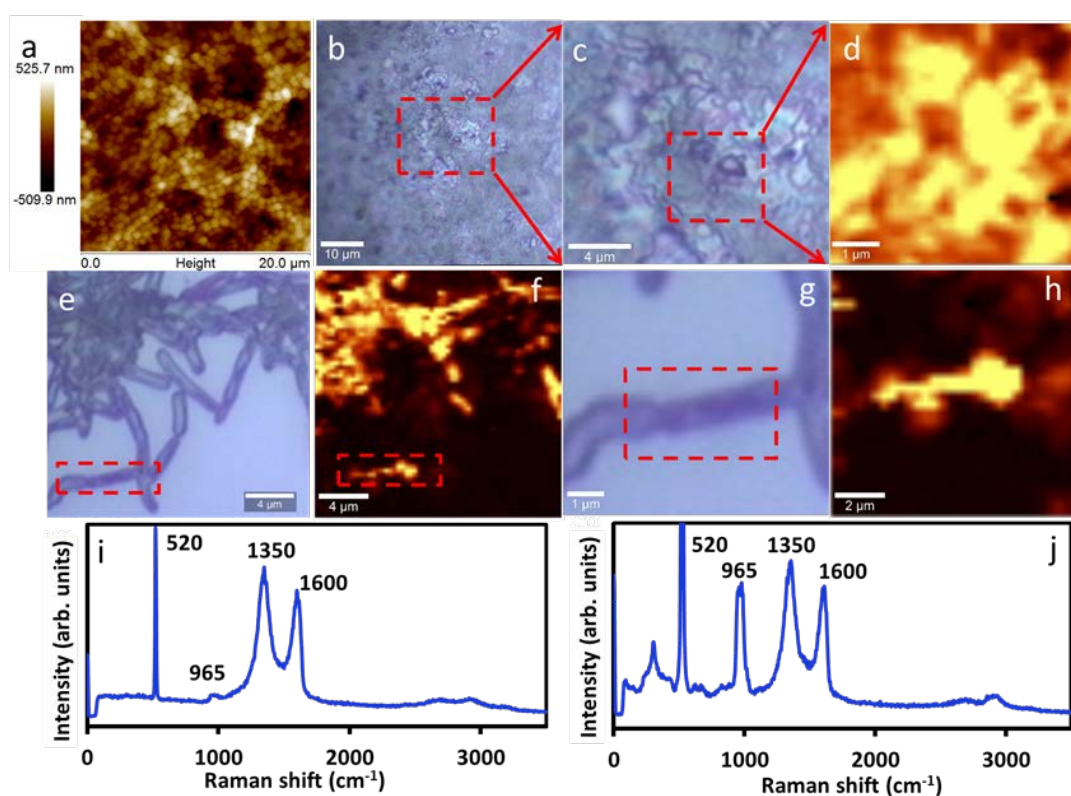


Figure 4.6. (a) AFM image acquired in approximately the same region as the optical micrographs of the *S. aureus* bacteria. (b) Optical microscope image (x100) of GO wrapped *S. aureus* deposited on a cleaned silicon surface and (c) Zoomed in image of (b). (d) Raman image, plotting the intensity of the 1600 cm^{-1} peak typical for the graphitic band of GO. (e)

Optical microscope image of GO wrapped *R.opacus*, (f) Raman image of (e), (g,h) Zoomed in image of (e,f) respectively. (i,j) Raman single spectra acquired on samples d and h respectively.

The growth of GO wrapped bacteria was monitored using optical density (OD) measurements (Appendix A5). The validity of using OD measurements for bacterial growth was also verified by its calibration with viable cell counting (Appendix A6).

According to these calibration curves, 1.0 OD unit (at 600 nm) is found to be equivalent to approximately 7×10^8 CFU.ml⁻¹ (colony forming units) *S. aureus* cells, and 4×10^7 CFU.ml⁻¹ *R. opacus* cells. For a better understanding on the differences between the growth of untreated bacteria and GO-wrapped bacterial cells, kinetic models were applied. Due to the more pronounced lag phase within the GO wrapped cells, a *logistic growth model* was applied for modelling the overall bacterial growth, including all three phases (i.e. lag, exponential, stationary). The amount of X bacterial concentration at time t is given according to the following equation, where X₀ is the initial and X_m is the maximum cell concentrations, and k_c is the apparent growth rate (see Appendix A7 for the detailed derivation stages of the following equation) [53]:

$$X = \frac{X_m}{1 + \left(\frac{X_m}{X_0} - 1\right) \cdot e^{-k_c \cdot t}} = \frac{a}{1 + b \cdot e^{-c \cdot t}} \quad (1)$$

Calculation of the logistic constants (a, b, and c), curve fitting, and the statistical analysis in the form of R² (coefficient of determination, as a parameter to show how well a statistical model fits the experimental observations) were carried out by a software program CurveExpert 1.4, and given in Fig. 4.7 and Fig. 4.8 below. In addition to the logistic model, specific growth rate of the exponential phase (μ_{exp}) were also found by calculating the slope of the linear data range of the exponential growth phase. Apparent growth rate (k_c) of the overall experiment and specific growth rate of the exponential phase (μ_{exp}) are given in Table 4.1.

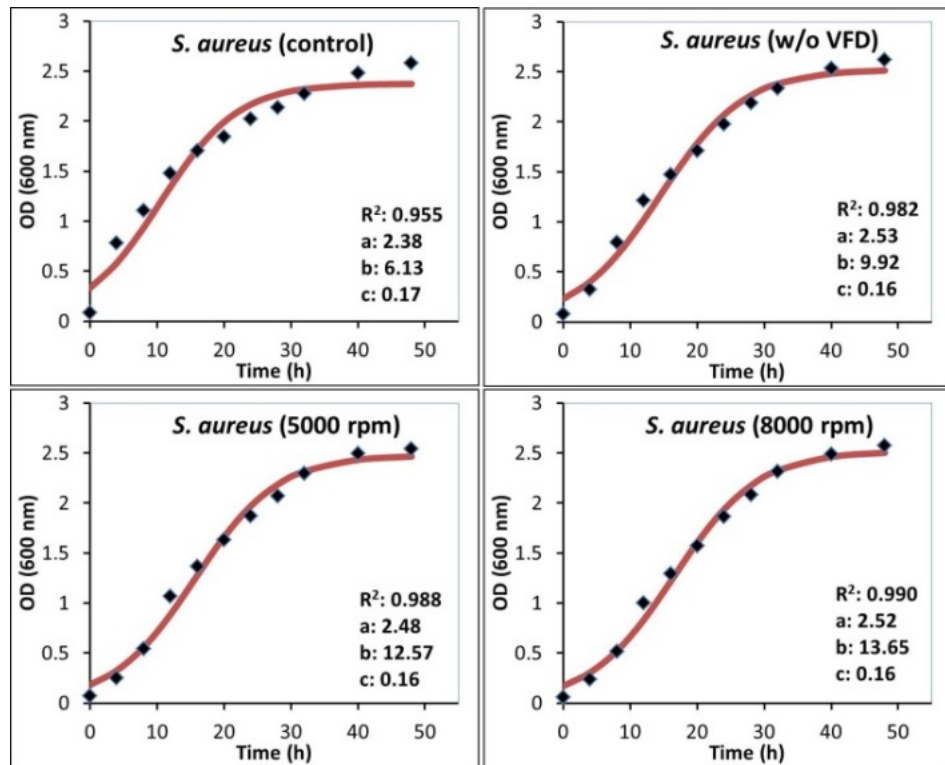


Figure 4.7. Bacterial growth curves for *S. aureus* cells regrown in nutrient media after wrapping with GO. Inset information of each figure shows the logistic model constants of equation-1 (a, b, and c), and the coefficient of determination (R^2).

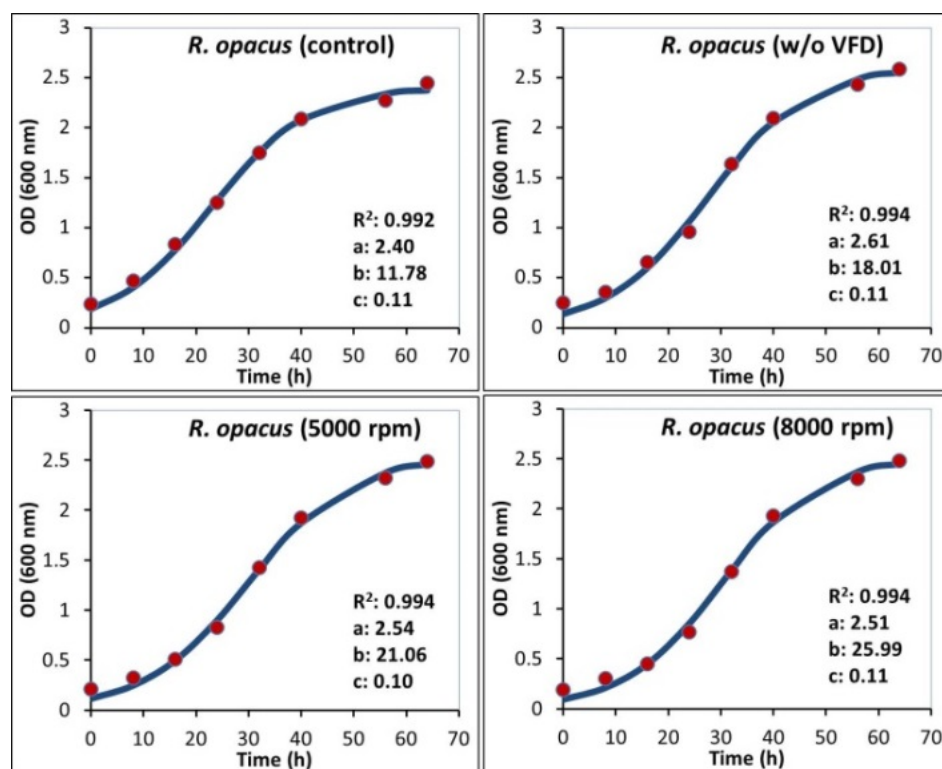


Figure 4.8. Bacterial growth curves for *R.opacus* cells regrown in nutrient media after wrapping with GO. Inset information of each figure shows the logistic model constants of equation-1 (a, b, and c), and the coefficient of determination (R^2).

Detailed growth analysis revealed that GO wrapped bacteria retained their biological activity even after interfacing with graphene oxide (Fig. 4.7, Fig. 4.8). While all cases showed a successful fit for *logistic growth model*, GO wrapped cells displayed relatively better fitting compared to their untreated bacteria controls, particularly for *S. aureus*. This might be caused by the more pronounced lag phase for the GO wrapped bacterial cells, due to the physical boundaries caused by the surrounding GO nano sheets for a certain time interval, which was ~8 hours for GO wrapped *S. aureus* and ~16 hours for GO wrapped *R. opacus*, with both processed in VFD. The main difference between the VFD processed and unprocessed GO-wrapped bacterial samples (w/o VFD) was that the lag time was longer for the samples processed in the VFD, allowing the cells a longer microencapsulation stage, whereas without VFD processing, samples escaped from their matrix faster (~4 hours for *S. aureus*, and ~8 hours for *R. opacus*). According to the growth rates given in Table 4.1 GO wrapped *S. aureus* cells had slightly lower apparent growth rates (k_c), while k_c values were quite similar for *R. opacus* cells compare to their unwrapped cell counterparts. On the other hand, both *S. aureus* and *R. opacus* cells showed distinctively higher

growth rates during their exponential phase once being released from their entrapment matrix, while maintaining their biological activity. A similar result was also observed in our previous studies with GO wrapped *Chlorella vulgaris* microalgal cultures [16]. The decrease in the cellular growth rate of the bacteria due to GO microencapsulation is a controllable immobilization strategy for processing industrially relevant bacteria while maintaining their biological activity [14].

Table 4.1 Kinetic model parameters for *S. aureus* and *R. opacus* bacteria; k_c is the apparent growth rate in h^{-1} , and μ_{exp} is the specific growth rate of the exponential phase in h^{-1} .

Samples	k_c (h^{-1})	μ_{exp} (h^{-1})
<i>S. aureus</i> (control)	0.173	0.038
<i>S. aureus</i> (5000)	0.162	0.060
<i>S. aureus</i> (8000)	0.159	0.063
<i>S. aureus</i> (w/o VFD)	0.159	0.071
<i>R. opacus</i> (control)	0.108	0.047
<i>R. opacus</i> (5000)	0.102	0.055
<i>R. opacus</i> (8000)	0.108	0.061
<i>R. opacus</i> (w/o VFD)	0.105	0.056

4.5 Conclusions

Facile wrapping of bacteria with GO using vortex fluidics has been successfully achieved while keeping the cells alive and biologically active. The wrapped cells had a longer lag time of growth due to their restricted environment within the GO sheets after processing in the VFD. In order to achieve higher microencapsulation efficiencies, keeping the GO-wrapped cells within their growth environment for extended periods may be an issue, in facilitating cell growth and escape from the GO matrix.

VFD processing is effective for wrapping or interfacing microorganisms with GO as a thin layered material. We note that other methods to interface graphene sheets onto the surface of microorganisms usually involves extensive chemical modification of the graphene sheets, such as functionalization with protein as reported by Mohanty *et al.* [28]. Similarly Kempaiah *et al.* established that calcium-ion functionalized graphene sheets can easily interface with yeast cells whereas unfunctionalized graphene sheets fail to interface with the cells [27]. Herein, we demonstrate the encapsulation of cells without the need for chemical modification of the graphene sheets. The process has potential for surface functionalization of bacteria cells, immobilizing them for applications in devices, sensors, controlled drug release and targeted delivery, wastewater treatment, for example. Other thin layered materials can also be considered for making composite materials involving VFD wrapping, including hexagonal boron nitride, and molybdenum and tungsten disulphides (MoS₂ and WS₂ respectively). Also noteworthy, is that interfacing soft material with GO or more conductive graphene sheets can provide a conductive layer around the material, without the need for pre-coating for SEM studies, for example with platinum. This offers scope as a general technique for SEM imaging, noting the VFD itself is a rather inexpensive technology [32].

4.6 Acknowledgements

We gratefully acknowledge support of this work by the Australian Research Council, the Government of South Australia and the National Health and Medical Research Council. M.H. Wahid would like to thank the Malaysian Government and Universiti Putra Malaysia for his PhD research funding. TEM, SEM and AFM studies were carried out using facilities in Adelaide Microscopy at The University of Adelaide and Flinders University, supported by the Australian Microscopy and Microanalysis Research Facility (AMMRF).

4.7 References

- 1 Todar, K. (2006) *Todar's online textbook of bacteriology*. University of Wisconsin-Madison Department of Bacteriology.
- 2 Rosenberg, E. (2006). Biotechnology and Applied Microbiology. In *The Prokaryotes* (284-298). Springer New York.

- 3 Brierly, C. L. (2001). Bacterial succession in bioheap leaching. *Hydrometallurgy*, 59(2), 249-255.
- 4 Valenzuela, L., Chi, A., Beard, S., Orell, A., Guiliani, N., Shabanowitz, J., Hunt, D. F. and Jerez, C. A. (2006). Genomics, metagenomics and proteomics in biomining microorganisms. *Biotechnology Advances*, 24(2), 197-211.
- 5 Rahman, K. S. M., Rahman, T. J., Kourkoutas, Y., Petsas, I., Marchant, R. and Banat, I. M. (2003). Enhanced bioremediation of n-alkane in petroleum sludge using bacterial consortium amended with rhamnolipid and micronutrients. *Bioresource Technology*, 90(2), 159-168.
- 6 Singh, R., Paul, D. and Jain, R. K. (2006). Biofilms: implications in bioremediation. *Trends in Microbiology*, 14(9), 389-397.
- 7 Nguyen, P. and Berry, V. (2012). Graphene interfaced with biological cells: opportunities and challenges. *The Journal of Physical Chemistry Letters*, 3(8), 1024-1029.
- 8 Raff, J., Soltmann, U., Matys, S., Selenska-Pobell, S., Böttcher, H. and Pompe, W. (2003). Biosorption of uranium and copper by biocers. *Chemistry of Materials*, 15(1), 240-244.
- 9 Perullini, M., Jobbágy, M., Mouso, N., Forchiassin, F. and Bilmes, S. A. (2010). Silica-alginate-fungi biocomposites for remediation of polluted water. *Journal of Materials Chemistry*, 20(31), 6479-6483.
- 10 Wahid, M. H., Eroglu, E., Chen, X., Smith, S. M. and Raston, C. L. (2013). Functional multi-layer graphene–algae hybrid material formed using vortex fluidics. *Green Chemistry*, 15(3), 650-655.
- 11 Sun, H., Cao, L. and Lu, L. (2012). Bacteria promoted hierarchical carbon materials for high-performance supercapacitor. *Energy & Environmental Science*, 5(3), 6206-6213.
- 12 Yang, D. P., Chen, S., Huang, P., Wang, X., Jiang, W., Pandoli, O. and Cui, D. (2010). Bacteria-template synthesized silver microspheres with hollow and porous structures as excellent SERS substrate. *Green Chemistry*, 12(11), 2038-2042.
- 13 Shim, H. W., Jin, Y. H., Seo, S. D., Lee, S. H. and Kim, D. W. (2010). Highly reversible lithium storage in bacillus subtilis-directed porous Co₃O₄ nanostructures. *ACS Nano*, 5(1), 443-449.
- 14 Liu, Y., Rafailovich, M. H., Malal, R., Cohn, D., & Chidambaram, D. (2009). Engineering of bio-hybrid materials by electrospinning polymer-

microbe fibers. *Proceedings of the National Academy of Sciences*, 106(34), 14201-14206.

- 15 Baca, H. K., Carnes, E., Singh, S., Ashley, C., Lopez, D. and Brinker, C. J. (2007). Cell-directed assembly of bio/nano interfaces—a new scheme for cell immobilization. *Accounts of Chemical Research*, 40(9), 836-845.
- 16 Wahid, M. H., Eroglu, E., Chen, X., Smith, S. M. and Raston, C. L. (2013). Entrapment of *Chlorella vulgaris* cells within graphene oxide layers. *RSC Advances*, 3(22), 8180-8183.
- 17 Anal, A. K. and Singh, H. (2007). Recent advances in microencapsulation of probiotics for industrial applications and targeted delivery. *Trends in Food Science & Technology*, 18(5), 240-251.
- 18 Islam, M. A., Yun, C. H., Choi, Y. J. and Cho, C. S. (2010). Review: Microencapsulation of Live Probiotic Bacteria. *Journal of Microbiology and Biotechnology*, 20(10), 1367-1377.
- 19 Cook, M. T., Tzortzis, G., Khutoryanskiy, V. V. and Charalampopoulos, D. (2013). Layer-by-layer coating of alginate matrices with chitosan–alginate for the improved survival and targeted delivery of probiotic bacteria after oral administration. *Journal of Materials Chemistry B*, 1(1), 52-60.
- 20 Bang, S. S. and Pazirandeh, M. (1999). Physical properties and heavy metal uptake of encapsulated *Escherichia coli* expressing a metal binding gene (NCP). *Journal of Microencapsulation*, 16(4), 489-499.
- 21 Tong, H. W., Mutlu, B. R., Wackett, L. P. and Aksan, A. (2014). Manufacturing of bioreactive nanofibers for bioremediation. *Biotechnology and Bioengineering*, 111(8), 1483-1493.
- 22 John, R. P., Tyagi, R. D., Brar, S. K., Surampalli, R. Y. and Prévost, D. (2011). Bio-encapsulation of microbial cells for targeted agricultural delivery. *Critical Reviews in Biotechnology*, 31(3), 211-226.
- 23 Kailasapathy, K. (2002). Microencapsulation of probiotic bacteria: technology and potential applications. *Current Issues in Intestinal Microbiology*, 3(2), 39-48.
- 24 Fakhrullin, R. F., García-Alonso, J. and Paunov, V. N. (2010). A direct technique for preparation of magnetically functionalised living yeast cells. *Soft Matter*, 6(2), 391-397.
- 25 Yang, S. H., Lee, T., Seo, E., Ko, E. H., Choi, I. S. and Kim, B. S. (2012). Interfacing living yeast cells with graphene oxide nanosheaths. *Macromolecular Bioscience*, 12(1), 61-66.

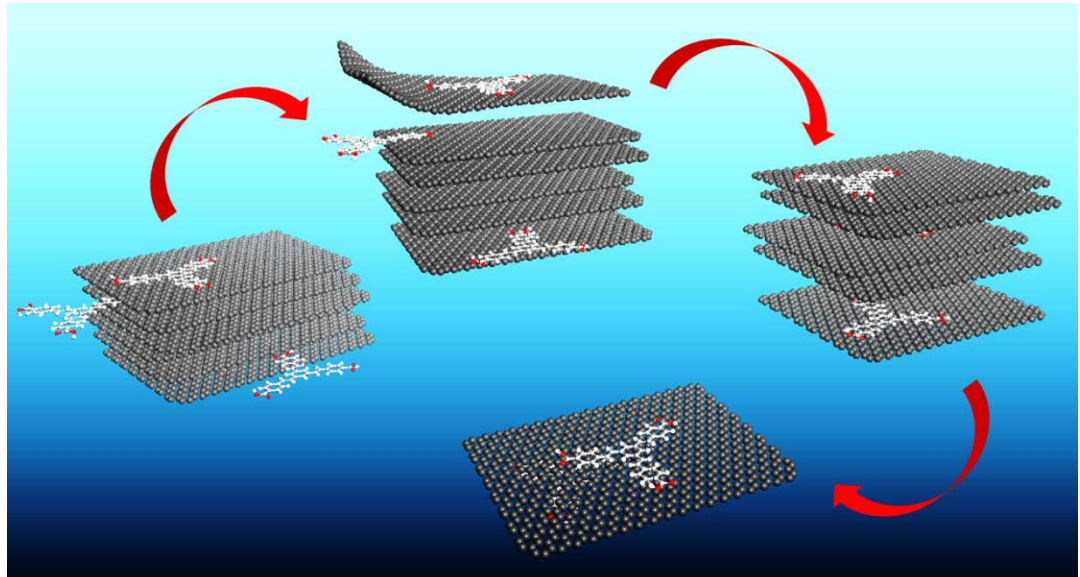
- 26 Wang, G., Wang, L., Liu, P., Yan, Y., Xu, X. and Tang, R. (2010). Extracellular silica nanocoat confers thermotolerance on individual cells: a case study of material-based functionalization of living cells. *ChemBioChem*, 11(17), 2368-2373.
- 27 Kempaiah, R., Salgado, S., Chung, W. L. and Maheshwari, V. (2011). Graphene as membrane for encapsulation of yeast cells: protective and electrically conducting. *Chemical Communications*, 47(41), 11480-11482.
- 28 Mohanty, N., Fahrenholtz, M., Nagaraja, A., Boyle, D. and Berry, V. (2011). Impermeable graphenic encasement of bacteria. *Nano letters*, 11(3), 1270-1275.
- 29 Salas, E. C., Sun, Z., Luttge, A. and Tour, J. M. (2010). Reduction of graphene oxide via bacterial respiration. *ACS Nano*, 4(8), 4852-4856.
- 30 Dikin, D. A., Stankovich, S., Zimney, E. J., Piner, R. D., Dommett, G. H., Evmenenko, G., Nguyen, S. T. and Ruoff, R. S. (2007). Preparation and characterization of graphene oxide paper. *Nature*, 448(7152), 457-460.
- 31 Kim, F., Cote, L. J. and Huang, J. (2010). Graphene Oxide: Surface Activity and Two-Dimensional Assembly. *Advanced Materials*, 22(17), 1954-1958.
- 32 Ruiz, O. N., Fernando, K. S., Wang, B., Brown, N. A., Luo, P. G., McNamara, N. D., Vangsnest, M., Sun, Y. P. and Bunker, C. E. (2011). Graphene oxide: a nonspecific enhancer of cellular growth. *ACS Nano*, 5(10), 8100-8107.
- 33 Yasmin, L., Chen, X., Stubbs, K. A. and Raston, C. L. (2013). Optimising a vortex fluidic device for controlling chemical reactivity and selectivity. *Scientific Reports*, 3.
- 34 Yasmin, L., Coyle, T., Stubbs, K. A. and Raston, C. L. (2013). Stereospecific synthesis of resorcin [4] arenes and pyrogallol [4] arenes in dynamic thin films. *Chemical Communications*, 49(93), 10932-10934.
- 35 Yasmin, L., Stubbs, K. A. and Raston, C. L. (2014). Vortex fluidic promoted Diels–Alder reactions in an aqueous medium. *Tetrahedron Letters*, 55(14), 2246-2248.
- 36 Britton, J., Dalziel, S. B. and Raston, C. L. (2015). Continuous flow Fischer esterifications harnessing vibrational-coupled thin film fluidics. *RSC Advances*, 5(3), 1655-1660.
- 37 Britton, J. and Raston, C. L. (2014). Continuous flow vortex fluidic production of biodiesel. *RSC Advances*, 4(91), 49850-49854.

- 38 Boulos, R. A., Zhang, F., Tjandra, E. S., Martin, A. D., Spagnoli, D. and Raston, C. L. (2014). Spinning up the polymorphs of calcium carbonate. *Scientific Reports*, 4.
- 39 Tong, C. L., Boulos, R. A., Yu, C., Iyer, K. S. and Raston, C. L. (2013). Continuous flow tuning of ordered mesoporous silica under ambient conditions. *RSC Advances*, 3(41), 18767-18770.
- 40 Vimalanathan, K., Chen, X. and Raston, C. L. (2014). Shear induced fabrication of intertwined single walled carbon nanotube rings. *Chemical Communications*, 50(77), 11295-11298.
- 41 Chen, X., Dobson, J. F. and Raston, C. L. (2012). Vortex fluidic exfoliation of graphite and boron nitride. *Chemical Communications*, 48(31), 3703-3705.
- 42 Yasin, F. M., Boulos, R. A., Hong, B. Y., Cornejo, A., Iyer, K. S., Gao, L., Chua, H. T. and Raston, C. L. (2012). Microfluidic size selective growth of palladium nano-particles on carbon nano-onions. *Chemical Communications*, 48(81), 10102-10104.
- 43 Yasin, F. M., Iyer, K. S. and Raston, C. L. (2013). Palladium nano-carbon-calixarene based devices for hydrogen sensing. *New Journal of Chemistry*, 37(10), 3289-3293.
- 44 Chen, X., Yasin, F. M., Eggers, P. K., Boulos, R. A., Duan, X., Lamb, R. N., Iyer, K. S. and Raston, C. L. (2013). Non-covalently modified graphene supported ultrafine nanoparticles of palladium for hydrogen gas sensing. *RSC Advances*, 3(10), 3213-3217.
- 45 Eroglu, E., D'Alonzo, N. J., Smith, S. M. and Raston, C. L. (2013). Vortex fluidic entrapment of functional microalgal cells in a magnetic polymer matrix. *Nanoscale*, 5(7), 2627-2631.
- 46 Yuan, T. Z., Ormonde, C. F., Kudlacek, S. T., Kunche, S., Smith, J. N., Brown, W. A., Pugliese, K. M., Olsen, T. J., Iftikhar, M., Raston, C. L. and Weiss, G. A. (2015). Shear-Stress-Mediated Refolding of Proteins from Aggregates and Inclusion Bodies. *ChemBioChem*, 16(3), 393-396.
- 47 Di Gennaro, P., Rescalli, E., Galli, E., Sello, G. and Bestetti, G. (2001). Characterization of *Rhodococcus opacus* R7, a strain able to degrade naphthalene and o-xylene isolated from a polycyclic aromatic hydrocarbon-contaminated soil. *Research in Microbiology*, 152(7), 641-651.
- 48 Zhang, W., Zhou, C., Zhou, W., Lei, A., Zhang, Q., Wan, Q. and Zou, B. (2011). Fast and considerable adsorption of methylene blue dye onto

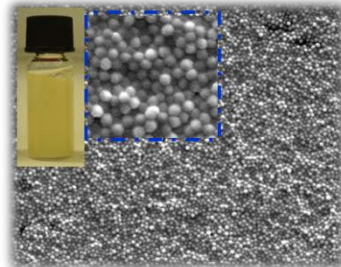
graphene oxide. *Bulletin of Environmental Contamination and Toxicology*, 87(1), 86-90.

- 49 Hummers Jr, W. S. and Offeman, R. E. (1958). Preparation of graphitic oxide. *Journal of the American Chemical Society*, 80(6), 1339-1339.
- 50 Kovtyukhova, N. I., Ollivier, P. J., Martin, B. R., Mallouk, T. E., Chizhik, S. A., Buzaneva, E. V. and Gorchinskiy, A. D. (1999). Layer-by-layer assembly of ultrathin composite films from micron-sized graphite oxide sheets and polycations. *Chemistry of Materials*, 11(3), 771-778.
- 51 Berney, M., Hammes, F., Bosshard, F., Weilenmann, H. U. and Egli, T. (2007). Assessment and interpretation of bacterial viability by using the LIVE/DEAD BacLight Kit in combination with flow cytometry. *Applied and Environmental Microbiology*, 73(10), 3283-3290.
- 52 Ramesha, G. K. and Sampath, S. (2009). Electrochemical reduction of oriented graphene oxide films: an in situ Raman spectroelectrochemical study. *The Journal of Physical Chemistry C*, 113(19), 7985-7989.
- 53 Shuler, M. L. and Kargi, F. (1992). *Bioprocess Engineering: Basic Concepts*. New York: Prentice Hall.

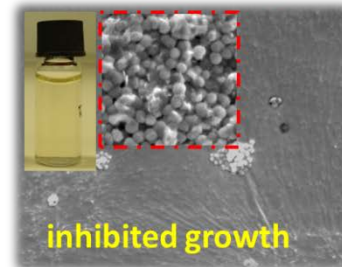
5. AQUEOUS BASED SYNTHESIS OF ANTIMICROBIAL-DECORATED GRAPHENE



S. aureus control



S. aureus + graphene/Ramizol®



This chapter is a reformatted version of the paper published in *Journal of Colloid and Interface Science*, Year 2015, Vol. 443, Pages 88-96.

5.1 Abstract

Ramizol[®] (1,3,5-tris[(1E)-2'-(4'-benzoic acid)vinyl]benzene) is a potent amphiphilic anti-microbial agent. It is essentially a planar molecule and can interact with the surface of graphene via extended π - π interactions. Herein we demonstrate the utility of Ramizol[®] in potentially acting as a molecular 'wedge' to exfoliate graphene and stabilize it in water. The non-covalent attachment of Ramizol[®] on the graphene surface enables release of Ramizol[®] by altering the pH of the solution. Furthermore, the stabilized composite material demonstrates antibacterial activity against *Staphylococcus aureus* which leads to potential in biomedical applications with graphene acting as a drug carrier as well as enhancing the structural strength of the composite material.

5.2 Introduction

The remarkable properties of graphene such as high electron mobility, high mechanical strength, flexibility and transparency, has led to extensive research efforts to produce the 2D material on a large scale [1-4]. Exfoliation is possible directly from graphite as a relatively cheap and abundant material, which requires overcoming relatively strong van der Waals interactions between the graphitic layers [5,6]. Developing processes to assist this exfoliation, as well as stabilising the sheets after exfoliation is important in advancing the diversity of applications of graphene, which includes its use as an antimicrobial agent in its own right [7,8]. Also important is avoiding the use of harsh chemical reagents or the production of toxic by-products, for developing sustainable technologies for the future.

Various methods have been reported for the production of graphene, from chemical vapour deposition [9], reduction of graphite oxide [10], micromechanical cleavage of graphite [11], ultra-sonication in an organic solvent such as N-methyl-2-pyrrolidone [12] or in water with the addition of a surfactant [13-16], dissolution in super acid [17], to the use of high shear forces [4,18]. We recently established the synthesis of multi-layer graphene from graphite in water using shear within a thin film microfluidic vortex fluidic device, without the need for a stabilising surfactant [19]. Given the antimicrobial property of graphene [7,8], we sought to use an antimicrobial agent to enhance this property of graphene, and also to facilitate the exfoliation process as well as acting as a stabilising agent at physiological pH.

Ramizol[®] (1,3,5-tris[(1E)-2'-(4'-benzoic acid)vinyl]benzene) is a potent and non-toxic synthetic antimicrobial agent [20-22], and features in this study, in developing a composite with graphene, along with the choice of water as the reaction medium. The latter was deemed important in incorporating green chemistry metrics into the synthesis from the outset.

Ramizol[®] is essentially a planar molecule and can in principle interact with the surface of graphene *via* extended π - π interactions, with potential then for stabilising the graphene in water. Intense shear and high cavitation forces [23-25] induced by ultrasonic mechanoenergy act on the bulk graphite, resulting in exfoliation [25]. In addition, the shape of Ramizol[®] lends itself to facilitate exfoliation of graphene from graphite in potentially acting as a molecular 'wedge' during sonication (Fig. 5.1), where the graphene sheets are prized apart. Such a process during sonication is likely to result in the exfoliation of graphene in water, as a related process to that established in the exfoliation of graphene in the presence of *p*-phosphonic acid calix[8]arene [15] and pyrene derivatives [13,14,16]. The presence of the ionisable carboxylic groups on the pendant arms of Ramizol[®] renders the molecule soluble in water at pH > 7. Ramizol[®] also exhibits antioxidant properties, similar to α -tocopherol (vitamin E), as a standard antioxidant [22], adding to its potent antimicrobial activity.

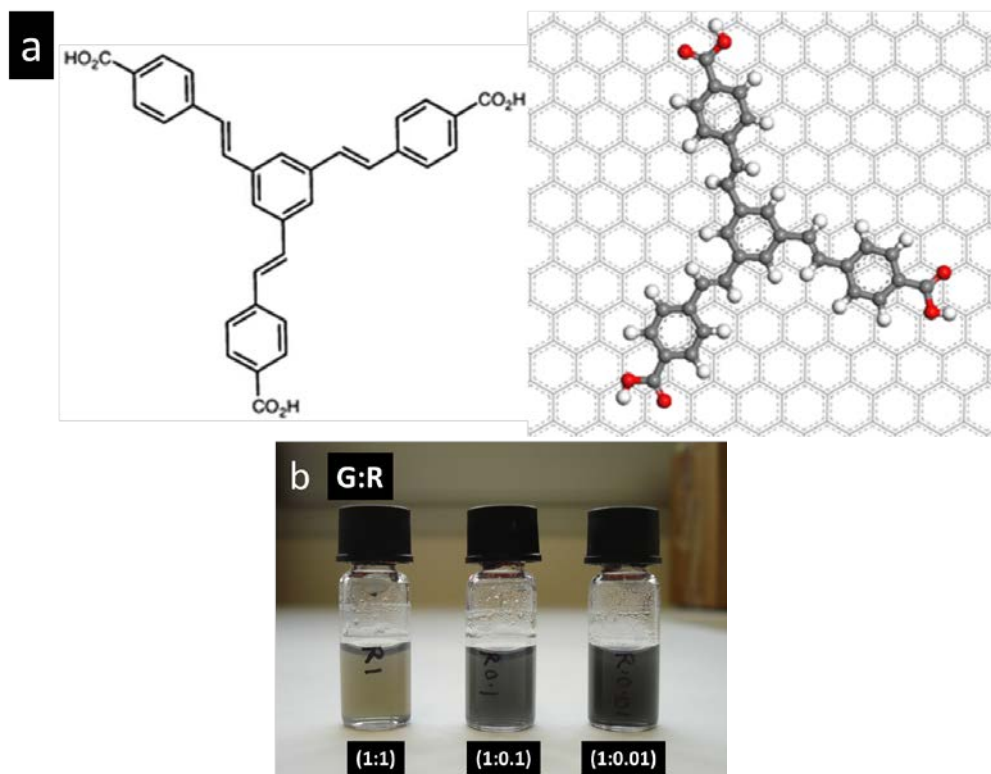


Figure 5.1. (a) Structure of Ramizol[®] (1,3,5-tris[(1E)-2'-(4'-benzoic acid) vinyl]benzene and a molecular dynamic simulation of it on the surface of graphene (Appendix A8). (b) Photograph of solutions derived from sonication of mixtures of different ratios of graphite and Ramizol[®] in water (G:R).

Functionalizing graphene with a biological active molecule is a design strategy for greater efficacy, noting composite nanomaterials are gaining prominence in applications in medicine [26-28]. Graphene and its derivative, namely graphene oxide, exhibit antibacterial property towards the Gram-negative bacteria, *Escherichia coli*, where it effectively cuts through the cell membrane of the bacteria releasing phospholipids, resulting in death of the bacteria [7]. In addition, composite materials of graphene, or graphene oxide with silver nanoparticles, and glutaraldehyde, are effective in killing *E. coli* and Gram-positive bacteria, *Staphylococcus aureus* [29-31]. More recently a composite of graphene oxide and curcumin has been developed for cancer therapy [32]. However, despite graphene oxide being more favourable for many applications because of its colloidal stability in aqueous media, the presence oxygen containing functional groups on its surface is a concern for biomedical applications [33]. Administration of graphene oxide into the lungs of mice results in severe and persistent lung injury [33]. In addition, graphene oxide increases the rate

of mitochondrial respiration and the generation of reactive oxygen species, activating inflammatory and apoptotic pathways of the cells. This is in contrast to pristine graphene which has minimal toxicity, which is reduced further by coating and stabilizing the graphene with block copolymer Pluronic [33]. Overall, the use of graphene in biomedical applications is advancing, for example, in the development the biocompatible graphene-based antibacterial paper [8].

We have established the facile exfoliation and stabilisation of graphene sheets in water at pH 10 by non-covalent functionalisation with Ramizol[®], with the resulting graphene/Ramizol[®] hybrid material exhibiting antibacterial properties. The exfoliated material is stable for more than 1 month, and unlike covalently functionalised graphene, the extended π conjugation on the graphene surface is maintained, and thus the electrical properties of the 2D sheets is preserved [34]. Interestingly Ramizol[®] is also fluorescent [21,22] and this was useful in terms of characterisation of the composite materials with graphene. From the perspective of drug delivery, the non-covalent functionalised graphene provides a platform for high drug loading and controlled release of the drug [26,35], with antimicrobial and antioxidant activity. Apart from acting as a drug carrier, graphene and multi-layer graphene can also impart mechanical stability, thermal conductivity [36] and flame retardant properties [37] which are promising for widespread applications.

5.3 Experimental methods

Ramizol[®] was synthesised following the literature procedure with minor changes to the method [38]. Ethyl acetate (20%) in hexane was used for monitoring the progress of the Heck cross coupling reaction between 1,3,5-tribromobenzene and ethyl 4-vinylbenzoate, using thin layer chromatography and 20:80 ethyl acetate–dichloromethane for eluting the product. Purification of the final product from the saponification reaction involved column chromatography using a 20:80 methanol–tetrahydrofuran solvent system, followed by the addition of diethyl ether as an anti-solvent to wash the product [38]. Graphite flakes (99%, particle size 7-10 μm in lineal dimension of the planar flakes) were purchased from Alfa Aesar and used as received.

Ramizol[®] was dissolved in Milli-Q water at a concentration of 0.1 mg mL⁻¹ after the addition of 0.1 M NaOH, such that the final pH of the solution was 10, noting Ramizol[®] has limited solubility at pH ≤ 7. Graphite flakes were added to the solution at a weight to weight (w/w) ratio of graphite to Ramizol[®] (G:R) of 1:1, 1:0.1 and 1:0.01 in a total of 20 mL of 0.1 mg.mL⁻¹ Ramizol[®] solution (Table 5.1).

Table 5.1 Composition of graphite and Ramizol[®] starting material

Sample	Graphite (mg/mL)	Ramizol[®] (mg/mL)
G:R (1:1)	0.1	0.1
G:R (1:0.1)	1.0	0.1
G:R (1:0.01)	10.0	0.1

The graphite-Ramizol[®] mixture were then ultrasonicated using a Sonics Vibra Cell ultrasonic liquid processor (130 Watt, 20 kHz) at 50% of the amplitude for 2 hours, whereupon they were centrifuged at 453 x g for 30 min to remove residual graphite flakes. Excess Ramizol[®] in the processed solution was removed from each reaction mixture by centrifugal washing with Milli-Q water at 18730 x g for 30 minutes. The final isolated mixture containing the exfoliated graphene sheets was redispersed in Milli-Q water, initially for characterisation purposes.

UV-Vis spectra of the samples were recorded using a Varian Cary 50 Bio UV/Visible spectrophotometer. Raman spectra were acquired using a WITec alpha300R confocal Raman microscope at 532 nm excitation wavelength. Transmission electron microscopy (TEM) characterization was carried out using the JEOL 2100 instrument operating at 120 kV. Atomic force microscopy (AFM) analysis in tapping mode was performed with a multimode AFM head and a NanoScope V controller (Digital Instruments, Veeco, Santa Barbra, USA) in ambient conditions. Scanning electron microscopy (SEM) analysis was performed on the FEI Quanta 450, with high voltage, 10 kV, and working distance, 10 mm. Antibacterial activity of graphene / Ramizol[®] against *Staphylococcus aureus* was investigated by monitoring the cell density by optical density measurements at 600 nm for a period

of 20 hours. The bacterial strain used was *S. aureus* ATCC 6538 which was grown overnight at 37 °C on Luria-Betani agar, the bacteria was then inoculated into 2x Mueller Hinton broth to give a starting concentration of 1×10^7 colony forming units per ml which equates to roughly an OD of 0.01. Subsequently, 5 mL of the bacterial suspension was added to tubes containing either 5 mL of NaOH in water at pH 10 as the negative control, pure Ramizol[®] [0.1 mg mL^{-1}], pure graphite sonicated in water [0.1 mg mL^{-1}] and the graphene/Ramizol[®] composite materials with the composition ratios presented in Table 5.2 below. pH of the starting media was pH 7.0 and upon addition of the sample the pH shifted slightly to 7.5.

Table 5.2 Composition of graphene and Ramizol[®] in graphene/Ramizol[®] composites used for antibacterial test against *S. aureus*.

Sample	Graphene (mg mL^{-1})	Ramizol [®] (mg mL^{-1})
G:R (1:1)	~0.09	0.1
G:R (1:0.1)	~0.90	0.1
G:R (1:0.01)	~1.80	0.1

The drug and bacterial mixture was then grown with shaking at ~250 rpm at 37 °C with samples taken every hour for 8 hours and the optical density determined at 600nm, and the final sample after overnight ($t = 20$ hours). The relevant media and pure Ramizol[®] samples (without bacteria) were used as a control for the optical density measurements. It is noteworthy that due to the high concentration of graphene in sample G:R (1:0.01), the sample was diluted 1:1 in water including the blank control and the optical density adjusted for this dilution.

5.4 Results and discussion

Ultrasonic mechanoenergy applied for 2 hours to the mixture of graphite and Ramizol[®] in water results in the exfoliation of graphite into multiple layers of graphene, affording a stable grey suspension, for all graphene:Ramizol[®] ratios (Fig. 5.1b). It is noteworthy that sonic energy and Ramizol[®] are both necessary for the exfoliation of graphene sheets. As shown in Figure 5.2, the use of Ramizol[®] in the

absence of the sonic energy (Fig. 5.2a) or the use of sonic energy in the absence of Ramizol[®] (Fig. 5.2b), no exfoliation and graphene stabilization occurred.

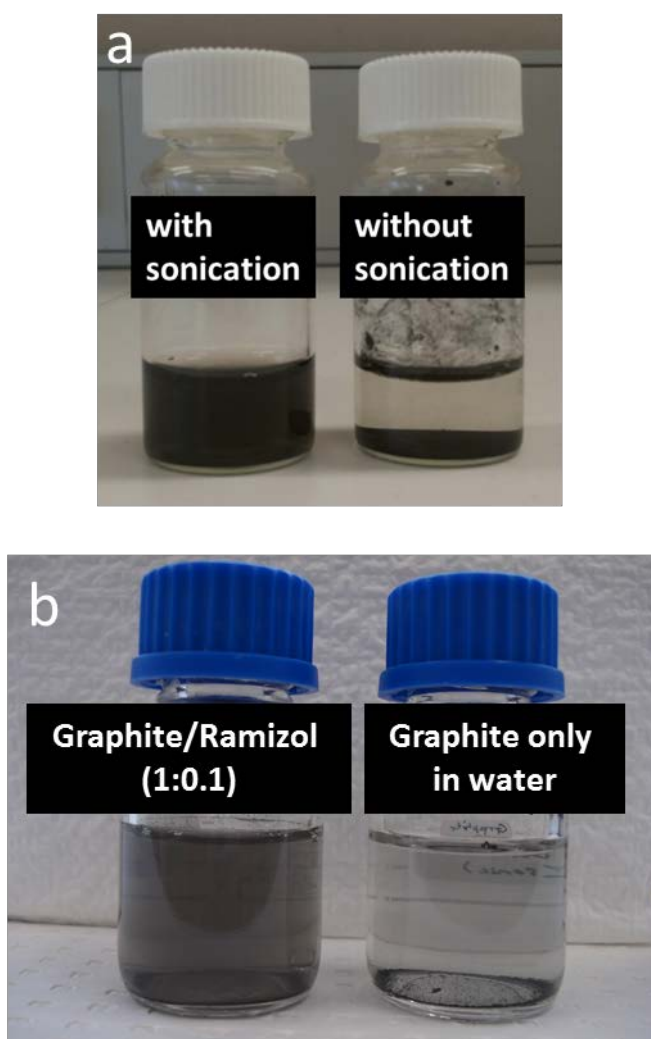


Figure 5.2. (a) Graphene/Ramizol[®] sample at the initial graphite to Ramizol[®] ratio, G:R (1:0.1) produced after sonication (image on the left) and a control sample prepared with the same starting material without sonication (image on the right). Sonication was carried out following the reported procedure, and the sample prepared without sonication involved manual shaking and left overnight) and (b) Photograph image of graphite in water, in the presence and absence of Ramizol[®]. Samples were sonicated following the described procedure and left overnight. In the case where no Ramizol[®] is present, any exfoliation is followed by rapid restacking.

The yield of exfoliated graphene sheets was determined by weighing the remaining graphite sediments after sonication, and subtracting it from the weight of initial graphite. This establishes an average yield of between 40% and 50% yield for G:R at

1:1 and 1:0.1, whereas for G:R 1:0.01 the yield was ca. 10%, presumably because of insufficient Ramizol[®] for effective graphene exfoliation and stabilisation of the colloidal particles. For the same ratio, increasing the concentration of Ramizol[®] to 0.15 mg mL⁻¹ resulted in a modest 4% increment in yield. Despite the high yields obtained for higher ratios, the thickness of graphene sheets obtained varied for different concentrations of Ramizol[®]. Importantly excess Ramizol[®] can be recovered and reused which is an advantage of using this processing method. A simple test to affirm that Ramizol[®] is non-covalently attached to at least the flat surface of the graphene, involved adding 0.1 mL of 1 M NaOH to 0.5 mL of the resulting solution, followed by mild sonication. This resulted in sedimentation of graphite following centrifugation at 453 x g, which is consistent with restacking of the previously stabilised colloidal solutions of graphene (Fig. 5.3). The formation of aggregates of restacked sheets due to the hydrophobic nature of graphite was verified using AFM and SEM (Fig. 5.3c and d).

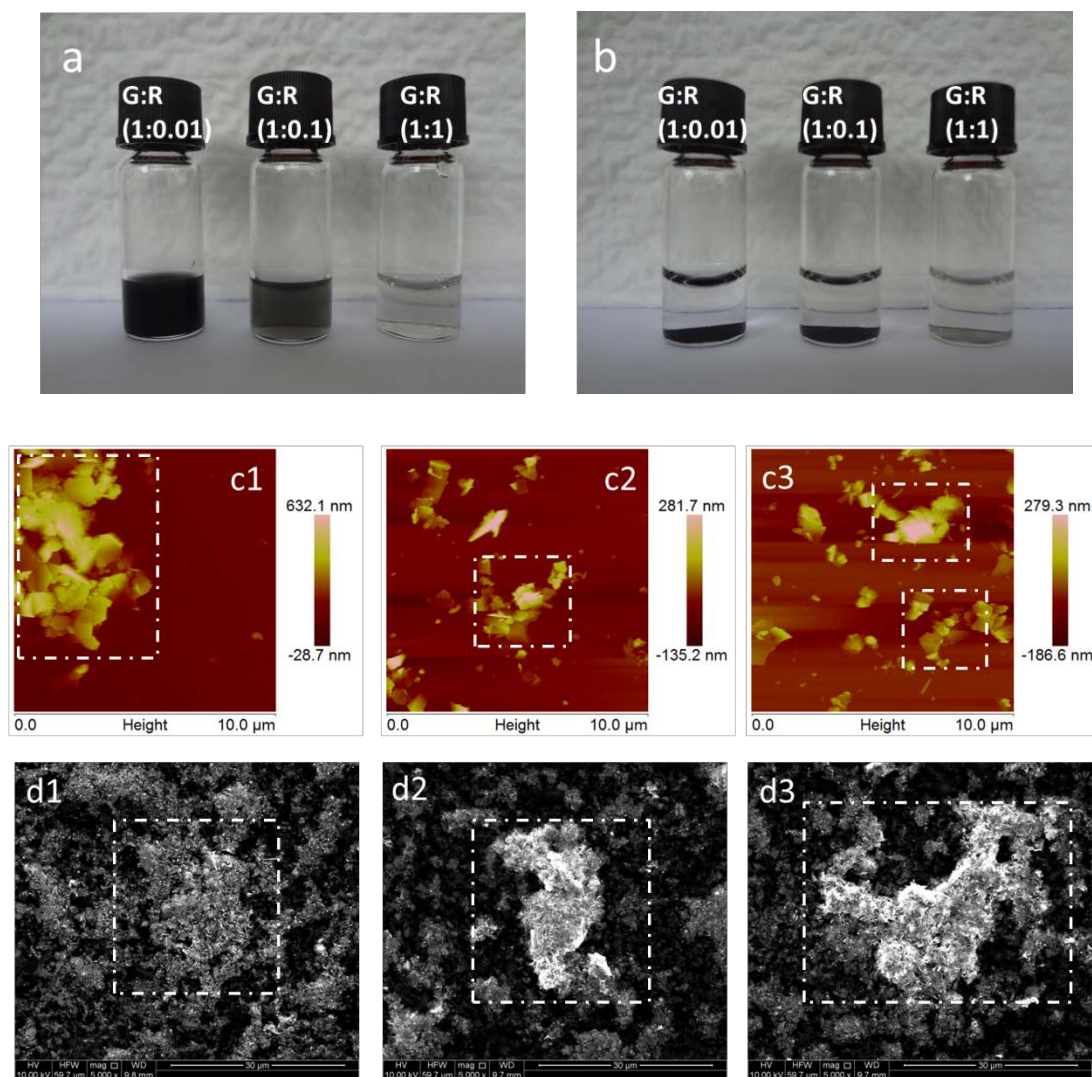


Figure 5.3. Photograph images of stabilised graphene/Ramizol[®] solutions, (a) before addition of aqueous NaOH (1 M), and (b) after the addition followed by mild sonication and centrifugation. AFM (c1-3) and SEM (d1-3) images at different regions of graphene/Ramizol[®] sample (initial graphite to Ramizol[®] ratio, G:R (1:0.1)) upon addition of NaOH followed by mild sonication and centrifugation. Rectangular dotted loops show formation of aggregates of restacked graphene sheets.

Ultraviolet (UV) - visible spectra of the graphene/Ramizol[®] composites are shown in Figure 5.4a. Pure Ramizol[®] (blue) shows strong absorption peaks at ~ 250 nm and ~ 320 nm which are weak for G:R 1:1 sample (red). For G:R 1:0.1 (light green) and G:R 1:0.01 (orange), the absorption peak of graphene at ~ 260 nm [39] is present which is consistent with the higher graphene to drug ratio. The effect of different graphene to Ramizol[®] ratios is also evident for fluorescence microscopy under FITC filters; green coloured regions represent Ramizol[®] within the sample (Fig. 5.4b). For

samples containing higher Ramizol[®] content, the contrast was clearer due to a higher drug concentration on the surface of graphene sheets (Fig. 5.4b).

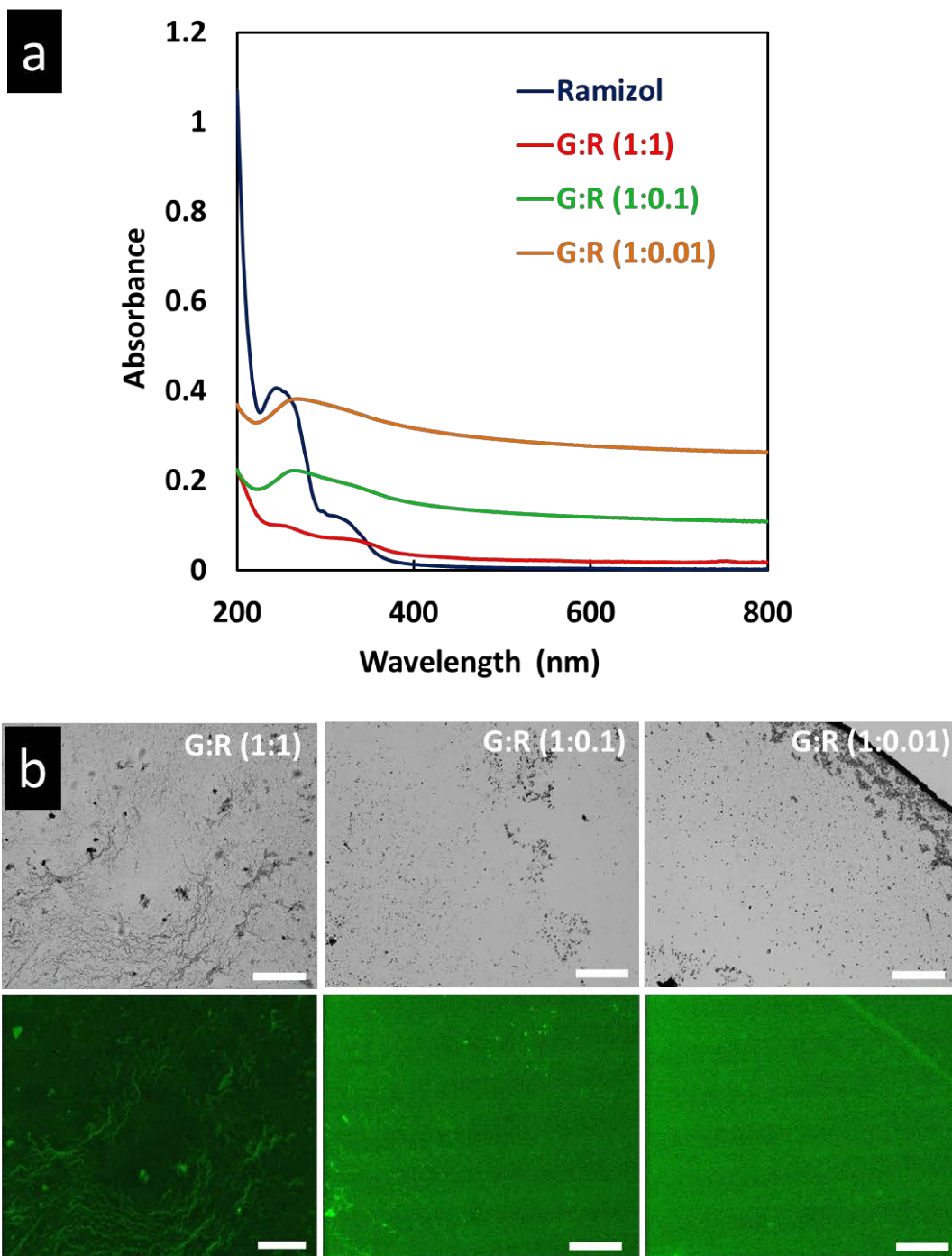


Figure 5.4. (a) UV-visible spectra of Ramizol[®] and graphene/Ramizol[®] composites at different ratios of graphite to Ramizol[®] (G:R) after centrifugal washing and redispersing in milli-Q water. (b) Bright field image (top row) of Ramizol[®] functionalised graphene and the corresponding fluorescence microscopy images (bottom row) at different w/w ratios of G:R (1:1), (1:0.1) and (1:0.01), respectively. (Scale bar: 100 μm).

Raman spectra of the graphene-containing samples were recorded using a 532 nm laser excitation wavelength, Figure 5.5. The prominent features of graphite/graphene are the G ($\sim 1580\text{ cm}^{-1}$), D ($\sim 1350\text{ cm}^{-1}$) and 2D ($\sim 2700\text{ cm}^{-1}$) bands [40], which are clearly observed for all samples. The D band represents graphitic disorder which is likely due to the edge effect and also structural defects introduced to graphene during the sonication process [15, 40]. The integrated intensity ratio, I_D/I_G for the D and G band, which is a measure of graphene defects [41], is higher for samples with a lower graphite concentration most likely due to smaller quantity of graphite being exposed to the sonic energy leading to deformation compared to graphite at a higher concentration. A small shoulder at 1900 cm^{-1} can be attributed to the presence of Ramizol[®] and/or partial oxidation of graphene arising from the sonication [15]. The 2D band profiles, Figure 5.5b, show the composite materials have narrower peaks compared to graphite, which is consistent with the few layers of graphene, as expected [40]. Raman spectra of graphene sheets composed of 5 layers or more are harder to distinguish from bulk graphite [40] and consequently transmission electron microscopy (TEM), atomic force microscopy (AFM) and scanning electron microscopy (SEM) were used as complementary tools to investigate the thickness of the sheets in such samples.

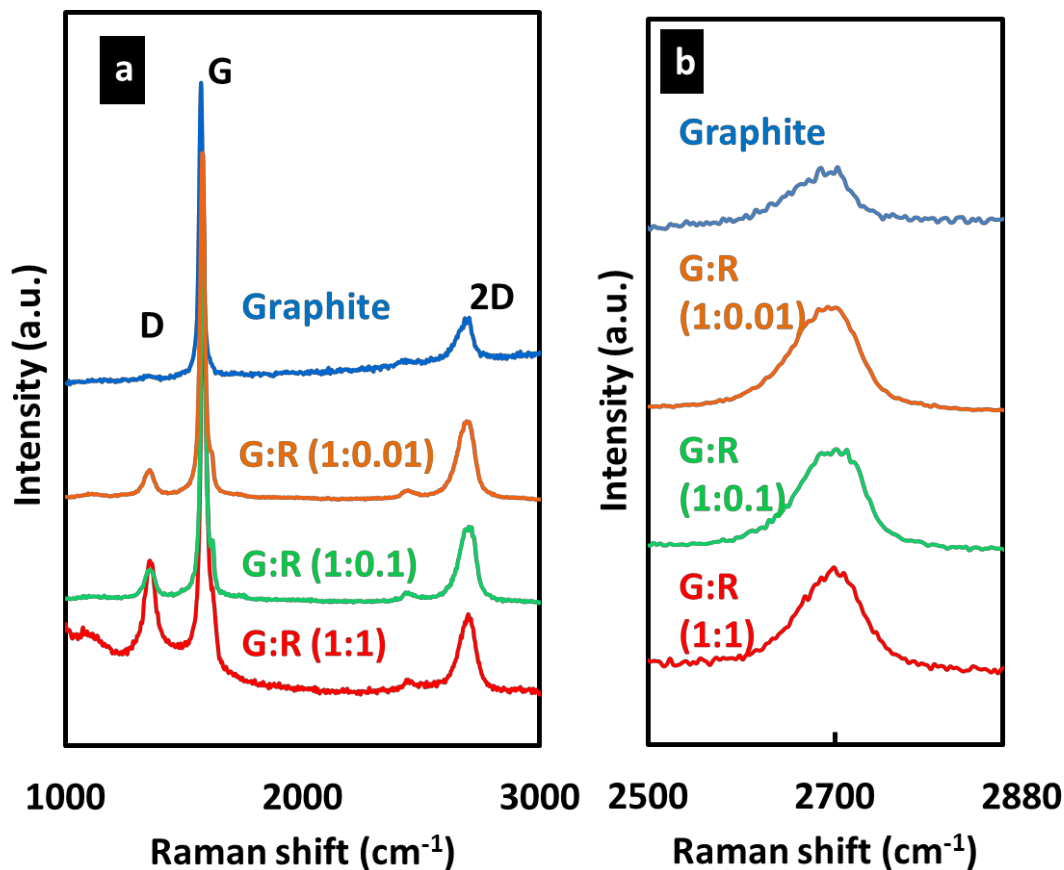


Figure 5.5. (a) Raman spectra at 532 nm of graphite flakes and graphene/Ramizol[®] composites at different ratios of graphite to Ramizol[®] (G:R). Dotted loops indicate a shoulder at 1900 cm⁻¹, and (b) comparison of scaled 2D band of the samples.

TEM images of the final product revealed few layers of graphene sheets with clear traces of Ramizol[®], particularly for G:R 1:1, Figure 5.6a, which corresponds to the highest loading of the compound. For G:R 1:1, the graphene sheets are more transparent compared to the other samples. For lower ratio of Ramizol[®], i.e. G:R 1:0.1, and G:R 1:0.01, possible partial restacking during sonication is evident by the presence of randomly stacked arrays, on the basis that a lower relative amount of Ramizol[®] is present to assist the exfoliation and stabilisation of graphene sheets. Electron diffraction of a selected area in Figure 5.6c displays the typical six-fold symmetry expected for graphite/graphene structure, Figure 5.6d. Sonication in water alone without any surfactant (Ramizol[®]) is significantly less effective in forming thin graphene sheets (Fig. 5.2b). Overall, the presence of Ramizol[®] is important in stabilising the graphene against restacking.

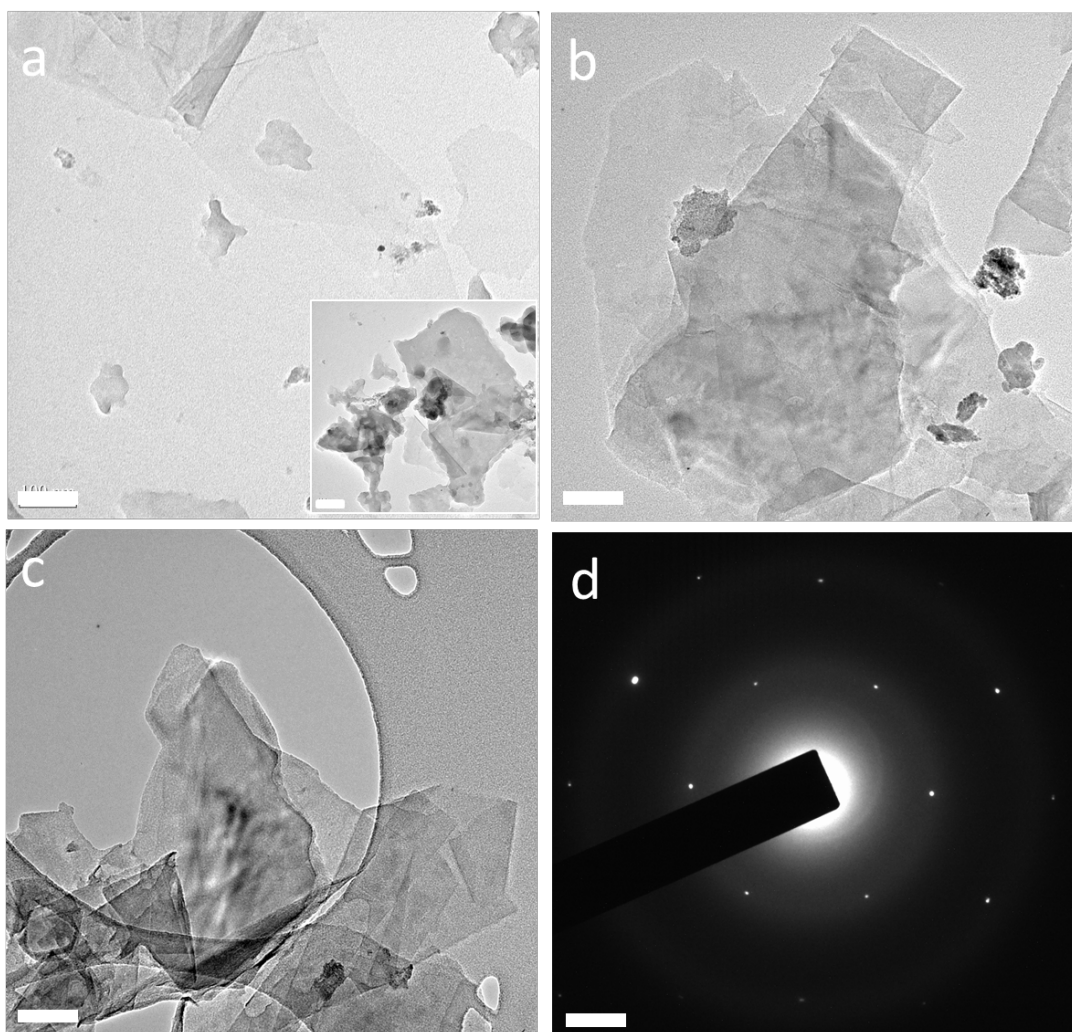
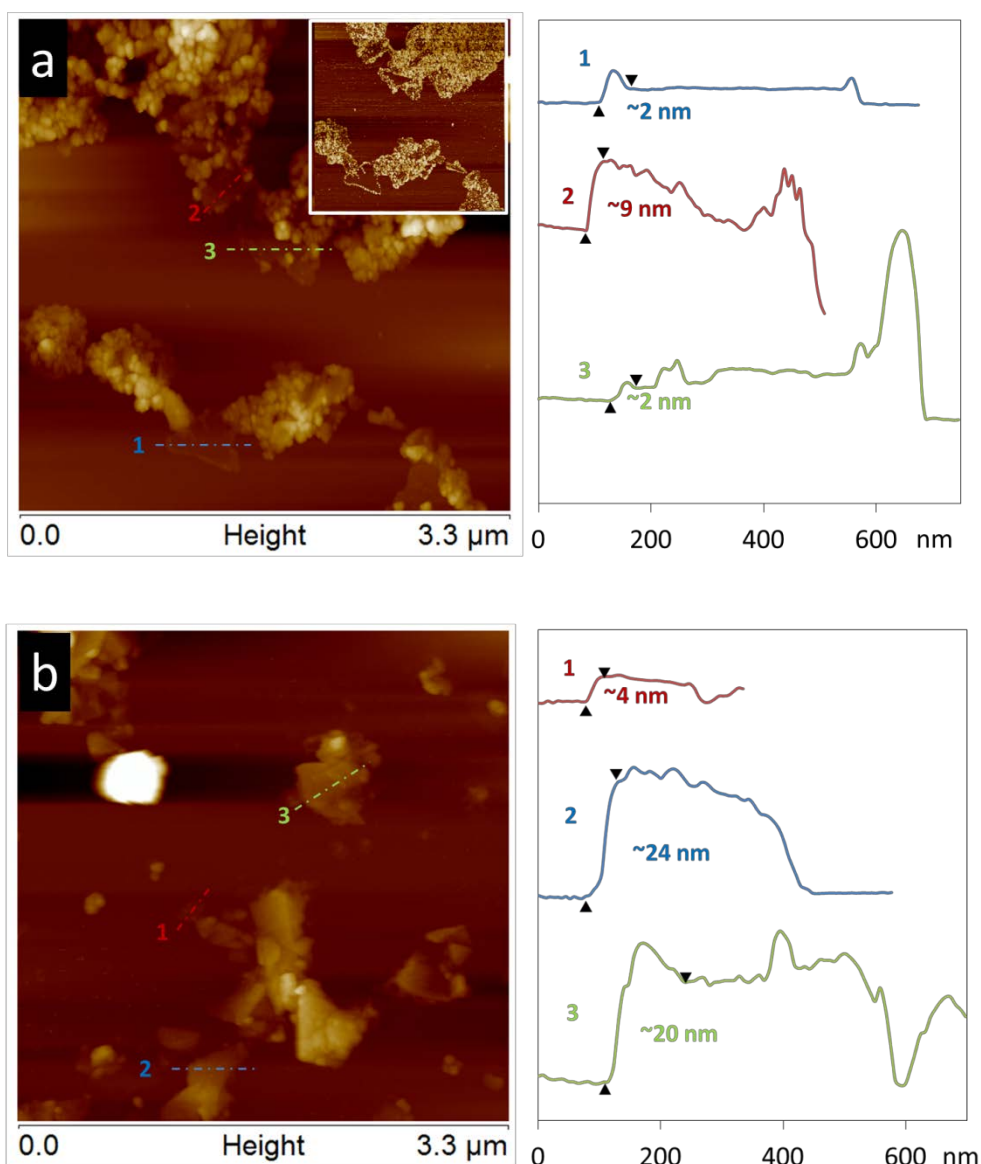


Figure 5.6. TEM images of graphene sheets prepared at different w/w ratios of graphite to Ramizol[®] (G:R). (a) 1:1. The inset TEM image shows significant traces of Ramizol[®] observed on graphene sheets from different area of the sample (b) 1:0.1 and (c) 1:0.01, and (d) electron diffraction pattern of a selected area in sample (c) (Scale bar: 100 nm).

AFM images using tapping mode revealed graphene sheets either partially or fully covered with Ramizol[®] which confirms the stabilising nature of the molecule, Figure 5.7. This is particularly evident for G:R 1:1, where the presence of Ramizol[®] can be clearly observed in both height (Fig. 5.7a) and phase (inset of Fig. 5.7a) AFM images. In all samples, the exfoliated graphene sheets have lateral dimensions of several hundred nanometers to ~1 μm . However, the presence of Ramizol[®] made it difficult to determine the thickness of graphene sheets especially for G:R 1:1. For G:R 1:1, the graphene sheets are discernible with different thicknesses ranging from 2 nm to 10 nm which is consistent with the presence of a few layers of graphene sheets. The effect of different ratios of drug to graphite towards the yield of graphene

is consistent with the results discussed above, i.e. thicker sheets are more prevalent as the amount of drug decreases. As expected, the presence of Ramizol[®] became less evident as the relative amount of compound decreased. Even though thin sheets (< 5 nm) are present, thicker sheets (> 20 nm) are common (Fig. 5.7b,c). Interestingly, some sheets have a higher height profile at the periphery compared to the centre and this is possibly due to the multi-layered stacking of drug molecules at the edges of the sheets which is in accord with computational energy minimisation studies (Appendix A9).



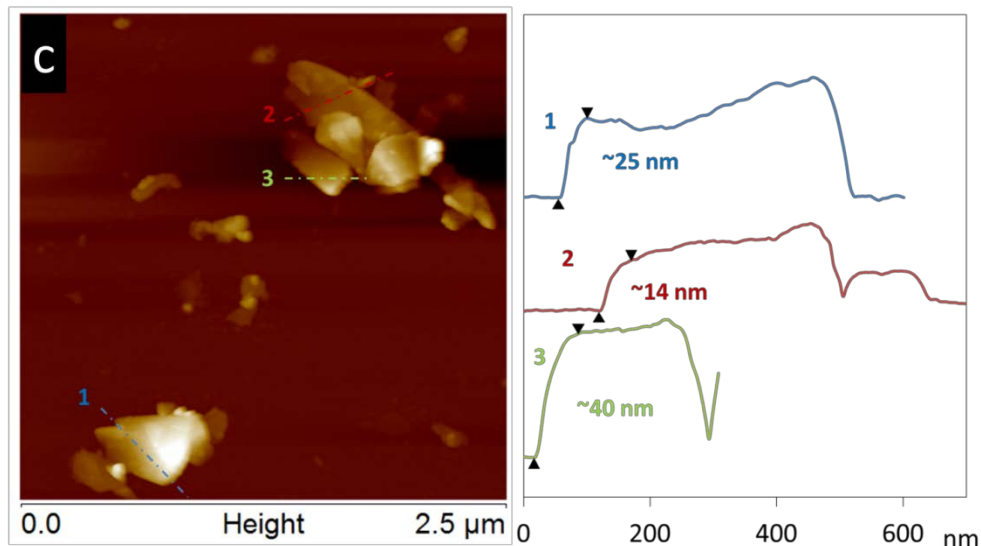


Figure 5.7. AFM height images of graphene/Ramizol[®] G:R (1:1) (a) with phase image in the inset, (1:0.1) (b), and (1:0.01) (c), respectively.

SEM was used to explore the surface decoration of graphene with Ramizol[®]. Even without coating, clear images can still be observed which indicates that the effect of exfoliation process on the electrical conductivity of graphene is minimal (Fig. 5.8, 5.9). The difference in thickness of the sheets after exfoliation in the presence of Ramizol[®] is also significantly different to that of bulk pristine graphite (Fig. 5.8). SEM results are consistent with the TEM and AFM analyses, where at G:R 1:1, Figure 5.9a, Ramizol[®] is aggregated, with lumpy structural features. However, aggregation becomes less evident for G:R 1:0.1 and G:R 1:0.01 where Ramizol[®] is present as small particles, ~ 2 nm in height based on AFM analysis. Elemental analysis for sample shown in Figure 5.6a using energy dispersive electron spectroscopy (EDS), shows the presence of oxygen and carbon peaks for the lumpy site which coincides with the elements in Ramizol[®] (Fig. 5.9d) whereas only carbon peak was observed for clear surface of the same sample (Fig. 5.9d inset).

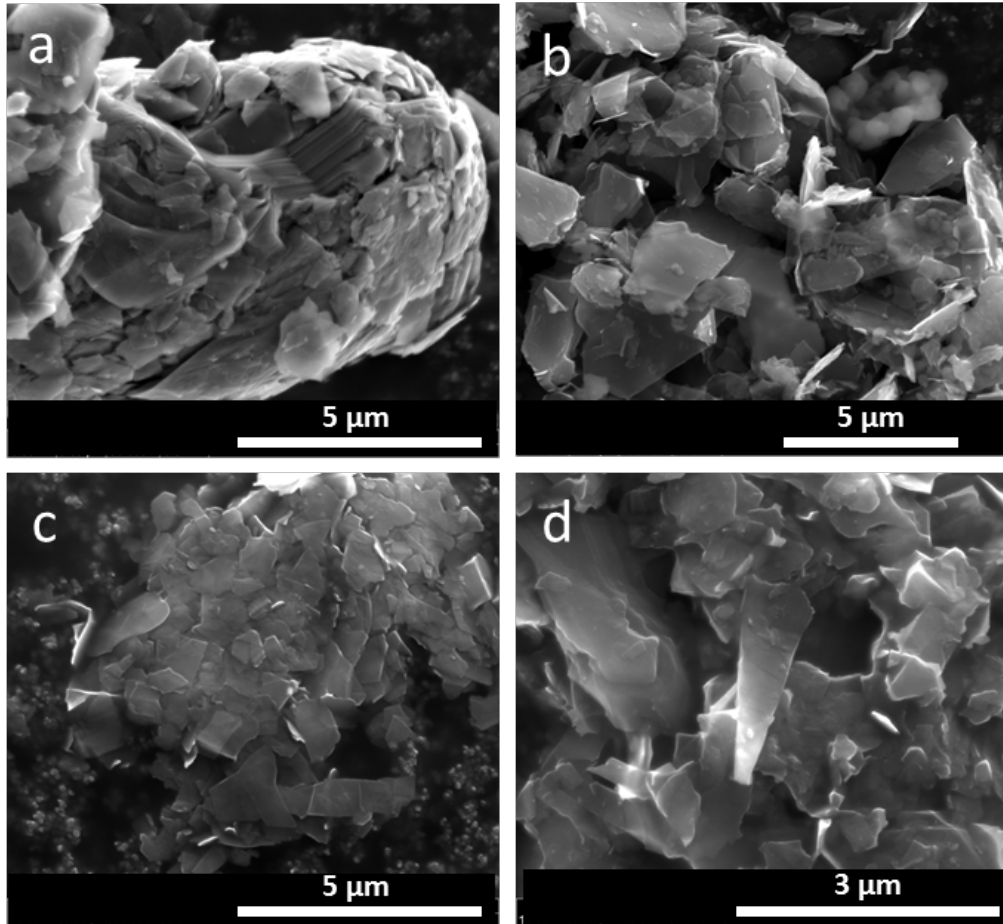


Figure 5.8. SEM images of (a) pristine graphite and graphene/Ramizol[®] samples; (b) G:R (1:1), (c) G:R (1:0.1) and (d) G:R (1:0.01) respectively. (Scale bar: 5 μm)

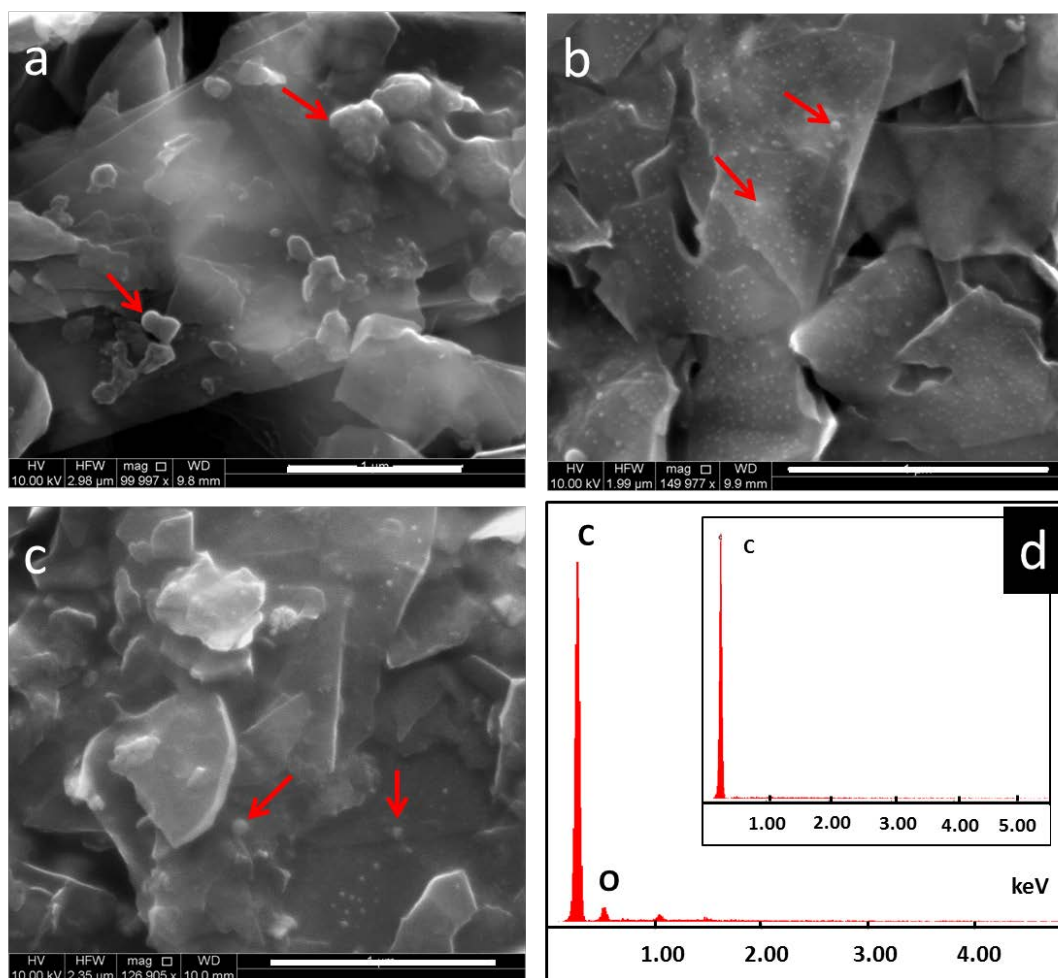


Figure 5.9. SEM images of graphene/Ramizol[®], G:R (a) 1:1 , (b) 1:0.1 and (c) 1:0.01, and (d) EDS analysis of lumpy sites in (a) and inset image showing EDS analysis on a clear surface for comparison. Red arrows indicating lumpy features on graphene sheets (Scale bar: 1 μ m).

The antibacterial property of the graphene/Ramizol[®] composite material was investigated using the model Gram-positive bacteria *S. aureus*. Optical density of the samples in media containing *S. aureus* was monitored at 600 nm after every 1 hour from 0 to 8 hours followed by the final measurement after overnight incubation. Preliminary test results in Figure 5.10 shows that effective bacterial growth inhibition was achieved with pure Ramizol[®], G:R 1:1 and G:R 1:0.1, whereas the antibacterial effect became less effective for higher graphene concentrations, i.e. G:R 1:0.01 and for graphite sonicated in water in the absence of Ramizol[®], the bacteria growth was hardly affected. Noteworthy mentioning is that the concentration of graphite alone in water was the same for the starting amount of graphite in sample G:R 1:1 (0.1 mg.mL⁻¹). The lack of efficacy is a direct result of the restacking of

graphene sheets in water to afford graphite, which unlike graphene, does not have antibacterial properties (Fig. 5.2b). Results are consistent with the high affinity of the drug to graphite reducing its bioavailability, and the low yield of exfoliated graphene sheets as a result of a low drug:graphite ratio. Both factors affect the observed antibacterial activity and at low concentrations of Ramizol[®] and graphene, the antibacterial activity of the G:R 1:0.01 mixture is thus quenched. The inset image displays the mixtures after 20 hours of incubation. For the control, a cloudy suspension is clearly observed which indicates uninhibited growth of the bacteria. With addition of Ramizol[®], a clear suspension was obtained due to the antibacterial effect which inhibits the growth of the bacteria. This was also observed for G:R 1:1 and G:R 1:0.1. However for G:R 1:0.01 and pure graphite sample a cloudy suspension was observed which suggests a lower antibacterial activity in this mixture.

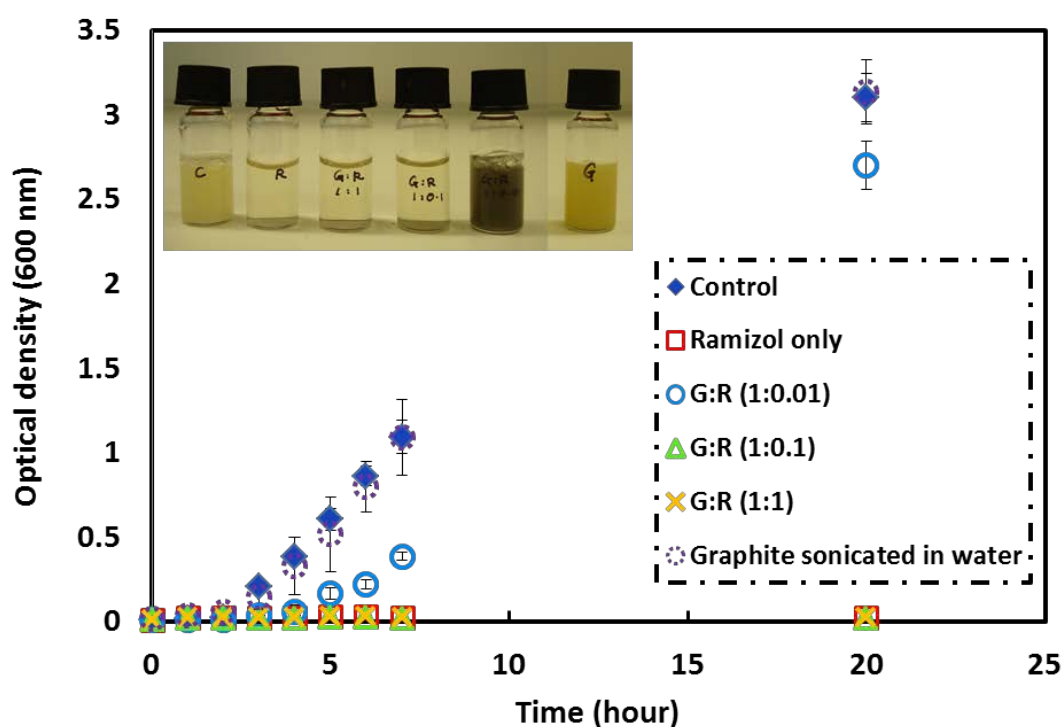


Figure 5.10. Bacterial growth monitoring by optical density measurements at 600 nm for pure Ramizol[®], pure graphite sonicated in water and graphene/Ramizol[®] composites of *S. aureus* in Mueller-Hinton media over a period of 20 hours. Inset photograph shows image of samples after incubation for 20 hours. First image on the left is bacteria only in media followed by pure Ramizol[®], G:R 1:1, G:R 1:0.1, G:R 1:0.01 and ultrasonicated graphite in water with bacteria in media, respectively.

5.5 Conclusion

Facile graphene exfoliation in water was successful in the presence of Ramizol[®] under sonication. The composite material incorporates the remarkable properties of graphene and Ramizol[®], with the latter being an antimicrobial and an antioxidant agent. This material has potential for developing wound dressing materials where graphene functions as a drug carrier as well as to impart toughness to the material. In addition this material may also be used for antibacterial coatings or other biomedical applications.

5.6 Acknowledgements

We gratefully acknowledge support of this work by the Australian Research Council, the National Health and Medical Research Council and the Government of South Australia. TEM, SEM and AFM studies were carried out using facilities in the Centre for Microscopy, Characterisation and Analysis, The University of Western Australia and Flinders University, supported by the Australian Microscopy and Microanalysis Research Facility. M.H. Wahid would like to thank the Malaysian Government and Universiti Putra Malaysia for the PhD research funding.

5.7 References

- 1 Geim, A. K. (2009). Graphene: status and prospects. *Science*, 324(5934), 1530-1534.
- 2 Meyer, J. C., Geim, A. K., Katsnelson, M. I., Novoselov, K. S., Booth, T. J. and Roth, S. (2007). The structure of suspended graphene sheets. *Nature*, 446(7131), 60-63.
- 3 Allen, M. J., Tung, V. C. and Kaner, R. B. (2009). Honeycomb carbon: a review of graphene. *Chemical Reviews*, 110(1), 132-145.
- 4 Paton, K. R., Varrla, E., Backes, C., Smith, R. J., Khan, U., O'Neill, A., Boland, C., Lotya, M., Istrate, O. M., King, P., Higgins, T., Barwich, S., May, P., Puczkarski, P., Ahmed, I., Moebius, M., Petterson, H., Long, E., Coelho, J., O'Brien, S. E., McGuire, E. K., Sanchez, B. M., Duesberg, G. S., McEvoy, N., Pennycook, T. J., Downing, C., Crossley, A., Nicolosi, V. and Coleman, J. N. (2014). Scalable production of large quantities of defect-free few-layer graphene by shear exfoliation in liquids. *Nature Materials*, 13(6), 624-630.

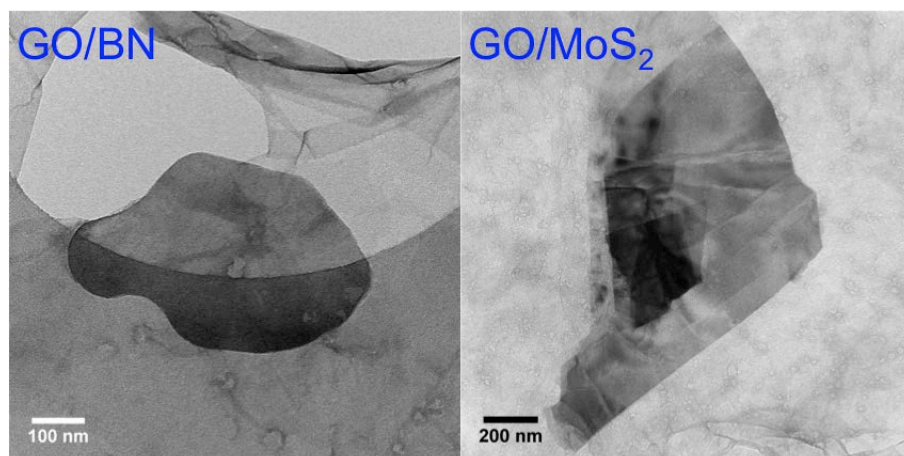
- 5 Yang, X., Zhu, J., Qiu, L. and Li, D. (2011). Bioinspired Effective Prevention of Restacking in Multilayered Graphene Films: Towards the Next Generation of High-Performance Supercapacitors. *Advanced Materials*, 23(25), 2833-2838.
- 6 Zacharia, R., Ulbricht, H. and Hertel, T. (2004). Interlayer cohesive energy of graphite from thermal desorption of polyaromatic hydrocarbons. *Physical Review B*, 69(15), 155406.
- 7 Tu, Y., Lv, M., Xiu, P., Huynh, T., Zhang, M., Castelli, M., Liu, Z., Huang, Q., Fan, C., Fang, H. and Zhou, R. (2013). Destructive extraction of phospholipids from *Escherichia coli* membranes by graphene nanosheets. *Nature Nanotechnology*, 8(8), 594-601.
- 8 Hu, W., Peng, C., Luo, W., Lv, M., Li, X., Li, D., Huang, Q. and Fan, C. (2010). Graphene-based antibacterial paper. *ACS Nano*, 4(7), 4317-4323.
- 9 Reina, A., Jia, X., Ho, J., Nezich, D., Son, H., Bulovic, V., Dresselhaus, M. S. and Kong, J. (2008). Large area, few-layer graphene films on arbitrary substrates by chemical vapor deposition. *Nano letters*, 9(1), 30-35.
- 10 Stankovich, S., Dikin, D. A., Piner, R. D., Kohlhaas, K. A., Kleinhammes, A., Jia, Y., Wu, Y., Nguyen, S. T. and Ruoff, R. S. (2007). Synthesis of graphene-based nanosheets via chemical reduction of exfoliated graphite oxide. *Carbon*, 45(7), 1558-1565.
- 11 Novoselov, K. S., Geim, A. K., Morozov, S. V., Jiang, D., Zhang, Y., Dubonos, S. V., Grigorieva, I. V. and Firsov, A. A. (2004). Electric field effect in atomically thin carbon films. *Science*, 306(5696), 666-669.
- 12 Hernandez, Y., Nicolosi, V., Lotya, M., Blighe, F. M., Sun, Z., De, S., McGovern, I. T., Holland, B., Byrne, M., Gun'Ko, Y. K., Boland, J. J., Niraj, P., Duesberg, G., Krishnamurthy, S., Goodhue, R., Hutchison, J., Scardaci, V., Ferrari, A. C. and Coleman, J. N. (2008). High-yield production of graphene by liquid-phase exfoliation of graphite. *Nature Nanotechnology*, 3(9), 563-568.
- 13 Zhang, M., Parajuli, R. R., Mastrogiovanni, D., Dai, B., Lo, P., Cheung, W., Brukh, R., Chiu, P. L., Zhau, T., Liu, Z., Garfunkel, E. and He, H. (2010). Production of graphene sheets by direct dispersion with aromatic healing agents. *Small*, 6(10), 1100-1107.
- 14 Lee, D. W., Kim, T. and Lee, M. (2011). An amphiphilic pyrene sheet for selective functionalization of graphene. *Chemical Communications*, 47(29), 8259-8261.
- 15 Chen, X., Boulos, R. A., Eggers, P. K. and Raston, C. L. (2012). p-Phosphonic acid calix [8] arene assisted exfoliation and stabilization of 2D materials in water. *Chemical Communications*, 48(93), 11407-11409.

- 16 Zhang, F., Chen, X., Boulos, R. A., Yasin, F. M., Lu, H., Raston, C. and Zhang, H. (2013). Pyrene-conjugated hyaluronan facilitated exfoliation and stabilisation of low dimensional nanomaterials in water. *Chemical Communications*, 49(42), 4845-4847.
- 17 Behabtu, N., Lomeda, J. R., Green, M. J., Higginbotham, A. L., Sinitskii, A., Kosynkin, D. V., Tsentlovich, D., Parra Vasquez, A. N. G., Schmidt, J., Kesselman, E., Cohen, Y., Talmon, Y., Tour, J. M. and Pasquali, M. (2010). Spontaneous high-concentration dispersions and liquid crystals of graphene. *Nature Nanotechnology*, 5(6), 406-411.
- 18 Chen, X., Dobson, J. F. and Raston, C. L. (2012). Vortex fluidic exfoliation of graphite and boron nitride. *Chemical Communications*, 48(31), 3703-3705.
- 19 Wahid, M. H., Eroglu, E., Chen, X., Smith, S. M. and Raston, C. L. (2013). Functional multi-layer graphene–algae hybrid material formed using vortex fluidics. *Green Chemistry*, 15(3), 650-655.
- 20 Boulos, R. A. (2013). Antimicrobial dyes and mechanosensitive channels. *Antonie van Leeuwenhoek*, 104(2), 155-167.
- 21 Boulos, R. A., Eroglu, E., Chen, X., Scaffidi, A., Edwards, B. R., Toster, J. and Raston, C. L. (2013). Unravelling the structure and function of human hair. *Green Chemistry*, 15(5), 1268-1273.
- 22 James, E., Viola, H., Hool, L., Eggers, P. K., Raston, C. L. and Boulos, R. A. (2013). A novel antimicrobial agent reduces oxidative stress in cells. *RSC Advances*, 3(20), 7277-7281.
- 23 Suslick, K. S., Didenko, Y., Fang, M. M., Hyeon, T., Kolbeck, K. J., McNamara, W. B., Mdleleni, M. M. and Wong, M. (1999). Acoustic cavitation and its chemical consequences. *Philosophical Transactions of the Royal Society of London. Series A: Mathematical, Physical and Engineering Sciences*, 357(1751), 335-353.
- 24 Esmaili, A. and Entezari, M. H. (2014). Facile and fast synthesis of graphene oxide nanosheets via bath ultrasonic irradiation. *Journal of Colloid and Interface Science*, 432, 19-25.
- 25 Ciesielski, A. and Samorì, P. (2014). Graphene via sonication assisted liquid-phase exfoliation. *Chemical Society Reviews*, 43(1), 381-398.
- 26 Yang, X., Zhang, X., Liu, Z., Ma, Y., Huang, Y. and Chen, Y. (2008). High-efficiency loading and controlled release of doxorubicin hydrochloride on graphene oxide. *The Journal of Physical Chemistry C*, 112(45), 17554-17558.

- 27 Yang, K., Zhang, S., Zhang, G., Sun, X., Lee, S. T. and Liu, Z. (2010). Graphene in mice: ultrahigh in vivo tumor uptake and efficient photothermal therapy. *Nano Letters*, 10(9), 3318-3323.
- 28 Yao, J., Sun, Y., Yang, M. and Duan, Y. (2012). Chemistry, physics and biology of graphene-based nanomaterials: new horizons for sensing, imaging and medicine. *Journal of Materials Chemistry*, 22(29), 14313-14329.
- 29 Tang, J., Chen, Q., Xu, L., Zhang, S., Feng, L., Cheng, L., Xu, H., Liu, Z. and Peng, R. (2013). Graphene oxide–silver nanocomposite as a highly effective antibacterial agent with species-specific mechanisms. *ACS Applied Materials & Interfaces*, 5(9), 3867-3874.
- 30 Wu, M. C., Deokar, A. R., Liao, J. H., Shih, P. Y. and Ling, Y. C. (2013). Graphene-based photothermal agent for rapid and effective killing of bacteria. *ACS Nano*, 7(2), 1281-1290.
- 31 Jiang, B., Tian, C., Song, G., Chang, W., Wang, G., Wu, Q. and Fu, H. (2013). A novel Ag/graphene composite: facile fabrication and enhanced antibacterial properties. *Journal of Materials Science*, 48(5), 1980-1985.
- 32 Some, S., Gwon, A. R., Hwang, E., Bahn, G. H., Yoon, Y., Kim, Y., Kim, S. H., Bak, S., Yang, J., Jo, D. G. and Lee, H. (2014). Cancer Therapy Using Ultrahigh Hydrophobic Drug-Loaded Graphene Derivatives. *Scientific Reports*, 4.
- 33 Duch, M. C., Budinger, G. S., Liang, Y. T., Soberanes, S., Urich, D., Chiarella, S. E., Campochiaro, L. A., Gonzalez, A., Chandel, N. S., Hersam, M. C. and Mutlu, G. M. (2011). Minimizing oxidation and stable nanoscale dispersion improves the biocompatibility of graphene in the lung. *Nano Letters*, 11(12), 5201-5207.
- 34 Loh, K. P., Bao, Q., Ang, P. K. and Yang, J. (2010). The chemistry of graphene. *Journal of Materials Chemistry*, 20(12), 2277-2289.
- 35 Depan, D., Shah, J. and Misra, R. D. K. (2011). Controlled release of drug from folate-decorated and graphene mediated drug delivery system: Synthesis, loading efficiency, and drug release response. *Materials Science and Engineering: C*, 31(7), 1305-1312.
- 36 Shahil, K. M. and Balandin, A. A. (2012). Graphene–multilayer graphene nanocomposites as highly efficient thermal interface materials. *Nano Letters*, 12(2), 861-867.
- 37 Dittrich, B., Wartig, K. A., Hofmann, D., Mülhaupt, R. and Scharrel, B. (2013). Flame retardancy through carbon nanomaterials: Carbon black, multiwall nanotubes, expanded graphite, multi-layer graphene and graphene in polypropylene. *Polymer Degradation and Stability*, 98(8), 1495-1505.

- 38 Lengkeek, N. A., Boulos, R. A., McKinley, A. J., Riley, T. V., Martinac, B. and Stewart, S. G. (2011). The Synthesis of Fluorescent DNA Intercalator Precursors through Efficient Multiple Heck Reactions. *Australian Journal of Chemistry*, 64(3), 316-323.
- 39 Wang, G., Shen, X., Yao, J. and Park, J. (2009). Graphene nanosheets for enhanced lithium storage in lithium ion batteries. *Carbon*, 47(8), 2049-2053.
- 40 Ferrari, A. C., Meyer, J. C., Scardaci, V., Casiraghi, C., Lazzeri, M., Mauri, F., Piscanec, S., Jiang, D., Novoselov, K. S., Roth, S and Geim, A. K. (2006). Raman spectrum of graphene and graphene layers. *Physical Review Letters*, 97(18), 187401.
- 41 Pimenta, M. A., Dresselhaus, G., Dresselhaus, M. S., Cancado, L. G., Jorio, A. and Saito, R. (2007). Studying disorder in graphite-based systems by Raman spectroscopy. *Physical Chemistry Chemical Physics*, 9(11), 1276-1290.

6. AMPHIPHILIC GRAPHENE OXIDE STABILISATION OF HEXAGONAL BN AND MoS₂ SHEETS



This chapter is a reformatted version of the paper published in *Chemical Communications*, Year 2015, Vol. 51, Pages 11709-11712.

6.1 Abstract

A simple and scalable method has been developed for directly forming water-dispersible van der Waals solids involving mixing aqueous solution of graphene oxide (GO) with hexagonal boron nitride (BN) or molybdenum disulphide (MoS_2) in *N*-methylpyrrolidone. The GO acts as an amphiphile in stabilising the colloidal solutions of the heterolaminar material in water.

6.2 Introduction

The breakthrough in unveiling the exceptional properties of graphene has triggered extensive research efforts in two-dimensional (2D) materials, including inorganic layered analogues such as hexagonal boron nitride (BN), and molybdenum disulfide (MoS_2), and other transition metal dichalcogenides, and layered oxides [1]. In addition to investigating the behaviour of monolayers, there is a rapidly emerging focus on constructing or reassembling isolated layers of such material into designer multi-layer heterostructures that are bound together primarily by van der Waals forces [2]. Such cohesion forces essentially preserve the distinct electronic properties of individual layers of the material [3], enabling tunable properties of the heterostructures, with potential for functioning as high performance electronic switches and optoelectronic devices that are still challenging to access for graphene due to the absence of an intrinsic energy bandgap [4].

Advancing the practical applications of the above heterolaminar van der Waals materials requires the development of scalable syntheses. In comparison to the well-developed strategies for fabricating graphene and quasi-graphene forms (graphene oxide or reduced graphene oxide), the possibility of making multi-layer van der Waals solids has only recently been achieved experimentally [5,6]. Significant efforts have been made towards growing graphene, monolayer BN and MoS_2 epitaxially on top of each other with controllable quality, although finding the right conditions for growing continuous layers is challenging [7-9]. Another approach is layer-by-layer deposition from 2D material suspensions *via* Langmuir-Blodgett techniques [10,11]. It is also possible to mix preformed colloidal suspensions of different 2D materials to generate layered flocculates [12]. This solution-based self-organising method is versatile and scalable, showing promise for producing van der Waals solids as ultrathin dielectrics [10], selectively permeable membranes [13], and

composite materials [14]. However, there are some limitations on the present approaches which involve the use of specific organic solvents that have similar surface tension to that of the stabilised 2D materials [15,16]. Organic solvents can only ensure temporary stability and finite concentration of the 2D material suspensions [17], and thus can restrict further processing of such materials. It is also difficult to produce stabilised inorganic lamellar materials, including BN and MoS₂, in aqueous media in the absence of additional surfactants due to their hydrophobic property [18,19]. Indeed access to water-processable quasi-graphene forms such as graphene oxide and reduced graphene oxide has dramatically advanced the potential of graphene-based materials into much broader areas [20,21]. Hence, there is significant scope for developing novel and versatile solution-based protocols to prepare water-dispersible heterolaminar van der Waals materials.

In this work we develop the use of graphene oxide (GO) sheets as both the composite material and the surfactant for supporting and stabilising BN and MoS₂ sheets in water. GO is amphiphilic due to the presence of carboxyl and hydroxyl groups at the edges and hydrophobic unoxidized polyaromatic islands within the basal plane [22,23]. This amphiphilic property has been used for effectively stabilising pristine graphite flakes and carbon nanotubes [23], creating highly stable Pickering emulsions [23,24], and constructing three-dimensional networks of GO hollow spheres [25]. This suggests that GO is capable of non-covalently assembling with BN or MoS₂ sheets *via* van der Waals interactions and/or hydrophobic effects, at the same time stabilising the heterolaminar materials in water, and this is the focus of the work reported herein.

6.3 Experimental methods

The overall procedure for preparing the heterolaminar materials is summarised in Figure 6.1. GO was prepared from high purity graphite flakes powder (99.9%, SP-1, Bay Carbon) using the modified Hummer's method [26,27]. Colloidal dispersions (10 mL) of BN (1 mg mL⁻¹) and MoS₂ (1 mg mL⁻¹) in *N*-methylpyrrolidone (NMP) were prepared using probe sonication for 1 hour. Each dispersion was then diluted to 0.2 mg mL⁻¹ (0.5 mL) and directly added drop-wise into 0.5 mL of colloidal suspension of GO (0.5 mg mL⁻¹), followed by mild sonication for 30 seconds. We selected a relatively low starting concentration for BN and MoS₂ dispersions,

because higher concentrations were observed to induce instability of the mixed solutions, presumably due to an increase in irreversible loading of BN or MoS₂ sheets onto GO sheets. The resulting mixed dispersions were centrifuged ($860 \times g$, 15 min) to remove any large flakes of the starting laminar materials, with the supernatants then separated, affording the colloidal dispersions of GO/BN and GO/MoS₂. NMP was the dispersing medium of choice for the exfoliation and stabilization due to the insolubility of BN and MoS₂ in water, but not in NMP, as well as the infinite miscibility of NMP with water. Despite the ability to directly exfoliate BN and MoS₂ in the presence of GO, pre-sonication of BN and MoS₂ in NMP effectively avoids any risk of damaging the structure of GO. The NMP in the resulting solutions can be further removed by centrifugal-washing the samples at $18370 \times g$ for 1 hour, and redispersing the sediments into water, affording stable dispersions, Figure 6.1. The colour difference between the solutions after mixing and after re-dispersing arises from the higher stability of the GO devoid of BN or MoS₂, whereas the heterolaminar materials are more readily separated centrifugally.

The overall sample preparation procedure is summarised in Figure 6.1. GO used in this study was prepared from natural graphite flakes powder (99.9%, SP-1, Bay Carbon) using the modified Hummer's method [26,27]. Probe sonication was carried out using a Vibra-Cell™ VCX130 sonicator at 60% amplitude for all samples. Centrifugations were performed using the Dynamica Velocity 14R. Zeta potential analysis was performed using a Malvern Zetasizer Nano series. Measurements for each sample were recorded in triplicate and 20 data acquisitions were recorded in each measurement. All measurements were recorded at 25°C in Malvern disposable clear Folded Capillary Cells. TEM samples were prepared by depositing a drop of the suspension onto a holey carbon coated copper grid (#2450-AB, SPI Supplies) and dried under ambient conditions. TEM analysis was carried out using a Philips CM200 instrument operating at 120-200 kV. Image J software was used for processing all the TEM images. Raman spectra were acquired using a Witec alpha300R Raman microscope with excitation laser wavelength of 532 nm (≤ 5 mW), at room temperature. The spectra were recorded with an x40 objective (Numerical Aperture 0.60) for each sample with typical integrations times between 10 to 20 seconds with 3 accumulations per spectrum. Atomic force microscopy (AFM) analysis in tapping mode was performed with a Bruker multimode AFM and a

NanoScope V under ambient conditions. AFM probes used were Mikromasch HQ:NSC15 Si probes with a nominal spring constant of 40 N/m and a nominal tip diameter of 16 nm. The AFM scanner was calibrated in the x, y and z axes using Si calibration grids (Bruker model numbers PG: 1 μm pitch, 110 nm depth, and VGRP: 10 μm pitch, 180 nm depth). Samples were deposited on mica substrates and dried in air prior to analysis. GO used in this study was prepared from high purity graphite flakes powder (99.9%, SP-1, Bay Carbon) using the modified Hummers method [26,27]. Colloidal dispersion (10 mL) of BN (1 mg mL^{-1}) and MoS₂ (1 mg mL^{-1}) in *N*-methylpyrrolidone (NMP) was prepared, respectively, *via* probe sonication using a Sonics Vibra Cell ultrasonic liquid processor (130 Watt, 20 kHz) at 60% of the amplitude for 1 hour. The dispersion was then diluted to 0.2 mg mL^{-1} (0.5 mL) and directly added drop-wise into 0.5 mL of colloidal suspension of GO (0.5 mg mL^{-1}), followed by mild sonication for 30 seconds. The stability of the suspensions were investigated under acidic (pH 1), neutral and basic (pH 12) conditions. We selected a relatively low starting concentration for BN and MoS₂ dispersions, because higher concentration can induce instability of the mixed solutions probably due to an increased irreversible loading of BN or MoS₂ sheets onto GO. The resulting mixed dispersions were centrifuged (860 $\times g$, 15 min) to remove any large flakes of the starting laminar materials. The supernatants were then separated affording the colloidal dispersions of GO/BN and GO/MoS₂. Centrifugation of samples prepared under acidic condition showed complete precipitation, and thus loss of stability of the material (Appendix A10). Noteworthy mentioning is the use of NMP as dispersant in the first place for the exfoliation and stabilization of BN and MoS₂ due to their inherent insolubility in water. Despite the direct exfoliation of BN and MoS₂ in GO solutions is applicable, the pre-sonication of BN and MoS₂ in NMP can effectively avoid the risk of damaging the structure of GO. The NMP in the resulting solutions can be further removed by centrifugal-washing the samples at 18370 $\times g$ for 1 hour, and redispersing the sediments into in water to generate stable dispersions, as shown in Figure 6.1.

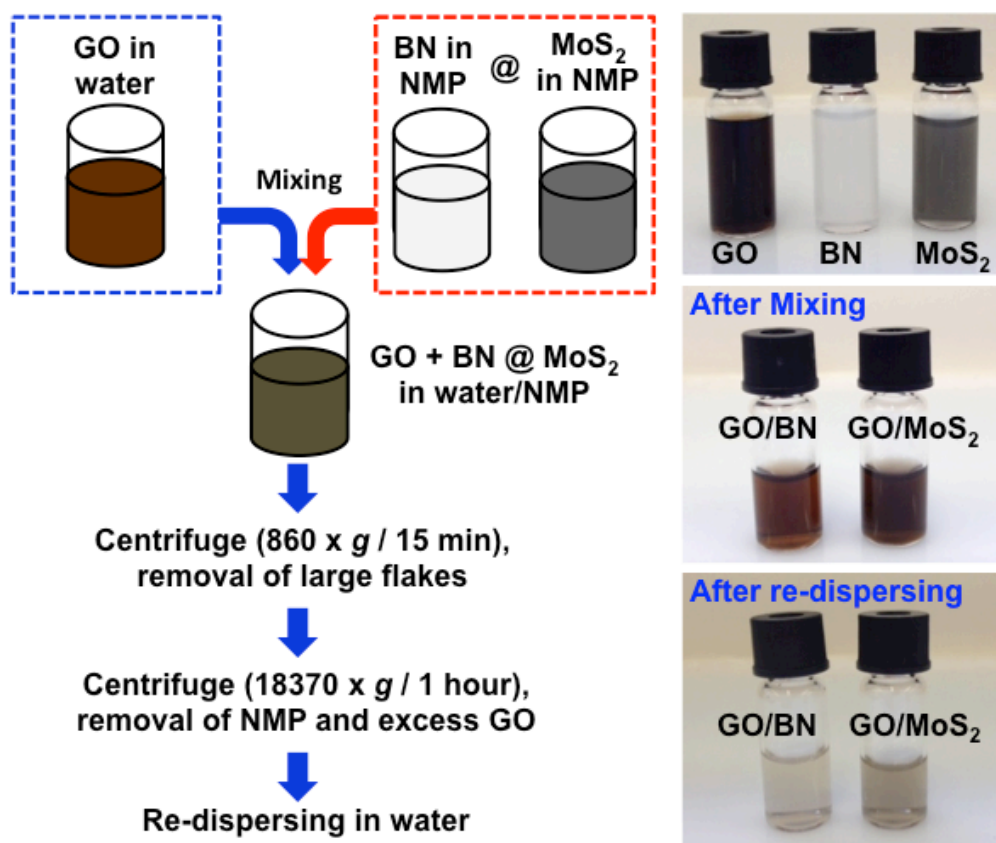


Figure 6.1. Schematic illustration of the sample preparation and corresponding photographs of the dispersions.

6.4 Results and discussion

Control experiments involving mixing NMP solutions of BN and MoS₂ with water showed no evidence for forming stable dispersions, clearly establishing that the formation of any dispersions in water requires the presence of GO. This supports our hypothesis that GO acts as an amphiphilic surfactant, in binding to BN and MoS₂ through the hydrophobic islands in lowering their interfacial energy, with hydrophilic groups on the outer surface of the GO stabilising the colloidal dispersion of the heterolaminar material in water. Pertaining to the effect of pH, under acidic conditions there is a loss in stability of the GO (Appendix A10) whereas stable dispersions formed under neutral and basic (pH 12) conditions. The electrostatic stability of the re-dispersed solutions of GO/BN and GO/MoS₂ at neutral pH was confirmed by zeta potentials, at -48.3 mV, -47.7 mV and -50.3 mV, respectively, for GO solution, and re-dispersed solutions of GO/BN and GO/MoS₂.

Transmission electron microscopy (TEM) was used to investigate the state of the re-dispersed composite materials in water, by dropping dispersions onto a holey carbon coated copper grid and drying under ambient conditions. TEM images for pristine GO, exfoliated BN and MoS₂ are shown in Figure 6.2a-d, respectively. Graphene oxide sheets (~200 nm to 10 μm in lateral dimensions) are evident in Figure 6.2a and 6.3a, with the corresponding electron diffraction (inset) revealing a typical pattern for monolayers. The pattern rings of electron diffraction in the inset of Figure 6.2b are consistent with randomly stacked layers of GO [28]. TEM images and corresponding electron diffraction patterns from selected areas in Figure 6.2c and d, for as prepared separate NMP solutions of BN and MoS₂, confirm the presence of exfoliated BN and MoS₂ sheets. The exfoliated sheets range in size from ~200 nm to 1 μm for both materials. While BN gives a similar shape and size due to the smaller cross section of the starting material (~1 μm), MoS₂ (~2 μm) shows an apparent fragmentation, presumably arising from high energy cavitation processes associated with the sonication and less strong in-plane stiffness compared with BN sheets [29]. Figures 6.2e and g show the composites of GO/BN and GO/MoS₂ in the re-dispersed solutions, respectively, with the size of the BN and MoS₂ consistent with that of the as-exfoliated sheets in NMP. Similar images were obtained for samples prepared under basic conditions (Appendix A11). The electron diffraction pattern in Figure 6.2f is similar to that of the stacking monolayers in Figure 6.2b. Even though it is difficult to determine the overlapping diffraction spots of BN in this pattern, as BN and graphene have very similar crystal structures with a lattice constant difference of ~2%, the difference in contrast, size and shape of BN and GO sheets provides a means to recognise BN. In the case of GO/MoS₂, the electron diffraction (Figure 6.2h) shows a typical pattern for MoS₂, along with the GO ring pattern. The TEM analysis also shows that BN and MoS₂ always accompany GO, which is in accordance with the BN and MoS₂ sheets being supported on the surface of GO in the re-dispersed solutions.

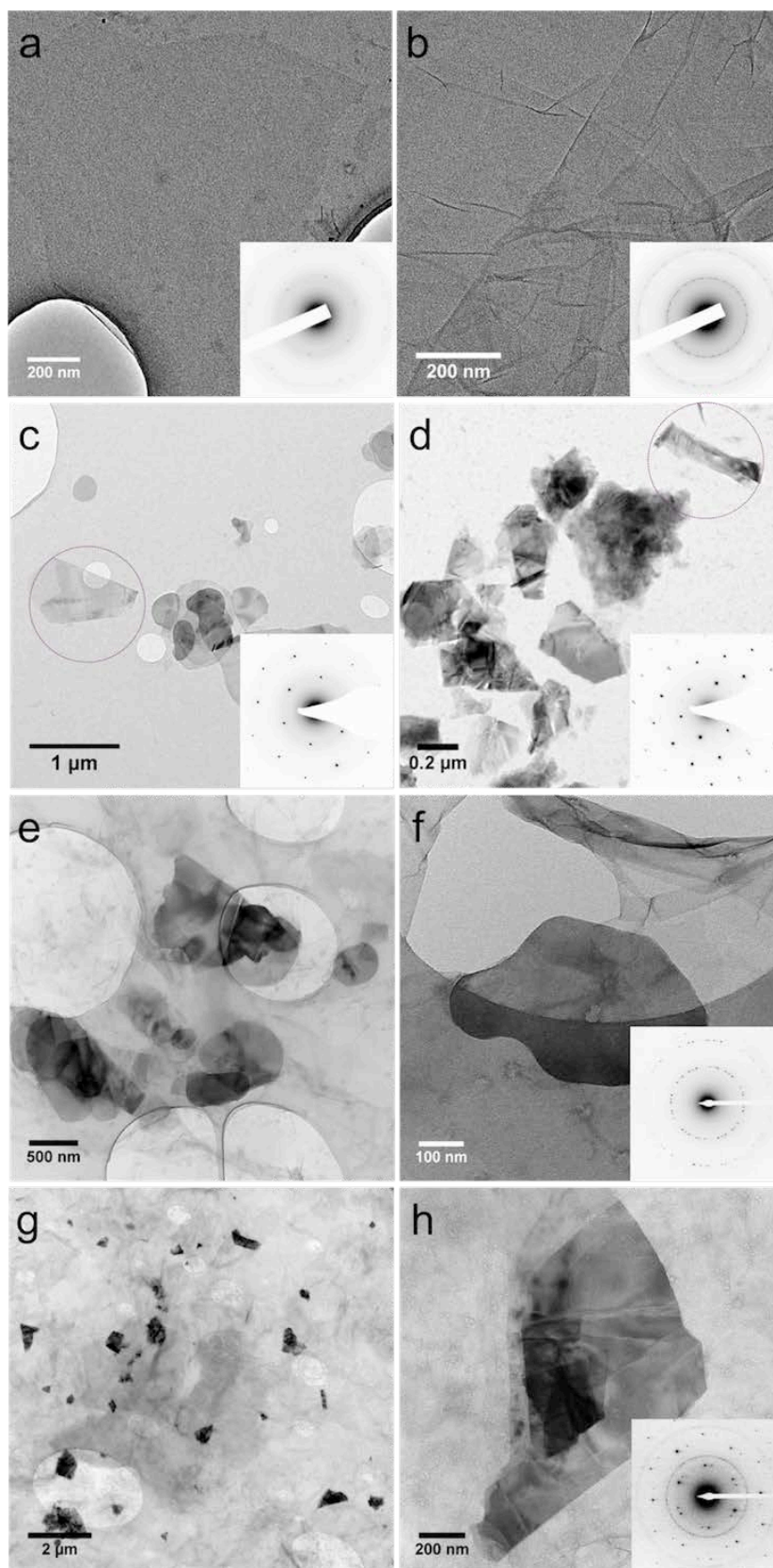


Figure 6.2. TEM images of (a,b) GO, (c) exfoliated BN and (d) MoS₂ sheets, (e,f) GO/BN and (g,h) GO/MoS₂. Electron diffraction patterns for all samples are as shown in the inset.

Atomic force microscopy (AFM) was undertaken to further investigate the morphology of the heterolaminar materials. The pristine GO is monolayered having a measured thickness of ~ 1 nm [21], Figure 6.3a and 6.3b. The structures of heterolaminar materials are consistent with TEM analysis, with BN and MoS₂ supported on GO evident in Figure 6.3c, 6.3e and 6.3f. The height profile measurement in Figure 6.3d along the orange line in Figure 6.3c reveals a thickness of ~ 5 nm for BN. The height profiles for the GO/MoS₂ show that the sheets of MoS₂ are ~ 8 - 12 nm thick, Figure 6.3g. The difference in thickness is related to the different interplanar distances between BN (~ 0.33 nm) and MoS₂ (~ 0.61 nm), as well as the higher surface energy of MoS₂ (>250 mJ m⁻²) compared to that of BN (~ 110 mJ m⁻²) [30,31], requiring higher energy input for exfoliation.

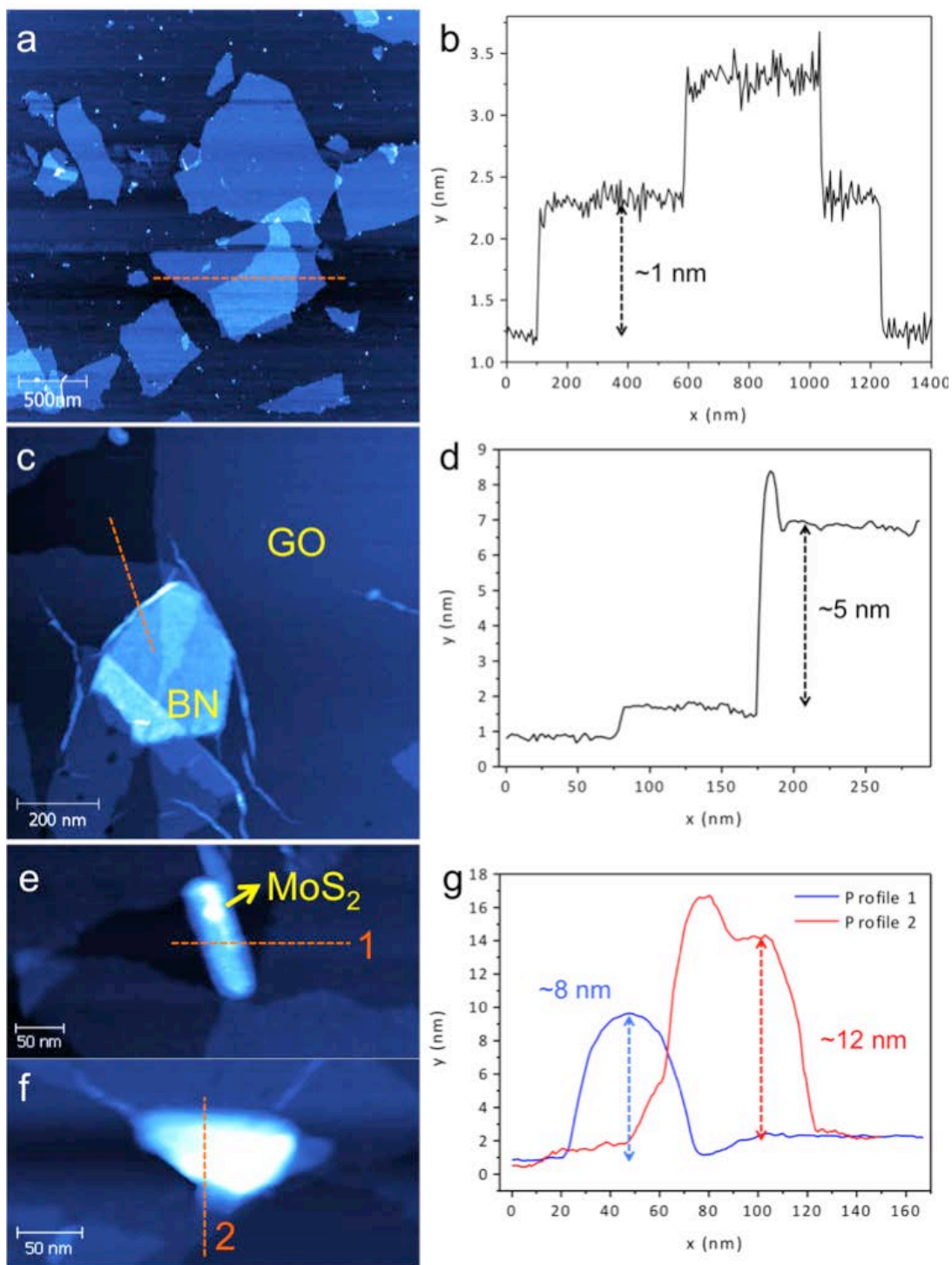


Figure 6.3. AFM images and height profiles of the indicated area in (a,b) GO, (c,d) GO/BN, and (e,f,g) MoS₂ samples.

Raman spectra were recorded for pristine GO, BN and MoS₂, and for the re-dispersed heterolaminar materials respectively (Figure 6.4). Typical spectra for GO displayed a D and G band at ~1370 cm⁻¹ and ~1570 cm⁻¹ respectively (Figure 6.4a) [32]. For BN (Figure 6.4b) and MoS₂ (Figure 6.4c), strong fluorescence background

was observed, possibly due to the remaining NMP which was used as the dispersant. BN exhibits a characteristic peak at $\sim 1360\text{ cm}^{-1}$ that is due to the E_{2g} phonon mode which is similar to the G peak in graphitic materials, as shown in the zoomed-in image in Figure 6.4(i) [33]. MoS_2 has characteristic peaks at $\sim 380\text{ cm}^{-1}$ and $\sim 400\text{ cm}^{-1}$ which are attributed to the E_{2g}^1 and A_{1g}^1 modes, respectively, Figure 6.4(ii) [34]. Strong D and G bands for GO are evident for both GO/BN and GO/ MoS_2 . The characteristic peak for BN cannot be seen due to overlap with the strong D band for GO, whereas for MoS_2 , both characteristic peaks are discernible, Figure 6.4(iii).

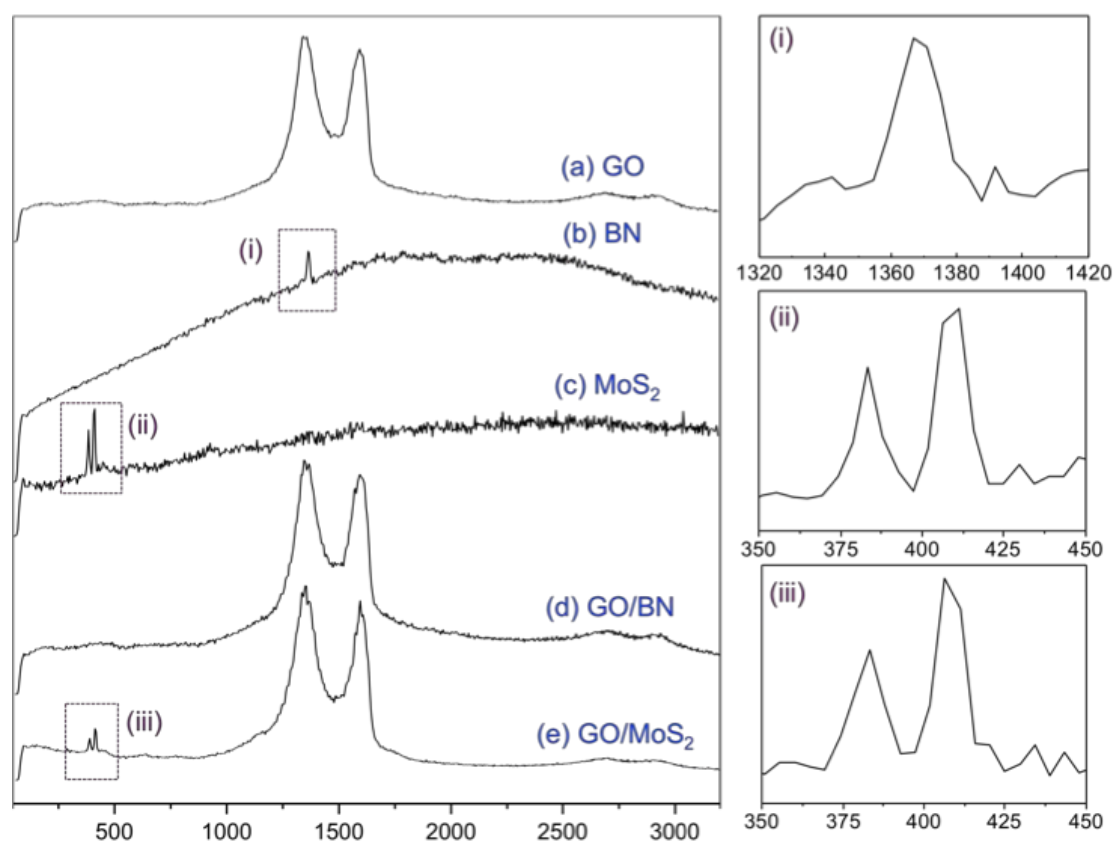


Figure 6.4. Raman spectra of pristine (a) GO, (b) BN, (c) MoS_2 and composite material of (d) GO/BN and (e) GO/ MoS_2 , respectively. Zoomed-in images of the peaks labelled as (i), (ii) and (iii) are shown on the right.

6.5 Conclusion

In conclusion, a facile method has been developed for stabilising pristine BN and MoS_2 in water. Since the 2D inorganic layered materials such as BN and MoS_2 are insoluble in water the presence of a surfactant is necessary in order to obtain stabilized dispersion of the 2D layered materials in water. Herein, we demonstrated

the use of GO to act as both the composite material and the surfactant for supporting and stabilising BN and MoS₂ sheets in water. Given that the synthesis of GO is already established and can be mass produced, this could lead to scalable synthesis of hydrophobic 2D laminar materials in water. Nonetheless, fine tuning of the processing controls such as ratio of GO to the other 2D layered materials, ultrasonication time and others is necessary to obtain the optimum yield. This work extends the utility of GO in stabilising 2D layered materials in water and consequently opening new facile processing avenues for 2D layered materials particularly in water.

6.6 Acknowledgements

We gratefully acknowledge support of this work by the Australian Research Council and the Government of South Australia. M.H. Wahid would like to thank the Malaysian Government and Universiti Putra Malaysia for the PhD research funding. TEM studies were carried out using facilities in Adelaide Microscopy at The University of Adelaide. AFM and Raman spectrometry studies were carried out at Flinders University, supported by the Australian Microscopy and Microanalysis Research Facility (AMMRF). The authors also would like to thank Dr. Sheng Dai for the assistance in zeta potential analysis.

6.7 References

- 1 Geim, A. K. and Novoselov, K. S. (2007). The rise of graphene. *Nature Materials*, 6(3), 183-191.
- 2 Geim, A. K. and Grigorieva, I. V. (2013). Van der Waals heterostructures. *Nature*, 499(7459), 419-425.
- 3 Radisavljevic, B. and Kis, A. (2013). Mobility engineering and a metal–insulator transition in monolayer MoS₂. *Nature Materials*, 12(9), 815-820.
- 4 Duesberg, G. S. (2014). Heterojunctions in 2D semiconductors: A perfect match. *Nature Materials*, 13(12), 1075-1076.
- 5 Dean, C. R., Young, A. F., Meric, I., Lee, C., Wang, L., Sorgenfrei, S., Watanabe, K., Taniguchi, T., Kim, P., Shepard, K. L. and Hone, J. (2010). Boron nitride substrates for high-quality graphene electronics. *Nature Nanotechnology*, 5(10), 722-726.

- 6 Ponomarenko, L. A., Geim, A. K., Zhukov, A. A., Jalil, R., Morozov, S. V., Novoselov, K. S., Grigorieva, I. V., Hill, E. H., Cheianov, V. V., Fal'co, V. I., Watanabe, K., Taniguchi, T. and Gorbachev, R. V. (2011). Tunable metal-insulator transition in double-layer graphene heterostructures. *Nature Physics*, 7(12), 958-961.
- 7 Tanaka, T., Ito, A., Tajima, A., Rokuta, E. and Oshima, C. (2003). Heteroepitaxial film of monolayer graphene/monolayer h-BN on Ni (111). *Surface Review and Letters*, 10(05), 721-726.
- 8 Liu, Z., Song, L., Zhao, S., Huang, J., Ma, L., Zhang, J., Lou, J. and Ajayan, P. M. (2011). Direct growth of graphene/hexagonal boron nitride stacked layers. *Nano Letters*, 11(5), 2032-2037.
- 9 Shi, Y., Zhou, W., Lu, A. Y., Fang, W., Lee, Y. H., Hsu, A. L., Kim, S. M., Kim, K. K., Yang, H. Y., Li, L. J., Idrobo, J. C. and Kong, J. (2012). Van der Waals epitaxy of MoS₂ layers using graphene as growth templates. *Nano Letters*, 12(6), 2784-2791.
- 10 Osada, M. and Sasaki, T. (2012). Two-Dimensional Dielectric Nanosheets: Novel Nanoelectronics from Nanocrystal Building Blocks. *Advanced Materials*, 24(2), 210-228.
- 11 Ariga, K., Ji, Q., Hill, J. P., Bando, Y. and Aono, M. (2012). Forming nanomaterials as layered functional structures toward materials nanoarchitectonics. *NPG Asia Materials*, 4(5), e17.
- 12 Gao, G., Gao, W., Cannuccia, E., Taha-Tijerina, J., Balicas, L., Mathkar, A., Narayanan, T. N., Liu, Z., Gupta, B. K., Peng, J., Yin, Y., Rubio, A. and Ajayan, P. M. (2012). Artificially stacked atomic layers: toward new van der Waals solids. *Nano Letters*, 12(7), 3518-3525.
- 13 Nair, R. R., Wu, H. A., Jayaram, P. N., Grigorieva, I. V. and Geim, A. K. (2012). Unimpeded permeation of water through helium-leak-tight graphene-based membranes. *Science*, 335(6067), 442-444.
- 14 Young, R. J., Kinloch, I. A., Gong, L. and Novoselov, K. S. (2012). The mechanics of graphene nanocomposites: a review. *Composites Science and Technology*, 72(12), 1459-1476.
- 15 Hernandez, Y., Nicolosi, V., Lotya, M., Blighe, F. M., Sun, Z., De, S., McGovern, I. T., Holland, B., Byrne, M., Gun'ko, Y. K., Boland, J. J., Niraj, P., Duesberg, G., Krishnamurthy, S., Goodhue, R., Hutchison, J., Scardaci, V., Ferrari, A. C. and Coleman, J. N. (2008). High-yield production of graphene by liquid-phase exfoliation of graphite. *Nature Nanotechnology*, 3(9), 563-568.

- 16 Coleman, J. N., Lotya, M., O'Neill, A., Bergin, S. D., King, P. J., Khan, U., Young, K., Gaucher, A., De, S., Smith, R. J., Shvets, I. V., Arora, S. K., Stanton, G., Kim, H. Y., Lee, K., Kim, G. T., Duesberg, G. S., Hallam, T., Boland, J. J., Wang, J. J., Donegan, J. F., Grunlan, J. C., Mariarty, G., Shmeliov, A., Nicholls, R. J., Perkins, J. M., Grieveson, E. M., Theuwissen, K., McComb, D. W., Nellist, P. D. and Nicolosi, V. (2011). Two-dimensional nanosheets produced by liquid exfoliation of layered materials. *Science*, 331(6017), 568-571.
- 17 Liu, W. W. and Wang, J. N. (2011). Direct exfoliation of graphene in organic solvents with addition of NaOH. *Chemical Communications*, 47(24), 6888-6890.
- 18 Chen, X., Boulos, R. A., Eggers, P. K. and Raston, C. L. (2012). p-Phosphonic acid calix [8] arene assisted exfoliation and stabilization of 2D materials in water. *Chemical Communications*, 48(93), 11407-11409.
- 19 Chen, X., Zang, W., Vimalanathan, K., Iyer, K. S. and Raston, C. L. (2013). A versatile approach for decorating 2D nanomaterials with Pd or Pt nanoparticles. *Chemical Communications*, 49(12), 1160-1162.
- 20 Si, Y. and Samulski, E. T. (2008). Synthesis of water soluble graphene. *Nano Letters*, 8(6), 1679-1682.
- 21 Li, D., Müller, M. B., Gilje, S., Kaner, R. B. and Wallace, G. G. (2008). Processable aqueous dispersions of graphene nanosheets. *Nature Nanotechnology*, 3(2), 101-105.
- 22 Dreyer, D. R., Park, S., Bielawski, C. W. and Ruoff, R. S. (2010). The chemistry of graphene oxide. *Chemical Society Reviews*, 39(1), 228-240.
- 23 Kim, J., Cote, L. J., Kim, F., Yuan, W., Shull, K. R. and Huang, J. (2010). Graphene oxide sheets at interfaces. *Journal of the American Chemical Society*, 132(23), 8180-8186.
- 24 Thickett, S. C. and Zetterlund, P. B. (2013). Preparation of Composite Materials by Using Graphene Oxide as a Surfactant in Ab Initio Emulsion Polymerization Systems. *ACS Macro Letters*, 2(7), 630-634.
- 25 Chen, X., Eggers, P. K., Slattery, A. D., Ogden, S. G. and Raston, C. L. (2014). Template-free assembly of three-dimensional networks of graphene hollow spheres at the water/toluene interface. *Journal of Colloid and Interface Science*, 430, 174-177.
- 26 Hummers Jr, W. S. and Offeman, R. E. (1958). Preparation of graphitic oxide. *Journal of the American Chemical Society*, 80(6), 1339-1339.

- 27 Kovtyukhova, N. I., Ollivier, P. J., Martin, B. R., Mallouk, T. E., Chizhik, S. A., Buzaneva, E. V. and Gorchinskiy, A. D. (1999). Layer-by-layer assembly of ultrathin composite films from micron-sized graphite oxide sheets and polycations. *Chemistry of Materials*, 11(3), 771-778.
- 28 Lee, J. K., Lee, S., Kim, Y. I., Kim, J. G., Min, B. K., Lee, K. I., Park, Y. and John, P. (2014). The seeded growth of graphene. *Scientific Reports*, 4.
- 29 Ataca, C., Sahin, H., Akturk, E. and Ciraci, S. (2011). Mechanical and electronic properties of MoS₂ nanoribbons and their defects. *The Journal of Physical Chemistry C*, 115(10), 3934-3941.
- 30 Weiss, K. and Phillips, J. M. (1976). Calculated specific surface energy of molybdenite (MoS₂). *Physical Review B*, 14(12), 5392.
- 31 Knowles, K. M. and Turan, S. (2000). High Resolution Transmission Electron Microscopy of Grain Boundaries between Hexagonal Boron Nitride Grains in Si₃N₄—SiC Particulate Composites. *Crystal Research and Technology*, 35(6/7), 751-758.
- 32 Stankovich, S., Dikin, D. A., Piner, R. D., Kohlhaas, K. A., Kleinhammes, A., Jia, Y., Wu, Y., Nguyen, S. T. and Ruoff, R. S. (2007). Synthesis of graphene-based nanosheets via chemical reduction of exfoliated graphite oxide. *Carbon*, 45(7), 1558-1565.
- 33 Gorbachev, R. V., Riaz, I., Nair, R. R., Jalil, R., Britnell, L., Belle, B. D., Hill, E. W., Novoselov, K. S., Watanabe, K., Taniguchi, T., Geim, A. K. and Blake, P. (2011). Hunting for monolayer boron nitride: optical and Raman signatures. *Small*, 7(4), 465-468.
- 34 Lee, C., Yan, H., Brus, L. E., Heinz, T. F., Hone, J. and Ryu, S. (2010). Anomalous lattice vibrations of single- and few-layer MoS₂. *ACS Nano*, 4(5), 2695-2700.

APPENDICES

A1. Zeta potential distribution of microalgae *C. vulgaris* free cells and GO wrapped cells

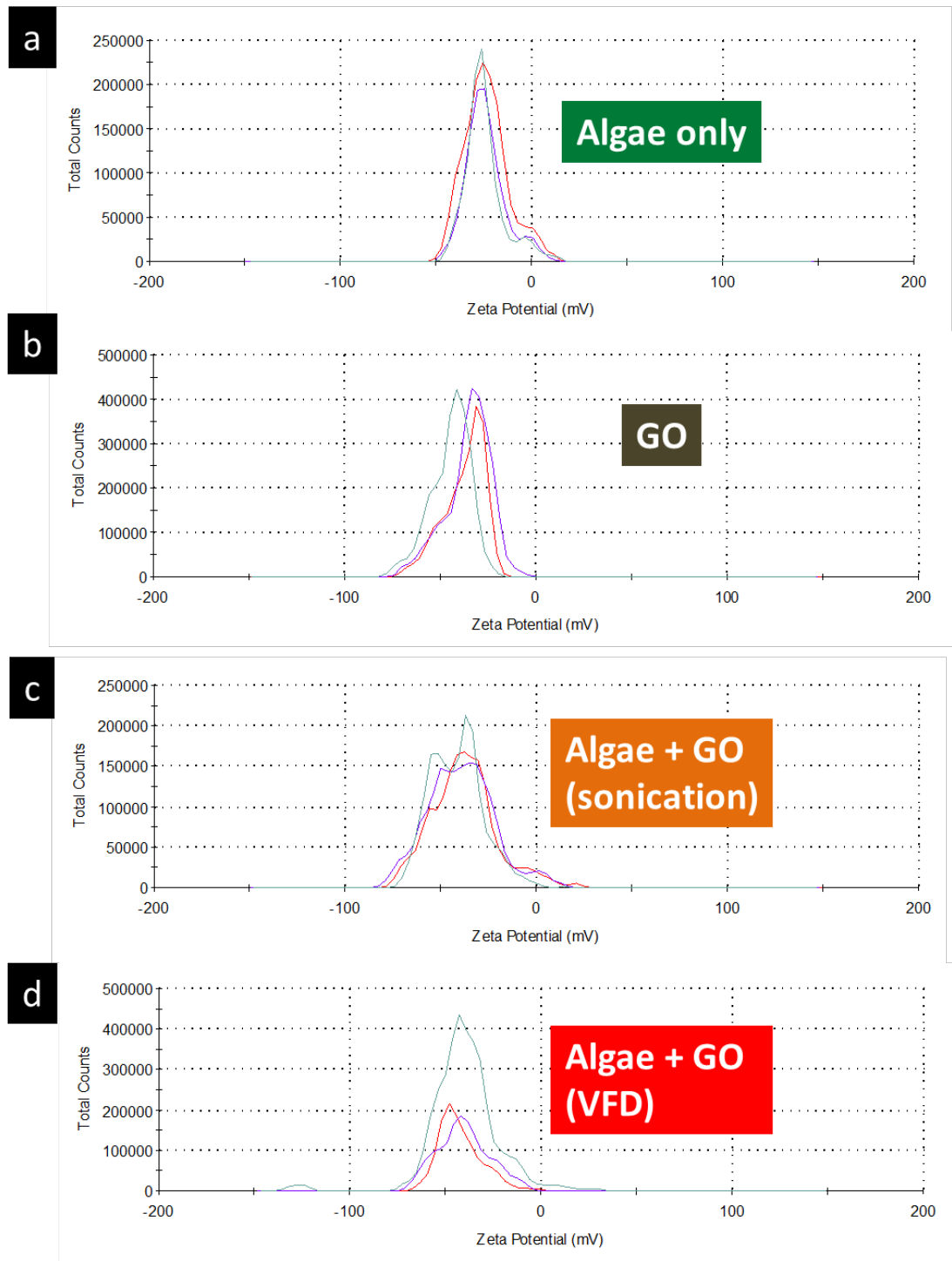


Figure A1. Zeta potential distribution of (a) free cells and (b) GO blank, and wrapped cells prepared via sonication, (c) and VFD, (d)

A2. Flow cytometry analysis

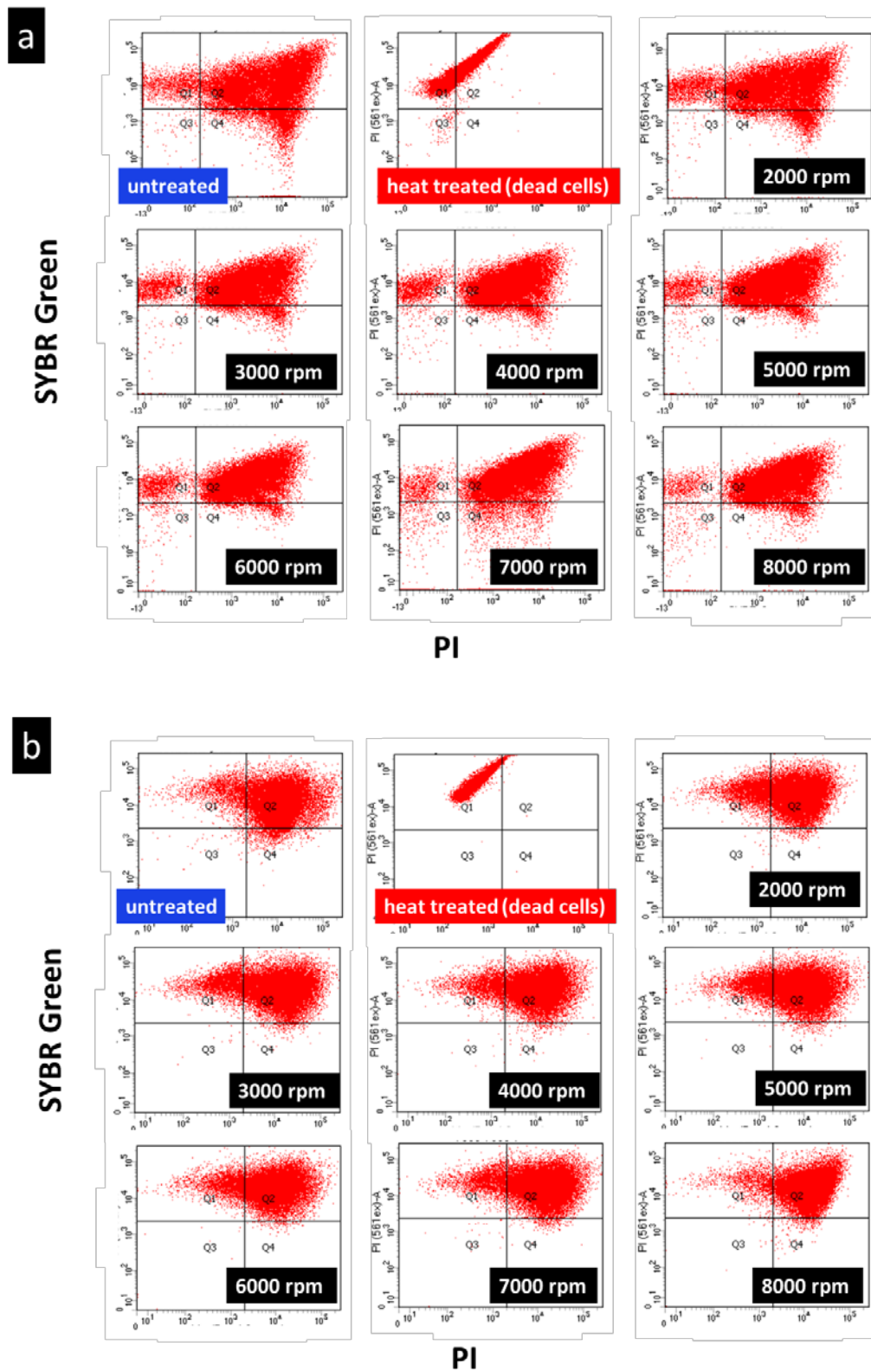


Figure A2. Flow cytometric analyses of (a) *S. aureus* and (b) *R. opacus* after processing in VFD at different speeds ranging from 2000-8000 rpm for 1 minute.

A3. AFM analysis

All AFM measurements were acquired using a Bruker Multimode AFM with a Nanoscope V controller. AFM images were acquired in tapping mode with imaging parameters, such as the set-point, scan rate and feedback gains, adjusted to optimize image quality. Images were analysed using the Nanoscope analysis program version 1.40. The AFM probes used were Mikromasch HQ:NSC15 Si probes with a nominal spring constant of 40 N/m and a nominal tip diameter of 16 nm. The scanner was calibrated in the x, y and z axes using Si calibration grids (Bruker model numbers PG: 1 μm pitch, 110 nm depth, and VGRP: 10 μm pitch, 180 nm depth).

A4. Raman analysis

Raman spectra and images were collected with a WiTEC alpha300R Microscope in confocal imaging Raman mode using 100 \times (Numerical Aperture 0.9) objective with a 532 nm Nd-YAG green ($E = 2.33$ eV) laser operating at constant power for each experiment. Laser power was kept below 5 mW during all measurements. Spectral images were acquired using integration times between 2.5 to 5 s per pixel with images composed of between 30 \times 30 and 150 \times 150 pixels depending on scan size. Each pixel corresponds to a separate Raman spectrum, allowing hundreds to thousands of spectra acquired during an image scan. Raman images were generated by selecting a region in each spectrum, in which a material specific peak is observed. For graphene oxide (GO) the peak chosen was the strong graphitic band at 1600 cm^{-1} . The intensity of this selected region is plotted relative to the x, y position of the scanning laser. Single spectra were also acquired at points on the Raman images with typical integrations times between 30 s to 60 s and 2 to 3 accumulations per spectra. Raman data was collected by the WiTEC Control software and analysed using the WiTEC Project software.

A5. Bacterial cell growth monitoring using optical density measurements at 600 nm

The growth of GO wrapped bacteria was monitored using the optical density (O.D.) method at 600 nm (Figure A3). O.D. measurements taken from GO

wrapped bacteria show that both *S. aureus* and *R. opacus* bacteria are still viable even after interfacing with graphene oxide. Interestingly, in the presence of GO the growth of bacteria is restricted until $t = 16$ hours for *S. aureus* and $t = 40$ hours for *R. opacus*, and this effect is even more pronounced for samples processed in the VFD.

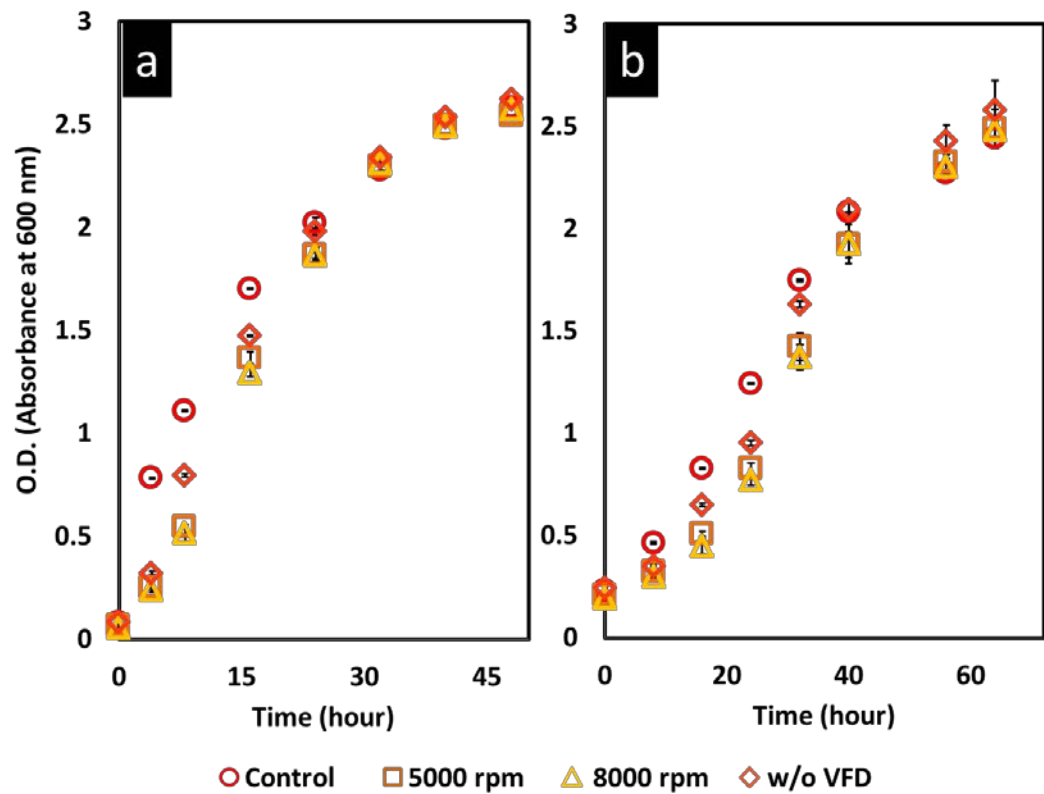


Figure A5. Optical density measurements of (a) *S.aureus*, and (b) *R.opacus* regrown in nutrient media after wrapping with GO.

A6. Calibration curve for optical density measurements at 600 nm versus viable cell count

The bacterial strains *S. aureus* and *R. opacus* were prepared by growing to an O.D.₆₀₀ of ~ 1 in Luria-Bertani (Miller) or GYM Streptomyces medium, respectively. Several dilutions of the O.D.₆₀₀ ~ 1 were prepared covering a wide region of optical density from 0.02 to 1. O.D.₆₀₀ measurements were taken and the samples were serially diluted and plated onto either Luria-Bertani Agar for *S. aureus* or GYM Streptomyces agar for *R. opacus* for viable cell determination. The plates were incubated for 16 hr at 37 °C for *S. aureus* and for 48 hr at 25 °C for *R. opacus* prior to counting the number of colony forming

units (CFU). Viable cell count results are given in $\text{CFU}\cdot\text{ml}^{-1}$. The gradients of the calibration curves in Figure S5 showed that OD unit (at 600 nm) of 1.0 is equivalent to approximately 7×10^8 $\text{CFU}\cdot\text{ml}^{-1}$ *S. aureus* cells, and 4×10^7 $\text{CFU}\cdot\text{ml}^{-1}$ *R. opacus* cells.

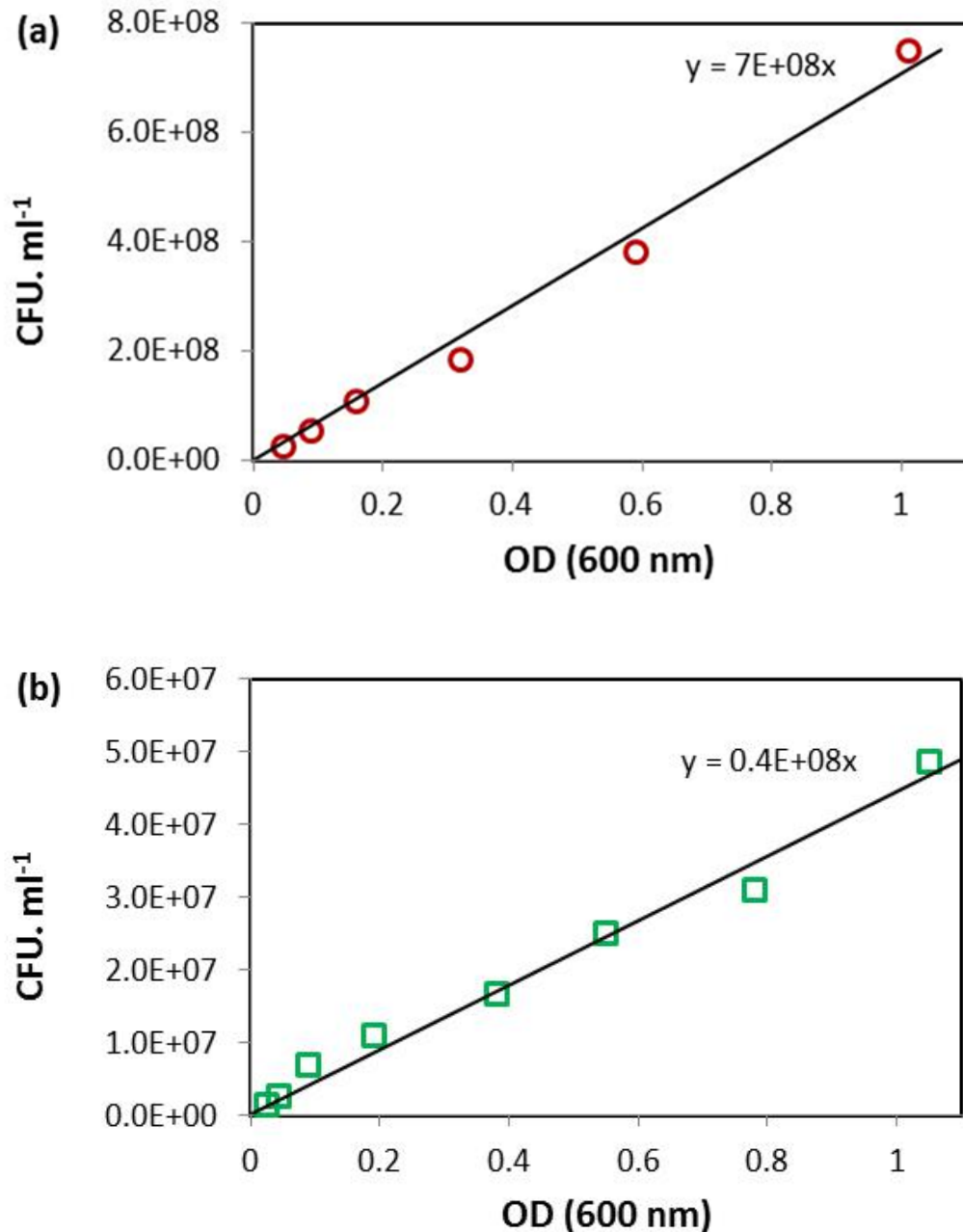


Figure A6. Calibration curves relating OD measurements (600 nm) versus viable cell count in $\text{CFU}\cdot\text{ml}^{-1}$ for (a) *S. aureus*, and (b) *R. opacus* cells. The slopes of the linear calibration curves are also given in each figure.

A7. Bacterial Growth Models

Cell growth rates for microbial cells are defined according to the general equation.

$$\frac{dX}{dt} = \mu X \quad (1)$$

where X is the amount of bacterial concentration at time t , and μ is the specific growth rate.

Due to the more pronounced lag phase within the GO wrapped cells, *logistic growth model* was applied for modelling the overall bacterial growth in all three phases (i.e. lag, exponential, stationary). Specific growth rate (μ) of the logistic model was defined⁶ with equation (2) below, where k_c is the apparent growth rate and X_m is the maximum cell concentration:

$$\mu = k_c \left(1 - \frac{X}{X_m}\right) \quad (2)$$

Rearranging the former equation after inserting into equation (1), and integrating between boundary conditions of X cell concentration at time t and X_0 initial cell concentration at time 0 yields the following:

$$X = \frac{X_m}{1 + \left(\frac{X_m}{X_0} - 1\right) \cdot e^{-k_c t}} \quad (3)$$

The model parameters were calculated by a computer program (CurveExpert 1.4), with a logistic model equation design in cordial to the following logistic function. The logistic model constants are $a = X_m$, $b = (X_m/X_0) - 1$, and $c = k_c$.

$$y = \frac{a}{1 + b \cdot e^{-c \cdot x}} \quad (4)$$

A8 Molecular dynamics simulation of graphene exfoliation using Ramizol[®]

The affinity of 1,3,5-Tris[(1E)-2'-(4'-benzoic acid)vinyl]benzene (Ramizol[®]) to graphene was studied using molecular dynamics. The Sketch Atom module was used to build Ramizol[®] with hydrogens attached. The molecule of interest was then brought in close proximity to the surface of a graphene sheet measuring 37 Å x 50 Å.

The structure was minimised *in vacuo* using the Smart Minimizer with 200,000 iterations, the PCFF forcefield and an atom-based summation method. For the dynamic simulations, the NVT ensemble was used at 298 k with a time step of 1.0 fs and 500,000 iterations giving a total dynamics time of 500 ps. The Andersen thermostat was implemented with a collision ratio of 1.0 and 5000 kcal/mol as the energy deviation. Following the simulation, a second optimization was performed to give the final structure, Fig A8.1a.

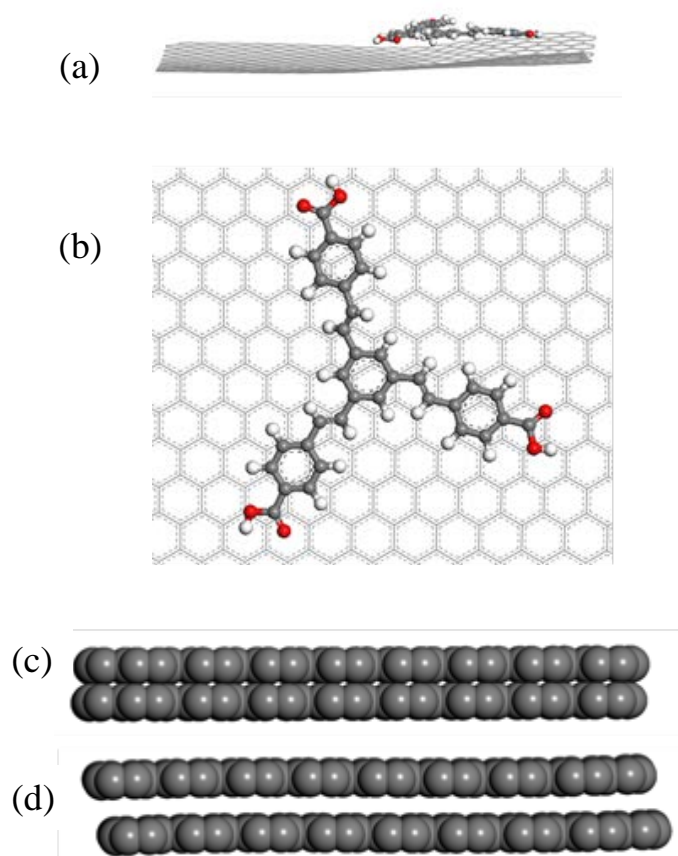


Figure A8.1. (a) Side view of final minimized structure of Ramizol[®] on graphene, (b) close up of top view of Ramizol[®] on graphene, (c) starting geometry of graphene on graphene, and (d) final structure of graphene on graphene.

Ramizol[®] is an aromatic molecule allowing π - π interactions with the graphene sheet, Fig A8.1b. These interactions increase the affinity of Ramizol[®] to graphene thus stabilising the hybrid material. Also noteworthy is the bending of the graphene sheet in the presence of Ramizol[®]. Similar bending of graphene in the presence of calix[8]arene has been observed using molecular modelling and the deformation of graphene may assist the exfoliation of graphene sheets from bulk graphite. The

minimisation of graphene on graphene was also undertaken with the starting geometry in Fig A8.1c. The minimised structure shows a shift of one of the graphene sheets with respect to the other, generating a true representation of stacked graphene, Fig A8.1d. Figure A8.2 shows the energies per atom extracted after the final minimisations. The data also shows that the electrostatic energy/atom in the interaction between Ramizol[®] and graphene sheet is lower than that of graphene on graphene (GOG), at -0.1 kcal/mol compared to 0 kcal/mol, however this difference is less than the difference in van der Waals energy/atom of the two systems of -0.4 kcal/mol. The result is a non-bond energy/atom that is higher for Ramizol[®] and graphene.

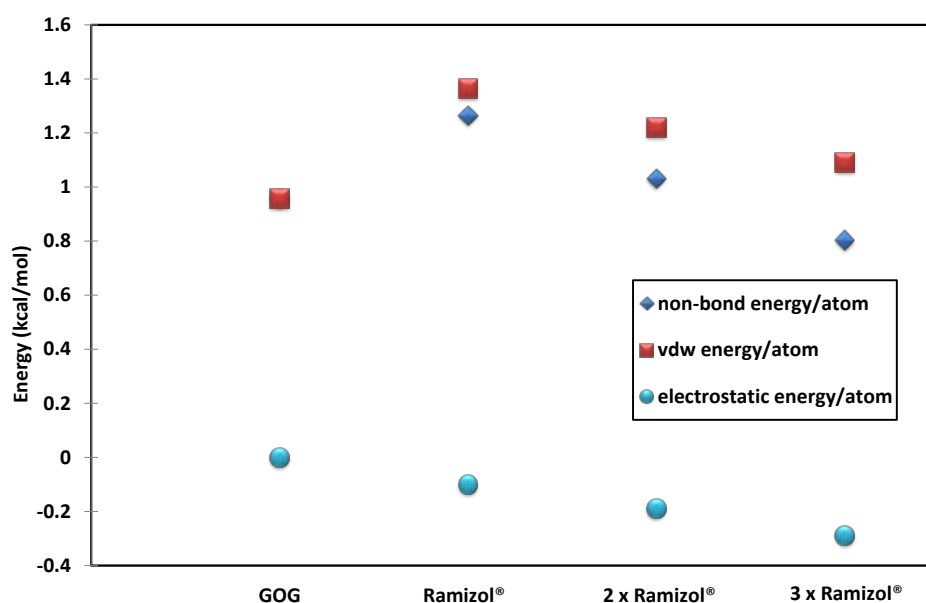


Figure A8.2. Various energies/atom extracted from the final optimised geometries.

Introducing a second Ramizol[®] molecule onto the surface of graphene gave a decrease in both the van der Waals energy and the electrostatic energy, yielding a non-bond energy/atom of 1.03 kcal/mol compared to 0.95 kcal/mol for graphene on graphene. Adding a third molecule of Ramizol[®] gave a lower non-bond energy/atom than graphene on graphene, and it is at this point that exfoliation may occur. The number of Ramizol[®] molecules on the surface translates to a coverage of 40.5% of the total surface area of a graphene sheet. Overall the molecular dynamics suggest that Ramizol[®] has potential in both exfoliating and stabilising graphene.

A9 Minimisation of Ramizol[®]-stabilised graphene sheets

Energy minimisation was carried out using the same parameters in A8 on a system where Ramizol[®] molecules are ‘sandwiched’ between graphene sheets with a higher number of molecules at the periphery versus the centre of the graphene sheet. This was done to gain insight into the increased height profile at the edge of graphene sheets in the composite material as determined by AFM analysis, Fig. 5.7 (a) and (b). Fig. A9a and A9b show the initial and final geometry of the system respectively. After minimisation, the graphene sheets move closer to each other in an attempt to make contact with the drug molecules via π - π interactions as discussed previously in A8. Moreover the minimised structure shows that the extremities of the graphene sheet are higher than the centre of the sheet.

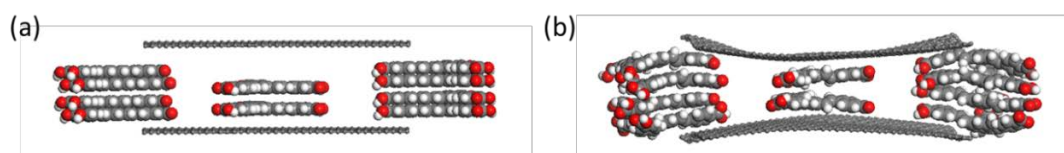


Figure A9. System of Ramizol[®]-graphene composite material: (a) Initial geometry. (b) Final geometry

A10. Effect of acidic and basic pH

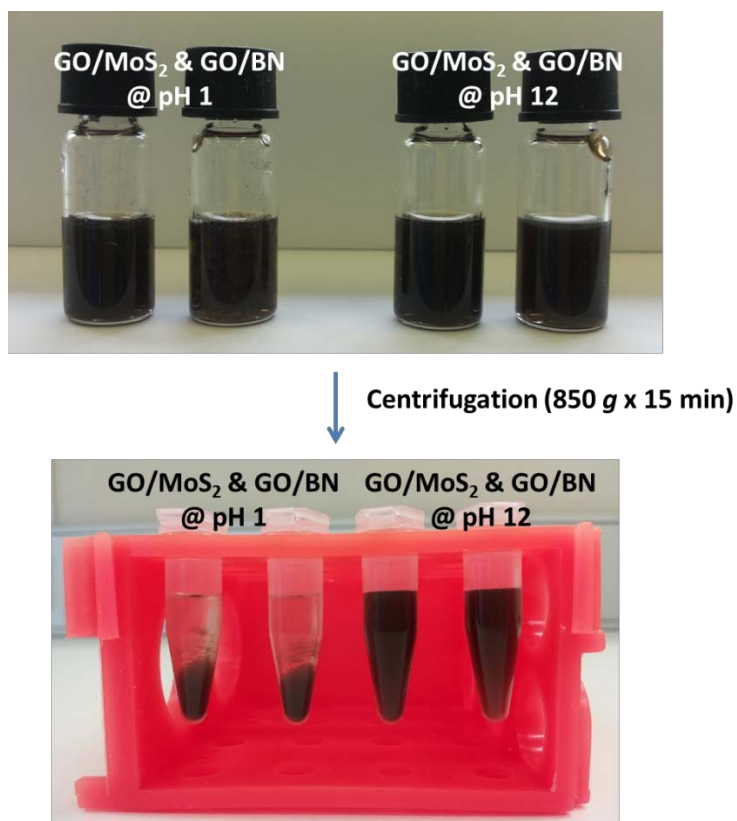


Figure A10. Photograph images of the resulting dispersions at pH 1 and pH 12 respectively, establishing the formation of stable dispersions at basic pH, as for the dispersions at neutral pH.

A11. TEM images of exfoliated BN and MoS₂ at pH 12

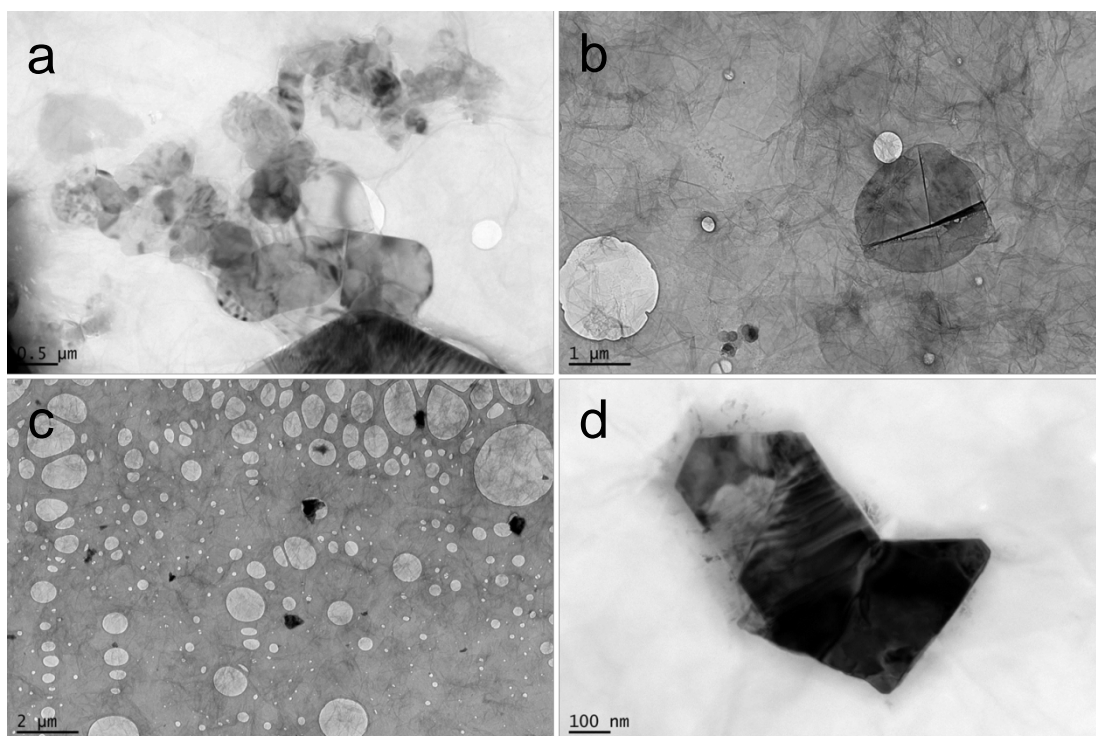


Figure A11. TEM images of the (a,b) GO/BN and (c,d) GO/MoS₂ obtained in basic conditions (pH 12).

7. CONCLUSIONS AND FUTURE WORK

7.1 Conclusions

In this dissertation, novel pathways for developing graphene based functional materials using mechanoenergy have been presented with potential to further expand the applications of graphene. Graphene is a remarkable material and it has been studied extensively in recent years. Pristine graphene alone possesses remarkable properties which has led to its use in energy and electronic applications [1,2]. Nevertheless graphene can be chemically modified or mixed with other materials resulting in the development of a wide range graphene based materials with the materials having interesting properties [1,2]. According to research analysis by IDTechEx, the graphene market is expected to reach nearly \$200 million by 2025 covering various applications sectors such as composites, energy storage and supercapacitors, inks and coatings, sensors, transparent film conductors and others [3]. Graphene also has potential to penetrate new areas, for example in healthcare [4], in the near future and addressing issues such as scalability in the production of graphene based materials offers scope in developing processes and products based on its remarkable properties.

Currently, there is a growing global concern on developing sustainable energy resources and this involves the use of renewable and benign materials. At the same time, there is also a need to incorporate environmentally friendly, scalable and cost efficient processing techniques as a requirement for improving the green chemistry metrics to render it industrially applicable [5]. Graphene can be isolated from relatively cheap graphite mineral and microorganisms are abundant in nature, and their combined usage can lead to sustainable technologies for the future. In Chapter 2, 3 and 4 of this thesis, the hybridization of graphene and microorganisms namely microalgae and bacteria has been explored and the VFD has been employed for the synthesis of the hybrid materials. Microalgae such as *Chlorella vulgaris* possess the capability to absorb nutrients such as nitrate and phosphate from water, and this can potentially reduce the treatment cost of wastewater [6,7]. Graphene itself shows promising properties as an efficient adsorbent [8,9], with high chemical stability [10], large specific area [11] and the possibility of mass production [10]. In this study the VFD features as a facile processing technique for the synthesis of materials. The

VFD has been used to exfoliate graphite flakes into multi-layer graphene (MLG) in water. Importantly, exfoliation of graphene via this technique results in graphene with much less defects compared to the high energy cavitation forces using ultrasonication [12] which is critical to preserve the electronic quality of the graphene [13]. While exfoliation of graphene in NMP is successful in generating monolayers [12], exfoliation in water results in multi-layer graphene due to the high surface energy of water which disfavours the formation of single layer graphene. Nevertheless, the possible mechanism of multi-layer graphene stabilisation in water described herein can be modelled like the stabilisation of an oil droplet in which attained stability arises from the preferential adsorption of hydroxide ions on its surface [14]. Cell viability tests revealed that the cells were sustained even after processing at different speeds in the VFD which was also observed in the study of encapsulating bacteria within GO sheets as presented in Chapter 4 of this thesis. This establishes that the VFD is an effective processing technique for manipulating living cells. Furthermore, VFD processed samples demonstrated complete removal of initial nitrate content within four days which surpassed the removal rate of the free cells, algae-MLG mixture without VFD, and MLG alone. This supports the fact that a more efficient interaction of the mixture is achieved through processing using the VFD. In addition, this processing established the potential for the exfoliation of other 2D laminar materials and their subsequent hybridization with various microorganisms.

Closely related to this study is the encapsulation of microalgal cells within ultrathin graphene oxide layers using the VFD which is presented in Chapter 3. From the previous work, it was established that the cells were viable towards different speeds of the VFD and that graphene is non-toxic towards the cells. In this study the main objective was to encapsulate algal cells within ultra-thin graphene oxide (GO) layers for immobilization purpose. Besides this study, immobilization of microalgal cells in magnetic polymer matrix using the VFD has also been reported by Eroglu *et al.* (2013) [15]. Microalgal growth test results established that the growth of GO encapsulated cells was significantly restrained for the first three days. However, the encapsulation was not very effective when algae and GO were simply mixed on the bench without using VFD or sonication thus showing the significance of an external force on the encapsulation process. Furthermore, GO wrapped cells using the VFD

showed slightly higher nitrate removal efficiency relative to the wrapped cells formed using mild sonication which indicates the advantage of using VFD for the encapsulation process. The unique dynamic thin film in the VFD provides a form of ‘soft energy’ resulting in a more uniform layer of GO relative to using high energy localized cavitation associated with sonication. As a result, they presumably have greater nitrate removal efficiencies while also entrapping the cells more effectively.

This work was also extended to the encapsulation of different shapes of bacteria within graphene oxide layers using the VFD as presented in Chapter 4. In a similar way to the immobilization of microalgal cells, facile wrapping of spherical and rod-shaped bacteria with GO using VFD was successful while maintaining the biological activity of the cells. Results established that the wrapped cells had a longer lag time of growth which relates to their restricted environment within the GO sheets after processing in the VFD. While other reported methods to interface graphene sheets onto the surface of microorganisms involves extensive chemical modification of the graphene, such as functionalization with protein [16] and metal ions [17], in the present work the encapsulation of cells were carried out without the need for further chemical modification of the graphene sheets. As mentioned earlier, interfacing cells with GO nanosheets has potential for surface functionalization of cells, and also immobilizing them for applications in devices, sensors, controlled drug release and targeted delivery, and wastewater treatment. In addition, interfacing soft materials with GO or more conductive graphene sheets can provide a conductive layer around the material, without the need for pre-coating for SEM studies, for example with platinum. This offers an alternative technique for SEM imaging, noting that VFD itself is a rather inexpensive technology.

Another emerging interest is to extend the use of graphene in biomedical applications. In Chapter 5 of this thesis the advantage of using 1,3,5-tris[(1E)-2’-(4’-benzoic acid)vinyl]benzene) (Ramizol[®]) to facilitate the exfoliation process, as well as acting as a stabilising agent has been established. Ramizol[®] is a potent and non-toxic synthetic antimicrobial agent and featured herein in developing a composite with graphene. Ramizol[®] which is a planar molecule and is similar to other pyrene moieties, can interact with the surface of graphene via extended π - π interactions, with potential for stabilising graphene in water. In addition, the shape of Ramizol[®]

lends itself to facilitate exfoliation of graphene from graphite in acting as a molecular ‘wedge’ during sonication where the graphene sheets are prized apart. The thickness of graphene sheets obtained through this method varies depending on concentration of Ramizol[®] with higher concentrations of Ramizol[®] results in thinner graphene sheets. For a graphite to Ramizol weight to weight ratio of 1:1, graphene sheets with thickness ranging from 2-10 nm were generated. This material has potential for developing wound dressing materials where graphene functions as a drug carrier, along with imparting toughness to the material which also has potential to be applied in antibacterial coatings or for other biomedical applications.

Recently there has been an emerging interest in stacking isolated layers of 2D materials into multi-layer heterostructures which can lead to composite materials with novel electronic, mechanical and optical properties. In principle, tailoring the properties of such heterostructures is possible, with potential for functioning as electronic switches which is challenging for graphene due to the absence of an intrinsic energy bandgap. Nevertheless, one of the key factors in advancing the practical applications of these materials is the development of scalable syntheses. In Chapter 6 of this thesis, a facile method for preparing hetero-laminar composites based on graphene oxide and h-BN or MoS₂ in water has been developed and the method can be readily scaled up into gram quantities of the material. This work extends the advantages of utilizing GO in stabilising 2D layered materials, and consequently introducing facile processing avenues for 2D layered materials in general, particularly in water.

7.1.1 Overall

The thesis primarily focuses on developing graphene based functional materials using process intensification technologies, in the form of the VFD and ultrasonic irradiation. Firstly, the exfoliation of graphene in water and its subsequent interfacing with microalgal cells was studied, resulting in material with enhanced nitrate removal efficiency. Secondly, the unique thin film processing in the VFD was used to wrap microalgae and bacterial cells within GO nanosheets results in temporal restriction of the growth of the cells which has a significant potential for immobilization purposes. In addition, given the oxygen-rich functional groups on the surface of GO, they can be modified to impart functionalities to the surface. Thirdly,

an aqueous based synthesis of graphene using an antimicrobial agent as a surfactant offers an alternative approach to produce graphene from graphite with antimicrobial property. Graphene acts as a drug carrier and also enhances the mechanical properties in applications such as wound dressing materials. Lastly, the amphiphilic property of GO has been utilized to develop a scalable syntheses of hetero-laminar materials in aqueous suspensions. Heterolaminar materials are deemed interesting due to their potential to gain access to material with tunable properties. The interaction within different layered materials is mainly van der Waals forces and thus the electronic properties of individual layers are preserved. Tailoring the properties of such material is possible especially in electronics and optoelectronics.

7.2 Future work

Future work includes the development and application of novel functional materials through manipulation of the shear forces and sonic cavitation energy. Since nanomaterials possess size/shape dependant behaviour, it would be interesting to explore possibilities for generating novel nanostructures or nanocomposites with potentially useful or enhanced properties. From this PhD study it is already established that the VFD is useful in generating graphene hybrid bionanomaterials. The VFD has featured in the exfoliation of graphene in water, although in the form of multilayers. It would be interesting to investigate the effect of the shear forces towards other 2D laminar materials in water particularly in the exfoliation of the layered materials. Another significant finding is that processing in the VFD does not appreciably affect the viability of the living cells. Therefore, the VFD has exciting possibilities as a processing tool to maximize reaction conditions involving living microorganisms or cells such as to functionalize surface of the microorganisms or cells with different properties possessing materials. For instance, microorganisms such as microalgae and bacteria, depending on the species, possess useful properties such as the ability to remove harmful substances from water [6,7,18], extract valuable metals from mineral ores, [19] and more. Interfacing them with nanomaterials such as graphene which has good adsorption properties can potentially enhance their properties. It is also interesting to investigate potential of this graphene hybrid material in cleaning oil spills. Moreover the VFD is also proven to be an effective technique for wrapping thin layers around micron sized cells with different

shapes. Similar approaches can be used to coat thin layers around other objects to impart properties such as electrical conductivity.

The VFD can be further designed, incorporating rotating tubes constructed from different materials, in order to create suitable conditions for different processes, in extending the versatility of the device. Also important is further investigation on the fluid dynamics of the VFD to understand the mechanism and effect of shear fluids in the various applications, which will be a major research project in its own right. This is likely to lead to better understanding the utility of the VFD and also generate new ideas on design strategies.

Other future work includes the implementation of the anti-microbial graphene/Ramizol[®] hybrid material into hydrogels. Hydrogels are currently used as wound dressing materials, but hydrogels consisting of natural or synthetic polymers usually exhibit poor mechanical properties [20]. Thus, by introducing graphene as filler, the mechanical stability of the hydrogel can be improved [21]. At the same time, Ramizol[®] will impart anti-bacterial properties to the hydrogel so as to prevent wound infection.

In Chapter 6 of this thesis where the preparation of simple and scalable water-dispersible van der Waals solids is presented, future work includes scaling up of the synthesis and to determine the optimum conditions such as the ratio of graphene oxide to the other 2D layered materials in order to increase the yield of the material. Study on building multilayered heterostructure materials is also warranted. The properties of the heterostructure need to be investigated followed by identifying their potential applications.

7.3 References

- 1 Geim, A. K. and Novoselov, K. S., (2007). The rise of graphene. *Nature Materials*, 6, 183-191.
- 2 Geim, A. K. (2009). Graphene: status and prospects. *Science*, 324(5934), 1530-1534.
- 3 Ghaffarzadeh, K. (2015). Graphene and 2D Materials: Markets, Technologies and Opportunities 2015 - 2025. Retrieved from [http://www.idtechex.com/research/reports/graphene and 2d materials markets](http://www.idtechex.com/research/reports/graphene%20and%202d%20materials%20markets)

- 4 Lee, M. S., Lee, K., Kim, S. Y., Lee, H., Park, J., Choi, K. H., Kim, H. K., Kim, D. G., Lee, D. Y., Nam, S. W., and Park, J. U. (2013). High-performance, transparent, and stretchable electrodes using graphene–metal nanowire hybrid structures. *Nano Letters*, 13(6), 2814-2821.
- 5 Tobiszewski, M., Marć, M., Gałuszka, A. and Namieśnik, J. (2015). Green Chemistry Metrics with Special Reference to Green Analytical Chemistry. *Molecules*, 20(6), 10928-10946.
- 6 Lau, P. S., Tam, N. F. Y. and Wong, Y. S. (1997). Wastewater nutrients (N and P) removal by carrageenan and alginate immobilized *Chlorella vulgaris*. *Environmental Technology*, 18(9), 945-951.
- 7 Sriram, S. and Seenivasan, R. (2012). Microalgae cultivation in wastewater for nutrient removal. *Algal Biomass Utiln*, 3(2), 9-13.
- 8 Li, Y., Zhang, P., Du, Q., Peng, X., Liu, T., Wang, Z., Xia, Y., Zhang, W., Wang, K., Zhu, H. and Wu, D. (2011). Adsorption of fluoride from aqueous solution by graphene. *Journal of Colloid and Interface Science*, 363(1), 348-354.
- 9 Xu, J., Wang, L. and Zhu, Y. (2012). Decontamination of bisphenol A from aqueous solution by graphene adsorption. *Langmuir*, 28(22), 8418-8425.
- 10 Geim, A. K. (2009). Graphene: status and prospects. *Science*, 324(5934), 1530-1534.
- 11 Zhu, Y., Murali, S., Cai, W., Li, X., Suk, J. W., Potts, J. R. and Ruoff, R. S. (2010). Graphene and graphene oxide: synthesis, properties, and applications. *Advanced Materials*, 22(35), 3906-3924.
- 12 Chen, X., Dobson, J. F. and Raston, C. L. (2012). Vortex fluidic exfoliation of graphite and boron nitride. *Chemical Communications*, 48(31), 3703-3705.
- 13 Ciesielski, A. and Samorì, P. (2014). Graphene via sonication assisted liquid-phase exfoliation. *Chemical Society Reviews*, 43(1), 381-398.
- 14 Creux, P., Lachaise, J., Graciaa, A., Beattie, J. K. and Djerdjev, A. M. (2009). Strong specific hydroxide ion binding at the pristine oil/water and air/water interfaces. *The Journal of Physical Chemistry B*, 113(43), 14146-14150.
- 15 Eroglu, E., D'Alonzo, N. J., Smith, S. M. and Raston, C. L. (2013). Vortex fluidic entrapment of functional microalgal cells in a magnetic polymer matrix. *Nanoscale*, 5(7), 2627-2631.

- 16 Mohanty, N., Fahrenholtz, M., Nagaraja, A., Boyle, D. and Berry, V. (2011). Impermeable graphenic encasement of bacteria. *Nano Letters*, 11(3), 1270-1275.
- 17 Kempaiah, R., Salgado, S., Chung, W. L. and Maheshwari, V. (2011). Graphene as membrane for encapsulation of yeast cells: protective and electrically conducting. *Chemical Communications*, 47(41), 11480-11482.
- 18 Pandey, V. C., Singh, J. S., Singh, D. P. and Singh, R. P. (2014). Methanotrophs: promising bacteria for environmental remediation. *International Journal of Environmental Science and Technology*, 11(1), 241-250.
- 19 Bosecker, K. (1997). Bioleaching: metal solubilization by microorganisms. *FEMS Microbiology Reviews*, 20(3-4), 591-604.
- 20 Gonzalez, J. S., Ludueña, L. N., Ponce, A. and Alvarez, V. A. (2014). Poly (vinyl alcohol)/cellulose nanowhiskers nanocomposite hydrogels for potential wound dressings. *Materials Science and Engineering: C*, 34, 54-61.
- 21 Fan, Z., Liu, B., Wang, J., Zhang, S., Lin, Q., Gong, P., Ma, L, and Yang, S. (2014). A Novel Wound Dressing Based on Ag/Graphene Polymer Hydrogel: Effectively Kill Bacteria and Accelerate Wound Healing. *Advanced Functional Materials*, 24(25), 3933-3943.